DETERMINATION OF DYNAMIC PROBLEMS ASSOCIATED WITH THE WIND POWER PLANTS IN TURKISH TRANSMISSION SYSTEM

A THESIS SUBMITTED TO
THE GRADUATE SCHOOL OF NATURAL AND APPLIED SCIENCES
OF
MIDDLE EAST TECHNICAL UNIVERSITY

BY

ANIL AKYEL

IN PARTIAL FULFILLMENT OF THE REQUIREMENTS
FOR
THE DEGREE OF MASTER OF SCIENCE
IN
ELECTRICAL AND ELECTRONICS ENGINEERING

SEPTEMBER 2015

Approval of the thesis:

DETERMINATION OF DYNAMIC PROBLEMS ASSOCIATED WITH THE WIND POWER PLANTS IN TURKISH TRANSMISSION SYSTEM

submitted by **ANIL AKYEL** in partial fulfillment of the requirements for the degree of **Master of Science in Electrical and Electronics Engineering Department, Middle East Technical University** by,

Prof. Dr. Gülbin Dural Ünver _____
Dean, Graduate School of **Natural and Applied Sciences**

Prof. Dr. Gönül Turhan Sayan _____
Head of Department, **Electrical and Electronics Engineering**

Prof. Dr. Osman Sevaioğlu _____
Supervisor, **Electrical and Electronics Engineering Dept., METU**

Examining Committee Members:

Prof. Dr. Mustafa Uğur Ünver _____
Electrical and Electronics Engineering Dept., Mevlana University

Prof. Dr. Osman Sevaioğlu _____
Electrical and Electronics Engineering Dept., METU

Prof. Dr. Müslüm Cengiz Taplamacıoğlu _____
Electrical and Electronics Engineering Dept., Gazi University

Assoc. Prof. Dr. Mehmet Timur Aydemir _____
Electrical and Electronics Engineering Dept., Gazi University

Assist. Prof. Dr. Murat Göl _____
Electrical and Electronics Engineering Dept., METU

Date: 08.09.2015

I hereby declare that all information in this document has been obtained and presented in accordance with academic rules and ethical conduct. I also declare that, as required by these rules and conduct, I have fully cited and referenced all material and results that are not original to this work.

Name, Last name : Anıl Akyel

Signature :

ABSTRACT

DETERMINATION OF DYNAMIC PROBLEMS ASSOCIATED WITH THE WIND POWER PLANTS IN TURKISH TRANSMISSION SYSTEM

Akyel, Anıl

M. S., Department of Electrical and Electronics Engineering

Supervisor: Prof.Dr. Osman Sevaioğlu

September 2015, 259 pages

From the early 20th Century, the intense population growth around the world resulted in large increases in the power plants, both by means of number and size. However, this increase brought many concerns, including environmental and human health related ones. This has resulted in renewable energy sources to rise over conventional power plants. Among renewable energy sources, thanks to their simplicity and convenience, wind turbines became of considerable importance. As a result, a large number of wind farms have been installed and integrated to the grid worldwide. As the wind oriented generation levels increased, several new concerns arose. Among them, the threat on system stability and security introduced by the wind farms present in the system which may play a role in the event of a fault is regarded as the main concern.

In order to investigate this problem and related concerns, a simplified yet realistic model of Turkish Generation/Transmission system is implemented on Digsilent Powerfactory computer software. With the present wind farms in operation added to the system model, transient analyses for three phase to ground faults are carried out. The analyses are performed individually for different wind farm installed capacity values and breaker operation times with the results recorded after each analysis. The installed capacity values for each wind farm are chosen to be equal to a given

percentage of the short circuit power at the bus that the wind farm is connected to. Regarding circuit breaker operation times; theoretical and practical minimum, average, above-average and maximum allowed durations are considered and their effect on the results are analyzed. The simulation results are examined and evaluated in a comparative manner, thus presenting the scales of dynamic effects of wind farms on the transmission system with respect to the wind oriented generation and wind farm installed capacity levels.

Keywords: Wind farms, Integration, Stability of transmission system, Dynamic effects, System security.

ÖZ

RÜZGAR SANTRALLERİNİN TÜRKİYE İLETİM SİSTEMİ ÜZERİNDE SEBEP OLDUĞU DİNAMİK PROBLEMLERİN BELİRLENMESİ

Akyel, Anıl

Yüksek Lisans, Elektrik Elektronik Mühendisliği Bölümü

Tez Yöneticisi: Prof.Dr. Osman Sevaioğlu

Eylül 2015, 259 sayfa

20. Yüzyıl'ın başlarından itibaren dünyadaki nüfus artışı enerji santrallerinin büyük bir hızla sayı ve boyut bakımından büyük artışlar göstermesini beraberinde getirmiştir. Ancak, bu artışın sonucu olarak başta çevre ve insan sağlığı sorunları olmak üzere birtakım endişeler gündeme gelmiştir. Bu da konvansiyonel santrallere alternatif olarak yenilenebilir enerji kaynaklarını ön plana çıkarmıştır. Yenilenebilir enerji kaynakları içinde ucuzluğu ve yaygınlığından dolayı rüzgar türbinleri ayrı bir önem kazanmış olup dünyanın dört bir yanında çok sayıda rüzgar enerji santralleri (RES) kurulmuş ve elektik sistemlerine bağlanmıştır. Gitgide artan rüzgar santraline dayalı üretim seviyeleri ortaya yeni endişeler çıkarmıştır. Bunların başında, yüksek üretim seviyelerinde sistemde meydana gelebilecek bir arızanın mevcut rüzgar santrallerinden dolayı sistem stabilite ve güvenliğininin tehlikeye gireceği endişesi yer almaktadır.

Bu ve benzeri sorunları ele alabilmek için Türkiye Üretim/İletim sisteminin gerçekçiliği korunarak detayları azaltılmış bir modeli Digsilent Powerfactory programı kullanılarak hazırlanmıştır. Mevcut rüzgar santralleri de modele eklenerek rüzgar santrallerinin bulunduğu bölgelerde üç faz-toprak arızaları için transient (anlık) analizler yapılmıştır. Analizler, söz konusu rüzgar santralleri için farklı kurulu güç değerlerinde ve farklı kesici açma süreleri için tekrarlanmış, sonuçlar

kaydedilmiştir. Santral kurulu güç değerleri için, santralin bağlı olduğu dağıtım sistemi barasının kısa devre gücü baz alınmış olup bu gücün belli bir yüzdesine eşit olan değerlerde analizler yapılmıştır. Kesici açma süreleri içinse teorik ve pratik minimum, ortalama, ortalamanın üstü ve maksimum izin verilen değerler baz alınmış olup bu sürelerin sonuçlara etkisi de incelenmiştir. Simülasyon sonuçları karşılaştırmalı olarak incelenmiş olup rüzgar santrallerinin iletim sistemine dinamik etkilerinin boyutları, rüzgara dayalı üretime ve santral kurulu güçlerine göre ortaya konmuştur.

Anahtar Kelimeler: Rüzgar santralleri, Entegrasyon, İletim sistemi stabilitesi,
Dinamik etkiler, Sistem güvenliği.

To My Late Grandfather…

ACKNOWLEDGMENTS

First of all, I would like to present my sincere thanks to my supervisor Prof. Dr. Osman Sevaioğlu for his guidance, suggestions and support throughout this study.

It is hard to describe how much I am grateful for the support and love from my dearest family, especially my mother who supported me with her endless and unconditional love and care, my aunt and uncle. I would not be able to complete this study without their encouragement.

I would also like to thank M. Erkut Cebeci and his colleagues for their advices during modeling processes.

I am thankful to my friend, Uğur Akyüz for his help and support during the hard times of this study.

I would like to express my great admiration to Vicky Leandros for making not only my thesis process but also my whole life much more beautiful with her presence and voice.

Finally, I present my sincere gratitude to TÜBİTAK for the scholarship granted regarding my M. Sc. study.

TABLE OF CONTENTS

LIST OF FIGURES

FIGURES

LIST OF TABLES

TABLES

LIST OF GRAPHS

GRAPHS

LIST OF SYMBOLS AND ABBREVIATIONS

HPP	Hydroelectric Power Plant
TPP	Thermal Power Plant
HVDC	High Voltage Direct Current
TEİAŞ	Türkiye Elektrik İletim Anonim Şirketi (Turkish Electricity Transmission Company)
S_{sc}	Short Circuit Power (MVA)
t	Time
r	Radius
E	Energy
P	Power
m'	Mass Flowing Through a Cylindrical Surface per Unit Time (kg/sec)
ρ	Density of Air Flow (kg/m^3)
A	Area
v	Wind Speed (m/sec)
F	Force (N)
C_B	Betz Limit
VOC	Volatile Organic Compounds
HAWT	Horizontal Axis Wind Turbine
VAWT	Vertical Axis Wind Turbine
v_e	Electrical Speed
v_m	Mechanical Speed
EÜAŞ	Elektrik Üretim Anonim Şirketi (Electricity Generation Company)
EMT	Electromagnetic Transient
DFIG	Double Fed Induction Generator

EPDK	T.C Enerji Piyasası Düzenleme Kurumu (Republic of Turkey Energy Market Regulatory Authority)
EMRA	Energy Market Regulatory Authority
RMS	Root Mean Square
RES	Rüzgar Enerji Santrali (Wind Power Plant)
HES	Hidroelektrik Santrali (Hydroelectric Power Plant)
u	Voltage
EMO	Elektrik Mühendisleri Odası (Chamber of Electrical Engineers)
p	Static Pressure (Pa)

CHAPTER 1

INTRODUCTION

This thesis investigates the dynamic problems associated with wind power plants in the transmission systems.

1.1 Evolution of Power Generation

With the industrial revolution, mankind has discovered the power of steam. In the early days of industrial revolution, steam machinery that were able to do "a thousand men's work" were developed and used by combustion of fossil fuels. As the technology has propagated further, the efficiency of these machinery has improved and their usage is spread worldwide. The invention of electricity generation was a milestone in this field. With electricity, mankind was not limited only to steam driven machines but also a variety of electrical machines which has provided a further boost to the technological developments [1]. To power these machines, constant generation of electricity is required, which was entirely provided by combustion of fossil fuels in the early years of electricity generation.

Fossil fuels, especially coal was the primary source of electricity generation since late 19th century. Despite hydroelectric generation was also started shortly after, at the dawn of 20th century, due to its geographical dependence, thermal power plants have become dominant since the very early days of electricity generation [2]. It was all good until the mid-20th century, when the consequences of fossil fuel based generation started to show up. Starting from the United States of America, pollution which was already enhanced by coal-burning residential heating, became a serious

problem concerning not only human health but also the environment worldwide. Replacement of coal burning stoves with natural gas heating systems has eventually eased up the pollution problem in the cities but the problem associated with large thermal plants remained unsolved, with increasing reaction from public, being informed by environmental organizations day by day. Moreover, the energy crisis that was effective in many parts of the world in the 1970's has drawn the attention to alternative sources of generating electricity.

People's search for less polluting and more abundant sources of energy resulted in the birth of a new concept: renewable energy. This concept includes, but not limited to, wind energy, solar energy, hydro energy, geothermal energy and biomass [3]. Among these, hydro energy was already in use by means of electricity production widely in the world, in the form of hydroelectric power plants (HPP). The remaining ones have also been in various usages apart from electricity generation. For example, wind energy was used in agriculture since 1st century A.D. or mankind had used biomass combustion for heating since the Neolithic Revolution (10.000 B.C). However, it wasn't until the late 20th century that they are started to be recognized as alternatives of electricity generation.

The idea of absorbing solar light had already been in usage for several centuries, by means of heating. Even today, roof mounted solar panels (hot water panels) are used to heat water for residential uses. However, with the developments in semiconductor technology, it became possible to use the absorbed solar light to free electrons from a surface, and therefore provide a current flow through a circuit. Following this idea, a few solar power plants, consisting of a large number of solar panels have been built. Moreover, roof-mounted solar panels are becoming of wider and wider usage in residential areas. These panels do not contribute to the country's electricity generation unless there's a Smart Grid system involved. However, they are still able to aid the generation by providing energy to individual houses and offices. On the other hand, they are expensive and due to their relatively low lifetime, on many occasions they are unable to even amortize their installation costs. Therefore, the

solar technology is only viable if the place of interest has exceptionally high solar power yield, which covers little portion of the available land worldwide.

Geothermal energy means the thermal energy generated and stored in the earth which is transferred to the surface via the hot springs. These springs are places where the water below the surface is heated by the Earth's internal heat. Their usage as a source for electricity generation has been started in the 1960's. However, due to their rarity when compared to other sources of energy, they have not become a common source for electricity generation. By 2010, the worldwide installed capacity of geothermal power plants is slightly above 10.000 MW.

Neolithic Revolution, corresponding to c.a. 10.000 B.C. was the wide scale transition of many cultures to settled lifestyle instead of nomad, enhanced with agricultural activities. With agriculture, followed by domestication of animals, the organic waste production of the tribes and their herds reached considerable amounts. Some cultures found a solution to increasing biological wastes. It was the idea of simply burning them. Therefore, they were able to obtain a certain amount of heat that could be used to warm their settlements during cold times. This can be considered as the first usage of biomass energy. The usage of biomass as a modern energy source is somewhat different. It mainly employs plants mostly grown for the specific purpose instead of animals. However, agricultural wastes are also being used in some parts of the world. The electricity generation from biomass is lead by a process very similar to conventional fossil fuels, enabling biomass power plants can be considered as "renewable thermal plants". This highlights the fact that, unlike other renewable sources, biomass does have an environmental impact that cannot be ignored. If necessary precautions are not taken, biomass power plants can cause significant air pollution problems.

In the first century A.D. a Greek engineer named Heron has developed the first ever known wind wheel. It was used to power an organ. Approximately 800 years later, in Persia (now Iran), the first windmills are believed to appear. They were able to grind corn and other grains or even pump water. However, they employed a vertical axis

configuration instead of horizontal axis which were found in later windmills, causing them to be relatively inefficient. However, development of horizontal axis windmills took approximately a millennium. They became of wide usage especially in Europe and Asia in the 19th century. The development of first wind turbines also correspond to the same era. The wind turbines converted the wind energy to electrical energy in a way similar to steam turbines. Here, the wind energy actually corresponds to the kinetic energy of the moving air mass. Wind, itself is created due to the pressure differences of different air masses. Since with the rotation of earth these pressure differences will always be present, wind energy can be indeed classified as a renewable and infinite energy source. This property differentiates wind energy from hydro and geothermal energy which are abundant but not infinite. The fact that wind energy does not cause any emissions also makes it advantageous over biomass energy. As will be discussed later, the cost of wind power plants are somewhat less than that of solar power plants of same capacity. Moreover, the amortization time of wind power plants, at sufficiently high wind speeds, are even shorter than any renewable power plant, including hydro generation. For all these reasons, electricity generation from wind energy proved more advantageous when compared to other renewable energy forms (excluding hydro energy) and therefore it is not surprising to see that wind power plants had gained more popularity and worldwide usage since late 20th century.

The conversion of wind energy to electrical energy takes place within the wind turbines. Wind turbines are the main element of wind generation [3]. Unlike conventional power plants, there is no general limitation on how many wind turbines can a wind power plant contain. Even a single turbine can be counted as a power plant itself and is enough to power a number of houses or offices.

The first wind turbine was designed and built by James Blyth in July 1887 and was used to supply his cottage in Maykirk/Scotland [1]. By means of axial configuration, wind turbines had a similar history with windmills. This early design, had vertical axis configurations and suffered from inefficiency problems worsened further by the low height-of-build. However, only a few months after Blyth built his turbine,

American inventor Charles F. Brush built the first horizontal axis wind turbine. It was a massive structure that looked something in between a windmill and a modern wind turbine. It had a rated output of 12 kW, which was revolutionary for the measures of that time. This was the first application of wind power plant technology since it was connected to an existent distribution system and operated as a power plant, unlike Blyth's design supplying an isolated house. In 1931, USSR has built the first "modern" wind turbine. It had a rating of 100kW and was almost as efficient as current wind turbines.

Modern wind turbines that are used in the industry have the horizontal axis configuration. Despite vertical axis turbines were also commercially produced until late 80's, later on they were of little usage. Horizontal axis turbines typically have a number of blades depending on the purpose of the wind turbine. For electricity generation, 3-blade turbines are dominant though 2-blade turbines have also found occasional usage. The low number of blades allows smaller and therefore lighter gearbox that is required to achieve the rated speed at the driving shaft of the generator. Turbines having 20 or more blades are used for mechanical water pumping and have no relation to electricity generation. For these reasons, the term "wind turbine" will cover exclusively 3-blade generating turbines for the rest of the thesis.

With the current technology, the ratings of wind turbines vary from a fraction of a Megawatt up to 8 MW. This value is claimed to be exceeded within a few years by some authorities. However, even these values are very small when compared with a conventional, fossil fuel based generator. For example, a medium-sized coal power plant may have a rating above 600 MW while a relatively large one, namely the Afşin-Elbistan B Thermal Power Plant can have a rating of approximately 1.500 MW. Therefore, to be able to contribute the generation system, a number of wind turbines are needed. This creates the idea of agglomeration of wind turbines, which is essentially the wind farm concept.

Wind farms may consist of from a mere dozen to several hundreads of wind turbines. However, interconnection of these turbines is not a simple task and therefore power electronics solutions are needed in order to turn a cluster of wind turbines to an actual wind farm that has similar characteristics with conventional power plants. This means that, wind farms are required to be able to behave as active controllable components in the power system. This includes the requirements of providing voltage and frequency control, regulating active and reactive power and being able to provide fast enough responses during transient periods.

In the traditional designs of wind turbines which do not employ a complicated control equipment, the active power control was simply carried out by pitching the blades or disconnecting the turbine [4]. However, these are not sufficient to contribute the power system stability. In addition, if wind farms consisting of these turbines are connected to the grid, since they will not be able to perform voltage control, voltage stability problems will also be introduced with them. Therefore, advanced power electronics systems are required when connecting a wind farm to the overall power system.

It is convenient to build a conventional power plant near a site of large consumption such as big cities or large industrial installations in order to maximize the power quality and minimize transmission losses. However, unlike coal or natural gas, wind which can be considered as the "fuel" of wind power plants, cannot be transported in the same manner. Therefore wind power plants must be located at sites with high wind speed and regular wind pattern so that wind power yield is sufficiently high. These areas can be briefly categorized as follows:

-Hill Tops
-Coastal
-Open Sea

These areas are, as can be intuitively predicted, mostly remote areas where little or no electrical loads are present. Therefore the grid connection for the wind farms can

be too far away or the existing lines may be too weak. In either case, new transmission investments are required which introduces a delay in wind power development and an increase in overall cost of wind farms. For continental or onshore (coastal) applications, the transmission is carried out by conventional overhead lines [5]. However, for wind power plants at open seas, which are called offshore wind farms, the distances to grid connection may be extremely long. For such cases, in order to prevent excessive losses or voltage drops due to capacitive impedances of A/C cables, High voltage DC (HVDC) links are used for grid connection.

In the early days of wind generation, the ratings of individual turbines, hence the wind farms were relatively low, and their numbers were scarce. Therefore, it was not of serious concern whether the existent wind farms were able to contribute to system stability or performing active and reactive power controls. However, as fuel prices have increased and the "clean energy" campaigns have been spread over the world, the renewable energy technologies have shown great progress, both by means of technology and commercial availability. Among the renewable energy technologies, thanks to its several advantages associated with the capacity and cost, wind energy has shown the largest development. This resulted in a drastic increase in both number and overall generation rating of wind farms worldwide. When the 21st century started, the contribution of wind energy, or wind power penetration, has become considerable with respect to overall generation capacity for many countries [6]. This introduced the fact that, an important fraction of the overall generation was now being provided by wind farms. However, due to aforementioned differences of wind generators from conventional generators, this large penetration has also brought certain problems and concerns.

With the increase in wind penetration in the power systems, there exists concerns about the system supply power quality. It is indicated that, in power systems with high wind power penetration, depending on the wind patterns in the regions with wind farms, there may be serious voltage fluctuations and hence deterioration in power quality [7].

This concern has been mentioned by TEİAŞ, as a report [8]. In the report, it is claimed that the system stability in case of a disturbance is severely endangered in case that the total wind farm(s) installed capacity exceeds %5 of the short circuit power (S_{sc}) at the bus that the relevant wind farm(s) is/are connected to. This claim implies that, the system will be unable to keep the normal operational state in case a disturbance occurs near to a bus that has a wind farm of high (more than %5 of the S_{sc}) capacity. This means that, if the claimed phenomenon is realistic, a disturbance in the system with high wind generation will result in large voltage swings (more than %10 of nominal voltage) or even loss of some nearby generators due to rotor angles exceeding 90 degrees. Therefore, the main concern focused on allowing or disallowing a wind farm to be installed and connected to a given bus should be, according to TEİAŞ, the rating of the plant to be installed and the short circuit power at that bus.

With this thesis, the aforementioned problems will be investigated. More specifically, the effects of wind power plants on the transmission system, the problems they can cause and the severity of these problems will be investigated. Among these effects, the cases which include a disturbance in the system such as short circuit events will be focused on.

Scope of the Thesis

This thesis will investigate the effects of a disturbance event in a power system with a nonzero penetration of wind power. For this purpose, the fluctuations in the system within the first 5 seconds of different dynamic events in a power system will be observed. These dynamic events will include several different line faults. Moreover, the line loadings to ensure secure system operation, as well as stability requirements will also be monitored to be satisfied throughout the processes.

Just like any other technology, the wind power plant technology, as well as its penetration with respect to conventional generation is uneven worldwide. The uneven distribution of worldwide wind generation is mainly due to the technological advancement as well as geographical and meteorological suitability of individual

countries. Moreover, being somewhat related with technological and economical welfare, a country's bias towards clean energy also plays significant role in that country's priority in wind installations [9]. When the wind penetration percentages in the world are examined, according to 2012 values Denmark is world leader with %34 and is followed by Portugal, Spain and Ireland all of which have approximately %20 penetration rates. United States of America follows the three countries with a rate of %4.5. On the other hand of the scale, there are still many undeveloped or developing countries without significant wind power penetration. A few examples of these countries can be given as Armenia with a total installed power of 2.6 MW, Madagascar having only 1.2 MW of capacity installed and Indonesia with a total capacity of 1.4 MW [4].

When the installed capacity and wind penetration figures of Turkey is examined, it is found that Turkey lies somewhere in-between the more developed countries with high wind penetration and the lesser developed countries that still don't have a determined wind power policy. By means of installed capacity, according to 2012 figures Turkey is at 16th place in the world with a total capacity of 2.960 MW [2]. Wind penetration of Turkey is reported to be approximately 4.3%, slightly below that of United States of America in 2013. For this position of Turkey among the countries in the world, it is possible to obtain the cases where wind penetration is lower by comparing with less developed countries. Moreover, the future cases when wind penetration will become higher can also be predicted by regarding more developed countries' wind power generation processes. Due to these facts, the analyses will be carried out with a power system model that is as similar as possible to the Turkish transmission system model. What is more, the wind farm ratings and positions will be selected taking the geographical and meteorological data of the regions of interest in Turkey into account.

1.2 Thesis Outline

In Chapter 2, a general background about definition, principles and types of wind turbines, different technologies used in wind farms and future of wind power

generation technology are given. Chapter 3 includes the construction of a power system model, as well as implementing wind farms into the power system model. This chapter also briefly describes the simulation process with which parameters are considered and observed alongside the methodology of analyzes and data acquisition. Chapter 4 includes the simulation results for different cases, each representing a defined event. Finally, in Chapter 5, the thesis is concluded and suggested future work is stated . The detailed explanations of relevant topics are provided in the appendices both by means of printed and digital material whenever necessary.

CHAPTER 2

GENERAL BACKGROUND

2.1 Definition of Wind Energy

In its most general form, wind energy is often referred as the kinetic energy of the moving air mass [10]. This kinetic energy of a mass is given by the expression

$$E= 0.5mv^2 \quad (2.1)$$

Where m is the mass of interest and v is its velocity. The standard units for mass and velocity are kg and m/s in SI unit system, respectively.

Since wind through turbine blades are of interest, it is convenient to define an cylindrical area through which wind flows.

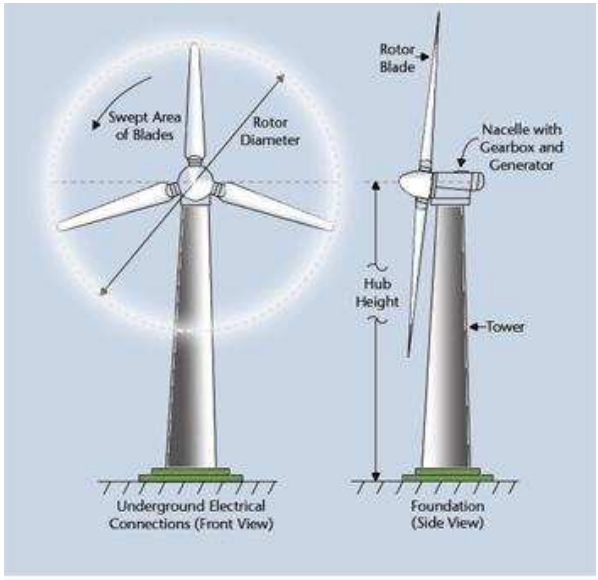

Fig.2.1. Area Swept by Rotor Blades

For horizontal axis wind turbines, the blades sweep, and hence capture energy from a cylindrical area, which can be assumed to be uniform and have a radius equal to blade length. This radius can be shown by "r". The mass of air confined in the cylindrical volume is equal to the mass whose energy will be captured by blades in a time equal to

$$t = h/v \tag{2.2}$$

where h is the length of the cylinder under consideration. To be able to express the energy in a more understandable way, it is necessary to focus on mass per unit time instead of mass. Therefore, if the mass in equation 2.1. is replaced by mass per unit time, the Energy (E) will become energy per unit time, which is essentially the power.

$$P = \frac{1}{2} m' v^2 \tag{2.3}$$

where P denotes power and m' is equal to mass flowing through the cylindrical surface per unit time. This expression can be modified further by using

$$m' = \rho A v \tag{2.4}$$

where ρ is the density of air flowing, A is the cylindrical cross section area and v is the velocity of air flow, or wind velocity. Substituting m' expression into eq. 2.3, eq. 2.5 is obtained.

$$P = \frac{1}{2}\rho A v^3 \tag{2.5}$$

According to SI unit system, the units for Power and density (denoted by p) are Watts and kg/m^3, respectively. Here, defining power is important since it illustrates how much energy per unit time is "carried" by the moving air mass, and therefore it is also related to how much energy a wind turbine can generate or namely, the rating of a wind turbine.

The cross sectional area of a cylinder of a radius r is given as

$$A = \pi r^2 \tag{2.6}$$

Where A is the cross sectional area and π is the constant 3,141519.. . Substituting this expression into eq. 2.5, a new equation relating power to turbine blade radius is obtained:

$$P = \frac{1}{2}\,\rho \pi r^2 v^3 \tag{2.7}$$

Here, it can be seen that power carried by an moving air mass through the blades of turbine is directly proportional to the length of blades squared. The effect of an infinitesimal change in blade radius to this power can be obtained by taking the derivative of eq. 2.7 with respect to radius.

$$\frac{dP}{dr} = \rho \pi r v^3 \tag{2.8}$$

By applying linearization, for small variations in r, the variation in P, namely ΔP is obtained as in eq. 2.8.

$$\Delta P = \rho \pi r v^3 \Delta r \qquad (2.9)$$

which can be modified to obtain the variation in P as a fraction of P leading to eq.2.10

$$\frac{\Delta P}{P} = \frac{2\Delta r}{r} \qquad (2.10)$$

This relation is important since it implies that any small change in radius (Δr) with respect to radius will result in a twice as large change in power with respect to the power yield of the moving air mass. That is, for instance, a 1 percent increase in turbine blade radius will result in a 2 percent increase in the power of the wind within the area spanned by the blades.

The effect of a change in wind speed (v) to the power carried by the wind can be found by taking the derivative of eq. 1.6 with respect to wind speed.

$$\frac{dP}{dv} = \frac{3}{2}\rho \pi r^2 v^2 \qquad (2.11)$$

In a similar manner, this equation can be modified to obtain the relation between the increase in power with respect to power and the increase in wind speed with respect to the wind speed.

$$\frac{\Delta P}{P} = \frac{3\Delta v}{v} \qquad (2.12)$$

Eq. 2.12 implies that any small change in wind speed, with respect to the magnitude of the wind speed, will result in a three times larger change in the power yield as a fraction of power of the wind. For example, a 1 percent decrease in wind speed will

cause the power carried by the wind decrease by 3 percent. It should, however be kept in mind that these linearizations are only valid for small changes. For large changes in values, actual Power relation must be used.

In order to understand how wind power is captured by turbine blades and transferred to the generator, the three essential laws of physics are needed to be understood. These laws are conservation of mass, conservation of energy and conservation of momentum. All of these equations will be handled by defining a volume of interest first. It is known that when the air flow comes across an obstacle, some of the air will hit the obstacle and therefore their energy will be absorbed, while the parts of the flow that is closer to the bounds of the obstacle will tend to flow around the obstacle, causing an outward expansion in the shape of the air flow. This can be illustrated in Fig. 2.2

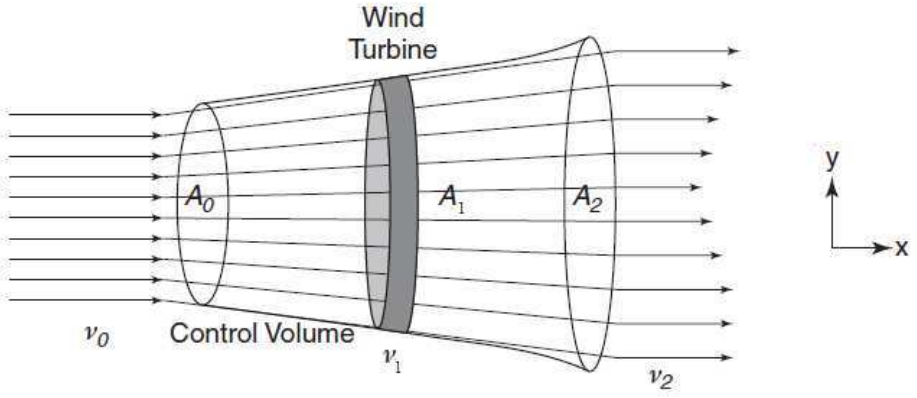

Fig.2.2 Illustration of Expansion in the Shape of Air Flow (Source: Jain, 2010)

As can be seen in the figure, A_0 is equal to the cross sectional area of air flow before the turbine. It is necessary to define the distance from the turbine to the point where this area is defined. For this purpose, a distance equal to the distance traveled by air in unit time will be assumed. That is, the distance between the area under consideration and wind turbine is

$$d_0 = v_0 \cdot 1 = v_0 \tag{2.13}$$

A_1 and v_1 are defined as the area spanned by the wind turbine blades and the wind velocity through the wind turbine area, respectively.

In a similar manner, A_2 is defined as the cross sectional area of wind flow, from a distance equal to that of traveled by air in unit time with a velocity of v_2 downwind.

For this case, the conservation of mass can be applied leading to eq. 2.13 [11].

$$m^{'} = \rho A_0 v_0 = \rho A_1 v_1 = \rho A_2 \bar{v}_2 \tag{2.14}$$

Where ρ is the density of air and $\bar{v}_2$ is the average wind speed over the cross sectional area A_2.
It should be noted that, since the wind turbine is extracting the wind energy, its speed from upwind to downwind direction should decrease. That is, $v_0 > v_1 > \bar{v}_2$.

The law of conservation of energy states that the total energy of an isolated system cannot change [12]. Here, total energy is defined as the sum of kinetic energy, pressure energy and potential energy. Kinetic energy refers to energy due to the movement of a mass while the pressure energy is because of the random motion of particles in a mass, applicable for liquids and gases [11]. The potential energy of a mass is not only due to the relative position of a mass but also to the state of compression of it. However, for the case of interest, compression of air in the atmosphere is zero, therefore will not be taken into account. Before moving any further, it is necessary to make some assumptions that will make the derivations of less complicated equations possible. These assumptions are:

-All the flow is along the streamlines.

-The work done by shear forces is zero.

-Air is not compressed during the power transfer process. Its density remains same.

-No heat exchange between air and its surroundings is present.

-The relative position change of air mass, hence the potential energy change is insignificant.

Taking these assumptions into account, the air flowing can now be defined as an ideal fluid. Therefore its total energy per unit volume is given by Bernoulli's equation which is given as eq. 2.14.

$$\dot{E} = \rho \frac{v^2}{2} + p_s = \text{Constant} \tag{2.14}$$

where $\dot{E}$ denotes the energy per unit volume, $\rho \frac{v^2}{2}$ is the kinetic energy per unit volume and p_s is the static pressure.

This equation states that, for a travelling air mass, the speed and the pressure are inversely related. That is, when the air mass along a streamline travels faster, its pressure will be lower and vice versa.

The conservation of momentum can be applied as follows: The moving air mass has a nonzero momentum before the wind turbine. When the air of interest interacts with the turbine blades and therefore will slow down. This will cause in a decrease in the air mass' momentum. According to the law of conservation of momentum, total momentum of the system is constant which implies that the momentum gained by the wind turbine is equal to the loss of momentum of the air mass. This gained momentum will allow the turbine blades to rotate at a speed and therefore, the generator will operate at a nonzero shaft speed.

The reason that the air flow expands, i.e. the cross sectional area A_2 is larger than A_1 can be explained by the following fact. The pressure will be low immediately after the wind has passed through the rotor. And after wind passes the rotor, its pressure will start to increase. From Bernoulli's equation, this implies that the wind velocity

will decrease and therefore the flow-through area of the wind will increase, leading to $A_2 > A_1$ [11].

It is possible to calculate how much energy that a moving air mass of specified velocity, flow area can yield in a given time interval. However, the amount of energy that can be captured by the wind turbine is always less than aforementioned energy. This can, very basically, be explained as follows. If the wind energy is to be absorbed by wind turbine completely, the moving air mass will lose all of its kinetic energy and hence momentum. If the momentum of a moving mass becomes zero, its velocity will also be zero. That is, $v_2=0$. However $v_2=0$ means that there is no wind passing through the wind turbine, which contradicts with the initial assumption stating that the whole wind energy is absorbed by the wind turbine [11]. To investigate this concept in more detail, the concept of Betz Limit needs to be provided.

In 1919, Albert Betz has came up with a theory stating that there is an upper limit for the efficiency of any wind turbine. He postulated that a wind turbine having a rotor of a disk-like shape, cannot capture more than %59.3 of the energy yielded by the air mass moving through the turbine. Betz has derived this conclusion by applying the aforementioned concepts, namely the conservation of mass, momentum and energy.

Taking the Fig.2.2 as reference again, the conservation of mass can be applied yielding to Eq.2.15.

$$A_0 v_0 = A_1 v_1 = A_2 \bar{v}_2 \tag{2.15}$$

To find the force exerted on the rotor by the wind can be found as

$$F = m'(v_0 - v_2) = \rho A_1 v_1 (v_0 - v_2) \tag{2.16}$$

This force is also equal to the pressure difference across the rotor. That is

$$F = A_1(p_1^0 - p_1^2) \tag{2.17}$$

where $p_1^0\ and\ p_1^2$ are the pressure values at rotor intake and outlet, respectively.

Equating Eq.2.16 and Eq. 2.17:

$$F = A_1(p_1^0 - p_1^2) = \rho A_1 v_1(v_0 - v_2) \tag{2.18}$$

Next, Bernoulli's law will be applied for both the air flow from A_0 to A_1 and from A_1 to A_2

For air flow from A_0 to A_1 :

$$\rho\frac{v_0^2}{2} + p_0 = \rho\frac{v_1^2}{2} + p_1^0 \tag{2.19}$$

For air flow from A_1 to A_2 :

$$\rho\frac{v_1^2}{2} + p_1^2 = \rho\frac{v_2^2}{2} + p_0 \tag{2.20}$$

In these equations, p_1^0 denotes the static pressure in the location immediately in front of the rotor while p_1^2 stands for the static pressure in the location immediately behind the rotor.

Subtracting Eq.2.19 from Eq.2.20 one obtains

$$p_1^0 - p_1^2 = \rho\frac{v_0^2 - v_2^2}{2} \tag{2.21}$$

It should be noted that, if the left hands side of Eq.2.21 is multiplied with A_1, Eq.2.18 is obtained. Therefore;

$$\frac{F}{A_1} = p_1^0 - p_1^2 = \rho v_1(v_0 - v_2) = \rho\frac{v_0^2 - v_2^2}{2} \tag{2.22}$$

Solving for v_1 one obtains:

$$v_1 = \frac{v_0 + v_2}{2} \tag{2.23}$$

which implies that the wind speed at the rotor is essentially the arithmetic mean of the wind speeds before and after the rotor.

The power delivered by the wind to the rotor is simply

$$P = F \cdot v_1 = A_1 v_1(p_1^0 - p_1^2) \tag{2.24}$$

Force F was given by Eq.1.17. Combining Eq.2.18 with Eq.2.24 power P is obtained as

$$P = A_1 v_1(p_1^0 - p_1^2) = \rho A_1 v_1 \frac{v_0^2 - v_2^2}{2} = \frac{\rho A_1 v_1}{2}(v_0 - v_2)(v_0 + v_2) \tag{2.25}$$

combining with Eq.2.23

$$P = \rho A_1 v_1^2(v_0 - v_2) = 2\rho A_1 v_1^2(v_0 - v_1) \tag{2.26}$$

To calculate the maximum power extracted possible, it is necessary to equate the derivative of Power with respect to wind speed at rotor (v_1) to zero.

$$\frac{dP}{dv_1} = 0 = 2\rho A_1(2v_1 v_0 - 3v_1^2) \tag{2.27}$$

implying

$$(2v_1 v_0 - 3v_1^2) = 0 \tag{2.28}$$

$$v_1 = \frac{2}{3} v_0 \tag{2.29}$$

Using Eq.2.23

$$v_2 = \frac{1}{3} v_0 \tag{2.30}$$

substituting these values into Eq. 2.24, maximum power is obtained as

$$P_{max} = \rho A_1 v_0^3 \left(\frac{8}{27}\right) \tag{2.31}$$

The total power P_t in the wind is equal to the kinetic energy of moving air mass. That is:

$$P_t = \frac{1}{2} m' v_0^2 = \frac{1}{2} \rho A_1 v_0 v_0^2 = \frac{1}{2} \rho A_1 v_0^3 \tag{2.32}$$

Therefore, the ratio of maximum power that can be extracted from a moving air mass to the total power available in the mass is:

$$\frac{P_{max}}{P_t} = \frac{\rho A_1 v_0^3 \left(\frac{8}{27}\right)}{\frac{1}{2} \rho A_1 v_0^3} = \frac{16}{27} = 0.593 = C_B \tag{2.33}$$

C_B is essentially the value known as Betz Limit stating that an ideal wind turbine can extract at most %59.3 of power yielded by the wind. In wind energy field, C_B is also referred as the power coefficient.

This limit is important since it defines the upper limit of the efficiency of any disk shaped rotor that is capturing the energy of a fluid in motion. For wind turbines, most of the %59.3 fraction of total energy is transferred to rotor and hence used in

electricity generation. Some of this energy, however, is lost due to drag forces at the blades, gearbox, bearings and electrical and magnetic losses at the generator and the power converter equipments. With the state of art technology, a typical 3-blade wind turbine usually has total efficiency of c.a. %50. For a rotor to approach Betz limit considerably, it is stated that a turbine with large number of blades and a high tip speed ratio is required [13].

2.2 Advantages of Wind Power Generation

Using wind to generate electricity has numerous advantages over both conventional generation methods and also other renewable energy methods. The main advantage of wind power generation over conventional generation methods is its low cost and zero emissions. Although the cost of wind power generation is higher than conventional generation methods at the establishment period, since the operation and generation costs of wind power plants are lower than that of conventional power plants, in the medium and long term, wind power plants proved to be cheaper. Generation costs for different power plants and generation costs of wind farms with respect to the turbine classes are given in Fig.2.3 and Fig.2.4, respectively [14]. All of the data is given for year 2010.

Technology	Installed Cost, €/kW	Fuel Price, €/MWh	O&M Cost, €/kW
Gas-fired	635–875	US: 16 EU: 27	19–30
Coal-fired	1300–2325	US: 12 EU: 18	30–60
Nuclear	1950–3400	3.6–5.5	80–96
Onshore wind	1300–1500	N/A	33–50
Offshore wind	3000	N/A	70

Fig.2.3 Costs of Different Power Plant Technologies
(Source: U.S. Department of Energy, 2010)

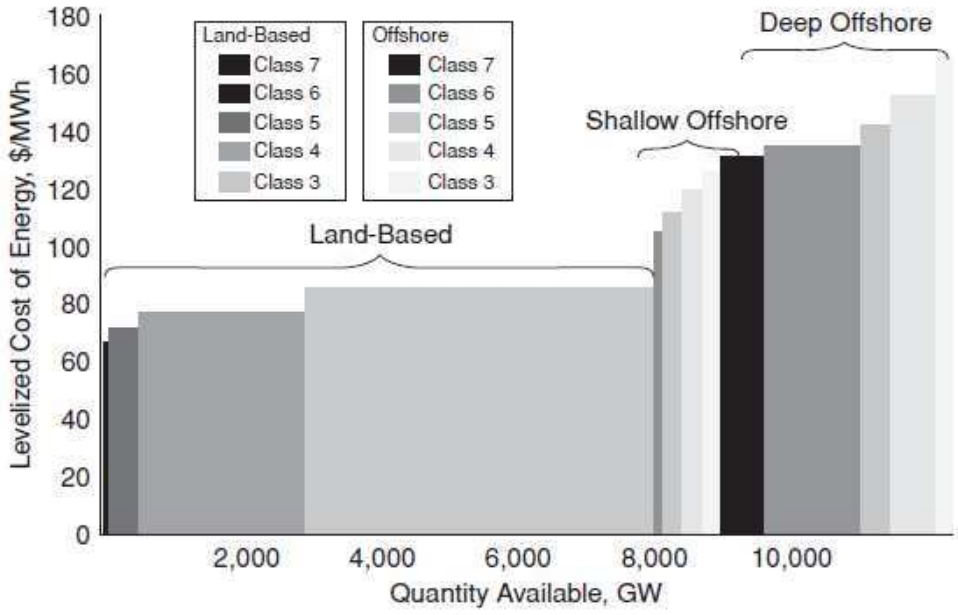

Fig.2.4. Costs of Different Wind Turbine Classes

(Source: U.S. Department of Energy, 2010)

When the charts above are examined, it is seen that at wind speeds close to 7m/s, cost of generation for relatively cheaper (€1300/kW onshore installed cost) wind power plants have a generation cost c.a. 80€/MWh. The generation costs estimated for conventional power plants are 120, 80 and 85€/MWh for coal, nuclear and gas power plants, respectively. Even at this wind speed, which can be considered as relatively low, a wind power plant has a total cost of generation that is comparable with a nuclear power plant that has a much higher installed cost. The costs of generation for conventional power plants that have lower installed cost than a nuclear power plant are already higher than that of a wind power plant. When the considered wind speed is increased to 8m/s, the cost of generation for a wind farm decreases to 60€/MWh which is equal to the half of the generation cost of a conventional power plant. At this wind speed, the generation cost of the wind power plant is 20€/MWh less than that of a nuclear power plant and 25€/MWh less than the generation cost of a gas power plant. For a advantageous case with a wind speed of about 9,5 m/s, the cost of generation for the wind farm decreases further to 50€/MWh. At this level,

generation cost of a wind farm is less than half of the generation cost of a coal power plant, and slightly higher than half of the generation costs of nuclear or gas power plants. Despite there is a nonzero operational cost for wind farms, from these figures, it is evident that they have a great economical advantage over conventional power plants, which can be further enhanced by installing wind power plants in the regions with high average wind speeds.

The environmental advantage of wind power plants over conventional power plants originates from the fact that wind power plants produce zero emissions. Here, the emissions include but not limited to CO_2, SO_2 , SO_3, NO, NO_2, Fly Ash, Volatile Organic Compounds (VOC) and heavy metals like Mercury or Arsenic. Since a wind turbine does not burn or react with a fuel in any way, it does not produce any waste. On the other hand, conventional generators, including nuclear power plants, do produce wastes and some of them are emitted to the atmosphere while the rest can be collected and recycled or used in the landfill.

A conventional coal power plant burns the coal in order to boil the water which will produce steam that can rotate the turbines. This rotation is transferred to the generator and therefore electricity is generated by electromechanical energy conversion. Combustion of coal is carried out at large furnaces. Before combustion, coal is mechanically processed by grinding into particles of a few centimeters in diameter. Power plants using fine-grinded coal particles with diameters less than a fraction of a centimeter also exist. The idea lying behind grinding of coal is to maximize the surface area and therefore increase combustion speed. The main emission for coal powered plants is Fly Ash, Carbon Dioxide, Sulfur Dioxide and Nitrogen Oxides. Fly Ash, as its name suggests, originates from unburned fine particles that are aviated from the coal and make their way to the atmosphere. The main pollution problem associated with fly ash is visibility degradation. Ash particles in the atmosphere scatter the incoming solar radiation and cause a considerable decrease in the visibility in the vicinity of the pollution source. Carbon Dioxide on the other hand, is a transparent gas that is already present in the atmosphere with a concentration of approximately %0.04. Carbon Dioxide would be at environmental

steady state if there were no human interference. However, since tremendous amounts of Carbon Dioxide is being released to atmosphere by human activity, its concentration is reported to be on rise since the industrial revolution [15]. The main environmental problem associated with this increase in Carbon Dioxide concentrations worldwide is global warming. Carbon Dioxide is considered as the main greenhouse gas [16]. Like all the other greenhouse gases, Carbon Dioxide keeps a fraction of the incoming, as well as reflected solar radiation and prevents it from escaping to space. This is done by absorption of the solar radiation by Carbon Dioxide molecules and results in heating up of these molecules. Since the atmosphere is a dynamical medium with continuous heat exchange, the atmosphere itself also heats up which eventually results in an increase in global average temperature figures. Sulfur Dioxide originates from combustion of Sulfur within the coal which is undesired. How much Sulfur Dioxide will be emitted from a given mass of coal depends on the quality (class) of the coal. The higher the Sulfur content, the lower the quality of a coal which also corresponds to a higher Sulfur Dioxide emission for a constant mass of coal. The main classes of coal are, from highest to lowest quality, Anthracite, Bituminous Coal, Sub-bituminous Coal, Lignite and Peat. Among these, for residential heating Anthracite and Bituminous coal are used while Lignite is the most commonly used coal class for thermal power plants. Nitrogen Oxide also originates from agricultural activities and fuel combustion, including coal and gasoline. According to the report of Inventory of U.S. Greenhouse Gas Emissions and Sinks: 1990-2012 [17], the main source of Nitrogen Oxides is agricultural activity. However, transportation and power generation related Nitrogen Oxide emissions are still considerably high.

It is stated that [18], in the United States of America, 558 kg of CO_2 emission is prevented by generating each MW of electricity by wind power plants instead of thermal power plants. According to the "%20 Wind Energy By 2030 Technical Report" [19], it is possible to reduce energy-generation related CO_2 emissions by %25 if the aim of %20 wind penetration of United States of America is realized. Moreover, by 2007, the CO_2 emissions are reported to be reduced by more than 28 million tons due to wind power generation [11].

Electricity generation by wind power plants, on the other hand, does not produce any emissions. It may be claimed that, during the installation process, the equipment for wind power plants does produce some emissions while being manufactured at relevant factories. Despite this claim is not wrong, it should be noted that it is also valid for any equipment that has usage in conventional power plants. Therefore, this does not cause any environmental disadvantage for wind power plants when compared with other power plant technologies. Despite wind power generation is no longer considered as a "fresh" concept as it was in the late 1980's, it is still a relatively new technology when compared to conventional generation methods and therefore it is still open to technological developments. Moreover, since it is the branch of renewable energy that has the widest usage and largest installed capacity worldwide, A considerable amount of the investment in the renewable energy field accounts for wind energy generation. According to the report of Frankfurt School FS-Unep Collaborating Centre[20], the investments to wind power in the year 2013 was $80 billion . The result of this investments, along with other renewable energy generation investments were renewable generation excluding large hydroelectric power plants made up 43.6% of the total new generating capacity installed worldwide in 2013, raising their share of world electricity generation from %7.8 in the preceding year, to %8.5 [21].

It is stated that, thanks to the recent developments in the wind power plant technology, the costs of onshore wind farms has dropped considerably [22]. Moreover, since fossil fuels that are used in conventional power plants are being consumed at a rate much faster than they are being produced by natural fossilization of organisms, they are becoming scarcer and scarcer as time propagates. This results in an inevitable rise in the prices of fossil fuels and hence, the cost of conventional electricity generation methods. Despite there are occasional falls in the fuel prices over time, it is clear that the prices have been, are and will show a net rise as long as their consumption by human activity keeps on. This general increase in coal, oil and gas prices can be seen in Fig.2.5.

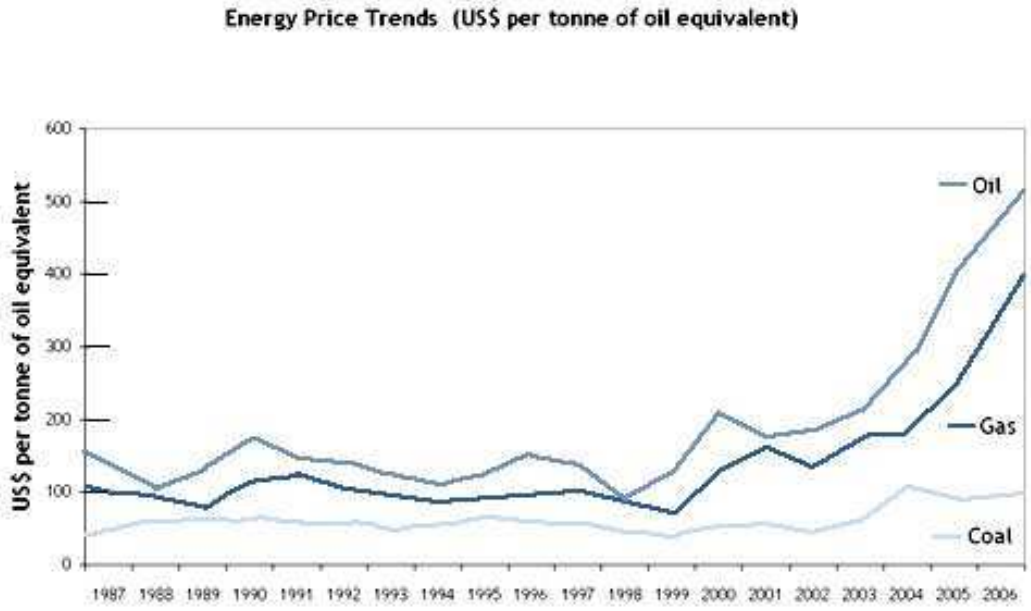

Fig.2.5. Prices of Oil, Gas and Coal for years 1987-2006
(Source: Woods et al., 2007)

On the other hand, despite both technologies rely on the principle of energy conversion, wind power generation does not consume any "fuel" for energy generation. The main difference between these technologies is the fact that, wind power plants transform the kinetic energy of a mass to electrical energy while thermal power plants transform the potential energy in a mass to electrical energy. Moreover, wind energy is free since it is generated by other mechanisms in the nature and does not require any human effort, and hence expense, to be put into a proper form that wind turbines can generate electricity from it. A wind turbine is able to generate electricity from a moving air mass regardless of the mechanism that wind is created as long as the wind is blowing at an appropriate speed. However, since a thermal power plant actually burns the fuel, it does consume the fuel, converting it into another material that cannot be reused for the same purpose. Moreover, the mechanism at which the fuel is generated is important since it defines the type and quality of the fuel. The type of the fuel, as well as the location of the source are the main factors determining the cost of the fuel. Despite the generation mechanism is,

as in the wind case, independent of human activity and therefore does not introduce any costs, the processes involving extraction, processing and transportation of the fuel which all require human effort and expenses, define the price of the fuel. Moreover, collection and disposal of combustion products at a thermal power plant introduces additional costs, which indirectly added to the fuel price since type and quality of the fuel directly affects the amount of products produced for unit energy generation, and also the methods used for removal of these products, which are in general, hazardous.

If the pollution generating alternative generation methods such as biomass electricity generation are taken aside, wind power generation is even with any renewable energy method by means of emissions. However, some renewable energy methods may have adverse effects on the environment. For instance, hydroelectric power plant dams may have a grave effect on the ecosystem by causing large number of flora and fauna to disappear with the flooding of a large portion of the land if the dam is not properly sited.

The main advantage of wind power generation over other renewable electricity generation technologies is its convenience. Wind is an atmospheric event that is present almost everywhere at anytime. Despite solar power generation may seem to be a serious alternative by means of availability, the simple fact that sun is present, on the best occasion, only half of the time possesses a serious disadvantage towards solar power generation. Moreover, solar power generation technologies have higher installation costs and relatively shorter plant lifetimes which allows them to be profitable only for very limited areas that yield very high solar energy which is possible by very high sunshine durations. These areas are on the other hand, usually on deserts which are in general, isolated areas with little or no settlement. Such isolated areas are very far away from the grid connection and in order to transfer the energy generated, additional transmission investments must be carried out first. Despite wind power plants might have to be installed in isolated areas as well, it may not be the case for many countries that have access to the coastal. Moreover, since the installation costs are relatively lower, wind power plants proved to be profitable

even at moderate wind speeds, making them to be suitable for a wide percentage of available land worldwide. If wind power generation and geothermal power generation are to be compared, the general picture is that geothermal power is only available in few gifted countries and even those countries are devoid of potentials that are comparable with wind power potentials in these countries [23]. As an expected consequence, installed capacities of wind power plants are much larger than that of geothermal power plants even in these countries. It is estimated that the worldwide wind power potential is 20 times more than what the entire human population needs [24] .United States comes first in the world by means of installed capacity of geothermal power plants with a total capacity of 3086 MW in the year 2010. On the other hand, in the same year, the total installed capacity of Wind Power Plants in United States is 40.180 MW, which is more than ten times of installed geothermal energy capacity. For Turkey, the installed geothermal power plant capacity is about 100MW, which turned out to be small when compared to the 500MW in 2010 aim which was set in 2005 [25]. On the other hand, the wind power plant capacity in Turkey by 2010 is reported to be 1274 MW and is continuing to grow by new installations from the energy companies, as well as smaller scaled off-grid applications, especially in remote areas.

Another advantage associated with wind power plants is about land usage. As mentioned earlier, hydroelectric power plants cause a large area within their vicinity to become unusable both for humans as well as animals. For solar power plants, the case is not very different either. Despite solar power plants do not cause any harm in their vicinities, they require large areas of land and use a large percentage of the land due to the dense arrangement of individual solar panels. Therefore, it is not possible to carry out any other activity in the areas devoted to solar power production [26]. Wind power plants, on the other hand, do not cause the land they are sited to become unusable. Despite a large wind power plant can take a few km^2 of land, since the wind turbines themselves are scarcely placed, most of the land within the wind farm can still be used for various activities including agriculture. This also makes it possible for land owners to obtain income by leasing their lands for wind farms while continuing their activities in a large portion of their lands.

Therefore, wind power generation is in general, much more convenient and appealing than other renewable energy alternatives since it possesses a wide area of applicability as well as lower installation costs.

2.3 Wind Turbines

A wind turbine is a wind powered electrical machine which uses the wind energy to generate electricity at generator unit.[27] It is considered as the main element of a wind power plant [28]. When in operation, a wind turbine absorbs the kinetic energy of the wind which exerts a rotational force on the blades of the turbine. This rotational energy is transferred to the rotor of the generator and converted to electrical energy there. The generated electrical energy can either transferred to the grid via an interconnection or can be used on site.

Despite this thesis and almost every electrical engineering research in this field focuses on the electricity generation at a wind turbine, it should be noted that wind turbines that can convert wind energy to other forms of energy also exist. However, for this thesis, wind power generation will always correspond to generation of electrical energy from wind energy.

When wind encounters with the turbine's blades, it causes a rotational motion at the blades which in turn rotates the shaft of the wind turbine. On the other end of the shaft, there is the generator of the turbine which produces electricity from the rotation of the rotor. As wind passes through the blades, it creates a lifting force (this is the case for horizontal axis wind turbines. For vertical axis wind turbines, the wind creates a drag i.e. frictional force). Except the hub and blades, all components of the wind turbine is contained in a section named nacelle. The shaft is the first element coming behind the turbine blades and is also positioned inside nacelle. The rotational motion is transferred from the blades to the shaft by direct mechanical coupling. Apart from the shaft, nacelle contains the gearbox, brake, generator and controller equipment. It should be noted that not all wind turbine models contain all of these mentioned above, as well as the orientation of the equipment inside nacelle may vary

from one wind turbine model to another. The gearbox is used to increase the rotational speed from the blades to the generator shaft. This is done in order to provide a generation at system frequency, which is 50 Hz. The generator, like any other power plant, is the unit where electricity is generated by electromechanical energy conversion. The generated electrical power is delivered to an interconnection substation. At the substation, the step-up transformer raises the voltage level to medium or high voltage levels so that the power generated will be
delivered and distributed with minimized losses.

2.4 Types of Wind Turbines

There exist two main types of wind turbines. These are horizontal axis wind turbine (HAWT) and vertical axis wind turbine (VAWT) types. Due to their higher efficiencies and lower mechanical stress levels, horizontal axis wind turbines have overtaken vertical axis wind turbines shortly after their invention. On the other hand, since their operation does not depend on the wind direction, vertical axis wind turbines can be advantageous in certain environments where wind direction changes very rapidly. There exist various sub-models of vertical axis wind turbines which will be presented in the following section. Horizontal axis wind turbines are the most common type of wind turbines in wind energy generation field.

2.4.1 Horizontal Axis Wind Turbines

As their name suggests, horizontal axis wind turbines employ a configuration so that the rotor hub and the shaft is parallel to the horizontal plane. They usually have three blades, connected to the hub with 120^{o} between each. The nacelle containing the main rotor shaft and generator is located at the top of the turbine tower and in most cases, able to rotate in order to provide perpendicular facing of turbine blades with the varying wind direction. The rotation is automated by either pitch control for smaller and older turbines, or with the aid of a servo motor which are generally found in newer and larger designs. This rotation property of nacelle is also used in emergency cases such as extreme wind speeds. In this case, the nacelle is rotated so

that the blades will face sideways to the wind direction, minimizing the force exerted on the blades. Most of the horizontal axis wind turbines contain a gearbox within the nacelle in order to increase the rotational speed of the rotor. In order to prevent any possible damage during extreme wind cases, the blades are located at a distance from the tower.

With today's technology, horizontal axis wind turbines have high efficiencies, approaching the Betz limit on certain occasions. Moreover, within the past decade, their reliability problems are come to the point of almost vanishing, increasing their overall advantage over conventional generators[29]. A standard commercial wind turbine can reach up to 320 km/h of tip speeds. This speed corresponds to a blade rotational speed ranging from 10 to 22 rpm (revolutions per minute) depending on the size of the blades.

The ratio of tip speed to the wind speed at a given moment is called tip speed ratio. Efficiency of a wind turbine is also related with the tip speed ratio. Generally, efficiency increases with increasing tip speed ratio up to some optimum point. However, high tip speed ratio values will also result in high noise levels and also high stress on turbine blades due to centrifugal forces. This makes it necessary to build blades strong enough to endure the centrifugal stress which implies a higher cost of construction.

Since wind speed increases with the height from ground, horizontal axis wind turbines are built with high turbine towers to benefit from this. The towers must be strong enough to carry the nacelle and endure highest wind speeds in the location they are installed. For this purpose, the towers are usually built from steel and its alloys.

Despite most of the commercially used generators have gearboxes to adjust the speed of the generator, there are also wind turbines without gearboxes. These wind turbines employ direct drive generators which are also referred as annular generators.

However, these generators generally have lower efficiency when compared to variable speed turbines.

2.4.2 Vertical Axis Wind Turbines

Vertical axis wind turbines employ a configuration so that the shaft containing the blades (which are sometimes referred as "wings" for this type) is perpendicular to the horizontal plane (ground). Despite there a number of designs with various number of blades, most commonly used ones have two blades, placed 180 degrees apart. Since the blades are mounted on two ends of the long shaft, there is no necessity of building a tower-like structure to carry the other turbine components. Instead, the components such as generator or gearbox are placed near the ground. This provides vertical axis turbines an advantage because the cost and complexity of construction is less than that of horizontal axis wind turbines. Moreover, since the equipment are close to the ground, the maintenance or replacement of the equipment is easier.

On the other hand, due to the physical alignment of the turbine blades, an inevitable pulsating torque problem is introduced in operation. This pulsating torque increases the stress on the structure and also decreases the operational efficiency which causes the power yield of vertical axis wind turbines to be smaller. Another reason that power yield is smaller for vertical axis wind turbines is the fact that their blades are also close to ground level. This means that the wind speeds at the vertical position that the vertical axis wind turbine is operating are smaller than that of a horizontal wind axis wind turbine would operate. These are the main reasons of vertical axis wind turbines have become overtaken by horizontal axis wind turbines.

Unlike horizontal axis turbines, there exists different blade shapes and configurations for vertical axis wind turbines, which allow them to be named depending on the blade style. These types are: Darrieus, Giromill and Savanius. Darrieus wind turbines are named after their inventor, Georges Darrieus. They provide relatively higher efficiency among vertical axis turbine types but their reliability is somehow poor. Moreover, due to the bulky design, the turbine is unable to start itself and therefore

require external initiation from a power source. They are distinguishable from other sub-models by their large, curved blades with external supports connected to the top beam. Giromills employ a similar structure to the Darrieus turbine, except that they have straight blades instead of curved ones. This results in a decreased pulsating torque which also decreases the stress on the structure thus increasing reliability and lifetime of the turbine. Moreover, thanks to variable pitch operation, Giromills are able to self-start. Savanius turbines employ smaller blades which are sometimes referred as "scoops" due to their similarity in shape. Unlike Darrieus and Giromills, since the blades are smaller, their number is usually more than 2. For Savanius turbines to have self-starting capacity, they must have at least 3 blades. [30]. With the usage of long and helical blades, operation with minimal torque pulsations is enabled. Examples of Darrieus and Giromill wind turbines can be seen on Fig.2.6 and Fig.2.7, respectively.

Fig.2.6. Darrieus Turbine
(source: Wacker, 2005)

Fig.2.7. Giromill Turbine
(source: Wacker, 2005)

Table 2.1 provides a comparative summary of horizontal and vertical axis wind turbines.

Table 2.1. Comparative Summary of HAWT and VAWT.

HAWT	VAWT
Variable blade pitch allowing optimal turbine blade angle for changing wind direction.	Can work at optimal efficiency regardless of wind direction.
Tall tower ensures higher wind speeds	No tall tower, has to work at lower wind speeds.
Maintenance is difficult since most of the equipment is on the top of the tower	Maintenance of equipment is easier since they are placed close to ground level
Provide higher efficiency in general	Provide lower efficiency due to operating principles.
Operational vibration and pulsating torques are smaller	Vibration and pulsating torques can be considerably high
Constructional cost is higher, more complicated design	Simpler design, constructional cost is lower

2.5 Wind Turbine Components

Despite there is impossible to define a single model for all wind turbine versions available, some of the most common components will be discussed here. Since vertical axis wind turbines have little commercial usage, a horizontal axis wind turbine model will be presented. A typical wind turbine model is presented in Fig.2.8 It can be assumed to consist of three main parts: The rotor, nacelle and the tower.

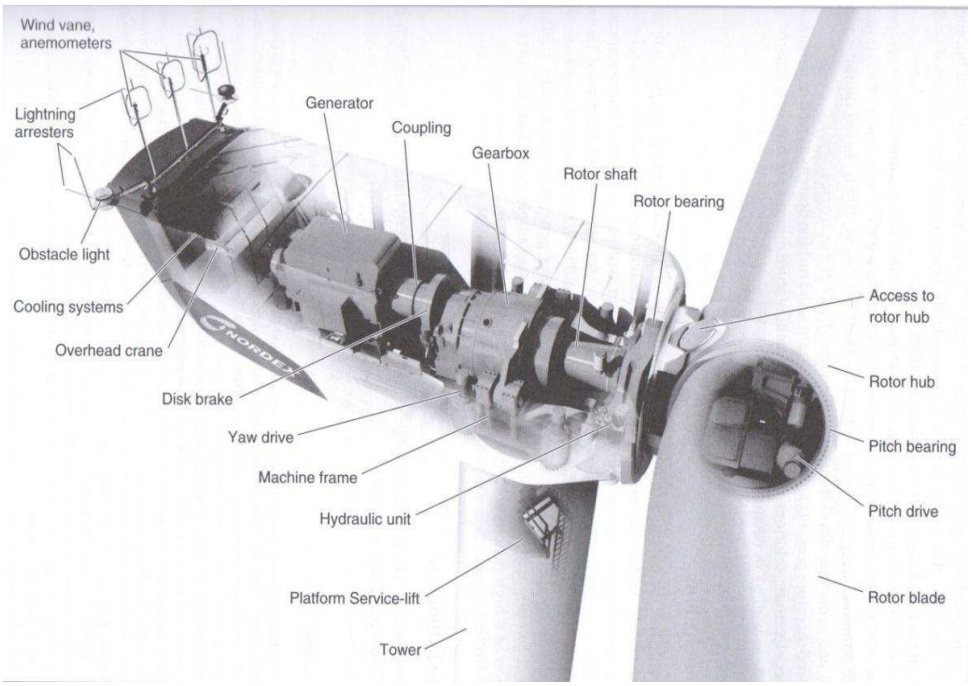

Fig.2.8. Schematic of a Wind Turbine

(source: Jain, 2010)

2.5.1 Rotor

The rotor, which should not be confused with the rotor of the generator, includes the rotor hub and the blades radially connected to it. The hub contains 2 or 3 blades in most turbines. The turbines with 2 blades have a lower efficiency but lower cost and weight too. The advantage of 3-blade turbines is their optimized efficiency. The rotor is made of high quality cast iron. The blades capture the wind power with the lifting force exerted on them by the wind. The rotor, turns the primary (main or low speed shaft) shaft at rotational speeds between 30 and 60 rpm for most turbines. This rotational velocity is mainly dependent on the wind speed. However, it can be varied by a mechanism called pitch control which adjust the blades' facing with respect to the plane of rotation. Pitch control allows the turbine to capture wind energy with optimum efficiency in a wide speed range. Some turbine models, especially smaller ones, do not have a separate pitch mechanism. They rely on the stall in order to regulate the rotational speed passively. Medium-sized and large turbines have an

active pitch control mechanism. The system used in these turbines can be one of three common mechanisms, namely; hydraulic pitch control, rack and pinion system and motorized pitch control. The hydraulic pitch control employs an oil pump in order to change the blades' alignment. Rack and pinion system, on the other hand, has a motor that drives the rack which changes the alignment of blades via the pinions. The motorized system employs individual motors for each blade, making it possible to change the blade alignment rapidly. However, since it needs multiple motors, it is the most expensive pitch control system.

2.5.2 Nacelle

Nacelle contains almost all the equipment of the wind turbine, except for the blades and the rotor hub. It encloses the generator, gearbox, most of the low-speed shaft, high speed (generator) shaft, controller equipment and the brake. Apart from these equipment, there may also be certain auxiliary equipment mounted on the top of the nacelle such as lightning arrester, anemometers, wind vanes or obstacle lights. Lightning arrester protects the turbine from lightning surges. Anemometers are used to measure the wind speed and wind vane measures the direction of the wind and commands the yaw drive to adjust the alignment of the blades according to this direction. Obstacle lights are used to warn the aircraft about the presence of the wind turbine. The material used in nacelle is usually plastic, fiberglass or their variants.

2.5.3 Generator

Generator is the crucial component for a wind turbine, as well as other turbines, since it is the part where electromechanical energy conversion takes place. In the early years of wind power generation, conventional induction or synchronous generators were used in the wind turbines, like any other power plant. However, with today's state of art technology, two different generator types are commonly used in wind turbines. These are, Fully Rated Converted Based Generator and Doubly Fed Induction Generator. Despite their technology is considerably different than classical induction or synchronous generators, their mechanical construction is quite similar to

the classical design. The main difference between them is the additional components such as converters providing operational difference. These generator types are used almost exclusively in modern wind turbines.

The fully rated converter based generator employs a fully rated voltage source converter [31]. This allows it to deliver full rated power at variable speeds. Despite there are also some induction motor applications, mostly synchronous generators are used as fully rated converter based generators. One of their major differences from conventional generators is that they allow permanent magnet excitation with high efficiency, instead of electromagnetic excitation found in conventional generators. Fig.2.9 presents a simple box-diagram representation of a fully rated converter based generator.

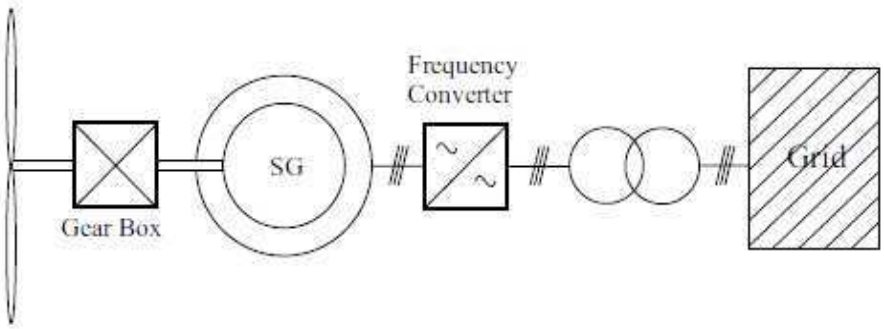

Fig.2.9. Box-diagram of a Fully Rated Converter Based Generator
(Source: Khalil, 2010)

The doubly fed induction generator is similar to conventional induction generators. But unlike the induction generator, it can provide power at variable speeds. Its difference is in its operational configuration, which actually leads to a double feeding via the crowbar-converter system. This system allows the voltage across the terminals of generator to be controlled. Here, the controllable voltage is the key element leading to variable speed operation. A box-diagram representation of doubly fed induction generator with proper configuration is given in Fig 2.10.

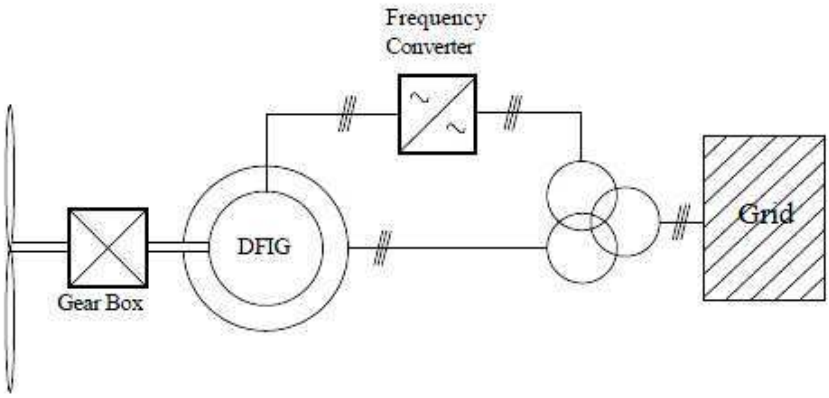

Fig.2.10. Box-diagram of a Doubly Fed Induction Generator
(Source: Khalil, 2010)

2.5.4 Gearbox

The gearbox is used to increase the rotational speed from the blades to the generator rotor while delivering the torque with minimal loss. It provides mechanical coupling between the main (primary, low speed) and secondary (high speed) shafts. The rotational speed at the low speed shaft is typically between 30 and 60 rpm. This speed is increased by the gearbox to 1000-1800 rpm. This speed is necessary for generators (except direct-drive generators) to produce electricity at the grid frequency. A typical generator that generates electricity at the grid frequency requires a gearbox in order to reach the required operational speed, which is typically at or above 1000 rpm.

There exist turbines without a main shaft. For these turbines, the rotor hub is directly connected to the gearbox. Most commonly, a double roller tapered bearing is mutually connected with rotor hub and nacelle frame and does serve the duty as the main shaft would, which is carrying the rotational motion from hub to gearbox. The bearing is also connected to the nacelle frame and the inner ring of the bearing is connected to the rotor shaft. The rotor shaft is generally shorter when compared to that of a turbine with a main shaft. This configuration allows the nacelle to be more

compact and reduces the weight of it. The drawback of this configuration, on the other hand, is the increased difficulty of performing maintenance operations on the gearbox [32].

There are also turbines without gearboxes [33]. For these turbines, the rotor hub is directly connected to the generator. Since there is not a gearbox to be able to determine the generator speed, the generator in these turbines must be of direct-drive type. Direct drive generators provide electrical power of variable frequency. Therefore, it is necessary to have a rectifier in order to convert the output of generator to rectified DC. Then, an inverter is employed to convert this DC power to AC at grid frequency. Since there is no gearbox to increase the rotational speed, the direct drive generator has a large number of poles. This allows the electrical speed to be very high while keeping the mechanical speed in a relatively low and safe range. For example, the direct drive generator of Enercon's E66 1.5 MW has 72 poles. The drawback introduced by having such large number of poles is the increase in the generator size, which is required to accommodate the high number of pole design structure. These turbine types also do not have a main shaft and the rotor hub is directly linked to the rotor of the generator. Similar to the configuration described above, the rotational load is transferred by the double roller taper bearing. The inner ring of the bearing is connected to the nacelle frame while the outer ring is connected to the rotor [34].

For non direct-drive turbines, the gearbox is an essential component. The main duty of the gearbox is to increase the rotational speed so that the generator can produce electricity at the grid frequency, which is 50 or 60 Hz. For instance, a turbine having a four pole generator can be assumed to have a rotor hub speed of 20 rpm. In order to generate power at system frequency (50 Hz), the generator must have an electrical speed of 50 rotations per second. The relation between electrical speed and mechanical speed is given by Eq. 2.34

$$v_e = \frac{p}{2} \times v_m \tag{2.34}$$

where v_e is the electrical speed (speed of the rotating field), v_m is the mechanical (rotor) speed and p is the number of poles, which is equal to 4 for this case.

Therefore, using Eq. 2.34, one obtains the necessary rotor speed as 25 rotations per second, or 25 x 60 = 1500 rpm. For this turbine, the gearbox ratio required can be found as 20/1500 = 1:75. Most gearboxes have multiple stages in order to reach the final required ratio. A common gearbox model having 1:75 ratio can be assumed to have 3 stages. The stage ratios from the rotor side to generator side are 1:5, 1:5 and 1:3. In general, the final stage has a lower ratio but higher size than the preceding stages.

Since it is mechanically one of the most complicated components of the wind turbine, its condition must be regularly checked to prevent a possible breakdown, which can result in loss of generation. For this purpose, certain gearbox monitoring systems can be employed.

2.5.5 Controller Equipment

The main purpose of the controller equipment to start the wind turbine when the wind speed reaches a threshold value which varies between 12-25 km/h depending on the wind turbine type and to shut down if the wind speed exceeds the safety limit, which is usually set as 80 km/h.

2.5.6 Brake

Brakes are used to bring the turbine blades to stop in emergency situations. For this purpose, in modern wind turbines disc brakes (which are similar to those used in automotive industry) are used. They can be mechanically, electrically or hydraulically boosted in order to ensure a more rapid stopping.

2.5.7 Tower

The tower provides structural support to the nacelle and the blades. It also includes the yaw drive and a servo-motor to move the nacelle, which is called yaw motor. As the construction material, usually steel and its variations are preferred in order to ensure durability. The tower is aimed to be as high as possible in order to be able to provide higher wind speeds to the blades. However, mechanical, environmental and economical factors set a limit to their limit. The yaw drive aligns the nacelle in a way that the rotor always faces to the wind direction. The servo motor is the source of mechanical power required for this operation. It adjust the nacelle according to the wind direction data obtained from the wind vane. If the yaw drive fails to perform its duty appropriately, there will be a nonzero angle between the wind direction and the normal to the plane of rotation, which will result in a reduction in the turbine efficiency, as well as introduction of pulsating torques due to unsymmetrical loading. Towers of modern wind turbines have an elevator inside in order to transport personnel for repair or maintenance operations in the nacelle. They may also have a staircase in order to provide access to the nacelle.

2.6 Wind Farms

With an increasing demand for electricity worldwide, a single wind turbine's power contribution is insignificant within a power system with hundreads, (or thousands) of conventional power plants that are in operation in order to meet the power demand of an entire country or in some cases, even a continent, via interconnected power systems. Therefore, in order to reach generation levels that are comparable to that of conventional generators, it is necessary to bring a number of wind turbines together. The number of wind turbines in a wind farm can vary from a mere dozen to a few hundreads, depending on the size of the wind farm. Therefore, the rated powers of wind farms can be in a wide range from a few tens of megawatts to several hundread or even thousand megawatts. By 2015, the largest wind farm in operation is Gansu Wind Farm with a rated power of 20.000 MW and is located in China. The wind

farms are mostly resided on land but there are also wind farms that are located on the sea, usually a few hundread meters from the shore, namely offshore wind farms.

The locations of wind farms are mainly chosen according to the wind speed and direction at the area. Despite meteorology stations also keep track of the wind speed and direction within their vicinities, they are in many cases unable to provide the required data due to the distance between measurement station and the land that the wind farm is to be installed onto. Therefore, it is often necessary to install the measuring equipment onto the wind farm site and take measurements of wind speed and wind direction at a given height (usually equal the turbine towers' height) for a sufficient time and with sufficiently high Intervals. The monitoring period often takes one or two years. The measurement interval most commonly used is once every ten minutes, resulting in 52.560 measurements within one year.
The measurements are carried out in order to determine the capacity factor of the plant to be installed as accurately as possible. Therefore, the measured wind data should be able to reflect the actual situation in the vicinity of the turbines' blades. For this purpose, towers containing the measuring equipment, which are often referred as Met Towers are placed onto the site of interest. In case that the Met towers' height do not match with the turbines' hub height, certain empirical relations can be used in order to determine the actual wind speed near the blades. One of the most commonly used relations is the Hellman exponent equation given in Eq.2.35.

$$v = v_0 \, x \left(\frac{h}{h_0}\right)^a \tag{2.35}$$

Here, v is the estimated wind speed and v_0 is the measured wind speed. h stands for the height for which the wind speed is to be estimated and h_0 is the height of measured wind speed, taken as the height of Met Tower. *a* is the exponent referred as the Hellman exponent. The Hellman exponent is dependent on many parameters, including temperature, air pressure, humidity or the surface roughness. Surface roughness is the one that affects the value of *a* most. For given area types, corresponding Hellman exponent values are given in Table 2.2 [35]. For practical calculations, *a* can be taken to be equal to 1/7 or 0,142.

Table 2.2. Friction Coefficients for Different Land Surfaces

Landscape type	Friction coefficient *a*
Lakes, ocean and smooth hard ground	0.10
Grasslands (ground level)	0.15
Tall crops, hedges and shrubs	0.20
Heavily forested land	0.25
Small town with some trees and shrubs	0.30
City areas with high rise buildings	0.40

Another formula, that putting emphasis on the effect of surface roughness is provided in Eq.2.36

$$\frac{v}{v_0} = \frac{\ln(H / z_0)}{\ln(H_0 / z_0)} \tag{2.36}$$

Here, v and v_0 are the same velocities described for the preceding Hellman equation. H and H_0 denote the heights of the desired wind velocity and measured wind velocity, respectively. The term z_0 is called the roughness coefficient length. Roughness coefficient length has the unit of meters. As its name suggests, roughness coefficient length is dependent on surface roughness, spacing and height of the obstacles on the surface and also the type of the surface (water, grass or soil).

2.7 Power Systems with Integrated Wind Farms

There are three main components in a power system regardless of its size, location or technological status of it. These components are; generators, transmission lines and loads. The loads are determined by the residential, commercial and industrial activity within the region of interest. The parties responsible for power system operation must establish the generation and transmission systems so that the load demand can be satisfied at all times. For this purpose, the analysis and forecast of loads in a

power system is regularly carried out. According to the results of these analyses and forecasts, a plan regarding the generation and transmission investments is prepared.

Apart from the aforementioned medium and long term forecast and planning operations, daily and hourly load forecasting and generation scheduling operations are essential for the healthy operation of a power system. In theory, to keep the grid frequency constant, the overall generation level in a system must be exactly equal to the sum of the loads connected to the system at every instant. In practice, however, this is impossible to satisfy and the aim is to keep the frequency variations as small as possible, usually within a pre-specified limit. What is more, the voltage levels in the system must also be kept within the normal limits in order to prevent damage to both power system equipment and end-user equipments.

2.8 Wind Power in Turkey

Turkey, thanks to its geographical and meteorological characteristics yields a considerable amount of wind potential. Most of this potential is reported to be located in the western coastline with average wind speeds approaching 10 m/s [36]. Especially in the northern Aegean region, wind energy potential is considerably high, promising a high contribution in the installed wind power plant capacity if the necessary investment is to be carried out [37]. EÜAŞ reported that, wind energy potential of Turkey for average wind speeds over 7m/s is 48 GW, which is roughly equal to the %85 of total installed capacity of Turkey [38]. If regions with average wind speeds over 6m/s are also taken into account, this potential rises to 131 GW. These potentials are important since it can be inferred that, theoretically, very high wind penetration can be achieved provided that the problems to be introduced by integration of wind power plants of large capacities can be managed appropriately. However, in reality, these values are rather optimistic and unlikely to be achieved without a perfect transmission system with infinite short circuit capacities, as well as being able to implement wind power plants all over the country, including settled areas or motorways which is practically impossible [39].

The development of wind power generation in Turkey, on the other hand, was relatively slow when compared to countries with considerable wind power penetration such as Germany or USA. The integration of first wind power plant to the Turkish grid took place in 1998 [40]. The total installed wind power capacity of Turkey with respect to the years is given in Graph 2.1 .It can be seen that in 1998, total installed wind power capacity was reported to be 9 MW, which is actually comparable to that of a single large wind turbine commercially available today [43]. The investments in the field started to gain speed in 2006 which is also the year that first official wind energy report of Turkey, REPA is prepared. The installed capacity has increased to 59 MW within 2006. The investments in wind power plants have continued with increasing pace each year. From 2007 to 2012, total installed capacity has increased from 146,3 MW to 2260,5 MW, corresponding to an increase of more than 15 times in magnitude. According to Turkish Wind Energy Statistics Report, by 2014 July total installed wind power capacity of Turkey has become 3424 MW [36]. It should be noted that Graph 2.1. coverts the time duration until March 2014, therefore the later developments are not reflected to the figures. Aegean region is the top contributor to this capacity by %42,8 while Marmara region follows it with a %38 contribution Mediterranean region is reported to have a %17 contribution to overall capacity while Black Sea region has a contribution of about %2.2 [41]. The other regions in Turkey have negligible contribution and therefore are not provided here. The wind power plant distribution within these regions is uneven, as expected. In the Aegean region, most of the existent wind farms are located within İzmir and Manisa while most of the wind generation in Marmara region is provided by the wind farms located in Balıkesir, Çanakkale and İstanbul. Wind farms around Hatay are the main contributors to the generation in the Mediterranean region. These locations, as can also be seen from the wind potential distribution map (Fig.2.11), are the ones where wind energy potentials are highest. The largest wind farm in Turkey, by 2013 is Balıkesir RES with 112,8 MW of installed capacity [42].

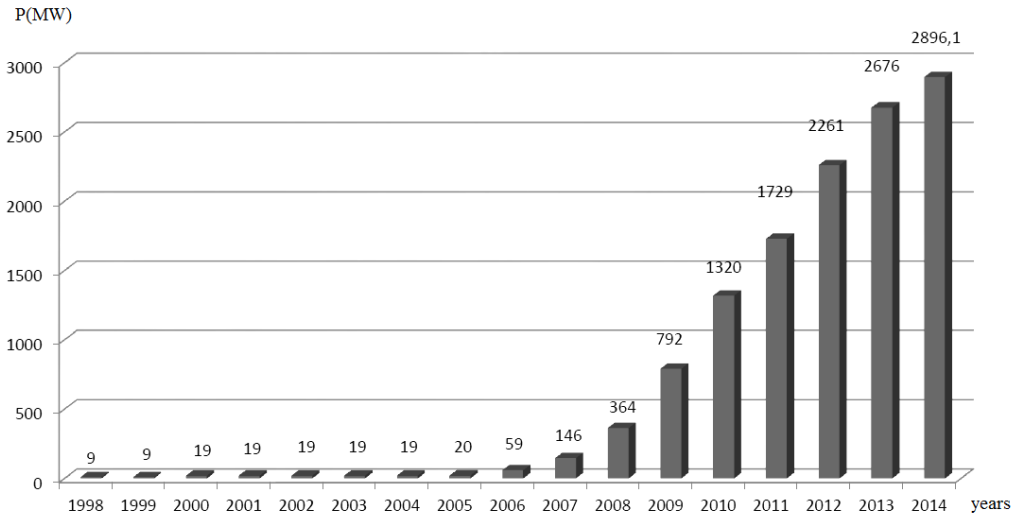

Graph 2.1.Total Installed Capacity Development of Wind Farms in Turkey

(Source: TEİAŞ, 2014)

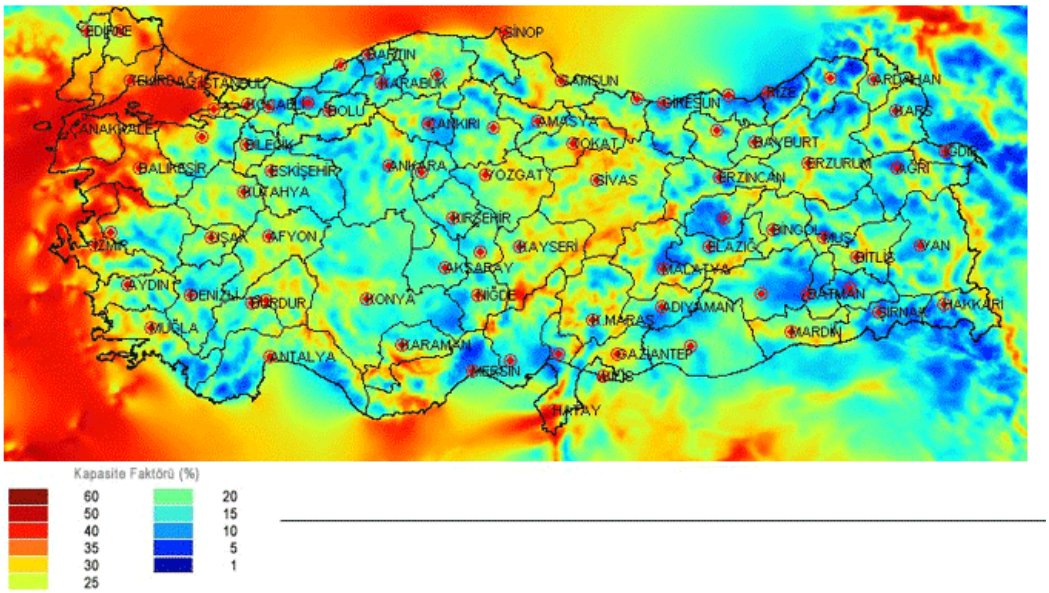

Fig.2.11. Wind Potential Map of Turkey

(Source: TEİAŞ, 2013)

Within the past decade, wind energy sector in Turkey have shown a large expansion, creating new job opportunities by means of project development, counseling and construction. Moreover, Turkish ministry of energy and natural resources have

started to follow a policy that supports the renewable energy investments by reduced taxes or guarantee to buy the generated electricity above regular energy trade prices from the private enterprises. Several national and foreign banks are also offering special credits for wind energy investments to the individuals [40].

By 2013, the total installed capacity of wind power plants in Turkey is %4,2 of the total installed capacity of generation. However, since wind is not continuously available over all the wind power plants during the whole year, this capacity cannot be fully realized in generation. In the same year, the wind penetration is reported to be %2,4 by 7 billion kWh. This value is still, smaller than that of the leading countries in wind energy generation. For instance, the wind penetration average of European Union is reported to be %7,8 for the same year while Denmark had a penetration of %20. EMO, reported that, in a realistic scale, it is possible to achieve %3,3 penetration with the available wind power plants [44].

In 2009, it is stated in the "Electrical Energy Market and Supply Security Strategy Document" [45] that Turkey aims to reach 20.000 MW of installed wind power plant capacity by the year 2023, which corresponds to approximately one third of the total installed capacity in the year 2013.

EPDK (EMRA, Energy Market Regulatory Authority), which is an independent authority whose duty is to inspect and regulate the energy market is also responsible for analyzing the wind power plant projects and approving them if they are decided to be applicable. Therefore, any entrepreneur individual or company needs to apply for a license to EPDK.

It is reported that [46] the total capacity of the wind power plant projects applied for a license has reached 85.000 MW by 2013. Most of this capacity (78.000 MW) is due to the applications made between 2006 and 2011, when EPDK removed the obligation of providing wind measurement data with the proposed projects. Due to the tremendous amount of applications done, this obligation is re-set in 05.04.2011 [47].

Despite it is stated that the licensing process for these applications is in progress, the total capacity is already above the total installed capacity of Turkey and therefore it is expected that a large portion of the applications will be rejected or suspended. On the other hand, the total installed capacity of existing wind power plants is noted to be account for only %36 of the total capacity of the projects that have approved by EPDK. The reasons for this fact can be given as the lengthy bureaucratic processes required even after the license has been approved, lack of coordination between related institutions or the inadequately planned projects as well as economical bottlenecks occurring at a considerable frequency.

The current situation regarding the license applications and their approval statuses can be summarized as "congested". This can be related with the large number of license applications of projects that are evaluated to be inadequately or incorrectly planned by various unofficial authorities. On the other hand, EPDK is criticized to suspend many applications that do not threaten the transmission system security unnecessarily due to its concern about keeping the transmission system secure [48]. Despite these are subjective and unofficial statements, they can imply that it is necessary to investigate the effects of wind power plants in the transmission system extensively in order to be able to benefit from this almost free and environmentally clean technology to maximum extend.

For the aforementioned reasons, this thesis aims to investigate the effects of wind power plants in the transmission system mainly by focusing on the system stability and continuity of healthy operation in case of disturbances in the regions where wind generation has the potential to be increased. With the analyzes to be made, it will be possible to propose a statement upon the size and severity of consequences of disturbances for different wind generation percentage levels in the power system.

CHAPTER 3

TECHNICAL ANALYSIS

3.1 Modeling Approach

Before observing the dynamic effects and problems related with wind farms' operation on the transmission system, it is necessary to have a transmission system in order to be able to connect the wind farms and observe their operation. For this reason, modeling of a transmission system is essential. In order to be able to reflect the effects of wind farms as close to real cases as possible, a realistic model of Turkish Transmission system is built. The model is built using the power system analysis software Digsilent Powerfactory. The detail level of simulation is optimized by including the 380 and 154 kV Transmission system, as well as 154/34,5 kV transformers and 34,5 kV buses. However, the entire distribution system is not modeled which includes distribution lines and cables, 34,5/0,4 kV transformers since it would be impossible to carry out by a single person and within a specified time. Moreover, introducing such a detail level would provide little increase on realism of the model as well as results that reflect the effects of wind farms on the transmission system and therefore, it is out of scope of this thesis.

During the modeling of the transmission system, the following elements are used in order to provide a fully functional system model:

-Buses: Buses are the first layer of the transmission system model since all other components are required to be connected to existing buses. All the bus types present in the Turkish transmission system are modeled. Though a

considerable majority of present buses are 380,154 and 34,5 kV bars; 66, 33.6 and 31.5 kV buses that are still in operation are also modeled.

-Lines: Lines correspond not only to aerial lines but also to high voltage cables that are existent in certain parts of the transmission system, mostly on 66 kV level. Transmission lines are essential to preserve the power system's monolithic characteristic, ensuring that every bus in the system has a direct or indirect connection with all other buses in the system.

-Generators: Generators are the only sources of active power in the power system. Therefore they are crucial for meeting the energy demand of the loads, which are active power consumption centers. Moreover, they are able to provide or absorb reactive power depending on the reactive power flow within the system.

-Loads: Loads stand for consumption centers in the power system. In the actual electricity system, the number of consumption points are too many to be modeled exactly. Therefore, it is assumed that the loads of each region is concentrated within the bus belonging to the nearest city. In addition, consumption centers of high importance and away from city centers are modeled separately.

-Shunt Reactors: Shunt Reactors are connected to various parts of the transmission system in order to protect the system against excessively high voltages at the buses that are relatively weakly connected to the rest of the system. The reactors that are connected to 380 and 154 kV systems are fully modeled.

3.2 Digsilent Powerfactory

Digsilent Powerfactory is a power system analysis software that is capable of building, modeling and analyzing large scale power systems including transmission systems, distribution systems or a combination of both.

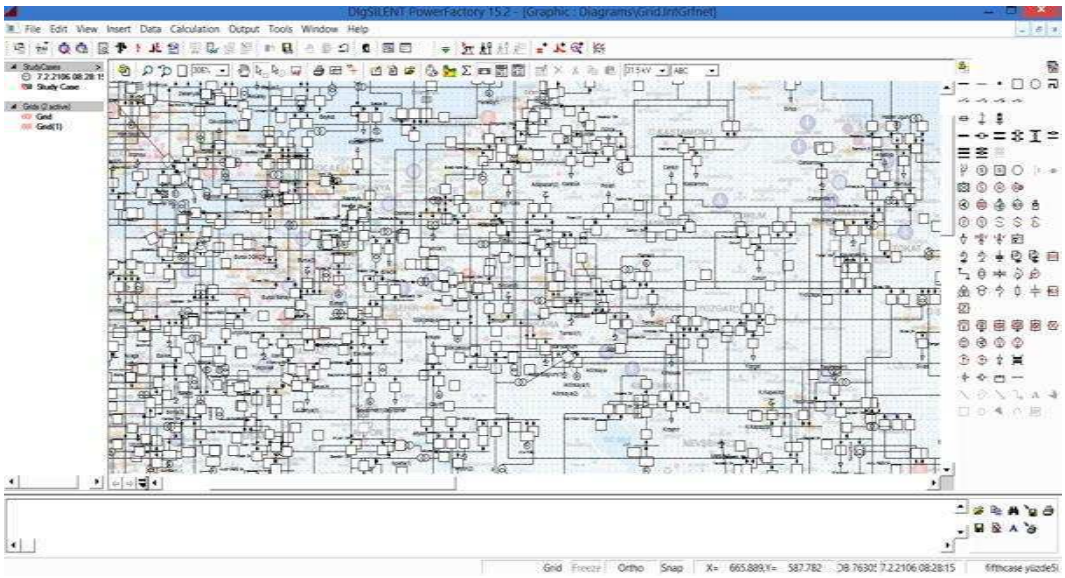

Fig.3.1. A Sample Screenshot of Digsilent Powerfactory

The software enables building a power system from scratch as well as taking an existing project as base. The user is relatively free by means of deciding on the level of detail of the system model thanks to a pre-existing library with IEC models as well as the option of designing his or her own component models. In case that the user does not want to create a component model from scratch, it is possible to take an existing model, either pre-created or created by the user himself or herself, and modify it in order to create a new model of desired component type. This implies that, despite being provided by commonly used wind generator models, one can define and build a highly realistic wind turbine model with the data of actual wind turbine in hand. The opportunities that Digsilent Powerfactory provides by means of renewable energy is not limited to wind generators. Geothermal or bio-fuel power plants can already be modeled by employing and modifying existing conventional generator

models. What is more, thanks to static generator model available, it is also possible to create realistic models of solar power plants as well.

The reason that Digsilent Powerfactory is chosen for the simulations required is the fact that it enables building a power system model and performing various simulations including but not limited to load-flow analysis, short circuit analysis or electromagnetic transient (EMT) analysis in a single software. Therefore, it is possible to build, troubleshoot and analyze a power system without using any third-party programs or extensions to set up a link between the mathematical model and the actual power system. This does not, however, disable the user from working with third party programs (such as Matlab) or extensions in an integrated manner with Powerfactory in order to perform more complicated activities whenever desired. Moreover, the calculations related with each analysis method are carried out in the lower-layer which is not directly accessible by the user and only the analysis related steps and results are displayed. This decreases the complexity of user interface greatly and allows the user to concentrate on what is going on in the power system during and after analysis instead of mathematical variables or results that are not directly interpretable as system components.

Just like any power system analysis program, Digsilent Powerfactory also employs mathematical models for every component in the system. Therefore, introducing a new component in the system actually results in a new mathematical model to be created under the system database with the necessary information and values stored within it. With its unique database concept, Digsilent Powerfactory then, stores the new system state with the new element introduced. This implies that, by every change made in the system, a new system state is created. This also means that, it is possible to undo a change made by simply returning to a previous state. To be able to benefit from this property as much as possible, Digsilent Powerfactory keeps the whole history of a project and allows returning to previous states even after the application is closed and re-opened, copied or even transferred to another computer.
The main analysis functions of Digsilent Powerfactory are load flow calculation, short circuit analysis, electromagnetic transient (EMT) analysis, as well as DC load

flow analysis for different simulation requirements. Moreover, despite the grid schematic shows (Fig.3.1) the single line diagram of the power system under consideration, it is possible to perform the aforementioned analysis' both as three phase balanced or unbalanced systems. When the latter is chosen as analysis method, it is possible to set up a system with unequal phase variables such as voltage magnitudes, currents or even impedances.

3.3 Wind Generation Impacts

Wind turbines are actually generators that convert the kinetic energy of the wind into electrical energy. Interestingly, despite they are named as "Wind Turbines", they do not contain turbines, unlike thermal or hydroelectric generators. The reasoning behind this naming is assumed to be due to the fact that Wind Generators are evolved decades after conventional generators that actually employ turbines within their structure, yet the naming of wind generators have suited that tradition [49]. If the name of the component that captures the kinetic energy is to be used as a name, a proper name suggested for wind turbines would be aerofoil-powered generator.

Despite being dominated by Horizontal axis wind turbines, the wind turbine market still contains both horizontal and vertical axis wind turbines over a wide range of ratings and variety of manufacturers. There are different types of horizontal wind turbines depending on the technology and size of the turbine such as the classical turbines with gearbox or direct-drive turbines which lack the gearbox yet maintain a high electrical speed thanks to the high number of poles of their generators. Except for earlier primitive models, all horizontal axis wind turbines' nacelles can be rotated, either by active or passive pitch control, so that the turbine will face the upcoming wind direction directly. Among horizontal axis wind turbines, the most popular type by means of number of blades is the three-bladed turbine type. Some manufacturers also offer two-bladed wind turbines despite they are outnumbered. Turbines having more than four blades are rare and have no commercial usage by means of electricity generation. Wind turbines are commercially categorized according to the generator

type employed. In the field, they are named with type numbers rather than describing their generators. Five available types of wind turbines are:

-Type I, squirrel cage induction generator
-Type II, squirrel cage wound rotor induction generator with external rotor resistance,
-Type III, double fed induction generator
-Type IV, fully rated converter generator
-Type V, synchronous generator mechanically connected through a torque converter.

Type I: Squirrel Cage Induction Generator

The Type I generator employs a squirrel cage induction machine. A basic schematic of Type I wind turbine generator can be seen in Fig.3.2. The induction machine is connected to the wind plant through a step-up transformer and a soft starter. The generator always operates at negative slip in order to generate power. There are power factor correction capacitors located at the base of the tower. Several steps of these capacitors are generally used for different operating speeds of the turbine. A major drawback of Type I wind turbines are the large currents the machine can draw during start up. In order to lessen these currents the turbine usually employs a soft starter and capacitor banks of a few steps within the turbine. The turbine shaft speed is kept around the rated value during operation. The squirrel cage generator is directly connected to the step-up transformer [50].

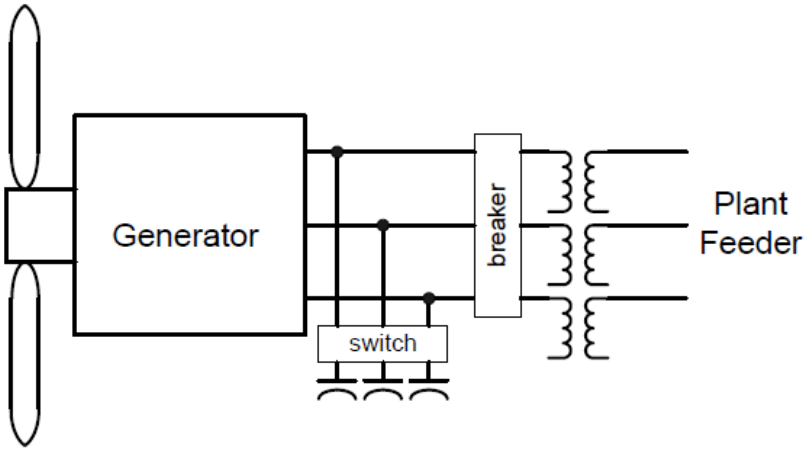

Fig.3.2. Basic Configuration of a Type I Wind Turbine Generator
(Source: Ackermann, 2012)

Type II: Squirrel Cage Induction Generator With External Rotor Resistance

Type II induction generators employ an external resistance inserted to the rotor circuit to allow variable speed, and hence variable slip operation. However, their slip range is still limited when compared to type III and IV generators. A basic schematic of Type II wind turbine generator can be seen in Fig.3.3. For this configuration, the external resistance is added to the actual rotor resistance. In some models, the external resistors are mounted on the rotor, eliminating the need for slip rings. This design is known as "Weiter Design". There are occasionally external controls allowing access and control to this resistance. The variable resistors that are connected into the rotor circuit are capable of controlling the rotor currents very rapidly which makes it possible to maintain a constant power generation even in case of gust winds. This ability improves the turbine's dynamic response characteristics during grid disturbances. The maximum fault contribution of Type II generators occur for an external resistance value of zero. The stator circuit is directly connected to the turbine's step-up transformer in this design.

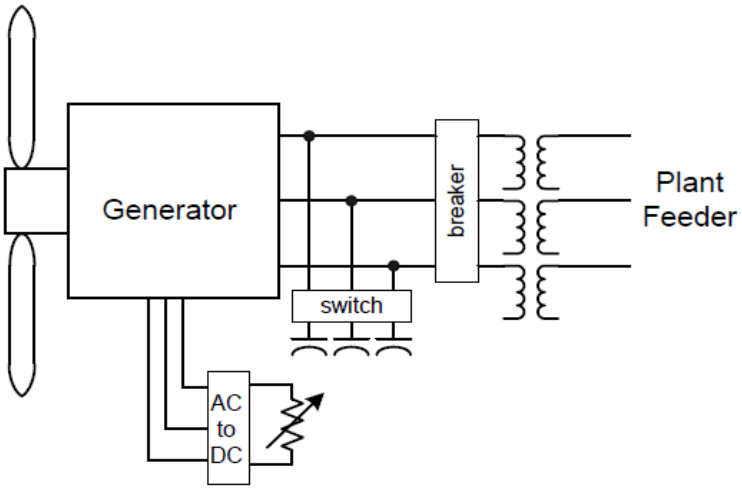

Fig.3.3. Basic Configuration of a Type II Wind Turbine Generator

(Source: Ackermann, 2012)

Type III: Double Fed Induction Generator

Double (or Doubly, as occasionally referred) fed induction generators (DFIG) are used in wind generation in order to provide variable speed operation over a wide range, typically between %70 and %130 of synchronous speed, and highly responsive to reactive power and AC voltage regulation capabilities. A basic schematic of Type III wind turbine generator can be seen in Fig.3.4. These state of art turbines have their line and rotor side converters as solid state. This enables the control to be very fast, typically within two or at most three cycles to achieve full response. These machines are also commonly called doubly-fed asynchronous generators. It should be noted that, despite they have structural similarity to conventional induction generators, their operation in wind turbines are considerably different than that of a conventional induction generator. Type III generators have three phase AC rotor windings with slip rings which allow the rotor to be excited by

an external converter. The additional rotor excitation is provided via the slip rings by a current regulated,

voltage source converter. The converter can adjust the rotor currents' magnitude and phase very rapidly. The stator of the DFIG is directly connected to the electric grid. The rotor windings of the generator are connected to a electronic converter that provides variable magnitude and the frequency of the rotor current. On the other side of this AC-DC-AC converter lies the grid connection. A DFIG is actually similar to a synchronous machine by means of excitation, however it should be noted that, the difference in the excitation of these generators is the fact that the rotor of a doubly fed induction generator is excited by variable frequency AC current. The AC excitation initiates a relative rotation of the rotor's magnetic field, with respect to the rotor itself. This relative rotation adds to, or subtracts from (in the case of a negative sequenced excitation is applied to the rotor) the physical rotation of the rotor. The stator field angular rotation, is the sum of the mechanical angular speed rotation of rotor and the rotor field voltage's frequency. This design makes even a small amount power injected into the rotor circuit to provide a large power control in the stator circuit [51]. This property of doubly fed induction generator is an important advantage since it is possible to control the output power with relatively small converter equipment (typically %20-30 of the rating of the generator).In addition to the real power that is delivered to the grid by the generator, an extra power is delivered to the grid through the inverter when the generator is moving faster than the synchronous speed. When the generator is rotating at a speed that is below the synchronous speed, real power flows from the grid, through converters, and also from rotor to stator. These two modes of operation, thanks to the power converters, allow a wide speed range in both directions, from %50 to %150 synchronous speed. However, for economical reasons, the speed range for a typical Type III wind turbine may be narrower than the given values.

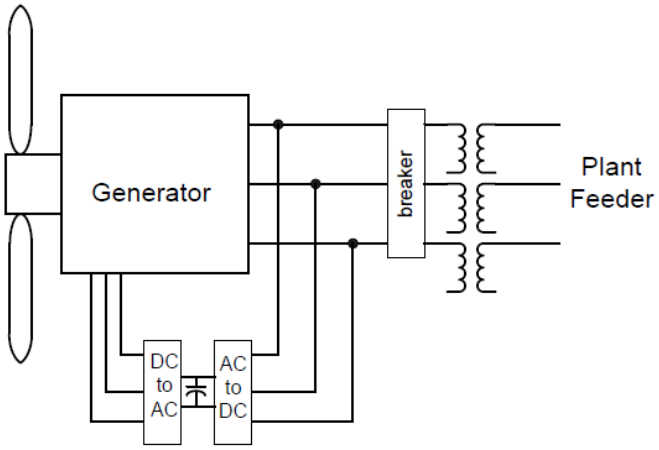

Fig.3.4 Basic Configuration of a Type III Wind Turbine Generator
(Source: Ackermann, 2012)

Type IV: Fully Rated Converter Generator

The Type IV generator consist of an electrical machine that is connected to the collector system through a full scale back-to-back frequency converter. A basic schematic of Type IV wind turbine generator can be seen in Fig.3.5. Type IV wind turbines come with three different generator options. They may use a synchronous machine excited either by permanent magnets or electrically , or an asynchronous generator instead. Unlike the aforementioned types, the generator of Type IV wind turbines is completely decoupled from the grid. This makes Type IV turbines to be able to designed without a gearbox, which are called direct-drive turbines. This, however, does not necessarily prevent the usage of gearbox in a Type IV turbine. Both direct-drive and gearboxed Type IV turbines are commercially available. Generally, in case that an asynchronous generator is used in the turbine, a gearbox is usually implemented in the design.

The electrical output of the generator is completely defined by power electronic equipment, i.e. the full scale converter. The inherent behavior of the generator itself has little effect on the output provided that the internal operation is within normal operational limits. This design allows Type IV turbines to rotate at an optimal

aerodynamic speed providing maximum flexibility by means generation and also excellent grid integration characteristics such as revolutionarily reactive power capabilities and a wide voltage and frequency operating range. The full scale frequency converter consists of a rectifying bridge, which generally resides in the nacelle, DC link, and the inverter, which is either located within the nacelle or in the basement of the turbine tower. The DC link allows the inverter to be controlled and provide output power independent of the input power of the generator within normal operational voltage ranges of the DC link. The inverter is controlled so that its output is in synchronization with the collector system frequency. Control properties of the inverter does vary considerably among different manufacturers. A unit transformer connected to the output of the inverter steps up the voltage from 690 V (which is typical rated voltage for majority of modern wind turbines) on the low voltage side to the wind farm's collector system voltage level, typically 34.5 or 33.6 kV for Turkey and Europe.

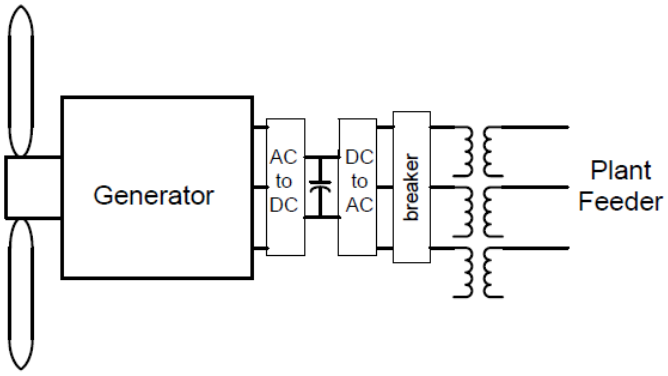

Fig.3.5 Basic Configuration of a Type IV Wind Turbine Generator
(Source: Ackermann, 2012)

Type V: Synchronous Generator Mechanically Connected Through A Torque Converter

Type V wind turbines are among the newest state-of-art models in the field. They exhibit typical synchronous generator behavior during faults. Therefore their

contributions to faults can be calculated from the generator machine constants just like any other synchronous machine. A basic schematic of Type V wind turbine generator can be seen in Fig.3.6. The synchronous generator can either be excited by a separate exciter or permanent magnets. When the latter method is the case for a turbine, it is named as "Permanent Magnet Synchronous Generator". The mechanical torque converter is resided between the rotor's low-speed shaft and the generator's high-speed shaft. It is responsible of controlling the generator speed in order to match with the electrical synchronous speed. Another interesting property of Type V wind turbines is that they operate at medium voltage levels, enabling them to be directly connected to MV grid if the voltage levels are the same[52].

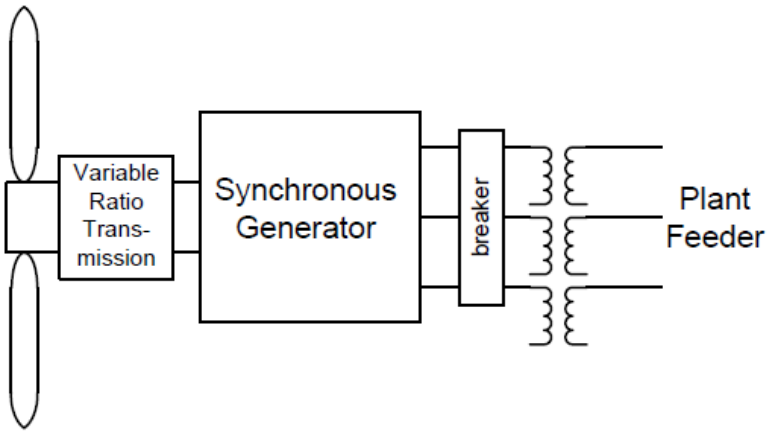

Fig.3.6. Basic Configuration of a Type V Wind Turbine Generator
(Source: Ackermann, 2012)

Just like any other type of generator, wind turbines can convert wind energy to electrical energy as long as an air flow of sufficient velocity is present in the vicinity of the turbine blades. If one is to set up a similarity between a conventional power plant and a wind farm, it is clear that wind can be regarded as the "fuel" of the wind power plant since the generator is able to generate electricity only when there is enough wind flow through the turbine blades. Therefore, when the turbine is "out of fuel" i.e. there is no sufficient wind flow through the blades, the wind turbine shuts

down. Moreover, if the wind velocity exceeds a certain value, known as cut-off wind speed, the controller of wind turbine locks the blades and stops generation in order to prevent damage to the turbine by excessive rotational velocity. The problem that differentiates wind generation from conventional generation is the fact that a fuel shortage in a conventional power plant is not abrupt but is predictable in the long run or there is no risk of over-accelerating the turbines due to excessive fuel combustion. On the other hand, wind velocity and direction at a region is predictable only up to some extent and abrupt changes in generation due to changes in wind velocity can always take place. These variations in generation cannot affect an entire power system if a single wind turbine is considered. However, as the number of turbines connected to the grid increases, the power contribution by these turbines to overall generation becomes more and more important. In power systems where wind power generation makes up a noticeable fraction of overall generation (typically above %3) it is necessary to analyze the effects of wind power plants to the system.

During steady-state operation where wind speed is constant or varies within the normal operational limits, a wind turbine's output power does not change abruptly. However, when the wind disappears or its velocity exceeds the turbines' cutoff velocity, wind turbines are unable to generate electricity. When large number of wind turbines in several wind farms within the country limits are considered, this phenomenon can be of high importance since when a large number of turbines cease their generation, the amount of generation lost can be significant. In such a case, it is necessary to prevent frequency drop in the system by primary and secondary controls and the interference of the system operator may be necessary.

Apart from being prone to sudden loss of generation, wind turbines show different characteristics during transient cases such as faults at buses, lines or transformers. Earlier wind turbines, which may still be in operation occasionally have very limited or no reactive power capabilities that make them impossible to contribute to system stability in the event of a fault. This reactive power incapability of wind turbines are solved up to some extent with the recent developments in the field. However, except for a number of state-of-art models which are generally more expensive than the rest

of the models occupying the market (mainly Type IV turbines), even modern wind turbines show somewhat worse characteristic than conventional generators by means of reactive power contribution. This reactive power contribution problem is actually not only limited to transient cases but also in normal operation since even in the absence of an extreme case in the system, due to continuously changing loads, losses and also generation of other plants, the system parameters such as voltage or reactive power flows change continuously . Wind turbines have to regulate their reactive power output in response to the voltage deviations at the grid connection.

The effects of wind generators on transmission system operation are primarily dependent on the contribution of wind generation within the overall generation of the power system, as well as the distribution of wind farms across the electrical system. It is expected by general experience that, the problems caused by wind turbines within the transmission system will tend to increase as the wind power penetration increases and the wind farms become more concentrated on certain parts of the system in contrast with uniform distribution. However, the severity of these effects will be made clear only after a realistic model of Turkish transmission system has been set up and certain analytical simulations have been carried out on it.

TEİAŞ (Turkish Electricity Transmission Company) is the authority in Turkey by means of electricity transmission services. Research, Planning and Coordination department (APK Daire Başkanlığı) of TEİAŞ has prepared an atlas containing the data of transmission system buses, terminals, transformers and transmission lines. The atlas both contains the tabulated data and the overall Turkish transmission system map, a variant of which is provided in Fig.3.7.

Fig.3.7. Turkish Electricity Generation-Transmission System Map
(Source: TEİAŞ, 2013)

By using the aforementioned data, the transmission system of Turkey will be modeled in detail. However, since modeling the exact system consisting of several thousand equipment is practically impossible to carry out by a single person within a specified duration, and also will provide little increase in realism of the actual system, the detail level of the transmission system will be reduced, roughly by a factor of 1/3. Necessary steps during the modeling process will be presented along with screenshots displaying the progress of constructing the Turkish transmission system on Digsilent.

Before starting to implement the transmission system, in order to place the system components accurately with respect to their geographical locations, a map of Turkish electrical system is set as the background of the project. Then, a list of the buses to be placed in the system is made regarding the transformer substation data provided by TEİAŞ. The listing process is made using Microsoft Office Excel. Then, in order to reduce the detail, the bus list is rearranged so that certain buses of less importance are merged to buses that are geographically close to each bus to be removed from the list. Then, the final bus list is modeled to Digsilent. The voltage levels used for buses

used in the system are 380, 154, 66, 34.5, 33.6 and 33 kV, among which 380 and 154 kV buses are dominant by means of quantity. The number of 66, 33.6 and 33 kV buses are relatively small since they are mostly belonging to earlier times of Turkish transmission system and majority of them are eventually taken out of service up to today. A number of 34.5 kV buses are also modeled since they belong to either important generation or important consumption centers, where the distribution transformers of higher ratings are located. The naming of the buses are carried out in order to effectively denote each bus with the naming provided by TEİAŞ. Moreover, the voltage level of each bus is added after the name of the bus in order to prevent any confusion between buses belonging to different voltage levels. Buses belonging to 380 kV system are denoted solely by their names. They will be clearly differentiated from the other voltage levels since the rest of the system has their voltage levels stated on the components' names.

After all the buses are implemented on Digsilent, the transformer data obtained from TEİAŞ is analyzed. Likewise, this transformer data is rewritten on Microsoft Excel in order to be able to successfully keep a track of the transformers that belong to the previously merged buses. The transformers belonging to previously merged buses are dispatched according to the merged bus they belong to. For instance, if there is a transformer between buses A and B, and if bus B is removed from the list and merged into a nearby bus C, then this transformer is implemented so that it is connected between buses A and C. If there is an actual transformer between buses A and C, then the two transformers are connected in parallel with each other. By this way, the realism of the system modeling is kept within levels close to the original while the system complexity is reduced.

A similar method like the aforementioned ones when implementing the buses and transformers in the system is used for the modeling of the transmission lines in the system. As expected, the transmission line data is the largest data set by means of quantity, since each bus is generally connected to the rest of the system via more than a single transmission line. For this reason, the tabulation of transmission lines in the system took relatively longer time when compared to other system components.

The lines connected to the merged buses are modeled in the same way as the transformers belonging to the merged buses. If there were an actual transmission line existing between the same buses, they are modeled in parallel to other (merged) transmission lines. It should be noted that here, transmission lines not only refer to aerial lines (overhead lines) but also to underground cables that are found in some parts of the transmission system. The naming of the transmission lines are carried out in a way so that the name of each transmission line is denoted by two buses names that the line is connected to, separated by a dash (-) and the voltage level of the transmission line, again omitting this notation if the transmission line belongs to the 380 kV system.

After all the transmission lines in the system are modeled, the transmission system model is partially complete. The transmission system is fully interconnected and it is able to provide power flow from/to any point in the system. However, in order to be able to do so, generators or power plants must also be implemented on the system. By the end of 2014, there exists more than 770 power plants connected to the Turkish electrical system, each contributing individually to the total installed capacity of approximately 69.500 MW. It should be noted that, however, a large percentage of these power plants can be considered as "smaller" power plants with ratings below 50 MW. However, as they are large in quantity, their contribution to total installed capacity of Turkey is not negligible. On the other hand, the peak demand of Turkey was 38.5 GW by 2014, implying that the installed capacity is never used completely, as expected from a secure system. For this reason, and for the scope of this thesis does not require the total installed capacity of Turkey is to be completely committed, the number of power plants modeled within the system is decreased. At this stage, only conventional power plants, namely, hydroelectric and combustion-type power plants are modeled since modeling of wind power plants is a different process, and chronologically carried out after all other components in the power system are modeled. Therefore, their modeling process is described in later parts of this section.

As the generators in the system are modeled and connected to the relevant buses which provide the monolithic property of the entire system, it is possible to dispatch the generators in order to achieve necessary generation levels. At this point, in order to allow generators to generate active power, there must be consumption centers that demand a specified amount of active, and also if desired, reactive power. These consumption centers are represented as loads connected to the electrical system created in Digsilent. Considering the fact that it would be practically impossible to model every single consumption point within the system, which corresponds to modeling all the factories, workshops, houses, or even street lamps and beyond, the consumption centers are modeled so that the consumption of every city in Turkey are modeled as a load connected to the distribution bus (commonly 34,5 or 31,5 kV) of the relevant city. This results in a total of 81 load elements to be implemented on the electrical system model. However, certain consumption centers that are of more importance are also modeled despite not being city centers. This resulted in a total of 113 load elements to be connected to the electrical system model.

Another component group that is of underestimated importance in the transmission system is the shunt reactors. The shunt reactors within the Turkish transmission system are modeled according to the data provided by TEİAŞ. By quantity and amount of time taken modeling, shunt reactors consisted the smallest portion among total system data. For this reason, it was possible to implement the exact number of shunt reactors in the given data set to the system. The naming of the shunt reactors are carried out in the same fashion that is described above for buses.

The modeling of wind farms in the system is carried out as the last step of system modeling. According to Turkish Wind Power Plant Atlas, there exists 101 wind farms connected to the Turkish power system by the first quarter of 2015. In order to stay in agreement with overall system detail, some wind farms that are geographically close to each other and share the connection points to the transmission system are merged into a single wind farm in the power system model constructed. When carrying out this process, the whole wind farm data, containing

the location of the wind farm, make and model of wind turbines belonging to each wind farm, as well as their numbers are used to construct an Excel worksheet.

Digsilent Powerfactory 15.2 already includes several wind turbine model templates with available buses and transformers in order to be able to connect them to the grid directly. These templates also include built-in turbine controllers that are widely used in the industry, including the ones present in the wind farms in Turkey. For this reason, as the first step, the wind farms are placed and connected to the grid according to the aforementioned Excel table as templates. Later, these templates are modified according to the actual wind turbine data provided by Turkish Wind Power Plant Atlas with necessary changes and additional controls defined. Transformers connecting the turbines to the main buses in the grid are also changed with transformer models used in Turkey in order to model the wind farms realistically.

The overall progress of construction of the Turkish transmission system, including the connected generation and consumption centers, is summarized in Fig.3.8.

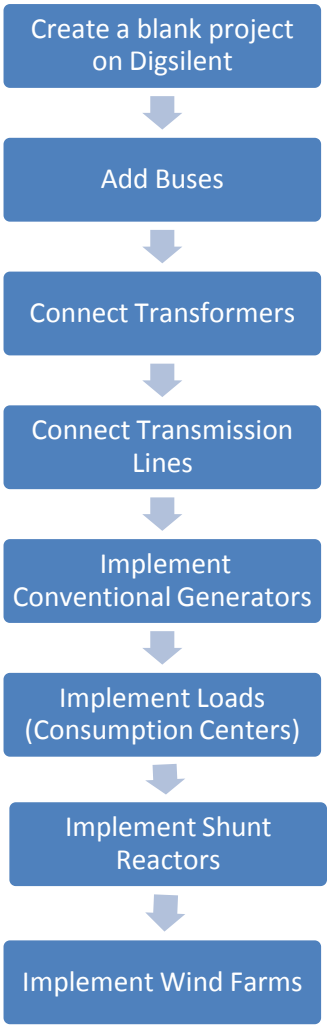

Fig.3.8. Summary of Implementation of the System Model

With all the buses, transformers, transmission lines, generators, loads, shunt reactors and wind farms connected in an unitary manner, the model of Turkish Transmission System is created and ready to be tested. The testing of the system, is carried out firstly by the topology checking. The topology check process is carried out under the "Network Data Assessment" tab of the program. This function enables to check the topology of the system and verify that the system is monolithic, with every single element has a direct or indirect connection to other elements in the system. After the system is verified to be completely interconnected, it is necessary to check if the modeling is correctly carried out so that the system is capable of supplying the

connected loads through the overall grid. To do so, firstly the power demands of the loads need to be specified. As a first step, average annual consumptions of 81 cities in Turkey, by 2014 are used as the demand values of the corresponding loads. In order to be able to supply this demand, generators within the system need to be dispatched to generate power that is enough to meet the demand and also grid losses. Since economic dispatch of generators, often referred as optimal load flow solution requires detailed data of every power plant in the system by means of fixed and variable costs, and is out of scope of this thesis, the dispatch is rather carried out in a way to keep the system losses and reactive power flow within reasonable limits. For initial load flow calculations, Karakaya HPP was chosen as the reference machine (hence bus Karakaya was the slack bus in the system). However, in order to benefit from maximum generation capacity of the plants, the reference machine is changed as Atatürk HPP with total installed capacity of 2400 MW. The load flow calculation is carried out simply by the "Load Flow" function of Digsilent available in the main toolbar menu. During analyses, load flow calculations are carried out several times, with necessary changes made between each calculations. This also includes testing the system's capability of meeting the demand when the demand is raised above the annual average consumption values of Turkey. In order to provide an uniform increase in demands of 113 consumption centers in the system, the "load scaling" property of Digsilent is used. This function allows to multiply a present demand (in Megawatts) assigned to a load with a variable coefficient in order to prevent the user from having to change each load value manually. With the aid of load scaling tool, the loading conditions from 0.7 to 1.4 times the average annual demand are tested by load flow analysis. It should however, be noted that generation dispatches had to varied manually in order to provide a secure system operation with minimized losses at each different loading state. The critically loaded (%80 to %100) equipments are denoted by orange colour in the resulting grid diagram after load flow calculation while the overloaded (above %100) equipments are denoted by red colour. Moreover, the undervoltage (below 0.95 p.u) and overvoltage (above 1.05 p.u.) at buses are denoted by blue and red colours, respectively. Since there are no overloaded elements or buses outside of normal operational range in the results of the analyses at different loading levels, it can be claimed that the system implemented successfully

represents a realistic electrical power system with secure operation within specified limits.

3.4 RMS Simulations

As mentioned in the previous section, the implemented power system model was able to successfully provide the power demand of consumption centers with the implemented conventional and wind power plants. This was verified by performing load flow analyses and observing that no element in the power system has gone outside their normal and secure operational ranges, as well as the voltage values at each bus is between 0.95 and 1.05 p.u. However, it is not enough only to consider normal operational states to analyze the effects of wind power plants in the transmission system operation. For this purpose, several transient analyses which will provide results of pre-specified disturbances (events) in the system with connected wind power plants of varying installed capacities are needed to be carried out.

In order to be able to observe the effects of wind farms in the power system in case of disturbances, the analyses are needed to be focused on disturbances in the regions which a considerable amount of wind generation exists. Moreover, in order to determine the extents of wind penetration that threatens the system stability and healthy operation, a worst case analysis must be considered when deciding upon the disturbance type. This implies that, a three phase to ground fault should be chosen as the disturbance event since it will result in highest short circuit power possible. What is more, in order to be able to compare the results analytically, the same set of scheduled events must be applied for each defined point to be analyzed.

Due to the reasons stated above, the analysis procedure described below will be applied for each wind farm modeled in the system which will result in 22 sets of analysis results.

Disturbance type: Three phase to ground fault with negligible (0.1 Ω) resistance

Location: Line connecting the wind farm to relevant bus (hence, the rest of the system).

Another important aspect affecting the severity of the consequences of a fault in the system is the fault clearing time. If the fault cannot be cleared within a given maximum duration, a power system, even the strongest one, may proceed to emergency state, or even collapse which will result in a wide scale blackout. Theoretically, it is stated that [16], the effect of a disturbance in the system is proportional to fault clearing time, which implies in order to minimize the effects of a disturbance, the fault must be cleared in the smallest time possible. According to Turkish Electricity Grid Code [53], the maximum permissible fault clearing time is determined to be 0.14 seconds for line-to-line faults and 1 second for ground faults, including three phase to ground faults. This implies that, under normal breaker operating conditions, a fault at any point of Turkish electrical system is cleared in at most 1 second. The minimum fault clearing time is limited by the state of circuit breaker and relay technology, electrical and mechanical limits. For a modern, state-of-art relay, the minimum time in order to detect the fault and provide the "open" signal to the relevant circuit breaker can be taken as 60 ms. However, there is also a defined time duration necessary in order the circuit breaker to perform "opening" action mechanically. With modern circuit breakers, the action duration can be as low as a few times of the system period ($T = 1/f = 1/50$ sec or 20 ms for Turkish System). For this reason, the circuit breaker can be assumed to clear the fault 60 or 80 ms after it receives the "open" command by the relay. Taking the time necessary for the relay to detect the fault and to provide the commanding signal to the breaker into account, the overall fault clearing time's minimum value can be taken as 60+60 = 120 ms for the current state of technology. It should, however be noted that this is the lower limit of the fault clearing time and the actual time to clear the fault can fall anywhere between this value and maximum allowable duration, which is 1 second for Turkish case. Considering the facts mentioned in this section, the analyses will be carried out with different fault clearing times. The fault clearing times for which all the simulations will be carried out is provided below with necessary explanations:

-60 ms: Despite being relatively optimistic for actual operational durations, analyzes for very low fault clearing times may provide an insight regarding the possibility of minimizing the severity of disturbances in the system.

-120 ms: Typical minimum fault clearing time for a 3 phase to ground fault in Turkish System. Can be achieved with a good coordination between relays and breakers as well as state-of-art technologies such as solid state circuit breakers.

-200 ms: Fault clearing time which falls to the "quick response" side of regular breakers

-500 ms: Fault clearing time that is still within the acceptable limits, can be typical for older breaker and/or relay systems.

-1000 ms (1 sec.): Maximum allowed fault clearing time in Turkish Grid Code [53] for 3 phase to ground faults, can be regarded as a "worst case scenario".

The installed capacities of the wind farms modeled in the system were set according to the actual values provided by Turkish Wind Power Plant Atlas. This, however, reflects only the present case in the Turkish electrical system since large numbers of wind farm applications had been rejected by EPDK and hence, the installed capacities of the wind farms are below or equal to %5 of the short circuit power at the bus that the wind farm is connected to. It can be claimed that, with the present situation, there is no threat by means of system stability caused by wind farms in operation since it is the actual case for Turkish Electrical System that holds no known records of emergency cases which originated from disturbances related to wind farms. This claim, however, does not remove the necessity of analyzing the possible results of disturbances within the current system. For this reason, a base case, for which the wind farm installed capacities are held at %5 of the short circuit power at relevant buses will be the first case for the analysis. Later, the installed capacities of the wind farms in the system will be increased in a stepwise manner to be equal to %7.5, %10, %12.5 and %15 of the short circuit power at relevant buses,

respectively. The RMS analyses will be carried out at each of these installed capacity values for each wind farm in the system. As the final step, each wind farm's installed capacity will be increased in order to approach the limit set by the ratings of the equipment in the system, i.e. the transformers and transmission lines which limit the amount of power that can be provided at a given bus to the rest of the system. For this installed capacity, RMS analyses will be carried out once more in order to determine the effects of such high wind penetration values in case of disturbances in the system.

The flowchart summarizing the analysis steps with relevant variables is provided in Fig.3.9.

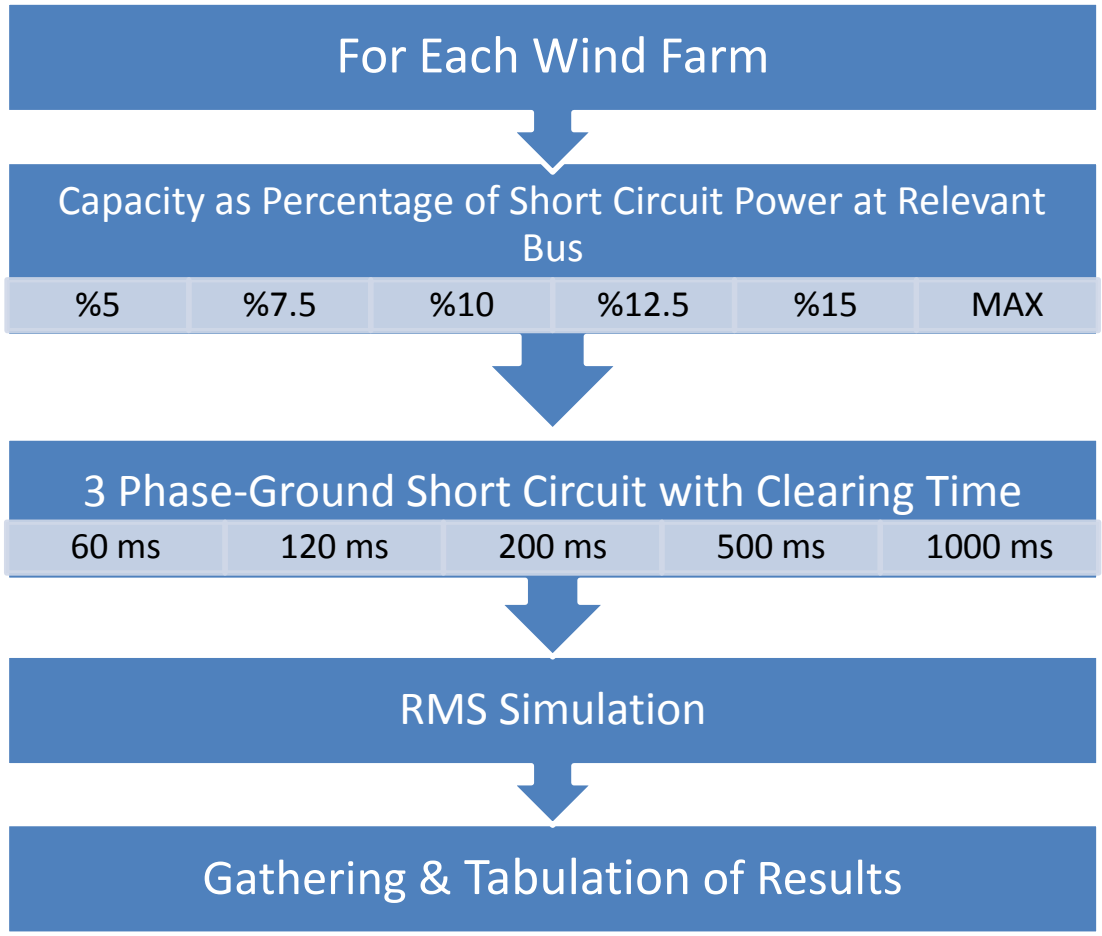

Fig.3.9. Summary of Analysis Steps

As can be implied from Fig.3.9, the total number of simulation analyses to be carried out is:

22 Plants x 6 Capacity Values x 5 Clearing Times = 660 different RMS simulations

In order to be able to observe the effects of the defined events, the output variables in Digsilent need to be properly defined. For the present analyses, voltage (rms) values at buses, line loadings and rotor angles of generators within the area defined as the circular area centered at fault location and is of 250 km radius will be monitored at each analysis step. In case that there are buses belonging to the same transformer substation with different voltage levels, for instance 34.5 and 154 kV buses connected via a transformer, only one of them will be monitored in order to keep the number of elements to be monitored within manageable limits. If the analysis results turns out to be addressing critical values for selected buses, the omitted buses will also be included in the elements to be monitored and the simulation will be carried out again.

The starting time of each simulation is set to be t= -100 ms in order to be able to trigger the fault event at absolute t=0 ms. This enables to set the breaker operating times to be exactly equal to the specified times. For instance, for the breaker set to operate 120 ms after the fault, the switching operation will be set to be performed at t= 120 ms and so forth. This configuration also allows to analyze the output of the simulations easily since each output variable will be displayed in a manner that the time (t) of the event of interest will be exactly equal to the time passed since the initiation of the disturbance in the system. In order to obtain results of high precision and accuracy, time step during analysis is set to be equal to 0.008 seconds. Moreover, error tolerance of the analyses are greatly reduced to improve precision. The stopping time of the analyses will be set to be t=5 sec. hence a total analysis duration of 5.1 sec. will be obtained.

As can be inferred from the aforementioned analysis steps, the resulting output data after each simulation will sum up to an enormous size which makes it impossible and

unnecessary to present every single output value separately within this study. Therefore, the output of each simulation will be transferred to MS.Excel worksheets and necessary portion of these data will be presented as numerical values and graphs providing the necessary information.

The wind farms modeled and to be analyzed, together with the lines connecting them to the grid, which are the lines that the short circuit event will be initiated on are presented in Table 3.1.

Table 3.1. List of Wind Farms to be Modeled.

No	Wind Farm	Line
1	Afyon RES	Afyon RES Line
2	Aksu RES	Aksu RES Line
3	Aydin RES	Aydin RES Line
4	Bandirma RES	Bandirma RES Line
5	Bozyaka RES	Bozyaka RES Line
6	Canakkale RES	Canakkale RES Line
7	Cesme RES	Cesme RES Line
8	Düzova RES	Düzova RES Line
9	Edincik RES	Edincik RES Line
10	Geycek RES	Geycek RES Line
11	GokRES	GokRES Line
12	Istanbul RES	Istanbul RES Line
13	Keltepe RES	Keltepe RES Line
14	Kirklareli RES	Kirklareli RES Line
15	Korkmaz RES	Korkmaz RES Line
16	Kuyucak RES	Kuyucak RES Line
17	Mersin RES	Mersin RES Line
18	Osmaniye RES	Osmaniye RES Line
19	Şenbük RES	Şenbük RES Line
20	Şenköy RES	Şenköy RES Line
21	Tekirdag RES	Tekirdag RES Line
22	Umurlar RES	Umurlar RES Line

3.5 Simulation Process

The simulations are carried out according to the method described in the previous section. Before each RMS analysis, the initial conditions of the system, i.e. the system state before any disturbance, is calculated with the "Calculate Initial

Conditions" function of Digsilent. Then, the RMS simulations are carried out for each individual case by using the "Start Simulation" function. During the simulations, no changes regarding the system or calculation methods can be made. Therefore any changes for the wind farm installed capacities or circuit breaker operation times are carried out after each simulation is completed and the results are printed on the output window.

CHAPTER 4

SIMULATION RESULTS

The simulation process consisting of a large number of individual transient analysis processes are carried out and the sets of output data that contain the information of simulation results are stored as Excel worksheets. In this section, some of these data will be presented with necessary explanations and comments.

For each of 22 wind farms, the simulation results have shown a similar pattern with, naturally, varying mathematical values. Five of these wind farms' simulation results will be presented here with necessary comments and highlights. The criteria used to determine which wind farms will be selected is based on the aim of effectively representing different wind farms according to their location, installed capacity and strength of the grid at the points of connection. Therefore, the five cases whose results will be analyzed in detail are provided below.

-Case 1: Bozyaka RES

-Case 2: Mersin RES

-Case 3: Şenköy RES

-Case 4:Aksu RES

-Case 5: Çanakkale RES

It is difficult to claim an exact definition of the strong points in the grid. However, in practice, the regions which are connected to the rest of the grid with relatively higher number of transmission lines or the regions with generators of high inertias nearby can be classified as strong regions in the grid while the regions lacking these features can be claimed to be weaker regions. The weak regions in the grid are assumed to be more prone to disturbances in the system and are expected to show lesser durability in case of such disturbances. That is, in the event of a disturbance, such as short circuit, a weaker region in the system will tend to suffer from more severe effects such as higher voltage oscillations, easier generator loss due to pole slip and so on. The example cases are mainly focused on to demonstrate the "worst case" results of weaker regions. However, there are also stronger regions taken under consideration to be able to demonstrate the results for the cases where the grid is strong and also to compare the effects of similar disturbances between the regions with different strengths among the system. Cases 2, 3 and 5 are examples of weaker regions where wind generation exists while cases 1 and 4 are the relatively strong regions with high wind penetration in the system.

4.1. Case 1: Bozyaka RES

The first case, Bozyaka RES is chosen to be demonstrated first since it is on the stronger side of the scale and therefore it can be regarded as a control case to compare with cases involving wind farms in weaker regions of the grid. Bozyaka wind farm is resided in Aliağa, a town within the limits of Izmir, the third largest city in Turkey. In the system, the wind farm is connected to the grid at Bornova 34.5 kV (denoted by Bornova 34 in the model) bus. Therefore, the connecting line is between the buses Bozyaka RES 34 and Bornova 34. The current installed capacity of Bozyaka RES (omitting the nearby wind farms which were actually included in the system model) is 12 MW. The short circuit power at Bornova 34 bus, on the other hand, is 2187 MVA [54]. If the wind farms included in the modeling are also considered, the total installed capacity of the wind farms that are denoted by Bozyaka RES in the model sum up to 85 MW. As can be inferred from its location, the grid where the wind farm is located is considerably strong since one of the largest

cities in Turkey is founded nearby with high power demands by means of residential, commercial and industrial consumption centers. Moreover, the fact that wind farms are concentrated mainly on the western coastline of Turkey makes it inevitable to have a strong transmission system with many connections enabling the wind generation to be provided to the rest of the system. For these reasons, the system strength around Izmir, and hence Bozyaka RES is expected to be high. This implies that, during simulations, the effects of disturbances will be relatively smaller than that would be expected to be observed at weaker regions of the grid.

As mentioned in the preceding section, the analyses will be carried out for installed capacities of Bozyaka RES that will be equal to %5, %7.5, %10, %12.5 and %15 of the short circuit MVA at Bornova 34 bus. The installed capacity values corresponding to these percentages of short circuit power are given in Table 4.1.

Table 4.1. Installed Capacity Values to be Analyzed in Case 1.

% of Ssc	5	7,5	10	12,5	15
Installed Capacity (MW)	109	164	219	273	328

The buses, transmission lines and generators within 250 km radius of the wind farm are chosen to be observed. However, to avoid overflow of output data, some elements among the initial set are omitted after they are proven not to show any significant variations during the analysis processes. The resulting set of elements to be observed and whose results will be provided in detail are given below.

-Buses (Voltages of) : Bornova 34, İzmir 34, Kuşadası 34

-Transmission Lines (Loading of): Bergama-Edremit 154, Yatagan-Yeniköy

-Generators (Rotor Angles of): Kemerköy

Analysis Results

For each given installed capacity value, five individual analyses are carried out regarding circuit breaker operating times. The results are provided in related sub-cases below.

4.1.1: %5 (109 MW) Installed capacity

4.1.1.1 Breaker operating time: 60 ms

For such a short fault clearing time, the variations of selected bus voltages are provided in graphs 4.1 to 4.3.

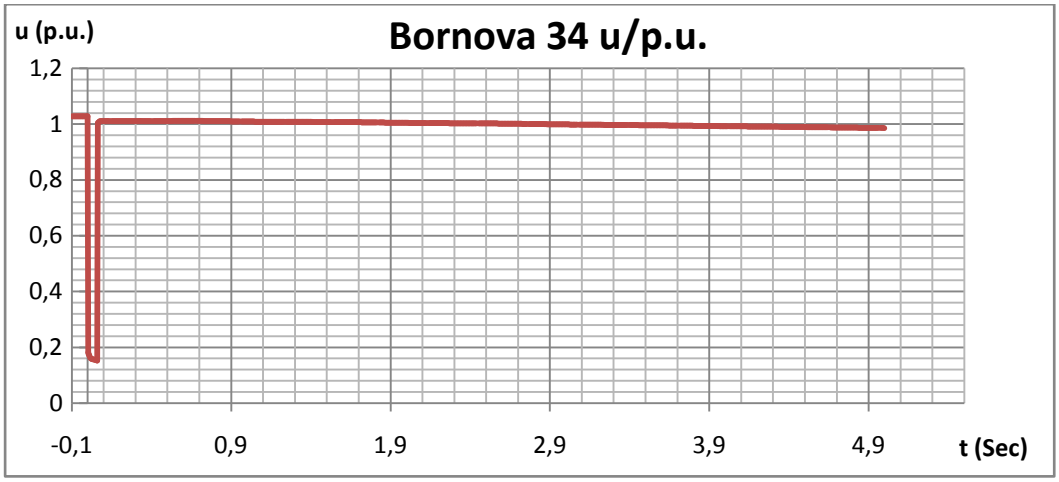

Graph 4.1. Voltage Variation of Bornova 34 Bus.

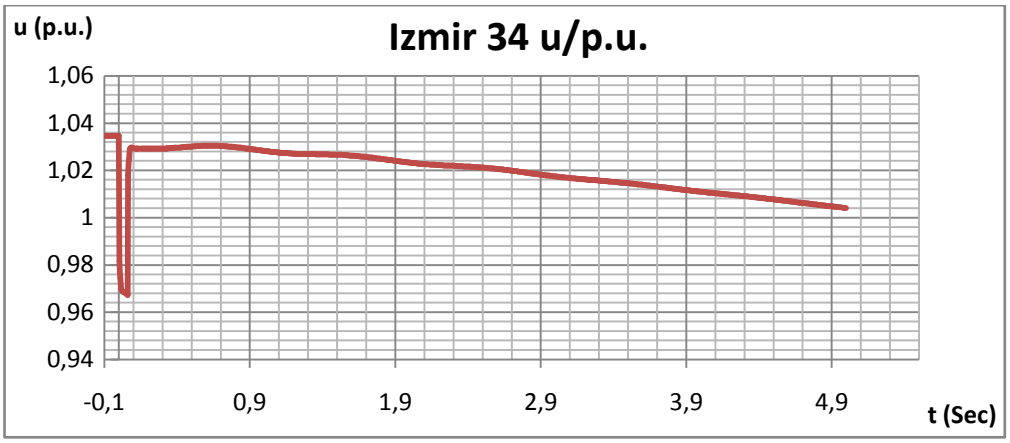

Graph 4.2. Voltage Variation of Izmir 34 Bus.

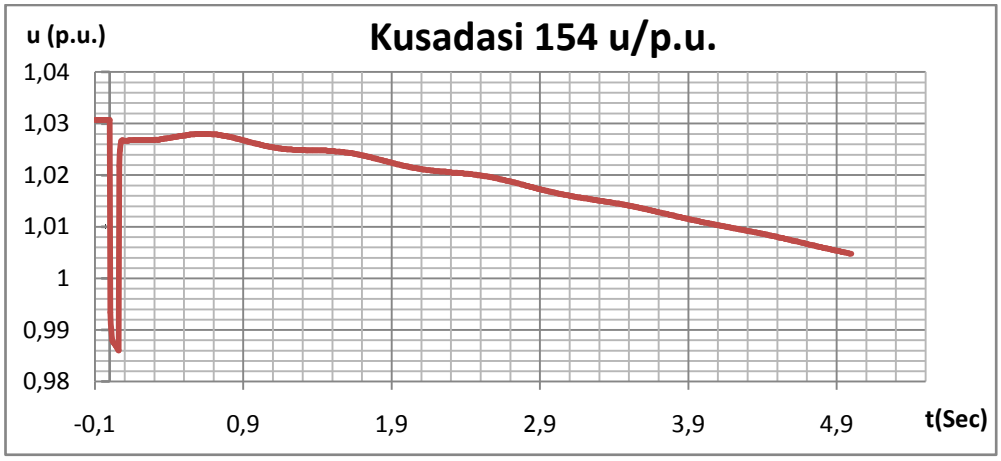

Graph 4.3. Voltage Variation of Kuşadası 154 Bus.

As can be seen from the three graphs above, the disturbance had a drastic and almost immediate effect on the bus voltages which caused the voltages at nearby buses to drop sharply. However, the size of the drop varied between different buses and mainly influenced by the connection strength and distance to the location of fault. Bornova 34 bus, being the closest one to the fault has suffered from the largest voltage drop in the event of a 3-phase short circuit. It can be seen that, at t=0.06 sec. the voltages at each bus rises sharply since the circuit breakers at the ends of faulted line are operated, thus, returning the rest of the system to fault-free state. However,

the voltage values are not constant at the post-fault state until the new stable system operating state is fully reached. During this state, the oscillations of the voltage values at each bus can be seen. In order to ensure the power quality in the grid, these oscillations should not exceed %10 of the nominal voltage, i.e. 0.1 p.u. during the post fault state. Moreover, the final voltages of the buses should be within normal operating limits, that is between 0.95 and 1.05 p.u. The maximum and minimum values of bus voltages after the fault clearing, as well as their difference in p.u. are provided in Table 4.2.

Table 4.2. Bus Voltages for Case 1.1.1.

	Bornova 34	Izmir 34	Kusadasi 154
Vmax	1.0063	1.0233	1.0225
Vmin	0.9859	1.0041	1.0048
Difference	0.0204	0.0192	0.0177
Vfinal	0.9859	1.0041	1.0048

As Table 4.2 clearly shows, the final values at the end of 5 seconds after the fault are within the normal operational limits. Moreover the voltage oscillatory peak for all buses are well below the specified %10 limit for this case.

The line loadings before, during and after the fault are also recorded and the related graphs are provided for lines Bergama-Edremit 154 and Yatagan-Yeniköy in graphs 4.4 and 4.5, respectively.

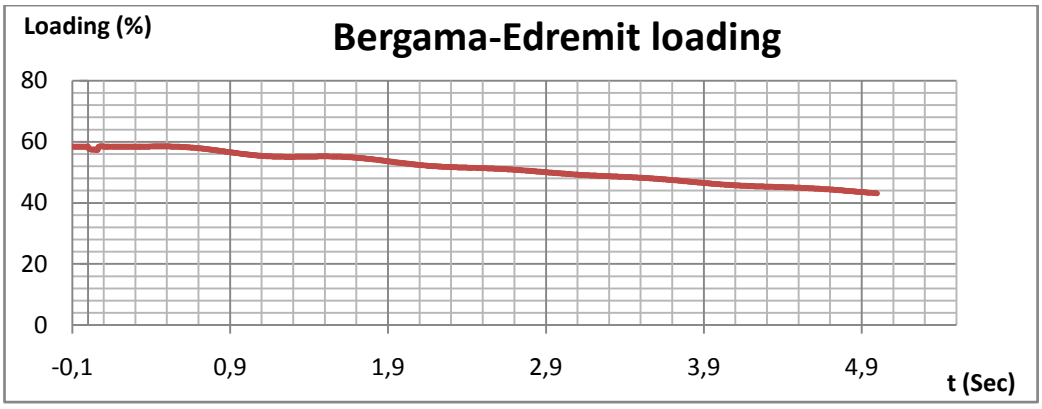

Graph 4.4. Loading of Bergama-Edremit Line.

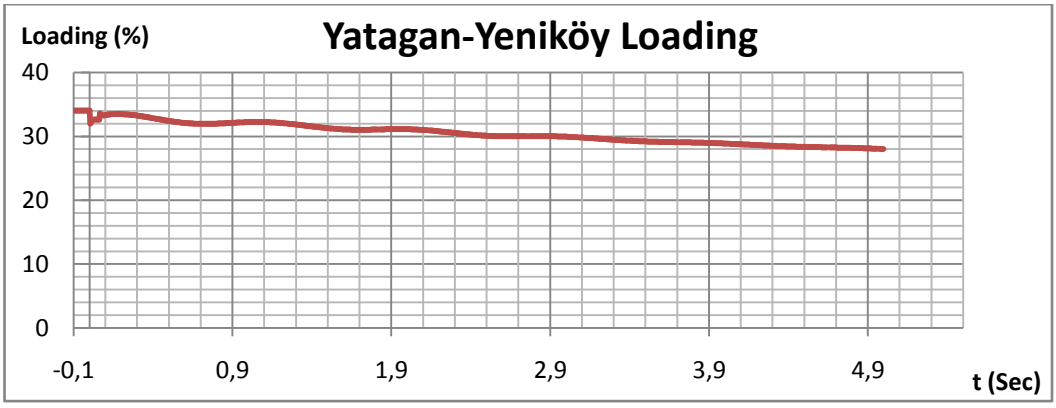

Graph 4.5. Loading of Yatagan-Yeniköy Line.

As can be seen from both graphs, the fault has caused a slight but immediate disturbance on the transmission lines. After the breaker operation, the line loadings have initially rose slightly and then, began decreasing to reach the new steady-state values. Since all the transmission lines residing within 250 km radius of the fault point remained under %100 loading at any time before, during or after the fault, it is safe to claim that this case has no threat to the transmission lines by means of overloading.

If a fault cannot be cleared within a certain time, it is possible for a nearby generator's rotor angle to increase at a high pace thus reaching 90 degrees which will result in the loss of the generator due to loss of synchronism or pole slip. The only synchronous generator that showed noticeable response to the fault was Kemerköy (Thermal Power Plant) . The rotor angle of generators should stay below 90 degrees, or approximately 1,57 radians in order the generator to stay in synchronism with the grid. Otherwise the generator will fall out of synchronism which will result in the loss of the generator. Therefore, the main criteria taken under consideration by means of fault ride through capabilities is to observe whether the generator is able to withstand the fault and also, post-fault cases so that the rotor angle stays below 1,57 radians. Table 4.3 provides the initial (t= -0,1 sec.), final (t=5 sec) and maximum rotor angles for Kemerköy TPP during this case.

Table 4.3. Rotor Angle Values for Kemerköy TPP

	Kemerköy Rotor Angle (rad)
Initial	1.2185
Final	1.2979
Maximum	1.2979

As can be seen from Table 4.3 the initial and final values of rotor angle differ only by a small amount (approximately 4,58^{o}) and the simulation results verify that the generator stays in synchronism with the system without any adverse effect.

4.1.1.2 Breaker operating time: 120 ms

120 milliseconds can be assumed to be a relatively quick fault clearing time. For this circuit breaker operation time, the variations of selected bus voltages are provided in graphs 4.6 to 4.8.

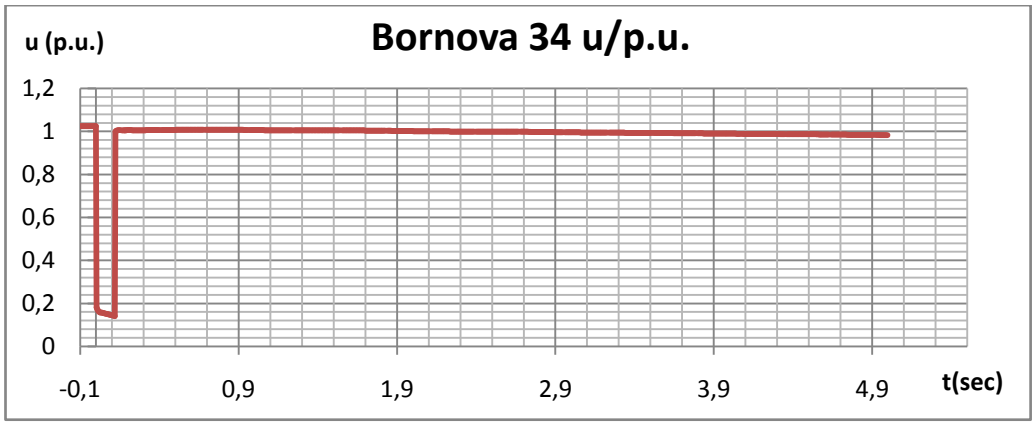

Graph 4.6. Voltage Variation of Bornova 34 Bus.

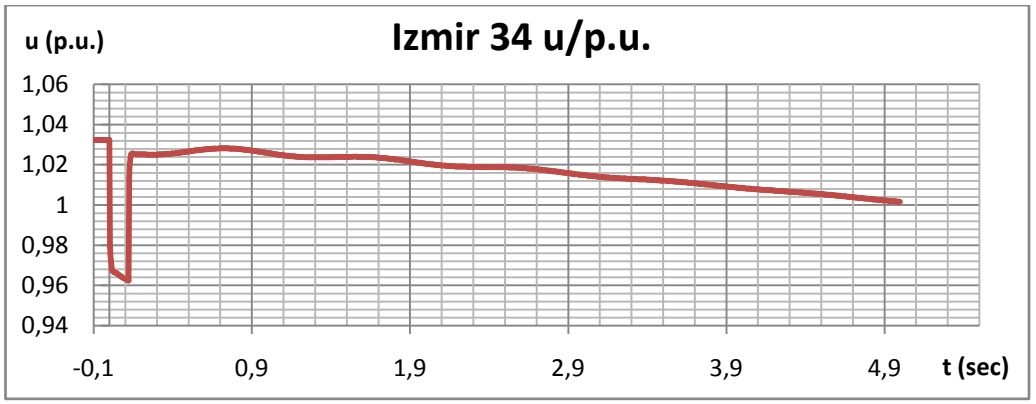

Graph 4.7. Voltage Variation of Izmir 34 Bus.

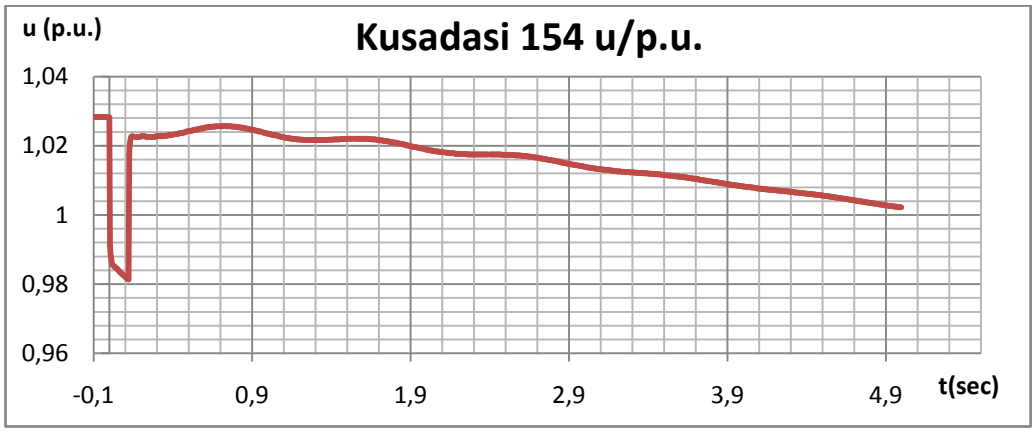

Graph 4.8. Voltage Variation of Kuşadası 154 Bus

As can be seen from the three graphs above, the disturbance had a drastic and almost immediate effect on the bus voltages which caused the voltages at nearby buses to drop sharply. However, the size of the drop varied between different buses and mainly influenced by the connection strength and distance to the location of fault. Bornova 34 bus, being the closest one to the fault has suffered from the largest voltage drop in the event of a 3-phase short circuit.

It can be seen that, at t=0.12 sec. the voltages at each bus rises sharply since the circuit breakers at the ends of faulted line are operated, thus, returning the rest of the system to fault-free state. However, the voltage values are not constant at the post-fault state until the new stable system operating state is fully reached. During this state, the oscillations of the voltage values at each bus can be seen. The maximum and minimum values of bus voltages after the fault clearing, as well as their difference in p.u. are provided in Table 4.4.

Table 4.4. Bus Voltages for Case 1.1.2.

	Bornova 34	Izmir 34	Kusadasi 154
Vmax	1.0039	1.0216	1.0199
Vmin	0.9834	1.0016	1.0022
Difference	0.0205	0.0200	0.0177
Vfinal	0.9834	1.0016	1.0022

As Table 4.4 clearly shows, the final values at the end of 5 seconds after the fault are, again, within the normal operational limits. Moreover the voltage oscillatory peak for all buses are well below the specified %10 limit for this case. The oscillation magnitude has increased when compared to the case 4.1.1 due to slower circuit breaker operation. However, this increase is very small for any bus and therefore it can be concluded that, even if it is possible to clear a fault in 60 milliseconds, the results by means of voltage oscillations will not change noticeably.

The line loadings before, during and after the fault are also recorded and the related graphs are provided for lines Bergama-Edremit 154 and Yatagan-Yeniköy in graphs 4.9 and 4.10, respectively.

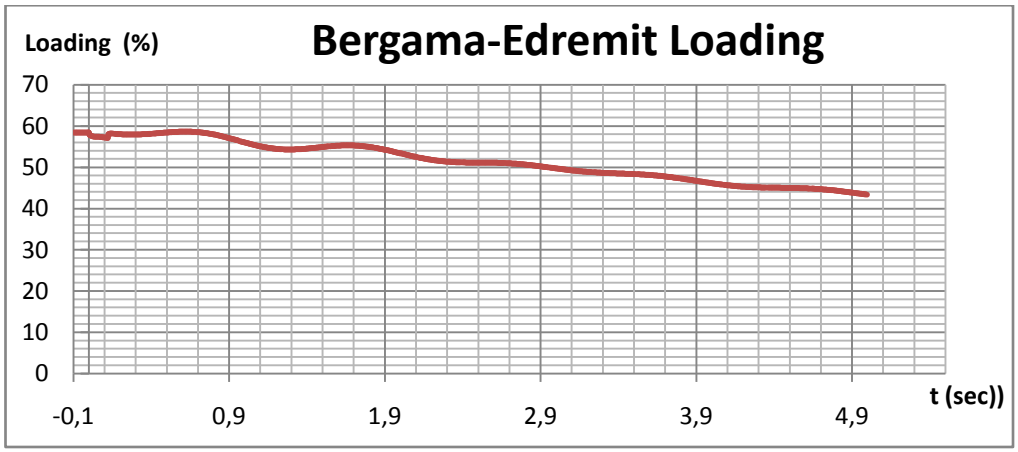

Graph 4.9. Loading of Bergama-Edremit Line

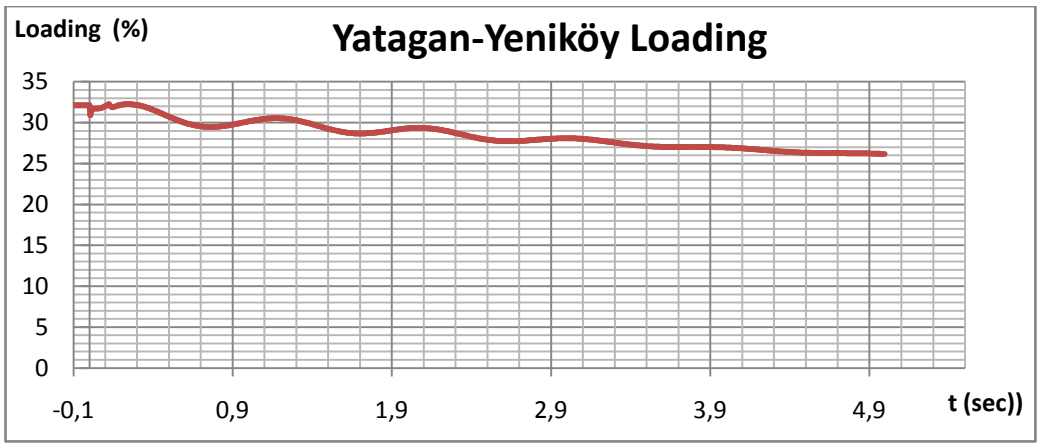

Graph 4.10. Loading of Yatagan-Yeniköy Line.

As can be seen from both graphs, the fault has caused a slight but immediate disturbance on the transmission lines. After the breaker operation, the line loadings have initially rose slightly and then, began decreasing to reach the new steady-state

values. The loading values and pattern does not vary from case 4.1.1. significantly. Since all the transmission lines residing within 250 km radius of the fault point remained under %100 loading at any time before, during or after the fault, it is safe to claim that this case has no threat to the transmission lines by means of overloading.

Table 4.5 provides the initial (t= -0,1 sec.), final (t=5 sec) and maximum rotor angles for Kemerköy TPP during this case.

Table 4.5. Rotor Angle Values for Kemerköy TPP

	Kemerköy Rotor Angle (rad)
Initial	1.3093
Final	1.3684
Maximum	1.3684

As can be seen from Table 4.5 the initial and final values of rotor angle differ only by a small amount (approximately 3,43^{o}) and the simulation results verify that the generator stays in synchronism with the system without any adverse effect. The difference in values existing between cases 4.1.1 and 4.1.2 is due to slight change made for analysis time steps for better convergence and it should be noted that the deviation between initial and final values are approximately the same for cases 4.1.1 and 4.1.2.

Taking the results provided above into consideration, the variations in bus voltages, line loadings and rotor angles are proven to stay within the limits to ensure a stable operation of the system.

4.1.1.3 Breaker operating time: 200 ms

200 milliseconds can be assumed to be a typical fault clearing time. For this circuit breaker operation time, the variations of selected bus voltages are provided in graphs 4.11 to 4.13.

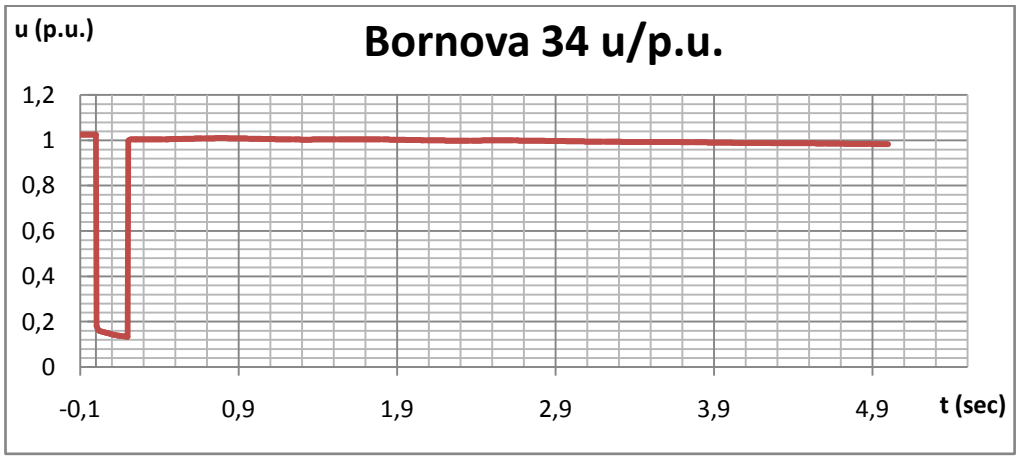

Graph 4.11. Voltage Variation of Bornova 34 Bus.

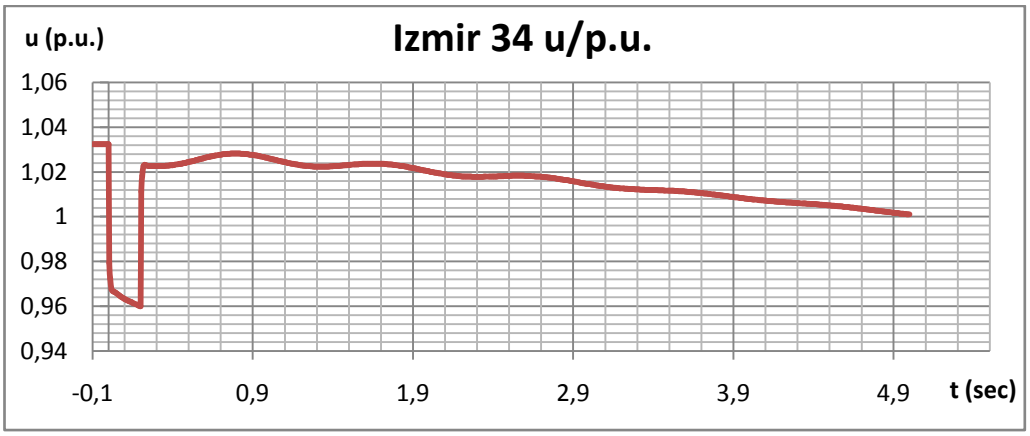

Graph 4.12. Voltage Variation of Izmir 34 Bus.

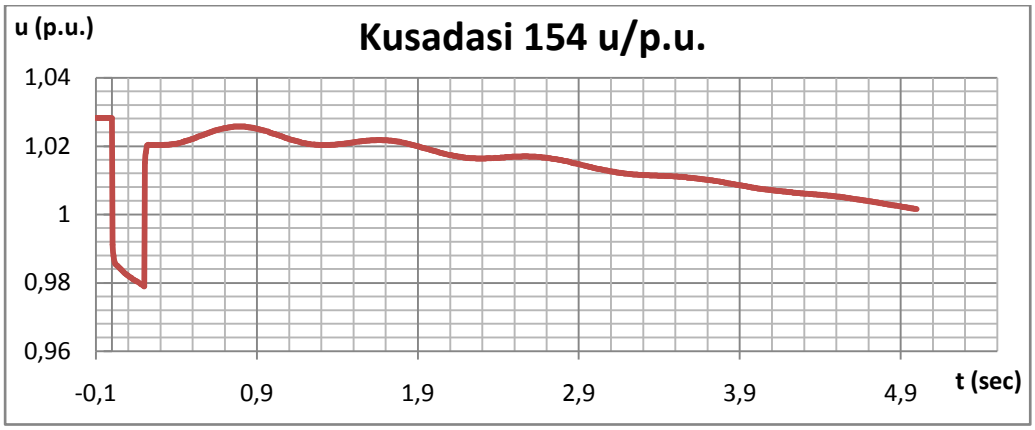

Graph 4.13. Voltage Variation of Kuşadası 154 Bus.

As can be seen from the three graphs above, the disturbance had a drastic and almost immediate effect on the bus voltages which caused the voltages at nearby buses to drop sharply. However, the size of the drop varied between different buses and mainly influenced by the connection strength and distance to the location of fault. Bornova 34 bus, being the closest one to the fault has suffered from the largest voltage drop in the event of a 3-phase short circuit.

It can be seen that, at t=0.2 sec. the voltages at each bus rises sharply since the circuit breakers at the ends of faulted line are operated, thus, returning the rest of the system to fault-free state. However, the voltage values are not constant at the post-fault state until the new stable system operating state is fully reached. During this state, the oscillations of the voltage values at each bus can be seen. The maximum and minimum values of bus voltages after the fault clearing, as well as their difference in p.u. are provided in Table 4.6.

Table 4.6. Bus Voltages for Case 1.1.3.

	Bornova 34	Izmir 34	Kusadasi 154
Vmax	1.0034	1.0215	1.0196
Vmin	0.9828	1.001	1.0016
Difference	0.0206	0.0205	0.0180
Vfinal	0.9828	1.001	1.0016

As Table 4.6 clearly shows, the final values at the end of 5 seconds after the fault are, again, within the normal operational limits. Moreover the voltage oscillatory peak for all buses are well below the specified %10 limit for this case. The oscillation magnitude has increased when compared to the case 4.1.1.2 due to slower circuit breaker operation. However, this increase is very small for any bus and therefore it can be concluded that, the oscillations in bus voltages does not vary considerably for the two different circuit breaker operation times. The line loadings before, during and after the fault are also recorded and the related graphs are provided for lines Bergama-Edremit 154 and Yatagan-Yeniköy in graphs 4.14 and 4.15, respectively.

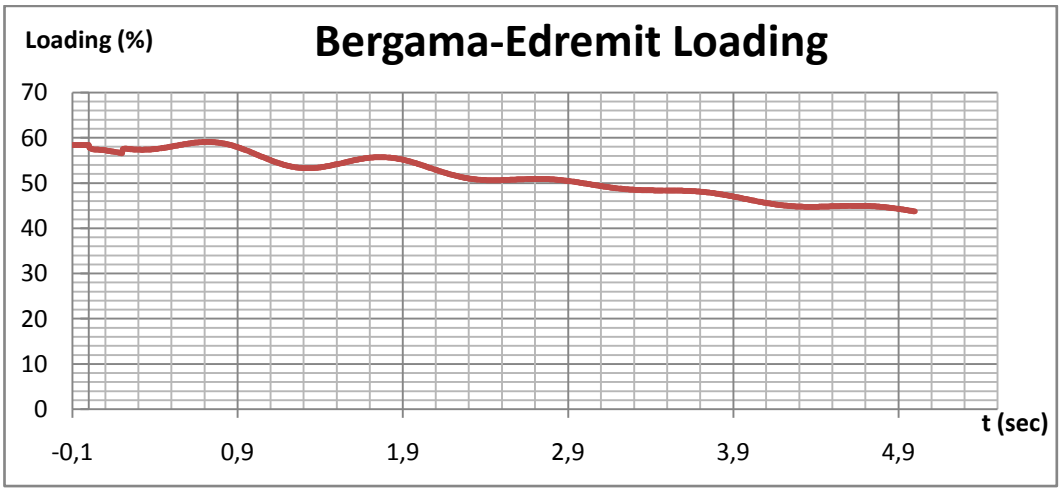

Graph 4.14. Loading of Bergama-Edremit Line.

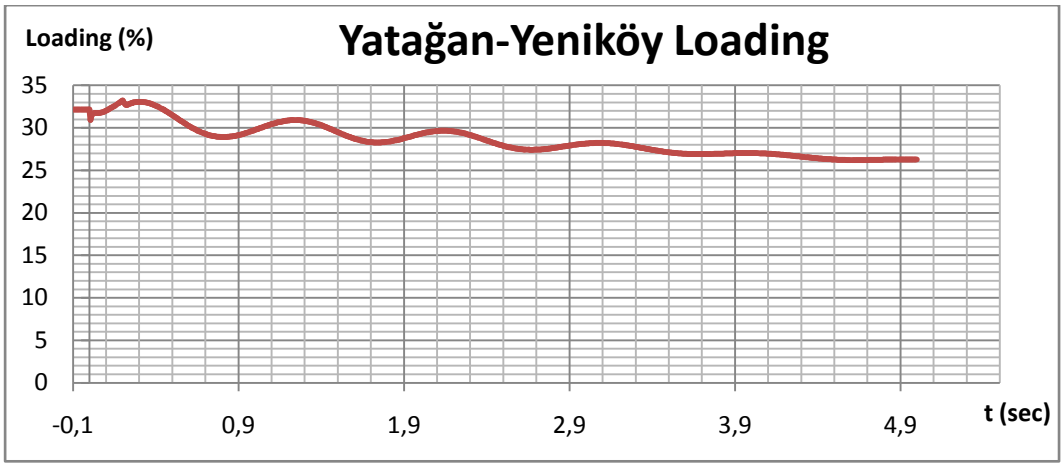

Graph 4.15. Loading of Yatagan-Yeniköy Line.

As can be seen from both graphs, the fault has caused a slight but immediate disturbance on the transmission lines. After the breaker operation, the line loadings have initially rose slightly and then, began decreasing to reach the new steady-state values. The loading values and pattern does not vary from previous cases significantly. Since all the transmission lines residing within 250 km radius of the fault point remained under %100 loading at any time before, during or after the fault, it is safe to claim that this case has no threat to the transmission lines by means of overloading.

Table 4.7 provides the initial (t= -0,1 sec.), final (t=5 sec) and maximum rotor angles for Kemerköy TPP during this case.

Table 4.7. Rotor Angle Values for Kemerköy TPP

	Kemerköy Rotor Angle (rad)
Initial	1.3093
Final	1.3785
Maximum	1.3787

As can be seen from Table 4.7 the initial and final values of rotor angle differ only by a small amount (approximately 4,01^{o}) and the simulation results verify that the generator stays in synchronism with the system without any adverse effect. It should however, be noted that the maximum value does not occur at t=5 sec. but instead, at an earlier time, t= 4.207 sec.

Taking the results provided above into consideration, the variations in bus voltages, line loadings and rotor angles are proven to stay within the limits to ensure a stable operation of the system.

4.1.1.4 Breaker operating time: 500 ms

500 milliseconds can still be assumed to be a typical fault clearing time for most relay-circuit breaker coordination. For this circuit breaker operation time, the variations of selected bus voltages are provided in graphs 4.16 to 4.18.

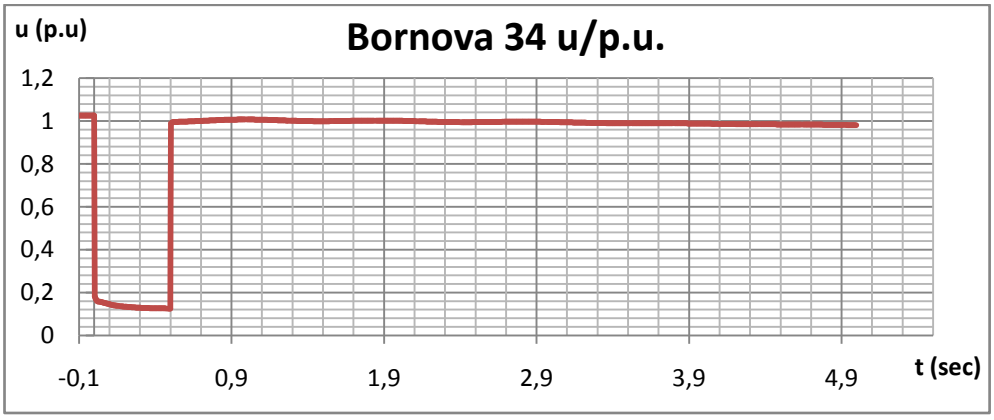

Graph 4.16. Voltage Variation Bornova 34 Bus.

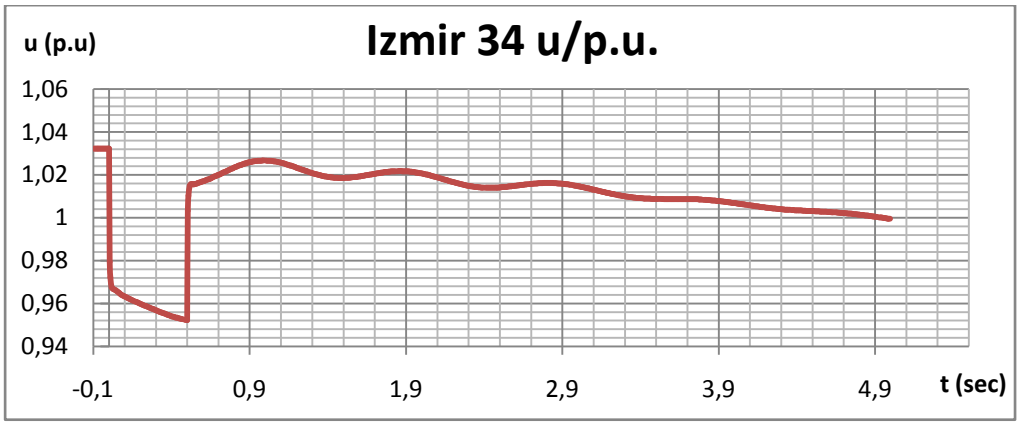

Graph 4.17. Voltage Variation of Izmir 34 Bus.

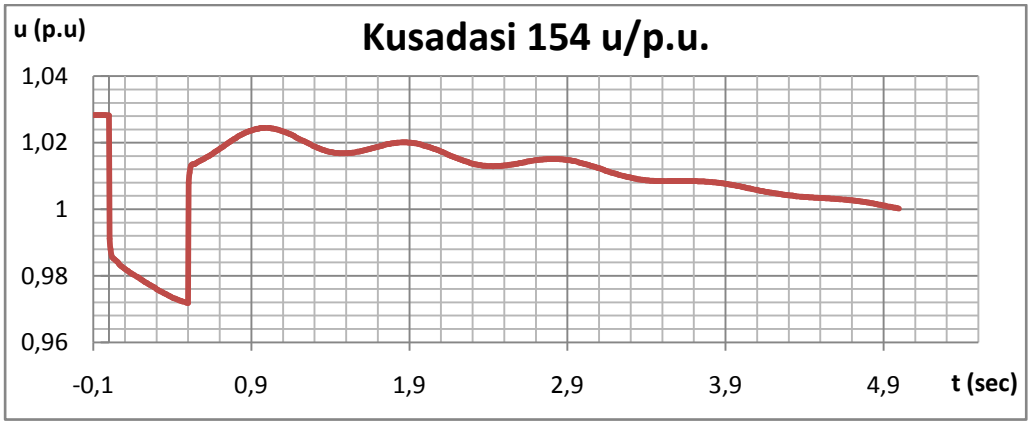

Graph 4.18. Voltage Variation of Kuşadası 154 Bus

As can be seen from the three graphs above, the disturbance had a drastic and almost immediate effect on the bus voltages which caused the voltages at nearby buses to drop sharply. However, the size of the drop varied between different buses and mainly influenced by the connection strength and distance to the location of fault. What is more, unlike previous cases, due to later breaker operating time, the voltages at each bus have continued to drop further until the fault is cleared. This phenomenon also occurred in previous cases but, due to short fault clearing time, the effect of it was relatively smaller, thus harder to observe. Bornova 34 bus, being the closest one

to the fault has suffered from the largest voltage drop in the event of a 3-phase short circuit.

It can be seen that, at t=0.5 sec. the voltages at each bus rises sharply since the circuit breakers at the ends of faulted line are operated, thus, returning the rest of the system to fault-free state. However, the voltage values are not constant at the post-fault state until the new stable system operating state is fully reached. During this state, the oscillations of the voltage values at each bus can be seen. The maximum and minimum values of bus voltages after the fault clearing, as well as their difference in p.u. are provided in Table 4.8.

Table 4.8. Bus Voltages for Case 1.1.4.

	Bornova 34	Izmir 34	Kusadasi 154
Vmax	1.002	1.0207	1.0187
Vmin	0.9813	0.9995	1.0002
Difference	0.0207	0.0212	0.0185
Vfinal	0.9813	0.9995	1.0002

As Table 4.8 clearly shows, the final values at the end of 5 seconds after the fault are, again, within the normal operational limits. Moreover the voltage oscillatory peak for all buses are well below the specified %10 limit for this case. The oscillation magnitude has almost remained the same when compared to the case 4.1.1.3 .Therefore it can be concluded that, the oscillations in bus voltages does not vary considerably for the two different circuit breaker operation times.

The line loadings before, during and after the fault are also recorded and the related graphs are provided for lines Bergama-Edremit 154 and Yatagan-Yeniköy in graphs 4.19 and 4.20, respectively.

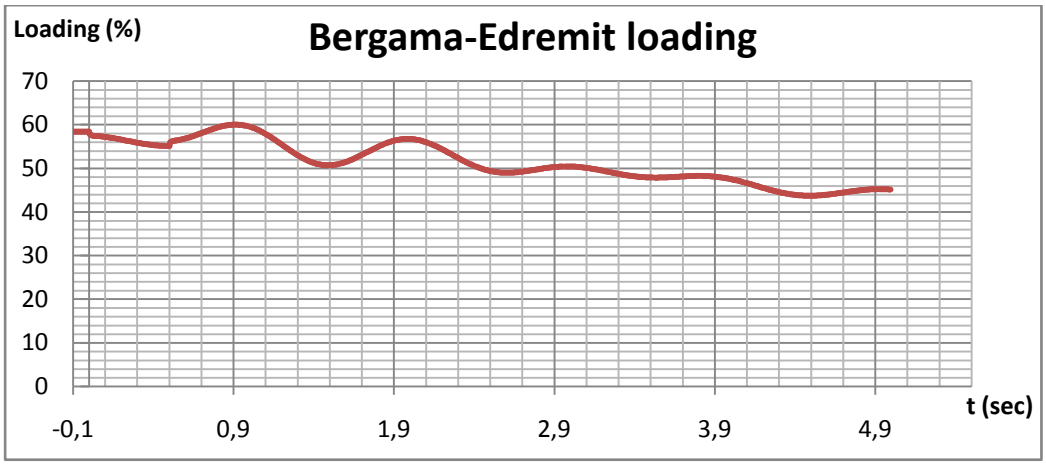

Graph 4.19. Loading of Bergama-Edremit Line.

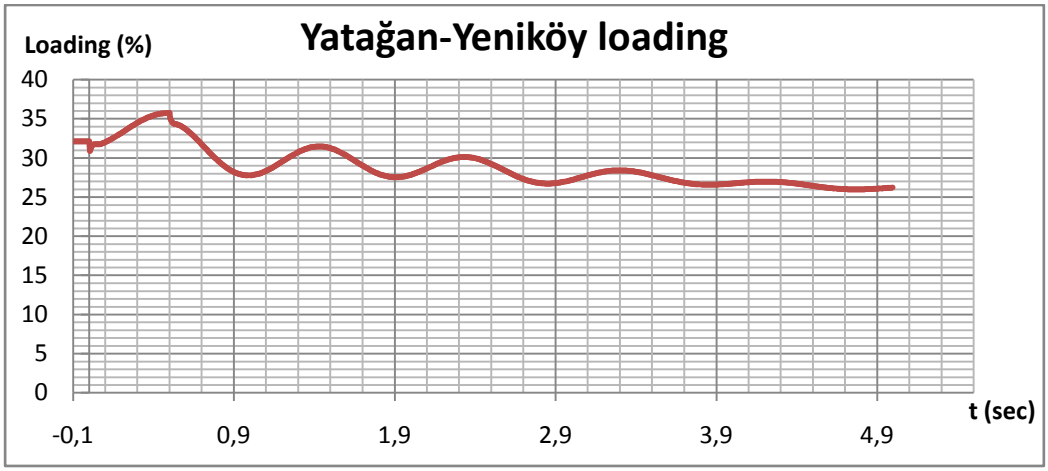

Graph 4.20. Loading of Yatagan-Yeniköy Line.

As can be seen from both graphs, the fault has caused a slight but immediate disturbance on the transmission lines. After the breaker operation, the line loadings have shown a slight step response and then, began decreasing to reach the new steady-state values with an attenuating oscillation pattern. The loading values and pattern do not vary from previous cases significantly. Since all the transmission lines residing within 250 km radius of the fault point remained under %100 loading at any

time before, during or after the fault, it is safe to claim that this case has no threat to the transmission lines by means of overloading.

Table 4.9 provides the initial (t= -0,1 sec.), final (t=5 sec) and maximum rotor angles for Kemerköy TPP during this case.

Table 4.9. Rotor Angle Values for Kemerköy TPP

	Kemerköy Rotor Angle (rad)
Initial	1.3093
Final	1.3597
Maximum	1.3723

As can be seen from Table 4.9 the initial and final values of rotor angle differ only by a small amount (approximately 2,89^{o}) and the simulation results verify that the generator stays in synchronism with the system without any adverse effect. It should however, be noted that the maximum value does not occur at t=5 sec. but instead, at an earlier time, t= 0.9853 sec.

Taking the results provided above into consideration, the variations in bus voltages, line loadings and rotor angles are proven to stay within the limits to ensure a stable operation of the system.

4.1.1.5 Breaker operating time: 1000 ms

1000 milliseconds is the maximum fault clearing time allowed by Turkish grid code for 3-phase to ground faults. Therefore, it is the worst-case for normal circuit breaker operating conditions which may incur in cases where the main circuit breaker may fail to operate or a delay in the related relay takes place. For this circuit breaker operation time, the variations of selected bus voltages are provided below.

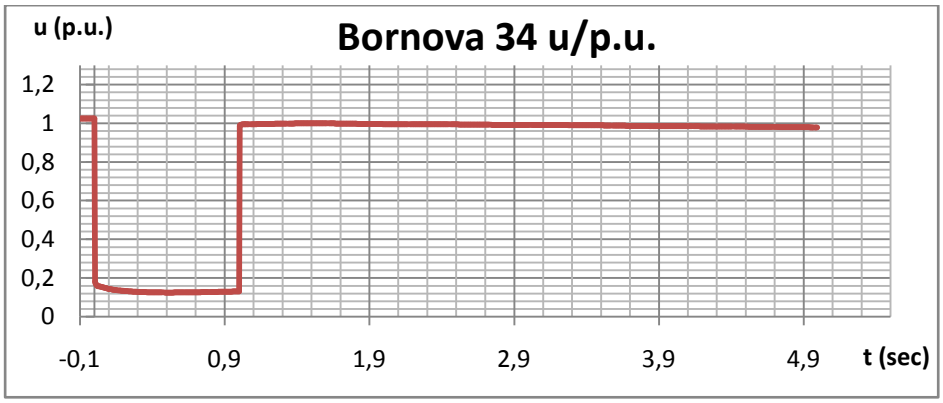

Graph 4.21. Voltage Variation of Bornova 34 Bus

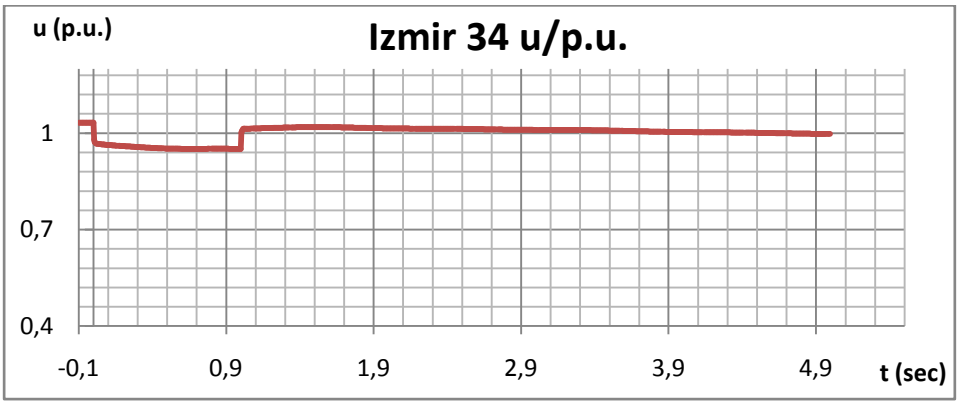

Graph 4.22. Voltage Variation of Izmir 34 Bus

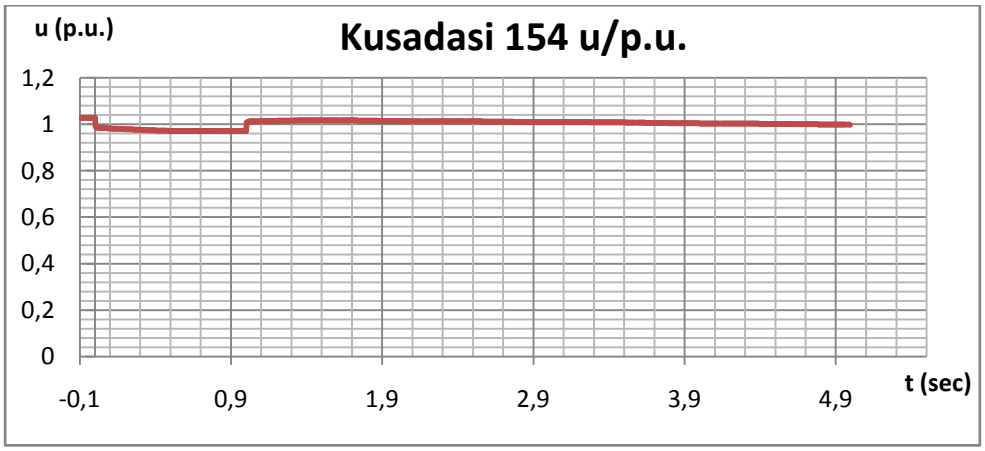

Graph 4.23. Voltage Variation of Kuşadası 154 Bus

As can be seen from the three graphs above, the disturbance had a drastic and almost immediate effect on the bus voltages which caused the voltages at nearby buses to drop sharply. However, the size of the drop varied between different buses and mainly influenced by the connection strength and distance to the location of fault. What is more, due to elongated breaker operating time, the voltages at each bus have continued to drop further until the fault is cleared. Bornova 34 bus, being the closest one to the fault has suffered from the largest voltage drop in the event of a 3-phase short circuit.

It can be seen that, at t=1 sec. the voltages at each bus rises sharply since the circuit breakers at the ends of faulted line are operated, thus, returning the rest of the system to fault-free state. However, the voltage values are not constant at the post-fault state until the new stable system operating state is fully reached. During this state, the oscillations of the voltage values at each bus can be seen. The maximum and minimum values of bus voltages after the fault clearing, as well as their difference in p.u. are provided in Table 4.10.

Table 4.10. Bus Voltages for Case 1.1.5.

	Bornova 34	Izmir 34	Kusadasi 154
Vmax	1	1.019	1.0175
Vmin	0.9792	0.9974	0.9982
Difference	0.0208	0.0216	0.0193
Vfinal	0.9792	0.9974	0.9982

As Table 4.10 clearly shows, the final values at the end of 5 seconds after the fault are, again, within the normal operational limits. Moreover the voltage oscillatory peak for all buses are well below the specified %10 limit for this case. The oscillation magnitude has increased slightly when compared to case 4.1.1.4 .It can still be claimed that, the oscillations in bus voltages does not vary considerably for

the two different circuit breaker operation times. For this reason, unless the oscillations approach the %10 limit, the circuit breaker operation time has little effect on determining the system security and quality of electricity by means of voltages at buses. The line loadings before, during and after the fault are also recorded and the related graphs are provided for lines Bergama-Edremit 154 and Yatagan-Yeniköy in graphs 4.24 and 4.25, respectively.

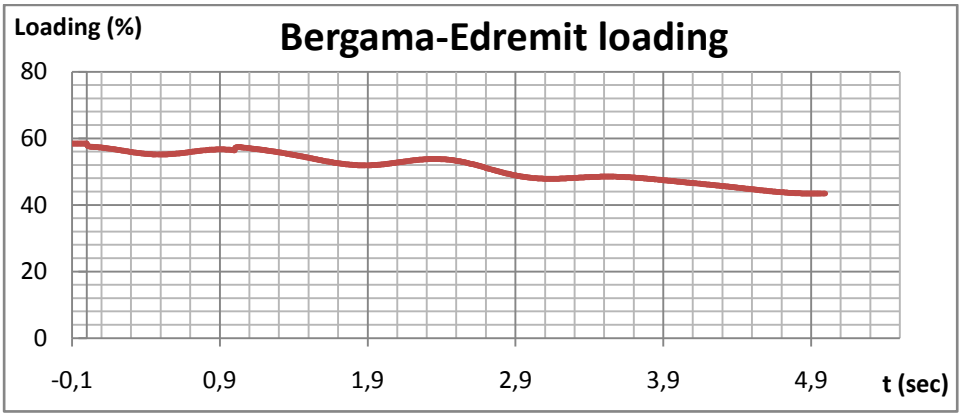

Graph 4.24. Loading of Bergama-Edremit Line.

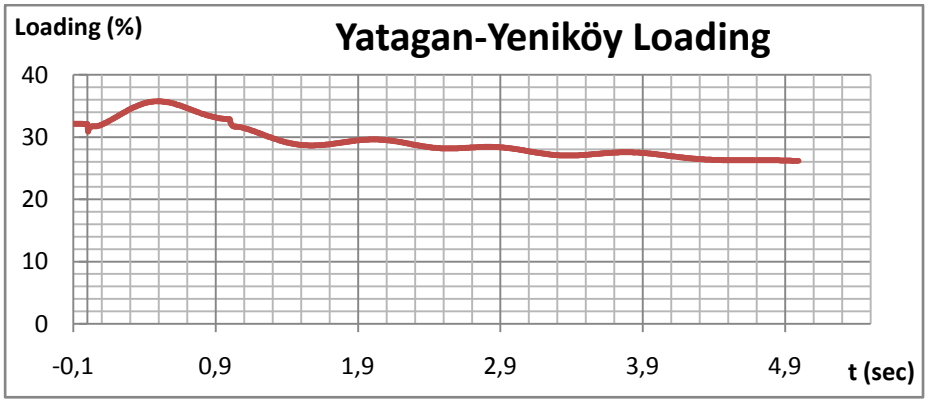

Graph 4.25. Loading of Yatagan-Yeniköy Line.

As can be seen from both graphs, the fault has caused a slight but immediate disturbance on the transmission lines. After the breaker operation, the line loadings have initially changed slightly and then, began decreasing to reach the new steady-state values with an attenuating oscillation pattern. The loading values and pattern do not vary from previous cases significantly. Since all the transmission lines residing within 250 km radius of the fault point remained under %100 loading at any time before, during or after the fault, it is safe to claim that this case has no threat to the transmission lines by means of overloading.

Table 4.11 provides the initial (t= -0,1 sec.), final (t=5 sec) and maximum rotor angles for Kemerköy TPP during this case.

Table 4.11. Rotor Angle Values for Kemerköy TPP

	Kemerköy Rotor Angle (rad)
Initial	1.3093
Final	1.3756
Maximum	1.3870

As can be seen from Table 4.11 the initial and final values of rotor angle differ only by a small amount (approximately 4^{o}) and the simulation results verify that the generator stays in synchronism with the system without any adverse effect. It should however, be noted that the maximum value does not occur at t=5 sec. but instead, at an earlier time, t= 4.698 sec.

Taking the results provided above into consideration, the variations in bus voltages, line loadings and rotor angles are proven to stay within the limits to ensure a stable operation of the system.

As cases 4.1.1.1 through 4.1.1.5 are taken under spotlight, it is seen that the breaker operation times have a small effect on the bus voltage pattern, line loadings and rotor angle variations. Despite not being negligible, these variations can be assumed to be of little importance unless stability limits are approached. For this reason and to ensure a compact presentation of results, the analysis results will be provided for the highest circuit breaker operation time, 1 seconds, for the rest of this section unless otherwise stated. This operation time is also the maximum allowed breaker operation time according to Turkish grid code [53] and therefore, the conditions for system stability and power quality need to be satisfied for this operating time.

4.1.2: %7,5 (164 MW) Installed capacity

Breaker operating time: 1000 ms

For the given fault clearing time, the variations of selected bus voltages are provided in Graphs 4.26 to 4.28.

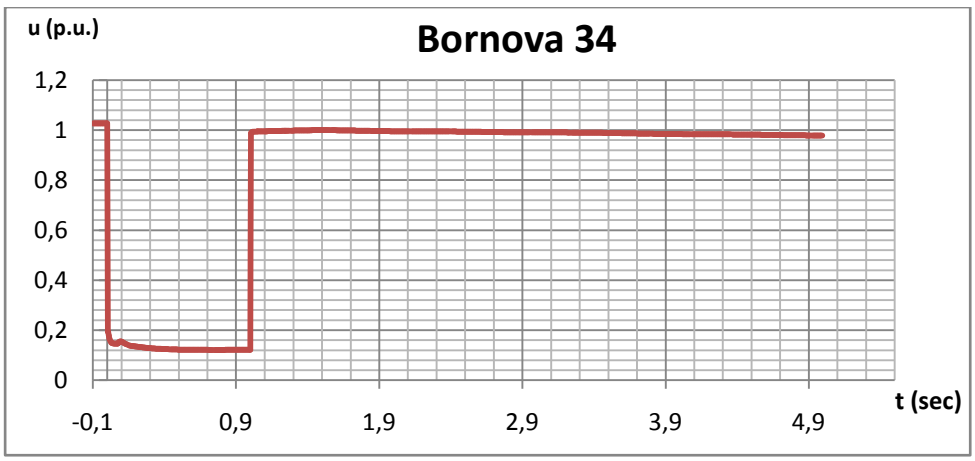

Graph 4.26. Voltage Variation of Bornova 34 Bus

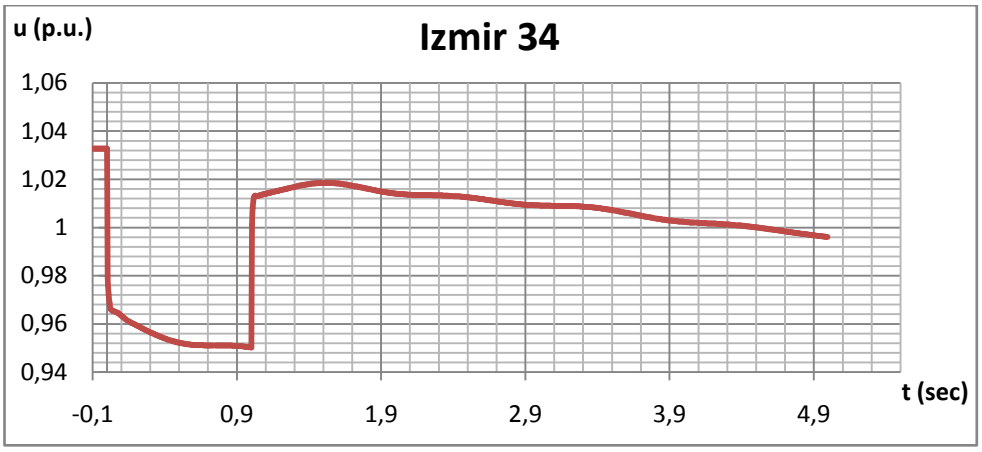

Graph 4.27. Voltage Variation of Izmir 34 Bus

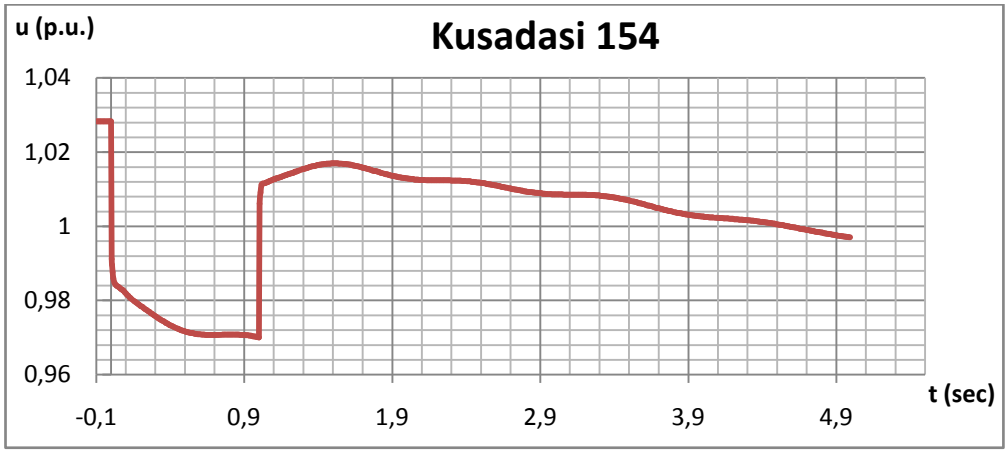

Graph 4.28. Voltage Variation of Kusadasi 154 Bus

As can be seen from the three graphs above, the disturbance had a drastic and almost immediate effect on the bus voltages which caused the voltages at nearby buses to drop sharply. However, the size of the drop varied between different buses and mainly influenced by the connection strength and distance to the location of fault. Bornova 34 bus, being the closest one to the fault has suffered from the largest voltage drop in the event of a 3-phase short circuit.

It can be seen that, at t=1 sec. the voltages at each bus rises sharply since the circuit breakers at the ends of faulted line are operated, thus, returning the rest of the system to fault-free state. However, the voltage values are not constant at the post-fault state until the new stable system operating state is fully reached. During this state, the oscillations of the voltage values at each bus can be seen. The maximum and minimum values of bus voltages after the fault clearing, as well as their difference in p.u. are provided in Table 4.12.

Table 4.12. Bus Voltages for Case 1.2

	Bornova 34	Izmir 34	Kusadasi 154
Vmax	0.9996	1.0185	1.017
Vmin	0.978	0.9961	0.997
Difference	0.0216	0.0224	0.02
Vfinal	0.978	0.9961	0.997

As Table 4.12 clearly shows, the final values at the end of 5 seconds after the fault are within the normal operational limits. Moreover the voltage oscillatory peak for all buses are well below the specified %10 limit for this case.

The line loadings before, during and after the fault are also recorded and the related graphs are provided for lines Bergama-Edremit 154 and Yatagan-Yeniköy in graphs 4.29 and 4.30, respectively.

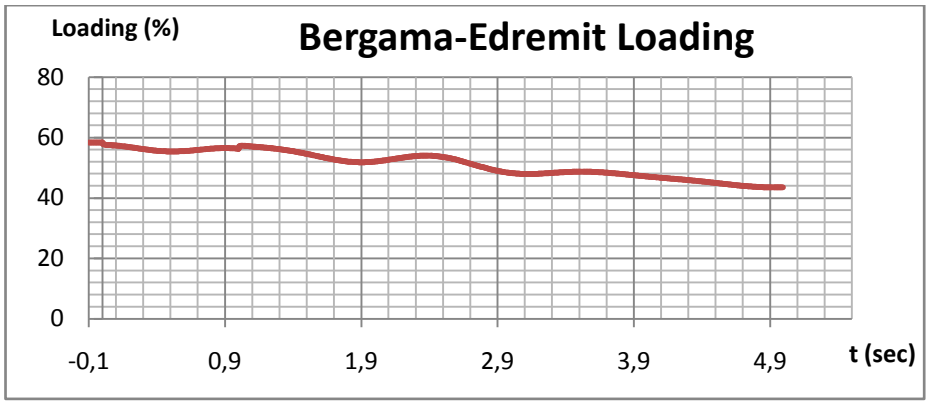

Graph 4.29. Loading of Bergama-Edremit Line

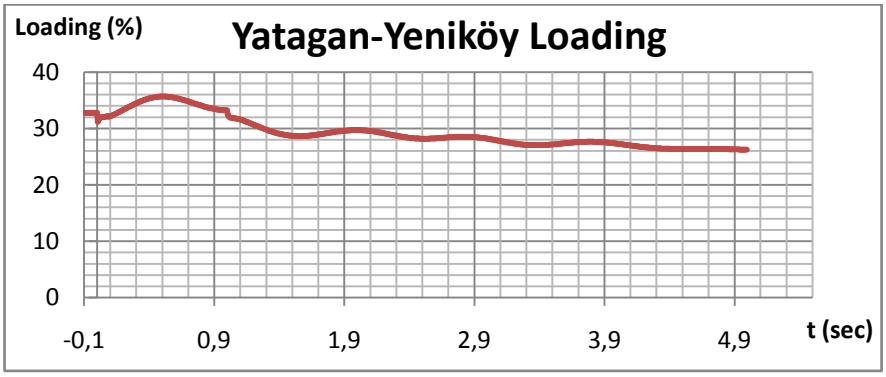

Graph 4.30. Loading of Yatagan-Yeniköy Line.

As can be seen from both graphs, the fault has caused a slight but immediate disturbance on the transmission lines. Since all the transmission lines residing within 250 km radius of the fault point remained under %100 loading at any time before, during or after the fault, it is safe to claim that this case has no threat to the transmission lines by means of overloading.

Table 4.13 provides the initial (t= -0,1 sec.), final (t=5 sec) and maximum rotor angles for Kemerköy TPP during this case.

Table 4.13. Rotor Angle Values for Kemerköy TPP

	Kemerköy Rotor Angle (rad)
Initial	1.2952
Final	1.3632
Maximum	1.3741

As can be seen from Table 4.13 the initial and final values of rotor angle differ only by a small amount (approximately 4^{o}) and the simulation results verify that the generator stays in synchronism with the system without any adverse effect.

Taking the results provided above into consideration, the variations in bus voltages, line loadings and rotor angles are proven to stay within the limits to ensure a stable operation of the system even the %5 limit of the short circuit capacity at related bus is exceeded by a factor of 1,5. Moreover, the observed parameter variations are considerably far from approaching the stability limits therefore they imply that the system may be able to handle disturbances for even higher values of installed capacity of the wind farm. This implication will prove true in the next analysis, involving a wind farm installed capacity equal to %10 of the short circuit MVA of the connecting bus.

4.1.3: %10 (219 MW) Installed capacity

Breaker operating time: 1000 ms

For the given fault clearing time, the variations of selected bus voltages are provided in graphs 4.31 to 4.33.

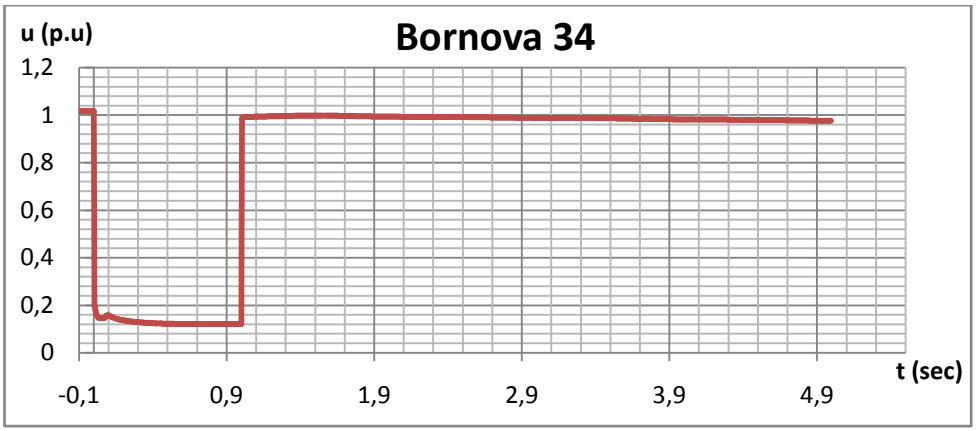

Graph 4.31 Voltage Variation of Bornova 34 Bus

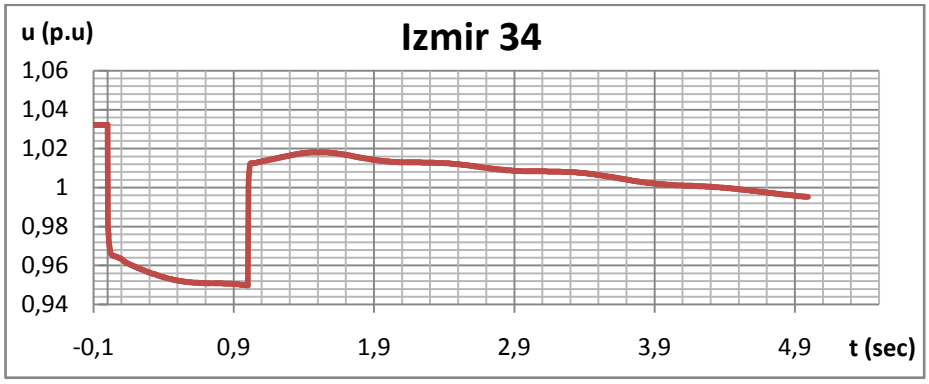

Graph 4.32. Voltage Variation of Izmir 34 Bus

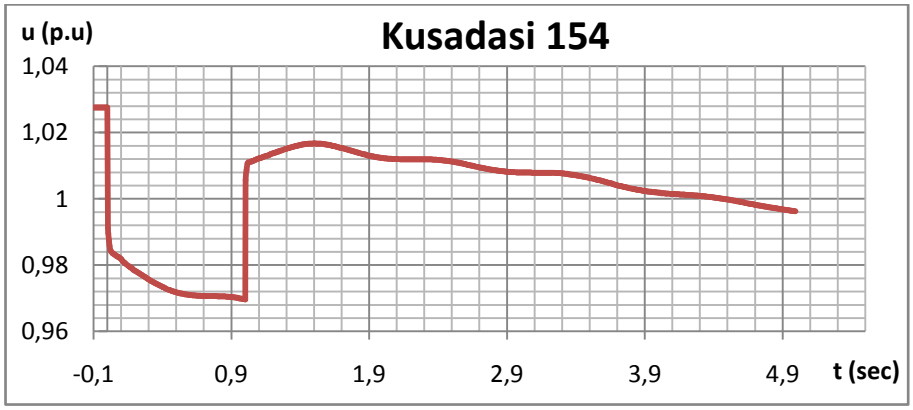

Graph 4.33. Voltage Variation of Kusadasi 154 Bus

As can be seen from the three graphs above, the disturbance had a drastic and almost immediate effect on the bus voltages which caused the voltages at nearby buses to drop sharply. However, the size of the drop varied between different buses and mainly influenced by the connection strength and distance to the location of fault. Bornova 34 bus, being the closest one to the fault has suffered from the largest voltage drop in the event of a 3-phase short circuit.

It can be seen that, at t=1 sec. the voltages at each bus rises sharply since the circuit breakers at the ends of faulted line are operated, thus, returning the rest of the system to fault-free state. However, the voltage values are not constant at the post-fault state until the new stable system operating state is fully reached. During this state, the oscillations of the voltage values at each bus can be seen. The maximum and minimum values of bus voltages after the fault clearing, as well as their difference in p.u. are provided in Table 4.14

Table 4.14. Bus Voltages for Case 1.3

	Bornova 34	Izmir 34	Kusadasi 154
Vmax	0.9985	1.0181	1.0167
Vmin	0.9764	0.9952	0.9962
Difference	0.0221	0.0229	0.0205
Vfinal	0.9764	0.9952	0.9962

As Table 4.14 clearly shows, the final values at the end of 5 seconds after the fault are within the normal operational limits. Moreover the voltage oscillatory peak for all buses are still well below the specified %10 limit for this case.

The line loadings before, during and after the fault are also recorded and the related graphs are provided for lines Yatagan-Yeniköy and Bergama-Edremit 154 in graphs 4.34 and 4.35, respectively.

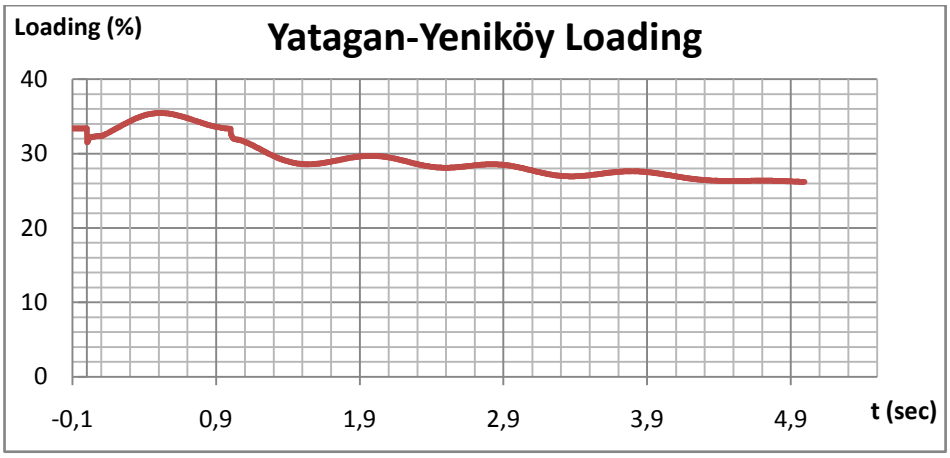

Graph 4.34. Loading of Yatagan-Yeniköy Line.

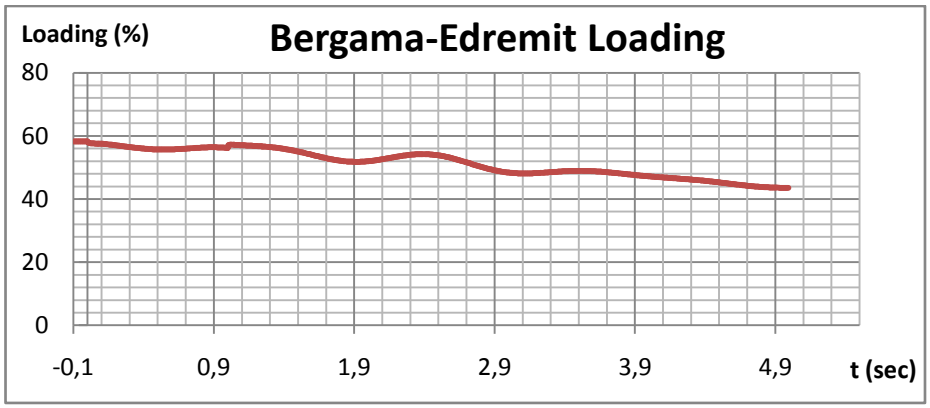

Graph 4.35. Loading of Bergama-Edremit Line.

As can be seen from both graphs, the fault has caused a slight but immediate disturbance on the transmission lines. After the breaker operation, the line loadings have initially shown a slight step response and then, began decreasing to reach the new steady-state values. Since all the transmission lines residing within 250 km radius of the fault point remained under %100 loading at any time before, during or after the fault, it is safe to claim that this case has no threat to the transmission lines by means of overloading. Table 4.15 provides the initial (t= -0,1 sec.), final (t=5 sec) and maximum rotor angles for Kemerköy TPP during this case.

Table 4.15. Rotor Angle Values for Kemerköy TPP

	Kemerköy Rotor Angle (rad)
Initial	1.2827
Final	1.3542
Maximum	1.3642

As can be seen from Table 4.15 the initial and final values of rotor angle differ only by a small amount (approximately $4{,}1^{o}$) and the simulation results verify that the generator stays in synchronism with the system without any adverse effect. Note that the initial and final angles are not necessarily the same as cases with different installed capacities since the overall system operation is affected by the power generation of the wind farm.

Taking the results provided above into consideration, the variations in bus voltages, line loadings and rotor angles are proven to stay within the limits to ensure a stable operation of the system even the %5 limit of the short circuit capacity at related bus is exceeded by a factor of 2. Moreover, the observed parameter variations are considerably far from approaching the stability limits therefore they imply that the system may be able to handle disturbances for even higher values of installed capacity of the wind farm. This implication will prove true in the next analysis, involving a wind farm installed capacity equal to %12.5 of the short circuit MVA of the connecting bus.

4.1.4: %12,5 (273 MW) Installed capacity

Breaker operating time: 1000 ms

For the given fault clearing time, the variations of selected bus voltages are provided in graphs 4.36 to 4.38.

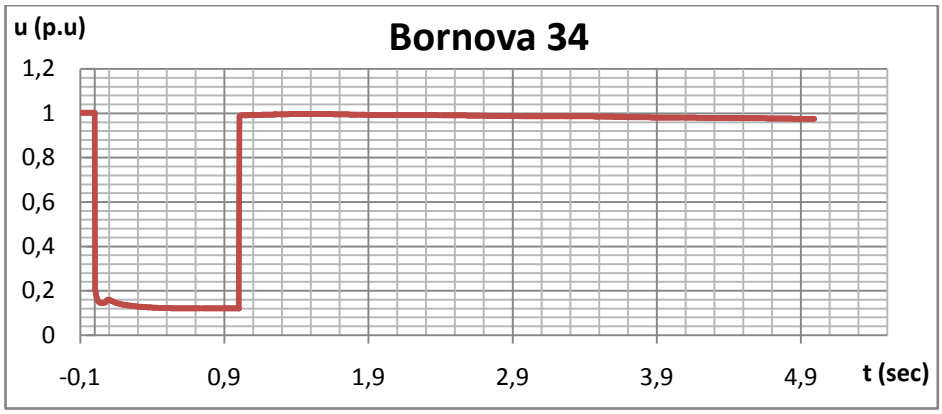

Graph 4.36. Voltage Variation of Bornova 34 Bus

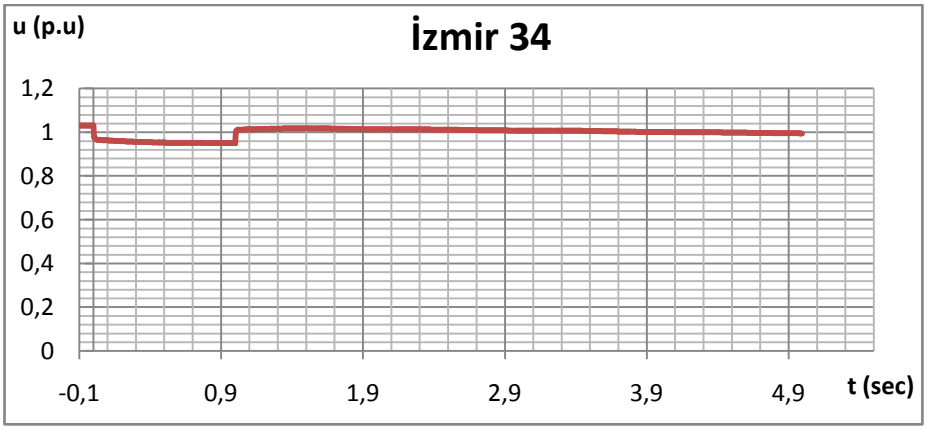

Graph 4.37. Voltage Variation of Izmir 34 Bus

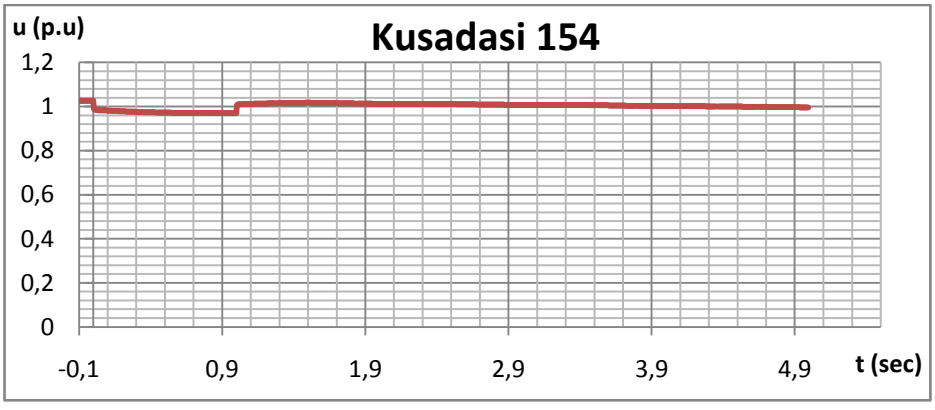

Graph 4.38. Voltage Variation of Kusadasi 154 Bus

As can be seen from the three graphs above, the disturbance had a drastic and almost immediate effect on the bus voltages which caused the voltages at nearby buses to drop sharply. However, the size of the drop varied between different buses and mainly influenced by the connection strength and distance to the location of fault. Bornova 34 bus, being the closest one to the fault has suffered from the largest voltage drop in the event of a 3-phase short circuit.

It can be seen that, at t=1 sec. the voltages at each bus rises sharply since the circuit breakers at the ends of faulted line are operated, thus, returning the rest of the system to fault-free state. However, the voltage values are not constant at the post-fault state until the new stable system operating state is fully reached. During this state, the oscillations of the voltage values at each bus can be seen. The maximum and minimum values of bus voltages after the fault clearing, as well as their difference in p.u. are provided in Table 4.16

Table 4.16. Bus Voltages for Case 1.4

	Bornova 34	Izmir 34	Kusadasi 154
Vmax	0.997	1.0177	1.0164
Vmin	0.9747	0.9945	0.9957
Difference	0.0223	0.0232	0.0207
Vfinal	0.9747	0.9945	0.9957

As Table 4.16 clearly shows, the final values at the end of 5 seconds after the fault are within the normal operational limits. Moreover the voltage oscillatory peak for all buses are still well below the specified %10 limit for this case.

The line loadings before, during and after the fault are also recorded and the related graphs are provided for lines Bergama-Edremit 154 and Yatagan-Yeniköy in graphs 4.39 and 4.40, respectively.

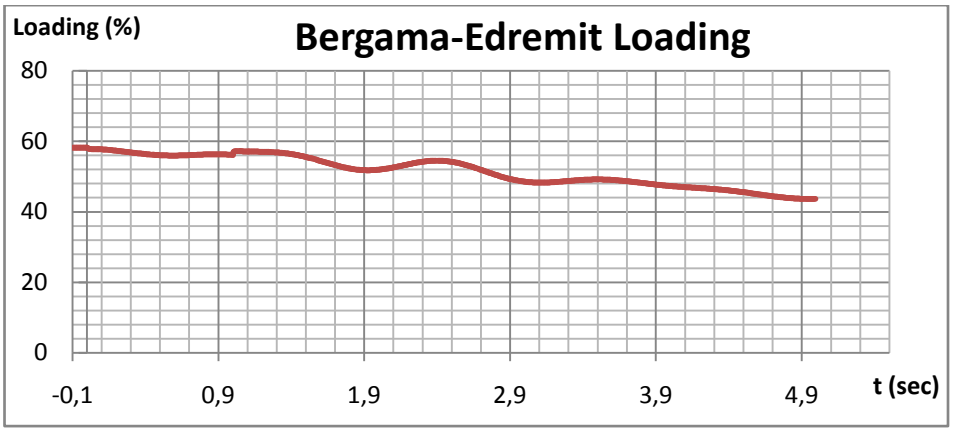

Graph 4.39. Loading of Bergama-Edremit Line.

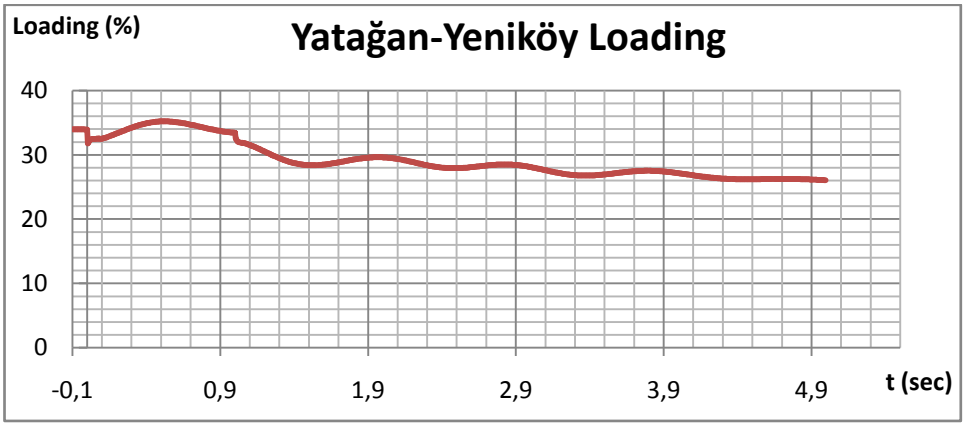

Graph 4.40. Loading of Yatagan-Yeniköy Line

As can be seen from both graphs, the fault has caused a slight but immediate disturbance on the transmission lines. After the breaker operation, the line loadings have changed very slightly and then, began decreasing to reach the new steady-state values. Since all the transmission lines residing within 250 km radius of the fault point remained under %100 loading at any time before, during or after the fault, it is safe to claim that this case has no threat to the transmission lines by means of overloading.

Table 4.17 provides the initial (t= -0,1 sec.), final (t=5 sec) and maximum rotor angles for Kemerköy TPP during this case.

Table 4.17. Rotor Angle Values for Kemerköy TPP

	Kemerköy Rotor Angle (rad)
Initial	1.2739
Final	1.3519
Maximum	1.3605

As can be seen from Table 4.17 the initial and final values of rotor angle differ only by a small amount (approximately 4,47^{o}) and the simulation results verify that the generator stays in synchronism with the system without any adverse effect. Note that the initial and final angles are not necessarily the same as cases with different installed capacities since the overall system operation is affected by the power generation of the wind farm.

Taking the results provided above into consideration, the variations in bus voltages, line loadings and rotor angles are proven to stay within the limits to ensure a stable operation of the system even the %5 limit of the short circuit capacity at related bus is exceeded by a factor of 2,5. Moreover, the observed parameter variations are considerably far from approaching the stability limits therefore they imply that the system may be able to handle disturbances for even higher values of installed capacity of the wind farm. This implication will prove true in the next analysis, involving a wind farm installed capacity equal to %15 of the short circuit MVA of the connecting bus.

4.1.5: %15 (328 MW) Installed capacity

Breaker operating time: 1000 ms

For the given fault clearing time, the variations of selected bus voltages are provided in graphs 4.41 to 4.43.

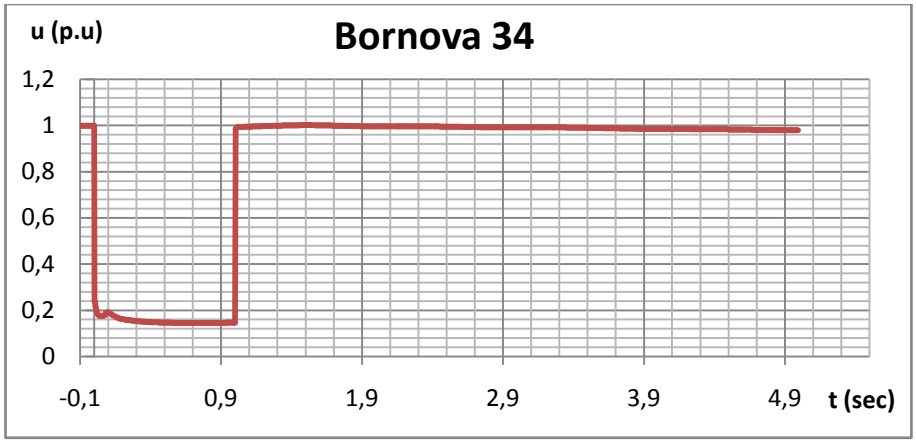

Graph 4.41. Voltage Variation of Bornova 34 Bus

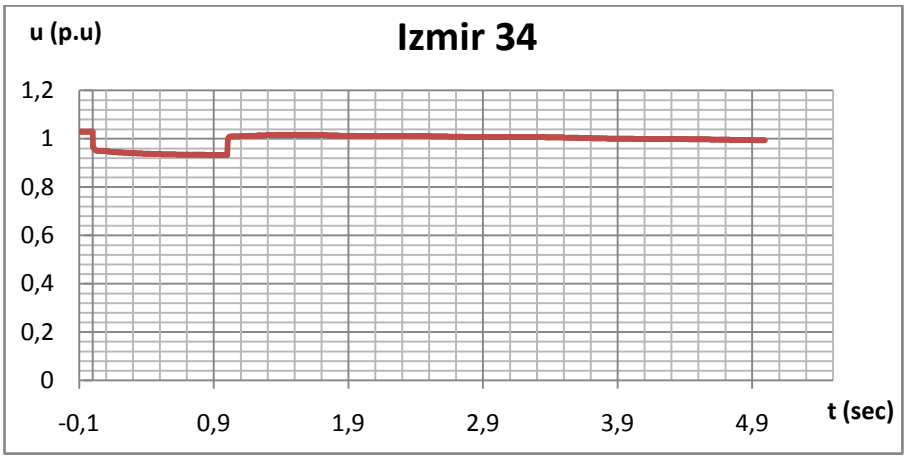

Graph 4.42. Voltage Variation of Izmir 34 Bus

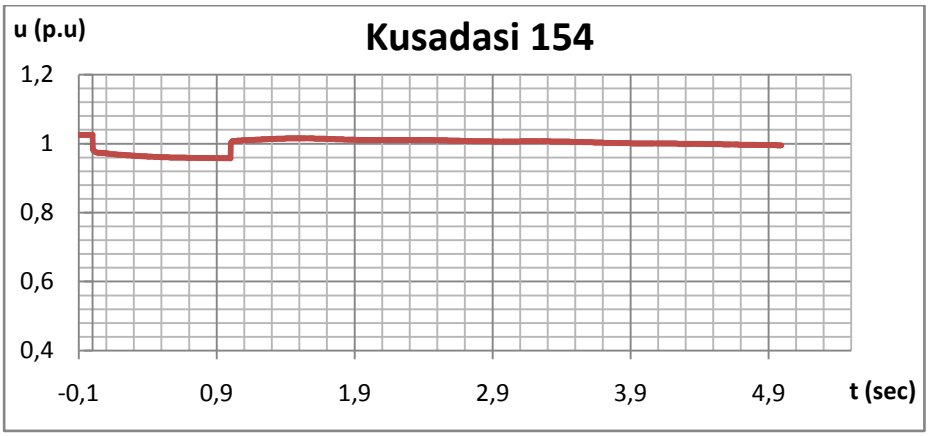

Graph 4.43. Voltage Variation of Kusadasi 154 Bus

As can be seen from the three graphs above, the disturbance had a drastic and almost immediate effect on the bus voltages which caused the voltages at nearby buses to drop sharply. However, the size of the drop varied between different buses and mainly influenced by the connection strength and distance to the location of fault. Bornova 34 bus, being the closest one to the fault has suffered from the largest voltage drop in the event of a 3-phase short circuit.

It can be seen that, at t=1 sec. the voltages at each bus rises sharply since the circuit breakers at the ends of faulted line are operated, thus, returning the rest of the system to fault-free state. However, the voltage values are not constant at the post-fault state until the new stable system operating state is fully reached. During this state, the oscillations of the voltage values at each bus can be seen. The maximum and minimum values of bus voltages after the fault clearing, as well as their difference in p.u. are provided in Table 4.18.

Table 4.18. Bus Voltages for Case 1.5.

	Bornova 34	Izmir 34	Kusadasi 154
Vmax	1.001	1.0292	1.0254
Vmin	0.9791	0.9939	0.9951
Difference	0.0219	0.0353	0.0303
Vfinal	0.9791	0.9939	0.9951

As Table 4.18 clearly shows, the final values at the end of 5 seconds after the fault are within the normal operational limits. Moreover the voltage oscillatory peak for all buses are still well below the specified %10 limit for this case.

The line loadings before, during and after the fault are also recorded and the related graphs are provided for lines Yatagan-Yeniköy and Bergama-Edremit 154 .in graphs 4.44 and 4.45, respectively.

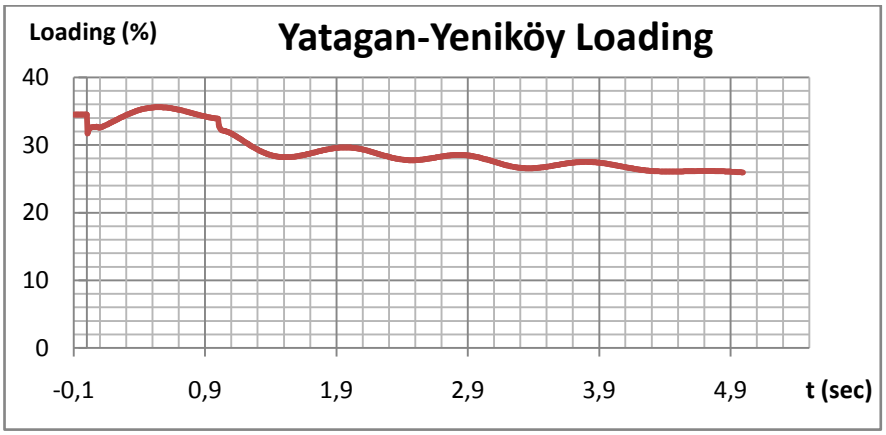

Graph 4.44. Loading of Yatagan-Yeniköy Line.

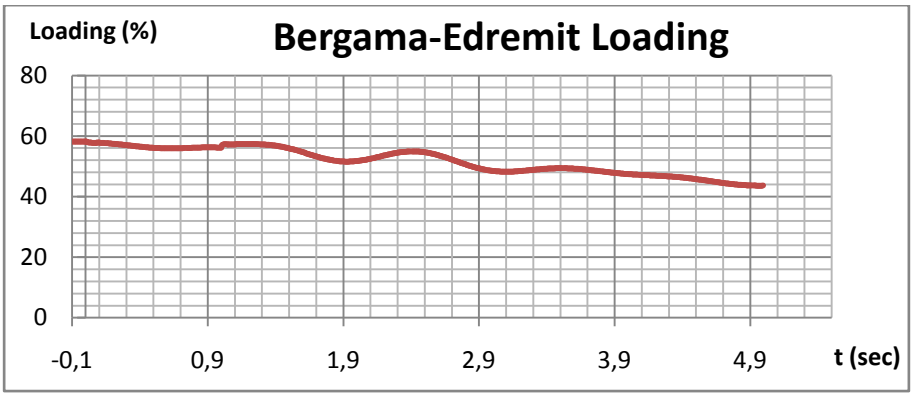

Graph 4.45. Loading of Bergama-Edremit Line

As can be seen from both graphs, the fault has caused a slight but immediate disturbance on the transmission lines. After the breaker operation, the line loadings have initially changed immediately but slightly and then, began decreasing to reach the new steady-state values. Since all the transmission lines residing within 250 km radius of the fault point remained under %100 loading at any time before, during or after the fault, it is safe to claim that this case has no threat to the transmission lines by means of overloading.

Table 4.19 provides the initial (t= -0,1 sec.), final (t=5 sec) and maximum rotor angles for Kemerköy TPP during this case.

Table 4.19. Rotor Angle Values for Kemerköy TPP

	Kemerköy Rotor Angle (rad)
Initial	1.2638
Final	1.3477
Maximum	1.3568

As can be seen from Table 4.19 the initial and final values of rotor angle differ only by a small amount (approximately 4,581^{o}) and the simulation results verify that the generator stays in synchronism with the system without any adverse effect. Note that the initial and final angles are not necessarily the same as cases with different installed capacities since the overall system operation is affected by the power generation of the wind farm.

Taking the results provided above into consideration, the variations in bus voltages, line loadings and rotor angles are proven to stay within the limits to ensure a stable operation of the system even the %5 limit of the short circuit capacity at related bus is exceeded by a factor of 3. Moreover, the observed parameter variations are considerably far from approaching the stability limits therefore they imply that the system may be able to handle disturbances for even higher values of installed capacity of the wind farm. The limits of stability will be tried to be found in the final sub-case of this analysis.

4.1.6: %27,5 (600 MW) Installed capacity

As the final analysis for this wind farm, the installed capacity is increased to a very high value, comparable with a medium-sized thermal power plant with the assumption that the wind power potential in the region is almost completely benefited from. The limit of 600 MW is primarily determined by the ratings of existing elements in the grid around the wind farm of interest. In other words, despite it is possible to increase the installed capacity even further, the transformers and transmission lines that will be responsible for transmitting the generated power to the rest of the grid are not able to carry higher amounts of power generated by the wind farm. Therefore, another analysis regarding the results of a 3-phase to ground fault in the case that a 600-MW wind farm exists in the region is carried out.

Breaker operating time: 120 ms

For the given fault clearing time, the variations of selected bus voltages are provided in graphs 4.46 to 4.48.

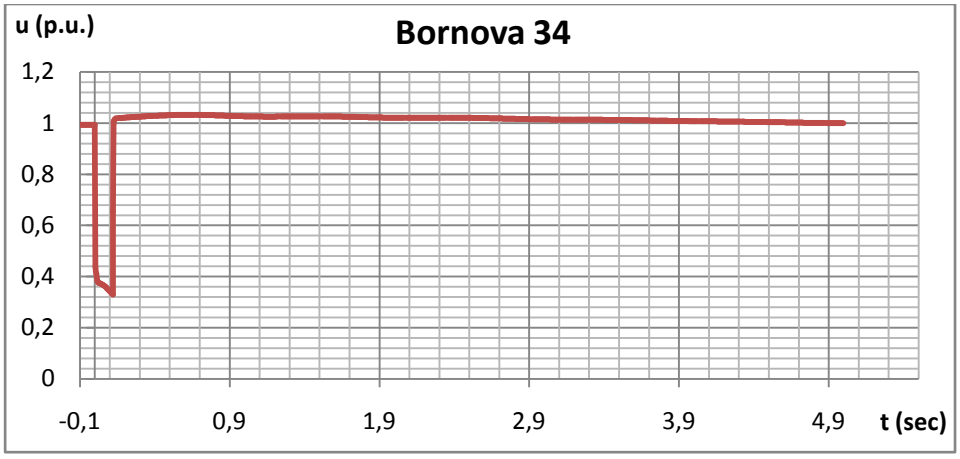

Graph 4.46. Voltage Variation of Bornova 34 Bus

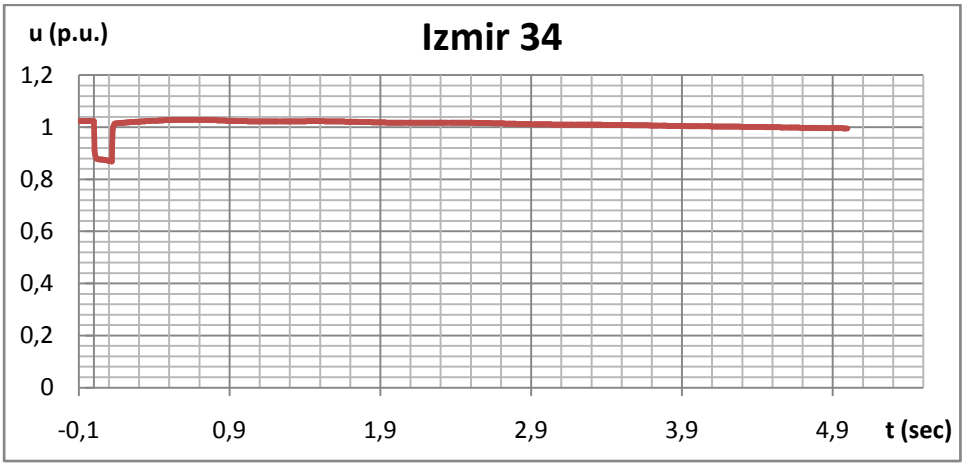

Graph 4.47. Voltage Variation of Izmir 34 Bus

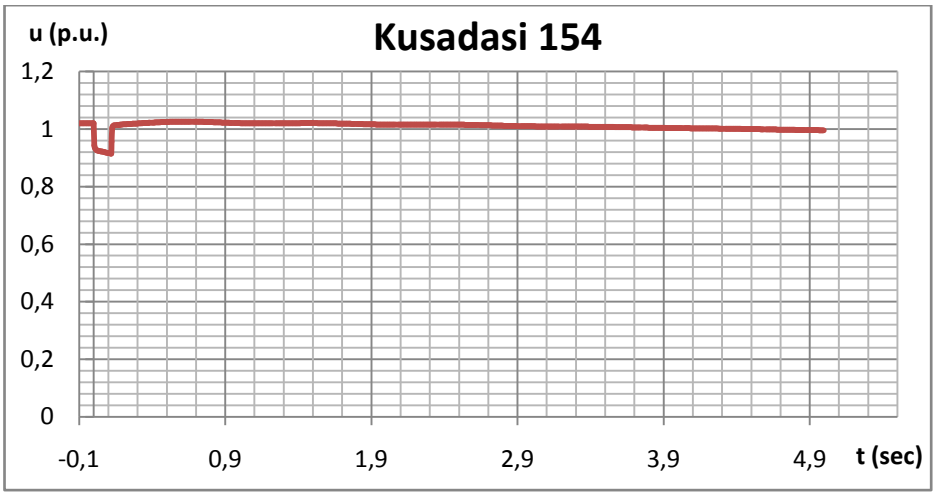

Graph 4.48. Voltage Variation of Kusadasi 154 Bus

As can be seen from the three graphs above, the disturbance had a drastic and almost immediate effect on the bus voltages which caused the voltages at nearby buses to drop sharply. However, the size of the drop varied between different buses and mainly influenced by the connection strength and distance to the location of fault. Bornova 34 bus, being the closest one to the fault has suffered from the largest voltage drop in the event of a 3-phase short circuit.

It can be seen that, at t=120 msec. the voltages at each bus rises sharply since the circuit breakers at the ends of faulted line are operated, thus, returning the rest of the system to fault-free state. However, the voltage values are not constant at the post-fault state until the new stable system operating state is fully reached. During this state, the oscillations of the voltage values at each bus can be seen. The maximum and minimum values of bus voltages after the fault clearing, as well as their difference in p.u. are provided in Table 4.20.

Table 4.20. Bus Voltages for Case 1.6

	Bornova 34	Izmir 34	Kusadasi 154
Vmax	1.0324	1.0289	1.026
Vmin	0.9997	0.9958	0.9959
Difference	0.0327	0.0331	0.0301
Vfinal	0.9997	0.9958	0.9959

As Table 4.20 clearly shows, the final values at the end of 5 seconds after the fault are within the normal operational limits. Moreover the voltage oscillatory peak for all buses are still well below the specified %10 limit for this case.

The line loadings before, during and after the fault are also recorded and the related graphs are provided for lines Yatagan-Yeniköy and Bergama-Edremit 154 in graphs 4.49 and 4.50, respectively.

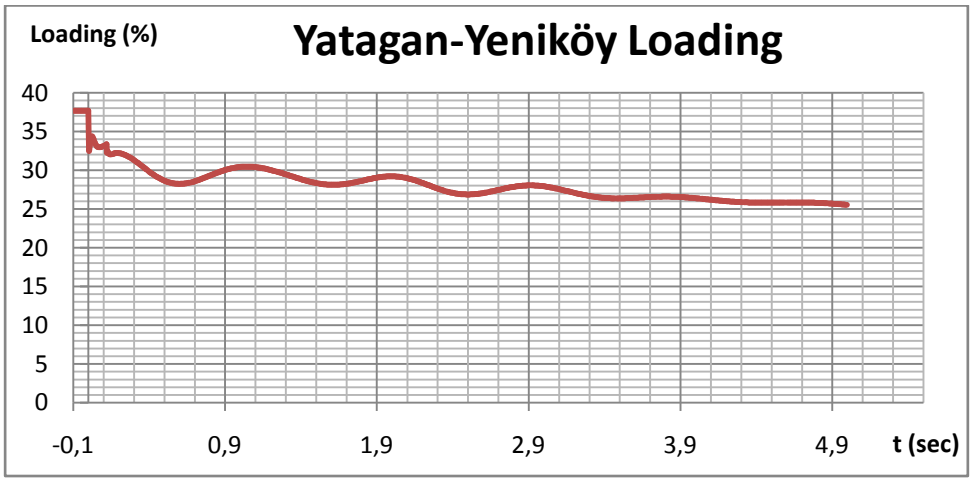

Graph 4.49. Loading of Yatagan-Yeniköy Line

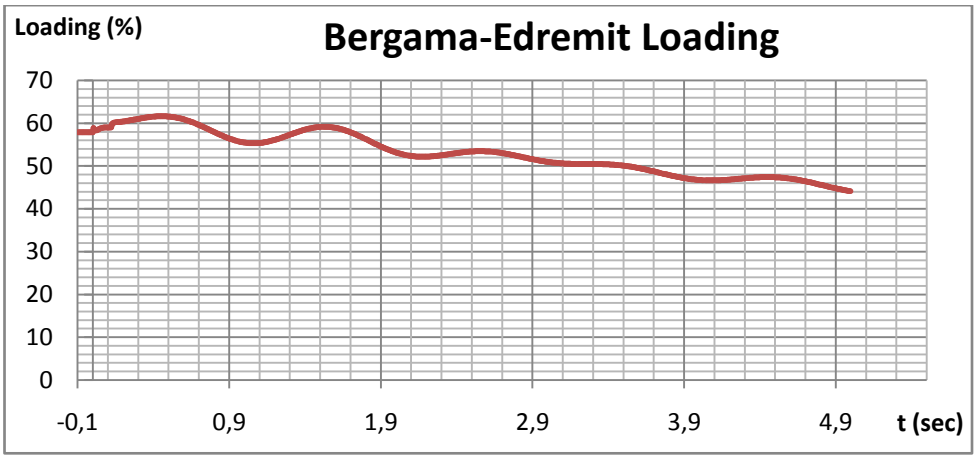

Graph 4.50. Loading of Bergama-Edremit Line

As can be seen from both graphs, the fault has caused a slight but immediate disturbance on the transmission lines. After the breaker operation, the line loadings have initially rose very slightly and then, began decreasing to reach the new steady-state values. Since all the transmission lines residing within 250 km radius of the fault point remained under %100 loading at any time before, during or after the fault, it is safe to claim that this case has no threat to the transmission lines by means of overloading.

Table 4.21 provides the initial (t= -0,1 sec.), final (t=5 sec) and maximum rotor angles for Kemerköy TPP during this case.

Table 4.21. Rotor Angle Values for Kemerköy TPP

	Kemerköy Rotor Angle (rad)
Initial	1.4459
Final	1.5817
Maximum	1.5817

As can be seen from Table 4.21 the initial and final values of rotor angle now differ considerably (approximately 9^o). Moreover, the final and maximum value of the rotor angle corresponds to 90,62 ^{o} which is above the limit for stability of 90^o. This occurrence is critical for it implies that Kemerköy's generators will go out of synchronization, finally resulting in loss of the generator, i.e. outage of Kemerköy TPP due to the generator slipping out of synchronization.

Taking the results provided above into consideration, despite the variations in bus voltages, line loadings are proven to stay within the limits to ensure a stable operation of the system in the event of a 3 phase to ground fault near the wind farm, the rotor angle variation of generators which exceed 90^o even after the fault which was cleared in 120 ms states that the system will be unable to preserve its solid structure and loss of nearby generators will occur which may have catastrophic effects on the overall grid such as black-outs or islanding for such a high-capacity (%27,5 of short circuit MVA at related bus) wind farm concentrated at this point in the grid.

4.2. Case 2: Mersin RES

The second case, Mersin RES is chosen to be demonstrated second since the grid around the area is argued to be relatively weak due to being on the south-end coast of the country with no connections from the southern side, yet due to large cities nearby, Mersin and Adana, the demand is relatively higher. Mersin wind farm is resided in Mut, a town within the limits of Mersin, the tenth largest city in Turkey. In the system, the wind farm is connected to the grid at Mersin 34.5 kV (denoted by Mersin 34 in the model) bus. Therefore, the connecting line is between the buses Mersin RES 34 and Mersin 34. The current installed capacity of Mersin RES (omitting the nearby wind farms which were actually included in the system model) is 42 MW. The short circuit power at Mersin 34 bus, on the other hand, is 2347 MVA [54]. If the wind farms included in the modeling are also considered, the total installed capacity of the wind farms that are denoted by Mersin RES in the model sum up to 87 MW. As can be inferred from its location, the grid where the wind farm is located

has both strong and weak points since despite being close to large consumption centers, the geographical location forces the grid to have connections from only three main directions, making Mersin as a semi-end point in the system. Despite being smaller in cumulative installed capacities when compared to western part of Turkey, the wind farm concentration in the southern part of the country is still comparably high, implying that the grid can be sufficiently strong to meet the increasing generation levels. For these reasons, the system strength around Mersin, and hence Mersin RES is expected to have both weak and strong points. This implies that, during simulations, the effects of disturbances will be comparable to what would be expected to be observed at weaker regions of the grid.

As mentioned in the preceding section, the analyses will be carried out for installed capacities of Mersin RES that will be equal to %5, %7.5, %10, %12.5 and %15 of the short circuit MVA at Mersin 34 bus. The installed capacity values corresponding to these percentages of short circuit power are given in Table 4.22

Table 4.22. Installed Capacity Values for Case 2

% of Ssc	5	7,5	10	12,5	15
Installed Capacity (MW)	117	176	235	293	352

The buses, transmission lines and generators within 250 km radius of the wind farm are chosen to be observed. However, to avoid overflow of output data, some elements among the initial set are omitted after they are proven not to show any significant variations during the analysis processes. The resulting set of elements to be observed and whose results will be provided in detail are given below.

-Buses (Voltages of) : Mersin 34, Adana 34, Ceyhan 154

-Transmission Lines (Loading of): Karaman-Mersin 154, Mersin-Adana

-Generators (Rotor Angles of): Berke HES

Analysis Results

For each given installed capacity value, five individual analyses are carried out regarding circuit breaker operating times. For keeping the data compact, only the cases corresponding to breaker operating time of 1000 ms will be presented.

4.2.1: %5 (117 MW) Installed capacity

Breaker operating time: 1000 ms

For the given fault clearing time, the variations of selected bus voltages are provided in graphs 4.51 to 4.53.

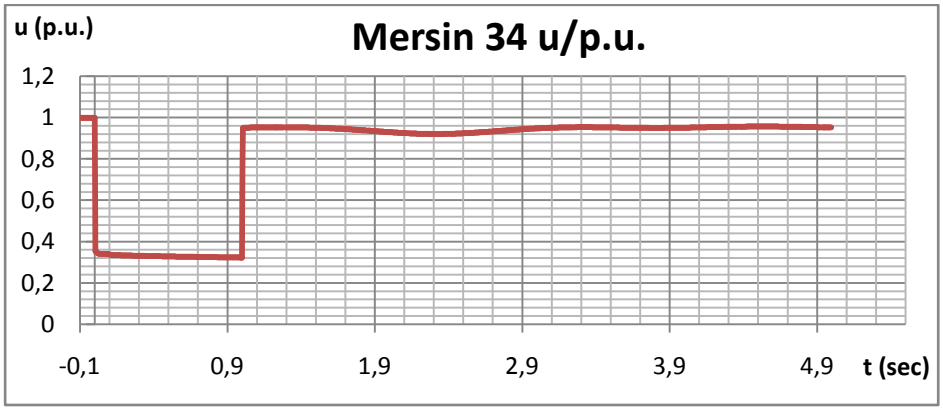

Graph 4.51. Voltage Variation of Mersin 34 Bus

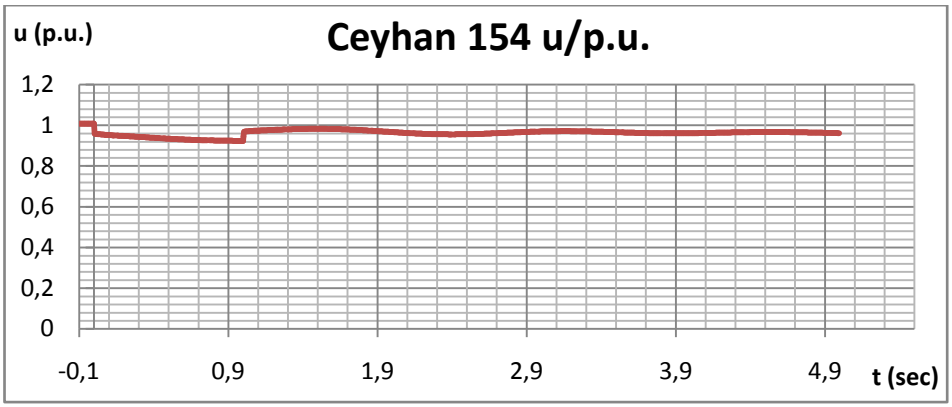

Graph 4.52. Voltage Variation of Ceyhan 154 Bus

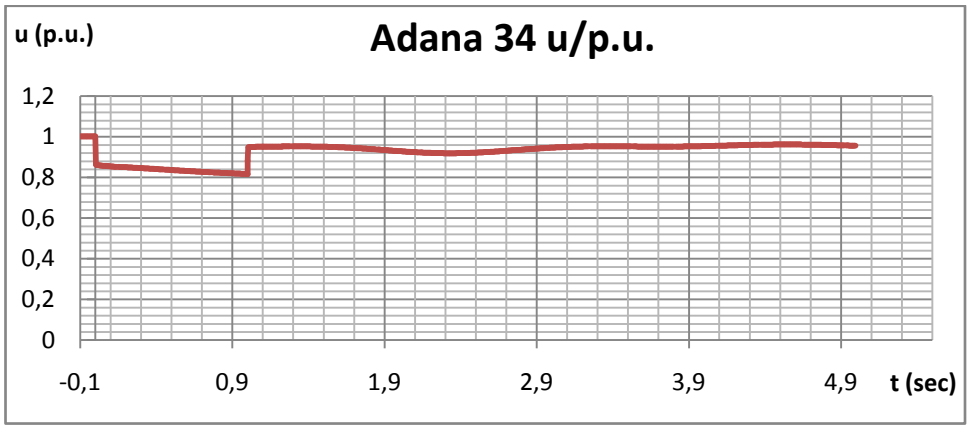

Graph 4.53. Voltage Variation of Adana 34 Bus

As can be seen from the three graphs above, the disturbance had a drastic and almost immediate effect on the bus voltages which caused the voltages at nearby buses to drop sharply. However, the size of the drop varied between different buses and mainly influenced by the connection strength and distance to the location of fault. Mersin 34 bus, being the closest one to the fault has suffered from the largest voltage drop in the event of a 3-phase short circuit while Adana 34 show a slightly more response when compared to Ceyhan 154 bus. It can be seen that, at t=1 sec. the voltages at each bus rises sharply since the circuit breakers at the ends of faulted line are operated, thus, returning the rest of the system to fault-free state. However, the

voltage values are not constant at the post-fault state until the new stable system operating state is fully reached. During this state, the oscillations of the voltage values at each bus can be seen. The maximum and minimum values of bus voltages after the fault clearing, as well as their difference in p.u. are provided in Table 4.23

Table 4.23. Bus Voltages for Case 2.1

	Mersin 34	Ceyhan 154	Adana 34
Vmax	0.9561	0.9829	0.9619
Vmin	0.9199	0.9557	0.9189
Difference	0.0362	0.0272	0.043
Vfinal	0.9513	0.9619	0.9561

As Table 4.23 clearly shows, the final values at the end of 5 seconds after the fault are within the normal operational limits. Moreover the voltage oscillatory peak for all buses are well below the specified %10 limit for this case. However, it should be noted that the voltage oscillations in this case are noticeably higher than case 4.1.1.5 which was the similar case by means of installed capacity and breaker operating time for Bozyaka RES. This implies that the grid strength is relatively lower for case 2 than case 1. This implication will be clarified in the next steps of this case which involve increasing the installed capacity of Mersin RES according to the aforementioned methodology. The line loadings before, during and after the fault are also recorded and the related graphs are provided for lines Karaman-Mersin 154 and Mersin-Adana in graphs 4.54 and 4.55, respectively.

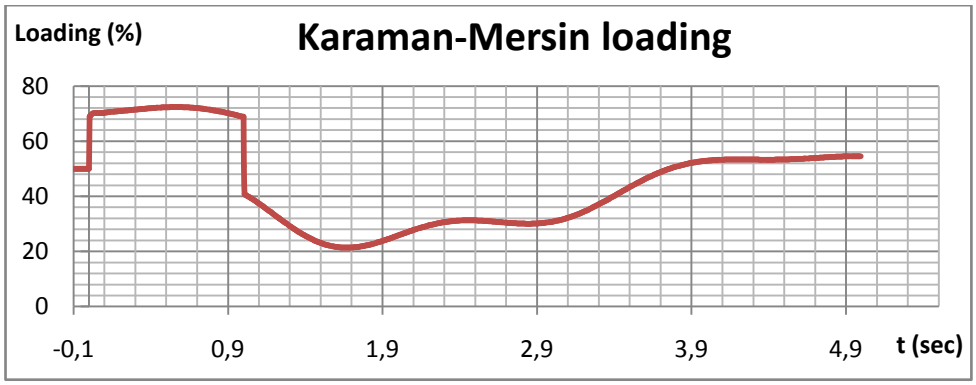

Graph 4.54. Loading of Karaman-Mersin Line

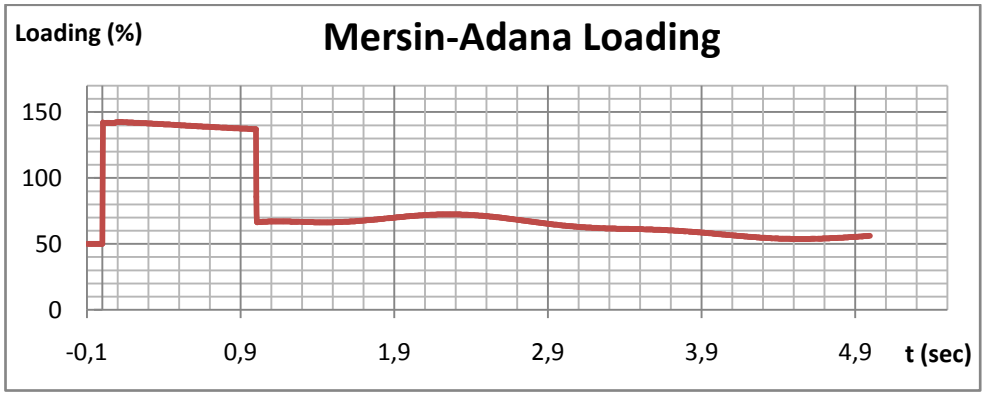

Graph 4.55. Loading of Mersin-Adana Line

As can be seen from both graphs, the fault has caused a slight but immediate disturbance on the transmission lines. After the breaker operation, the line loadings have initially decreased sharply and then, continued changing slowly to reach the new steady-state values. Despite the line Karaman-Mersin remained under %100 loading at any time before, during or after the fault, the transmission line Mersin-Adana has exceeded %140 loading during the fault, i.e. between t=0 and t=1 sec. This may initially seem as a catastrophic event, however the line is actually able to withstand this overloading for such a short duration according to the characteristics of the line type for Karaman-Mersin 154 (477 mcm Hawk). Since after fault clearing loading of the line is below %100 it can be said that this transmission line is still able

to withstand the given short circuit event. No other line within 250 km radius of the fault location exceeded %100 loading which implies that it is safe to claim this case has no threat to the transmission lines by means of overloading.

Table 4.24 provides the initial (t= -0,1 sec.), final (t=5 sec) and maximum rotor angles for Berke HPP during this case.

Table 4.24. Rotor Angle Values for Berke HPP

	Berke Rotor Angle (rad)
Initial	1.1501
Final	1.2015
Maximum	1.2395

As can be seen from Table 4.24 the initial and final values of rotor angle differ only by a small amount (approximately 2,86^{o}) and the simulation results verify that the generator stays in synchronism with the system without any adverse effect.

Taking the results provided above into consideration, the variations in bus voltages, line loadings after the fault clearance and rotor angles are proven to stay within the limits to ensure a stable operation of the system even with an installed capacity, and hence generation equal to the %5 of the short circuit MVA at the bus that the wind farm is connected to. Moreover, the observed parameter variations are considerably far from approaching the stability limits therefore they imply that the system may be able to handle disturbances for even higher values of installed capacity of the wind farm. This implication will prove true in the next analysis, involving a wind farm installed capacity equal to %7,5 of the short circuit MVA of the connecting bus.

4.2.2: %7,5 (176 MW) Installed capacity

Breaker operating time: 1000 ms

For the given fault clearing time, the variations of selected bus voltages are provided in graphs 4.56 to 4.58.

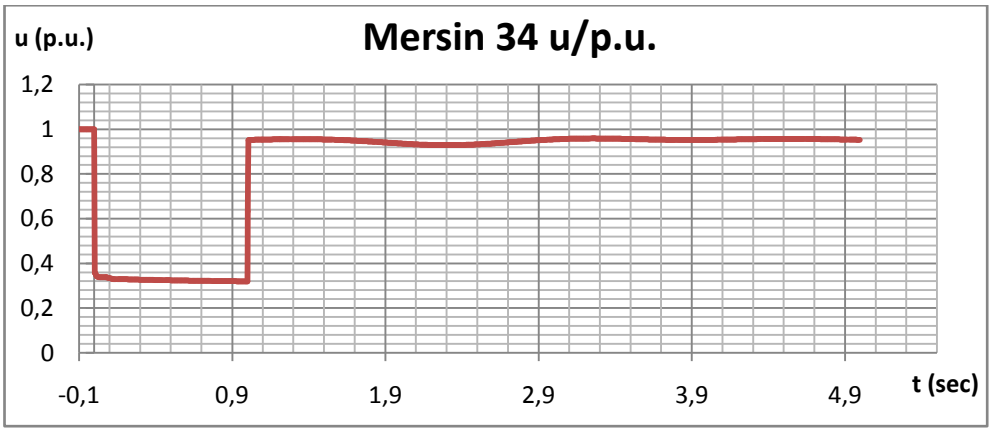

Graph 4.56. Voltage Variation of Mersin 34 Bus

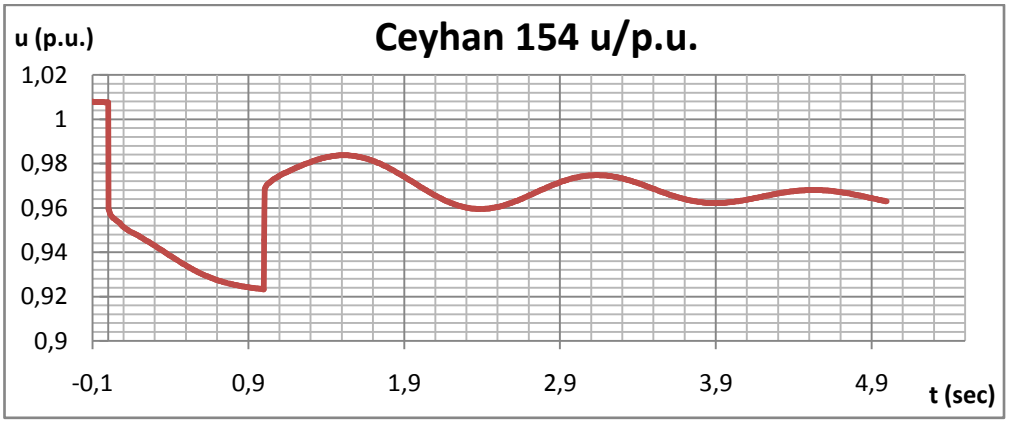

Graph 4.57. Voltage Variation of Ceyhan 154 Bus

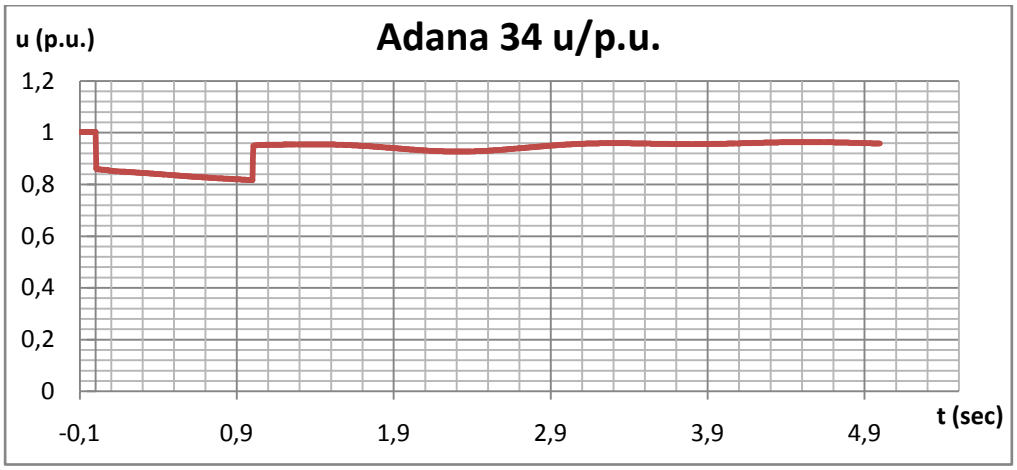

Graph 4.58. Voltage Variation of Adana 34 Bus

As can be seen from the three graphs above, the disturbance had a drastic and almost immediate effect on the bus voltages which caused the voltages at nearby buses to drop sharply. However, the size of the drop varied between different buses and mainly influenced by the connection strength and distance to the location of fault. Mersin 34 bus, being the closest one to the fault has suffered from the largest voltage drop in the event of a 3-phase short circuit while Adana 34 show a slightly more response when compared to Ceyhan 154 bus.

It can be seen that, at t=1 sec. the voltages at each bus rises sharply since the circuit breakers at the ends of faulted line are operated, thus, returning the rest of the system to fault-free state. However, the voltage values are not constant at the post-fault state until the new stable system operating state is fully reached. During this state, the oscillations of the voltage values at each bus can be seen. The maximum and minimum values of bus voltages after the fault clearing, as well as their difference in p.u. are provided in Table 4.25.

Table 4.25. Bus Voltages for Case 2.2.

	Mersin 34	Ceyhan 154	Adana 34
Vmax	0.9586	0.9837	1.0028
Vmin	0.9205	0.9455	0.9272
Difference	0.0381	0.0382	0.0756
Vfinal	0.9526	0.9629	0.9583

As Table 4.25 clearly shows, the final values at the end of 5 seconds after the fault are within the normal operational limits. Moreover the voltage oscillatory peak for all buses except Adana 34 are well below the specified %10 limit for this case. Adana 34 bus voltage variation has increased considerably when compared to case 4.2.1. However, it should be noted that the voltage oscillations in this case are still within acceptable limits. However, for the cases involving Bozyaka RES (4.1) such high oscillations were not observed at similar installed capacity levels. This is in agreement with the claim that the grid strength is relatively lower for case 2 than case 1. This claim will be clarified further in the next steps of this case, as the installed capacity of Mersin RES is increased further.

The line loadings before, during and after the fault are also recorded and the related graphs are provided for lines Karaman-Mersin 154 and Mersin-Adana in graphs 4.59 and 4.60, respectively.

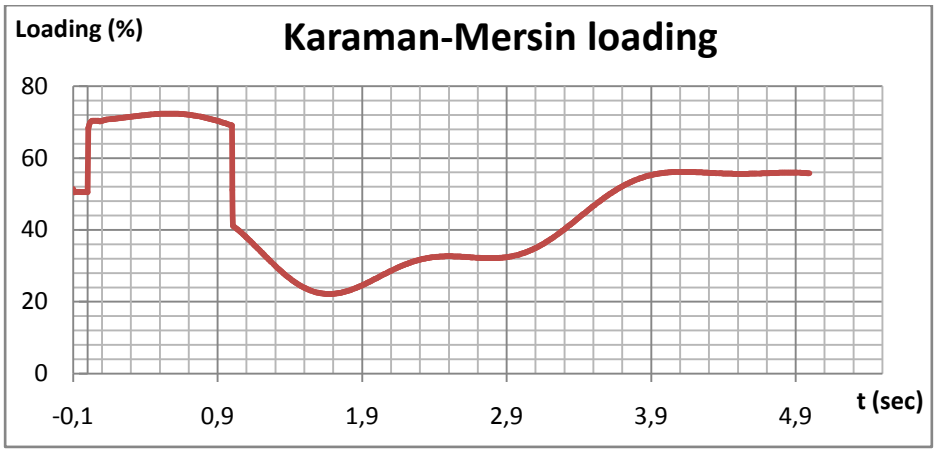

Graph 4.59. Loading of Karaman-Mersin Line

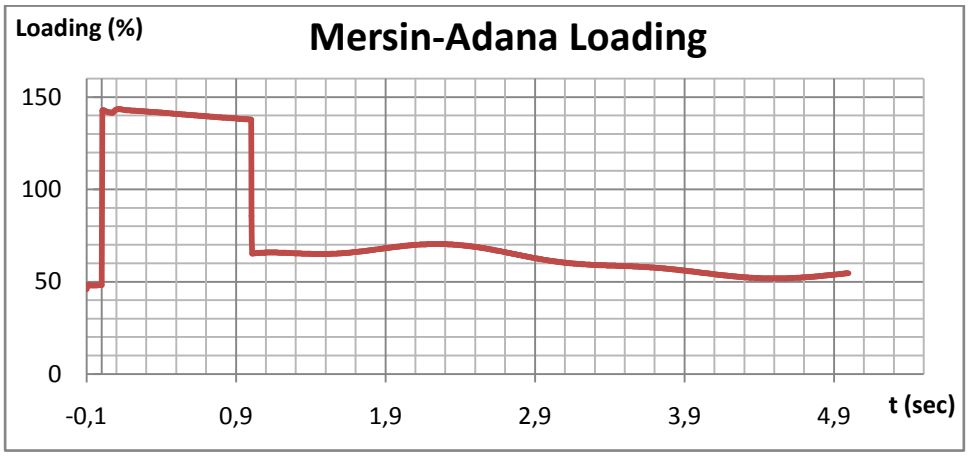

Graph 4.60. Loading of Mersin-Adana Line

As can be seen from both graphs, the fault has caused a slight but immediate disturbance on the transmission lines. After the breaker operation, the line loadings have initially decreased sharply and then, continued changing slowly to reach the new steady-state values. Despite the line Karaman-Mersin remained under %100 loading at any time before, during or after the fault, the transmission line Mersin-Adana has, as expected from previous case, exceeded %140 loading during the fault, i.e. between t=0 and t=1 sec. However the line is actually able to withstand this overloading for such a short duration according to the characteristics of the line type

for Karaman-Mersin 154 (477 mcm Hawk). Since after fault clearing loading of the line is below %100 it can be said that this transmission line is still able to withstand the given short circuit event. No other line within 250 km radius of the fault location exceeded %100 loading which implies that it is safe to claim this case has no threat to the transmission lines by means of overloading.

Table 4.26 provides the initial (t= -0,1 sec.), final (t=5 sec) and maximum rotor angles for Berke HPP during this case.

Table 4.26. Rotor Angle Values for Berke HPP

	Berke Rotor Angle (rad)
Initial	1.1282
Final	1.1756
Maximum	1.212

As can be seen from Table 4.26 the initial and final values of rotor angle differ only by a small amount (approximately 2,86^{o}) and the simulation results verify that the generator stays in synchronism with the system without any adverse effect.

Taking the results provided above into consideration, the variations in bus voltages, line loadings after the fault clearance and rotor angles are proven to stay within the limits to ensure a stable operation of the system even with an installed capacity, and hence generation equal to the %7,5 of the short circuit MVA at the bus that the wind farm is connected to. Moreover, the observed parameter variations excluding a single bus voltage variation (Adana 34) are considerably far from approaching the stability limits therefore they imply that the system may be able to handle disturbances for even higher values of installed capacity of the wind farm. This implication will be checked to be true in the next analysis, involving a wind farm installed capacity equal to %10 of the short circuit MVA of the connecting bus.

4.2.3: %10 (235 MW) Installed capacity

Breaker operating time: 1000 ms

For the given fault clearing time, the variations of selected bus voltages are provided in graphs 4.61 to 4.63.

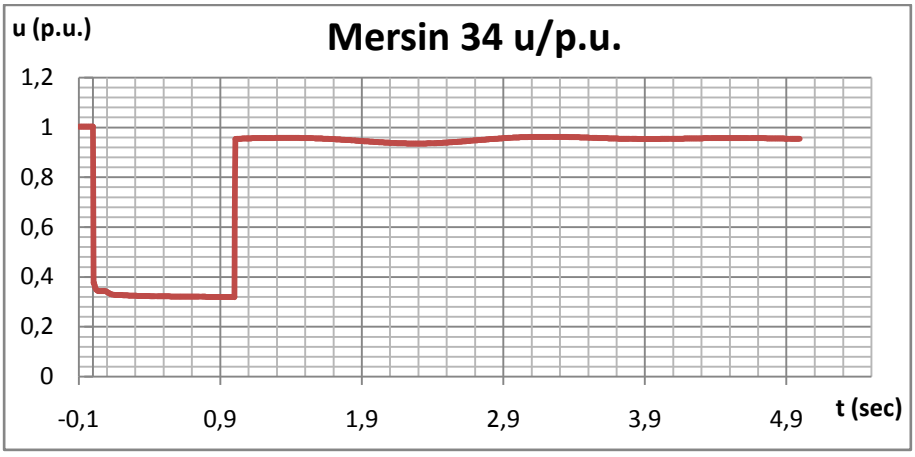

Graph 4.61. Voltage Variation of Mersin 34 Bus.

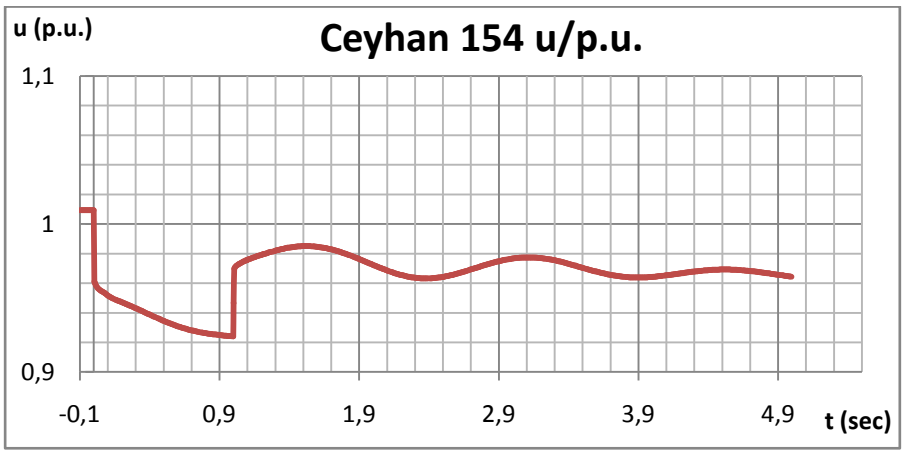

Graph 4.62. Voltage Variation of Ceyhan 154 Bus.

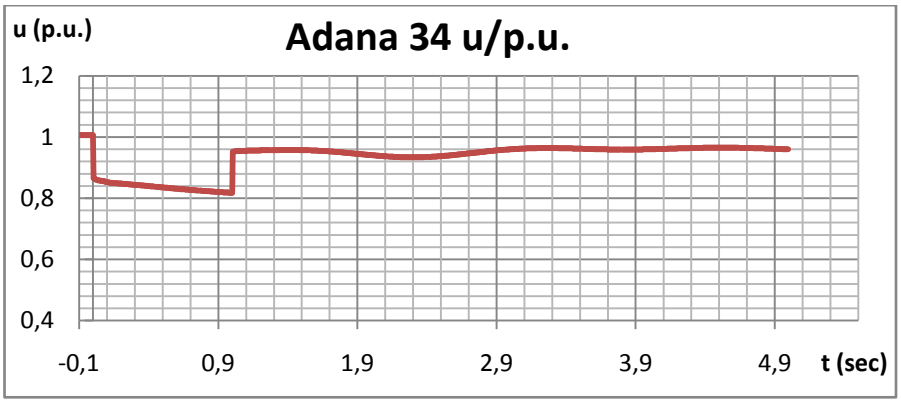

Graph 4.63. Voltage Variation of Adana 34 Bus.

As can be seen from the three graphs above, the disturbance had a drastic and almost immediate effect on the bus voltages which caused the voltages at nearby buses to drop sharply. However, the size of the drop varied between different buses and mainly influenced by the connection strength and distance to the location of fault. Mersin 34 bus, being the closest one to the fault has suffered from the largest voltage drop in the event of a 3-phase short circuit while Adana 34 show a slightly more response when compared to Ceyhan 154 bus.

It can be seen that, at t=1 sec. the voltages at each bus rises sharply since the circuit breakers at the ends of faulted line are operated, thus, returning the rest of the system to fault-free state. However, the voltage values are not constant at the post-fault state until the new stable system operating state is fully reached. During this state, the oscillations of the voltage values at each bus can be seen. The maximum and minimum values of bus voltages after the fault clearing, as well as their difference in p.u. are provided in Table 4.27.

Table 4.27 Bus Voltages for Case 2.3

	Mersin 34	Ceyhan 154	Adana 34
Vmax	0.9738	0.985	0.9656
Vmin	0.9352	0.9466	0.8843
Difference	0.0386	0.0384	0.0813
Vfinal	0.9539	0.9644	0.9601

As Table 4.27 clearly shows, the final values at the end of 5 seconds after the fault are within the normal operational limits. Moreover the voltage oscillatory peak for all buses except Adana 34 are well below the specified %10 limit for this case. Adana 34 bus voltage variation has increased slightly when compared to case 4.2.2. However, it should be noted that the voltage oscillations in this case are still within acceptable limits. However, for the cases involving Bozyaka RES (4.1) such high oscillations were not observed at similar installed capacity levels. This is in agreement with the claim that the grid strength is relatively lower for case 2 than case 1. This claim will be clarified further in the next steps of this case, as the installed capacity of Mersin RES is increased further.

The line loadings before, during and after the fault are also recorded and the related graphs are provided for lines Karaman-Mersin 154 and Mersin-Adana in graphs 4.64 and 4.65, respectively.

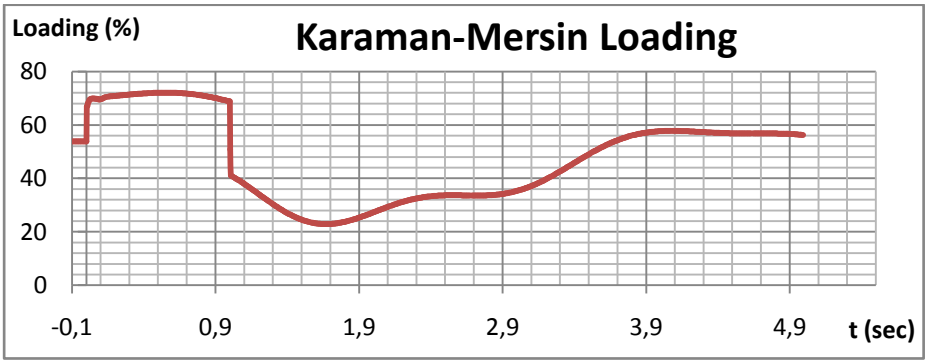

Graph 4.64 Loading of Karaman-Mersin Line.

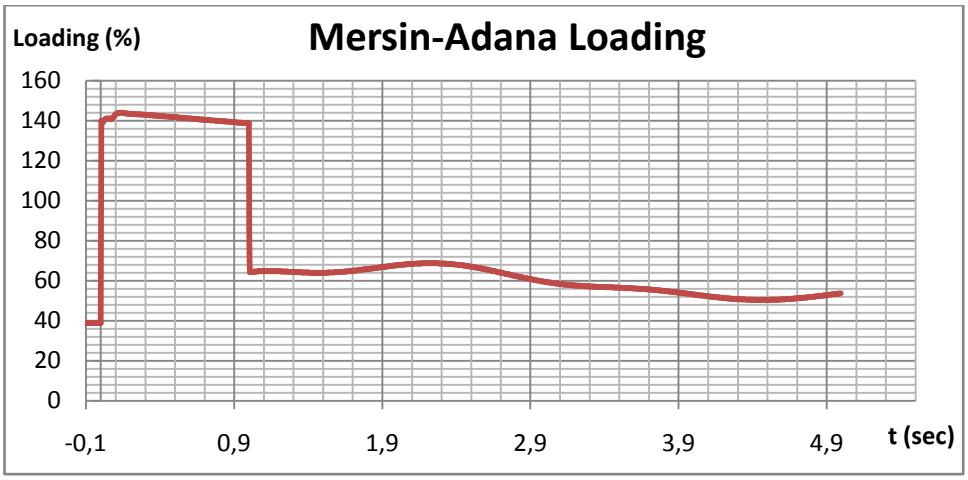

Graph 4.65 Loading of Mersin-Adana Line

As can be seen from both graphs, the fault has caused a slight but immediate disturbance on the transmission lines. After the breaker operation, the line loadings have initially decreased sharply and then, continued changing slowly to reach the new steady-state values. Despite the line Karaman-Mersin remained under %100 loading at any time before, during or after the fault, the transmission line Mersin-Adana has, as expected from previous case, exceeded %140 loading during the fault, i.e. between t=0 and t=1 sec. However the line is actually able to withstand this overloading for such a short duration according to the characteristics of the line type for Karaman-Mersin 154 (477 mcm Hawk). Since after fault clearing loading of the line is below %100 it can be said that this transmission line is still able to withstand the given short circuit event. No other line within 250 km radius of the fault location exceeded %100 loading which implies that it is safe to claim this case has no threat to the transmission lines by means of overloading. Table 4.28 provides the initial (t= -0,1 sec.), final (t=5 sec) and maximum rotor angles for Berke HPP during this case.

Table 4.28 Rotor Angle Values for Berke HPP

	Berke Rotor Angle (rad)
Initial	1.1099
Final	1.155
Maximum	1.1892

As can be seen from Table 4.28 the initial and final values of rotor angle differ only by a small amount (approximately 2,86^{o}) and the simulation results verify that the generator stays in synchronism with the system without any adverse effect.

Taking the results provided above into consideration, the variations in bus voltages, line loadings after the fault clearance and rotor angles are proven to stay within the limits to ensure a stable operation of the system even with an installed capacity, and hence generation equal to the %10 of the short circuit MVA at the bus that the wind farm is connected to. Moreover, the observed parameter variations excluding a single bus voltage variation (Adana 34) are considerably far from approaching the stability limits therefore they imply that the system may be able to handle disturbances for even higher values of installed capacity of the wind farm. This implication will be checked to be true in the next analysis, involving a wind farm installed capacity equal to %12,5 of the short circuit MVA of the connecting bus.

4.2.4: %12,5 (293 MW) Installed capacity

Breaker operating time: 1000 ms
For the given fault clearing time, the variations of selected bus voltages are provided in graphs 4.66 to 4.68.

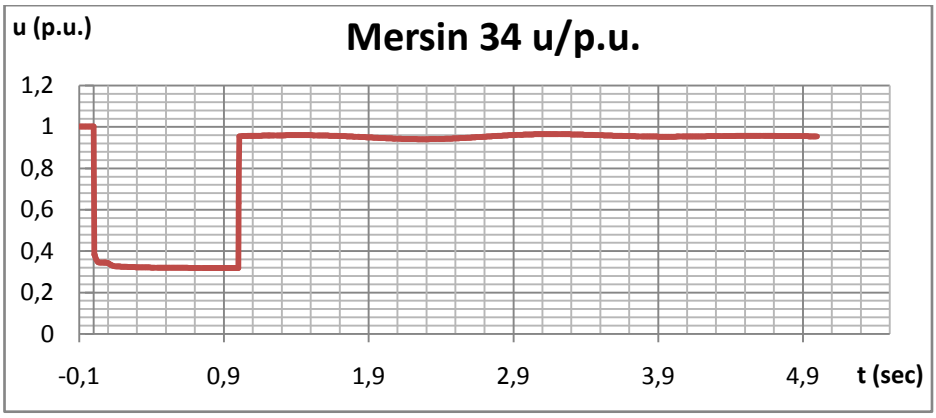

Graph 4.66 Voltage Variation of Mersin 34 Bus.

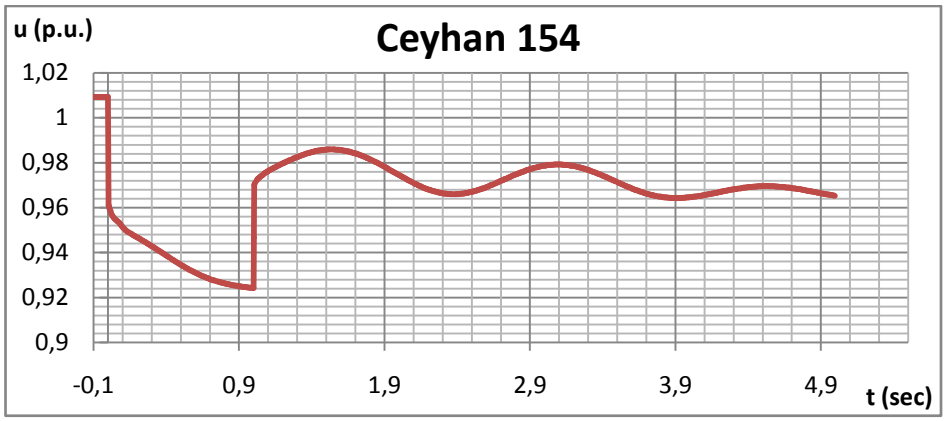

Graph 4.67 Voltage Variation of Ceyhan 154 Bus

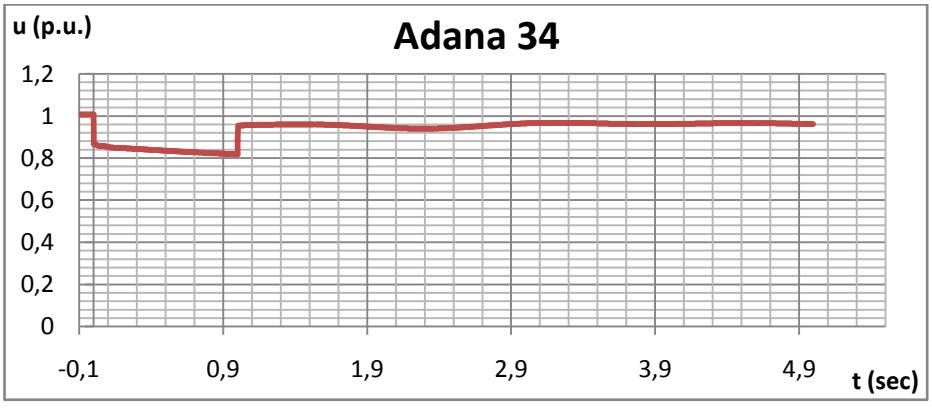

Graph 4.68 Voltage Variation of Adana 34 Bus

As can be seen from the three graphs above, the disturbance had a drastic and almost immediate effect on the bus voltages which caused the voltages at nearby buses to drop sharply. However, the size of the drop varied between different buses and mainly influenced by the connection strength and distance to the location of fault. Mersin 34 bus, being the closest one to the fault has suffered from the largest voltage drop in the event of a 3-phase short circuit while Adana 34 show a slightly more response when compared to Ceyhan 154 bus.

It can be seen that, at t=1 sec. the voltages at each bus rises sharply since the circuit breakers at the ends of faulted line are operated, thus, returning the rest of the system to fault-free state. However, the voltage values are not constant at the post-fault state until the new stable system operating state is fully reached. During this state, the oscillations of the voltage values at each bus can be seen. The maximum and minimum values of bus voltages after the fault clearing, as well as their difference in p.u. are provided in Table 4.29.

Table 4.29. Bus Voltages for Case 2.4.

	Mersin 34	Ceyhan 154	Adana 34
Vmax	0.9814	0.9859	0.9679
Vmin	0.9408	0.9468	0.8852
Difference	0.0406	0.0391	0.0827
Vfinal	0.9544	0.9653	0.9613

As Table 4.29 clearly shows, the final values at the end of 5 seconds after the fault are within the normal operational limits. Moreover the voltage oscillatory peak for all buses except Adana 34 are well below the specified %10 limit for this case. Adana 34 bus voltage variation has increased very slightly when compared to case 4.2.2. However, it should be noted that the voltage oscillations in this case are still within acceptable limits. However, for the cases involving Bozyaka RES (4.1) such high

oscillations were not observed at similar installed capacity levels. This is in agreement with the claim that the grid strength is relatively lower for case 2 than case 1. This claim will be clarified further in the next steps of this case, as the installed capacity of Mersin RES is increased further.

The line loadings before, during and after the fault are also recorded and the related graphs are provided for lines Karaman-Mersin 154 and Mersin-Adana in graphs 4.69 and 4.70, respectively.

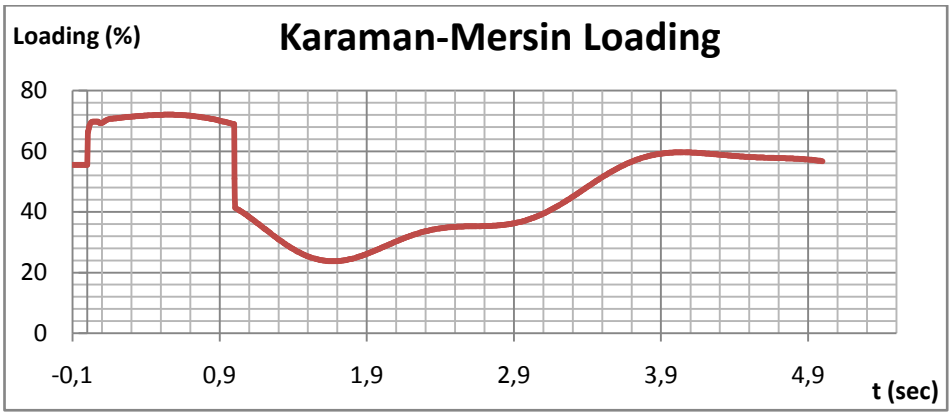

Graph 4.69 Loading of Karaman-Mersin Line

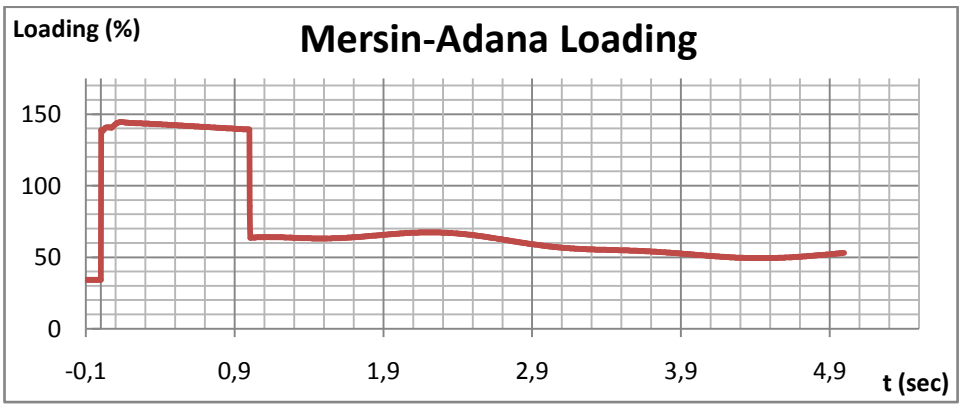

Graph 4.70 Loading of Mersin-Adana Line

As can be seen from both graphs, the fault has caused a slight but immediate disturbance on the transmission lines. After the breaker operation, the line loadings have initially decreased sharply and then, continued changing slowly to reach the new steady-state values. Despite the line Karaman-Mersin remained under %100 loading at any time before, during or after the fault, the transmission line Mersin-Adana has, as expected from previous case, exceeded %140 loading during the fault, i.e. between t=0 and t=1 sec. However the line is again, able to withstand this overloading for such a short duration according to the characteristics of the line type for Karaman-Mersin 154 (477 mcm Hawk). Since after fault clearing loading of the line is below %100 it can be said that this transmission line is still able to withstand the given short circuit event. No other line within 250 km radius of the fault location exceeded %100 loading which implies that it is safe to claim this case has no threat to the transmission lines by means of overloading.

Table 4.30 provides the initial (t= -0,1 sec.), final (t=5 sec) and maximum rotor angles for Berke HPP during this case.

Table 4.30 Rotor Angle Values for Berke HPP

	Berke Rotor Angle (rad)
Initial	1.0975
Final	1.141
Maximum	1.1733

As can be seen from Table 4.30 the initial and final values of rotor angle differ only by a small amount (approximately 2,86^{o}) and the simulation results verify that the generator stays in synchronism with the system without any adverse effect.

Taking the results provided above into consideration, the variations in bus voltages, line loadings after the fault clearance and rotor angles are proven to stay within the

limits to ensure a stable operation of the system even with an installed capacity, and hence generation equal to the %12,5 of the short circuit MVA at the bus that the wind farm is connected to. Moreover, the observed parameter variations excluding a single bus voltage variation (Adana 34) are considerably far from approaching the stability limits therefore they imply that the system may be able to handle disturbances for even higher values of installed capacity of the wind farm. This implication will be checked in the next analysis, involving a wind farm installed capacity equal to %15 of the short circuit MVA, 3 times the stated limit, of the connecting bus.

4.2.5: %15 (352 MW) Installed capacity

Breaker operating time: 1000 ms

For the given fault clearing time, the variations of selected bus voltages are provided in graphs 4.71 to 4.73.

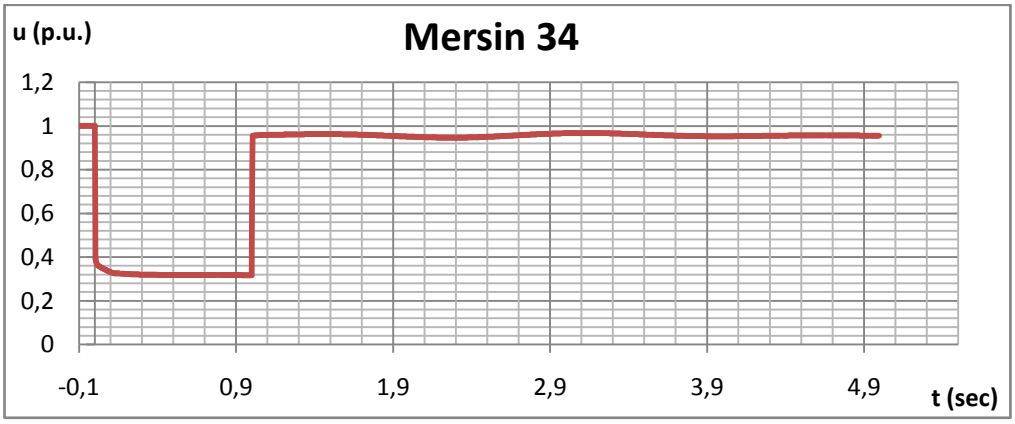

Graph 4.71 Voltage Variation of Mersin 34 Bus

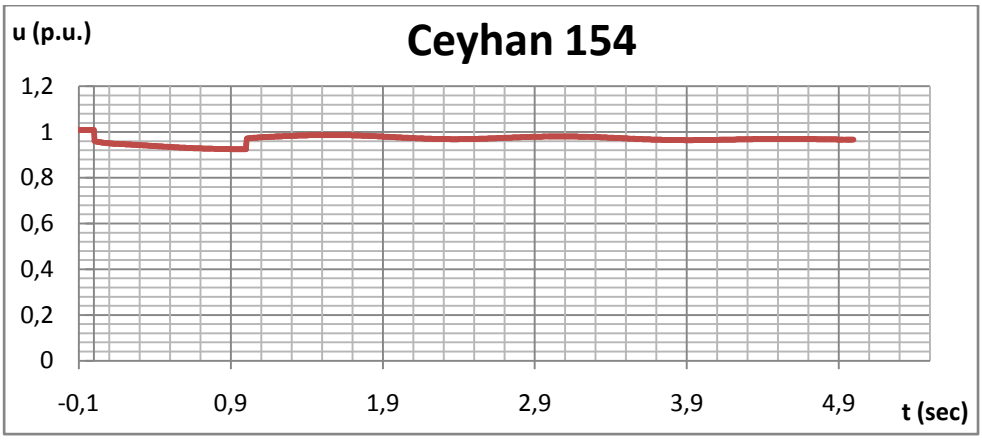

Graph 4.72 Voltage Variation of Ceyhan 154 Bus

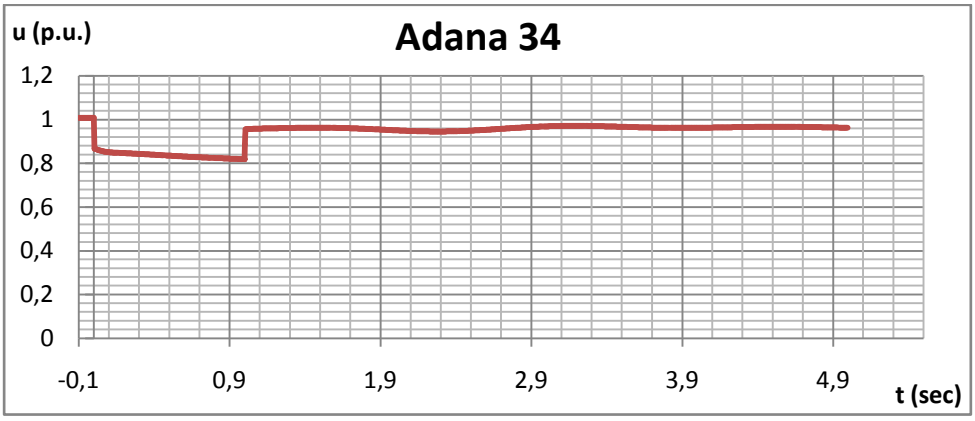

Graph 4.73 Voltage Variation of Adana 34 Bus

As can be seen from the three graphs above, the disturbance had a drastic and almost immediate effect on the bus voltages which caused the voltages at nearby buses to drop sharply. However, the size of the drop varied between different buses and mainly influenced by the connection strength and distance to the location of fault. Mersin 34 bus, being the closest one to the fault has suffered from the largest voltage drop in the event of a 3-phase short circuit while Adana 34 shows slightly more response when compared to Ceyhan 154 bus.

It can be seen that, at t=1 sec. the voltages at each bus rises sharply since the circuit breakers at the ends of faulted line are operated, thus, returning the rest of the system to fault-free state. However, the voltage values are not constant at the post-fault state until the new stable system operating state is fully reached. During this state, the oscillations of the voltage values at each bus can be seen. The maximum and minimum values of bus voltages after the fault clearing, as well as their difference in p.u. are provided in Table 4.31

Table 4.31. Bus Voltages for Case 2.5

	Mersin 34	Ceyhan 154	Adana 34
Vmax	1.0006	1.0093	1.0078
Vmin	0.946	0.9645	0.8861
Difference	0.0546	0.0448	0.1217
Vfinal	0.9549	0.9662	0.9625

As Table 4.31 clearly shows, the final values at the end of 5 seconds after the fault are within the normal operational limits. Moreover the voltage oscillatory peak for all buses except Adana 34 are below the specified %10 limit for this case. Adana 34 bus voltage variation has increased considerably when compared to case 4.2.3. Moreover, the maximum oscillation has turned out to exceed the %10 limit slightly. This possesses a danger to the system by means of power quality and although being slightly off-limits, a wind farm with such a high installed capacity in this region can be claimed to be a threat to the system stability and quality of electricity in case of a fault nearby. Since case 1 (Bozyaka RES) was successfully able to preserve the solid characteristics of grid with similar installed capacity of wind farm by means of percentage of short circuit MVA at related bus, the claim the grid strength is relatively lower for case 2 than case 1 is proved. The line loadings before, during and after the fault are also recorded and the related graphs are provided for lines Karaman-Mersin 154 and Mersin-Adana in graphs 4.74 and 4.75, respectively.

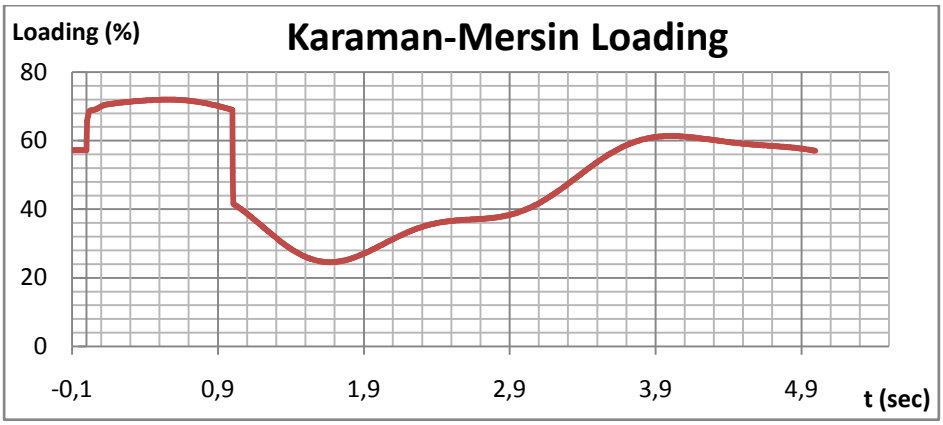

Graph 4.74 Loading of Karaman-Mersin 154 Line

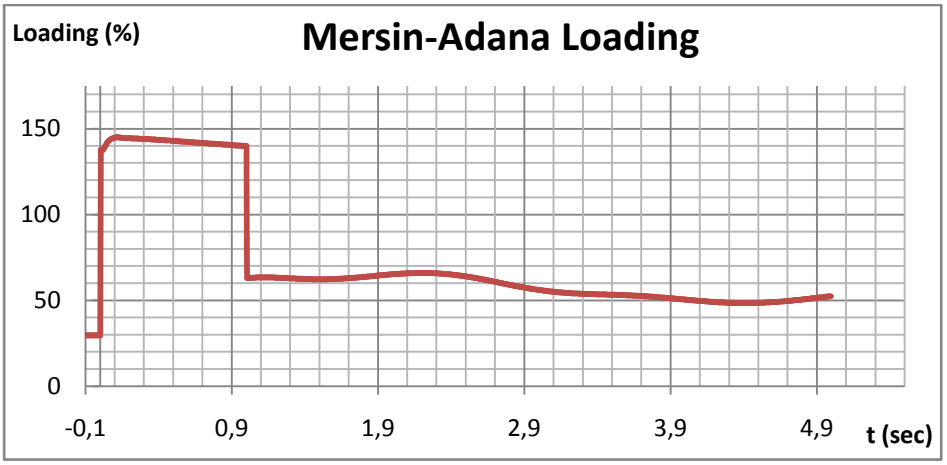

Graph 4.75 Loading of Mersin-Adana Line

As can be seen from both graphs, the fault has caused an immediate disturbance on the transmission lines. After the breaker operation, the line loadings have initially decreased sharply and then, began approaching to the new steady-state values.

Despite the line Karaman-Mersin remained under %100 loading at any time before, during or after the fault, the transmission line Mersin-Adana has, as expected from previous case, exceeded %140 loading during the fault, i.e. between t=0 and t=1 sec.

However the line is still able to withstand this overloading for such a short duration according to the characteristics of the line type for Karaman-Mersin 154 (477 mcm Hawk). Since after fault clearing loading of the line is below %100 it can be said that this transmission line is still able to withstand the given short circuit event. No other line within 250 km radius of the fault location exceeded %100 loading which implies that it is safe to claim this case has no threat to the transmission lines by means of overloading. Table 4.32 provides the initial (t= -0,1 sec.), final (t=5 sec) and maximum rotor angles for Berke HPP during this case.

Table 4.32 Rotor Angle Values for Berke HPP.

	Berke Rotor Angle (rad)
Initial	1.0861
Final	1.1285
Maximum	1.1584

As can be seen from Table 4.32 the initial and final values of rotor angle differ only by a small amount (approximately 2,43^{o}) and the simulation results verify that the generator stays in synchronism with the system without any adverse effect.

Taking the results provided above into consideration, despite the variations in most of the bus voltages and all line loadings after the fault clearance and rotor angles are proven to stay within the limits, the observed voltage variations of Adana 34 have exceeded the %10 limit to ensure power quality which can arguably be a proof to the claim that the stability and power quality conditions are threatened by the presence of a wind farm with such high installed capacity corresponding to %15 of the short circuit MVA of the connecting bus. Therefore, presence of a wind farm with very large installed capacity can cause aforementioned problems in the regions where the grid is not of a certain strength.

Since the analysis results of case 4.2.5 shown that the installed capacity of wind farm corresponding to %15 of the short circuit MVA of the connecting bus causes problems in the system in case of a short circuit event, no further analyses involving higher installed capacities of Mersin RES will be presented here. If desired, the results displaying variations in system parameters due to the same short circuit events for highest installed capacity simulated (corresponding to %33,4 of short circuit MVA of the related bus) can be accessed from the appendix CD as an Excel file.

4.3. Case 3: Şenköy RES

The third case, Şenköy RES is chosen to be demonstrated third since it also resides in the southern end of Turkey where the grid is relatively weak. Unlike Mersin Wind farm, the area where Şenköy RES is resided is somewhat less developed with the largest city in the close distance is Hatay with approximate population of 350.000 . Şenköy wind farm is resided within the city limits of Hatay, the province also including the central town Antakya. In the system, the wind farm is connected to the grid at Antakya 31.5 kV (denoted by Antakya 31 in the model) bus. Therefore, the connecting line is between the buses Şenköy RES 34 and Antakya 31 The current installed capacity of Şenköy RES (omitting the nearby wind farms which were actually included in the system model) is 35 MW. The short circuit power at Mersin 34 bus, on the other hand, is 1200 MVA [54]. If the wind farms included in the modeling are also considered, the total installed capacity of the wind farms that are denoted by Şenköy RES in the model sum up to 62 MW. As can be inferred from its location, the grid where the wind farm is can be considered to be weak since being noticeably far away to large consumption centers. Despite being smaller in cumulative installed capacities when compared to western part of Turkey, the wind farm concentration in the southern part of the country is still comparably high, implying that the grid may still be sufficiently strong to meet the increasing generation levels. However, the position of Şenköy RES makes it to be relatively far away from stronger points in the grid due to being the eastern-end of Turkish wind farm distribution geographically. For these reasons, the system strength around

Şenköy RES is expected to be relatively weaker among the regions where wind farms of significant size exists. This implies that, during simulations, the effects of disturbances will be comparable to what would be expected to be observed at weaker regions of the grid.

As mentioned in the preceding section, the analyses will be carried out for installed capacities of Şenköy RES that will be equal to %5, %7.5, %10, %12.5 and %15 of the short circuit MVA at Antakya 31 bus. The installed capacity values corresponding to these percentages of short circuit power are given in Table 4.33

Table 4.33. Installed Capacity Values for Case 3.

% of Ssc	5	7,5	10	12,5	15
Installed Capacity (MW)	60	90	120	150	180

The buses, transmission lines and generators within 250 km radius of the wind farm are chosen to be observed. However, to avoid overflow of output data, some elements among the initial set are omitted after they are proven not to show any significant variations during the analysis processes. The resulting set of elements to be observed and whose results will be provided in detail are given below.

-Buses (Voltages of) : Antakya 31, İskenderun 34, Taşucu

-Transmission Lines (Loading of): Erzin-Andırın, Yumurtalık-Adana 154

-Generators (Rotor Angles of): Atatürk HPP, İskenderun TPP

Analysis Results

For each given installed capacity value, five individual analyses are carried out regarding circuit breaker operating times. For the sake of keeping the data given here compact, only the cases corresponding to breaker operating time of 1000 ms will be presented.

4.3.1: %5 (60 MW) Installed capacity

Breaker operating time: 1000 ms

For the given fault clearing time, the variations of selected bus voltages are provided in graphs 4.76 to 4.78.

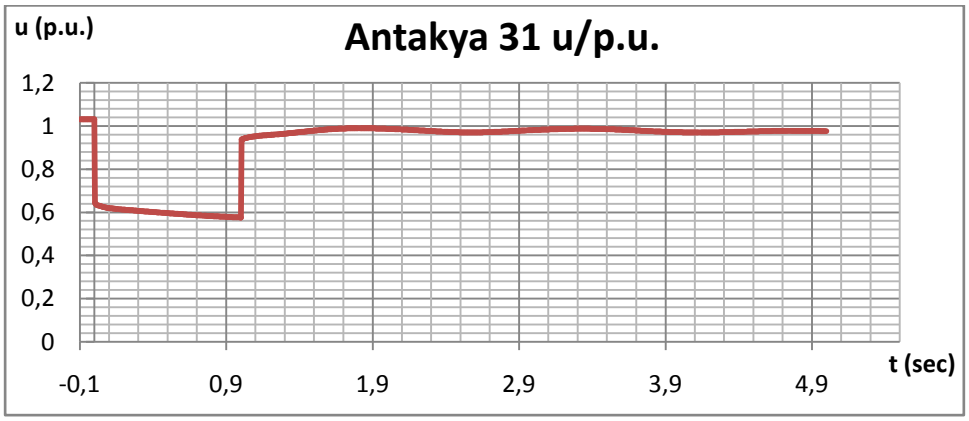

Graph 4.76. Voltage Variations of Antakya 31 Bus

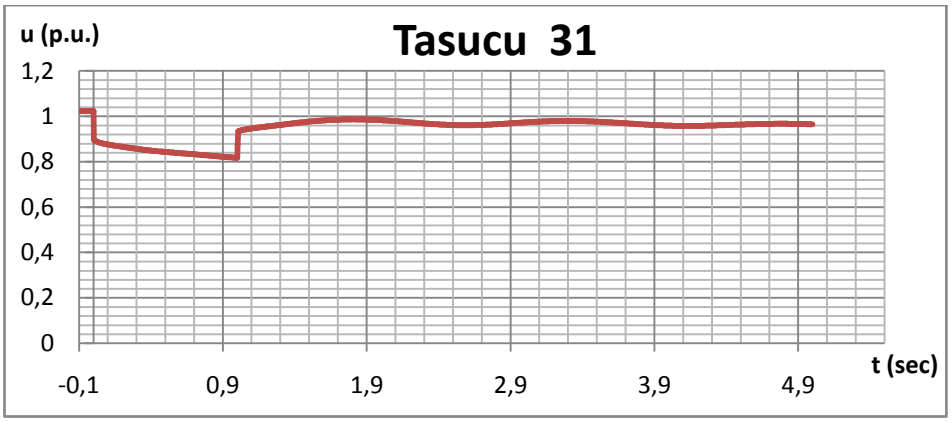

Graph 4.77. Voltage Variations of Tasucu 31 Bus

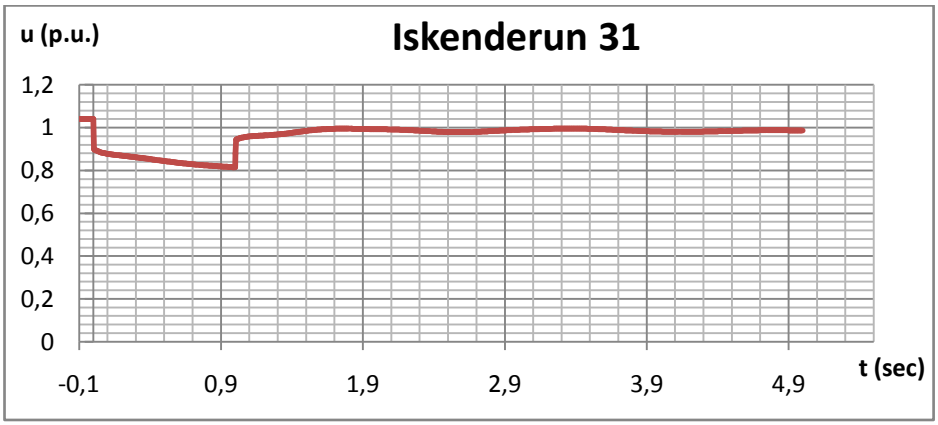

Graph 4.78. Voltage Variations of Iskenderun 31 Bus

As can be seen from the three graphs above, the disturbance had a drastic and almost immediate effect on the bus voltages which caused the voltages at nearby buses to drop sharply. However, the size of the drop varied between different buses and mainly influenced by the connection strength and distance to the location of fault. Antakya 31 bus, being the closest one to the fault has suffered from the largest voltage drop in the event of a 3-phase short circuit while Tasucu 31 and Iskenderun buses showed a similar response that is smaller than that of Antakya 31.

It can be seen that, at t=1 sec. the voltages at each bus rises sharply since the circuit breakers at the ends of faulted line are operated, thus, returning the rest of the system to fault-free state. However, the voltage values are not constant at the post-fault state until the new stable system operating state is fully reached. During this state, the oscillations of the voltage values at each bus can be seen. The maximum and minimum values of bus voltages after the fault clearing, as well as their difference in p.u. are provided in Table 4.34.

Table 4.34. Bus Voltages for Case 3.1

	Antakya 31	Tasucu 31	Iskenderun 31
Vmax	0.99	0.9863	0.9958
Vmin	0.939	0.9345	0.9445
Difference	0.051	0.0518	0.0513
Vfinal	0.9765	0.9648	0.9861

As Table 4.34 clearly shows, the final values at the end of 5 seconds after the fault are within the normal operational limits. Moreover the voltage oscillatory peak for all buses are well below the specified %10 limit for this case. However, it should be noted that the voltage oscillations in this case are noticeably higher than case 4.1.1.5 which was the similar case by means of installed capacity and breaker operating time for Bozyaka RES. This implies that the grid strength is relatively lower for case 3 than case 1. This implication will be clarified in the next steps of this case which involve increasing the installed capacity of Şenköy RES according to the aforementioned methodology. The line loadings before, during and after the fault are also recorded and the related graphs are provided for lines Erzin-Andırın and Yumurtalık-Adana in graphs 4.79 and 4.80, respectively.

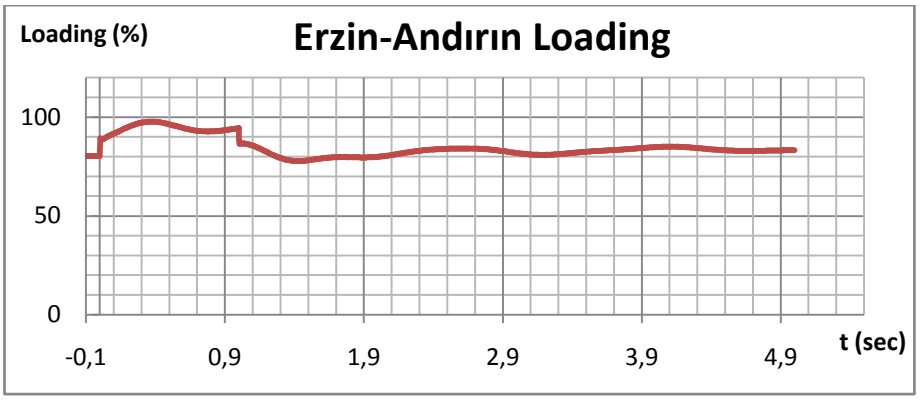

Graph 4.79. Loading of Erzin-Andırın Line

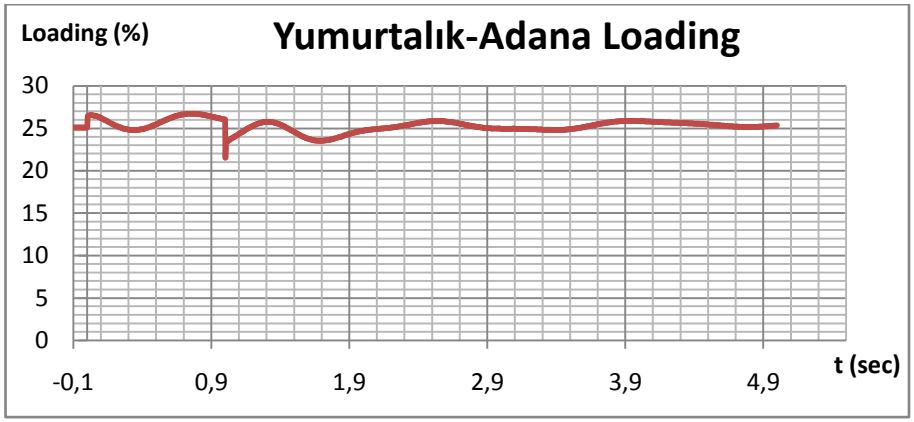

Graph 4.80. Loading of Yumurtalık-Adana Line

As can be seen from both graphs, the fault has caused a slight but immediate disturbance on the transmission lines. After the breaker operation, the line loadings have initially decreased immediately but slightly and then, began increasing in an attenuating oscillatory manner to reach the new steady-state values. Since all the transmission lines residing within 250 km radius of the fault point remained under %100 loading at any time before, during or after the fault, it is safe to claim that this case has no threat to the transmission lines by means of overloading. It is advisable to note that despite the loading of line Erzin-Andırın approaches %100, it never reaches or exceeds full loading at any time.

Table 4.35 provides the initial (t= -0,1 sec.), final (t=5 sec) and maximum rotor angles for Atatürk HPP and İskenderun (Atlas) TPP during this case.

Table 4.35. Rotor Angle Values for Atatürk and Iskenderun Plants

	Atatürk Rotor Angle (rad)	Iskenderun Rotor Angle (rad)
Initial	0.493	1.3701
Final	0.493	1.4194
Maximum	0.493	1.4546

As can be seen from Table 4.35, the initial and final values of Iskenderun TPP's rotor angle differ only by a small amount (approximately 2,29^{o}) while the Atatürk HPP's rotor angle shows no detectable response to the fault at all. Therefore, the simulation results verify that the generators stay in synchronism with the system without any adverse effect.

Taking the results provided above into consideration, the variations in bus voltages, line loadings after the fault clearance and rotor angles are proven to stay within the limits to ensure a stable operation of the system with an installed capacity, and hence generation equal to the %5 of the short circuit MVA at the bus that the wind farm is connected to. Moreover, the observed parameter variations are far away from approaching the stability limits therefore they imply that the system may be able to handle disturbances for even higher values of installed capacity of the wind farm. This implication will prove true in the next analysis, involving a wind farm installed capacity equal to %7,5 of the short circuit MVA of the connecting bus.

4.3.2: %7,5 (90 MW) Installed capacity

Breaker operating time: 1000 ms

For the given fault clearing time, the variations of selected bus voltages are provided in graphs 4.81 to 4.83.

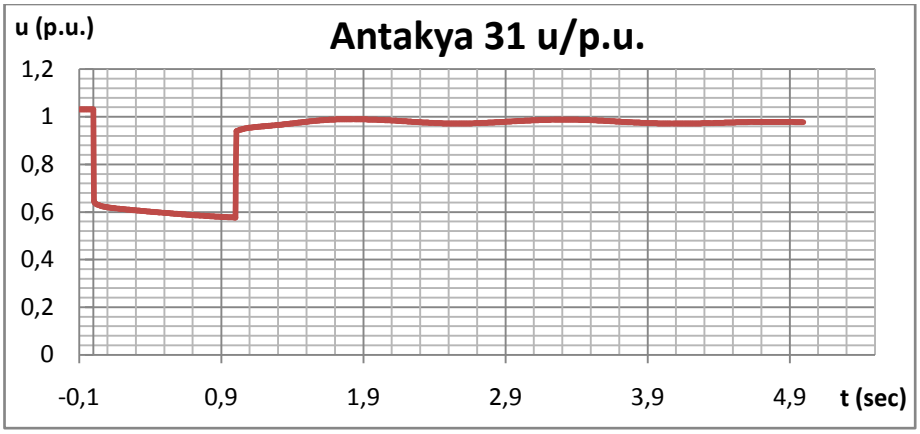

Graph 4.81. Voltage Variations of Antakya 31 Bus

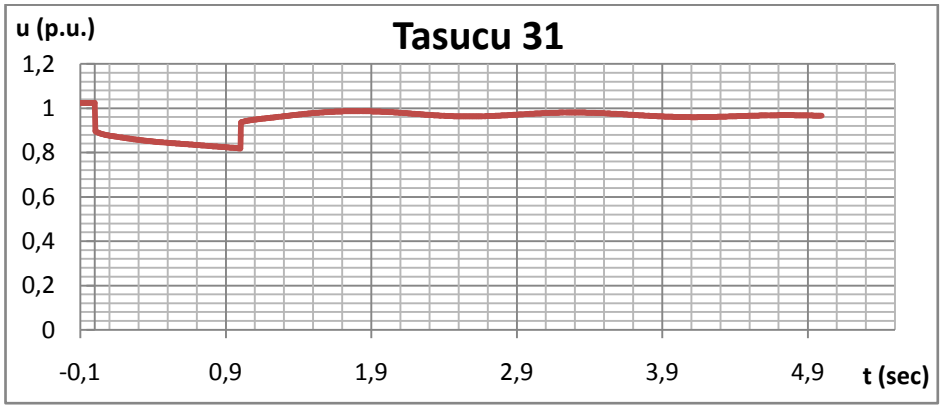

Graph 4.82. Voltage Variations of Tasucu 31 Bus

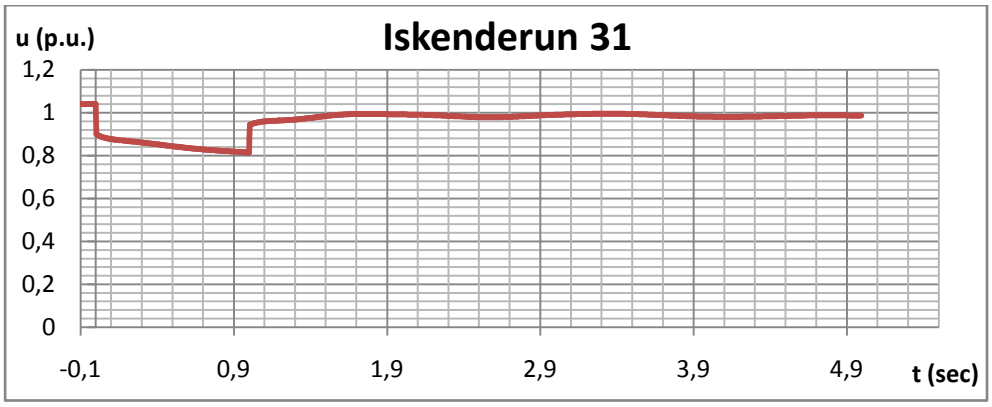

Graph 4.83. Voltage Variations of Iskenderun 31 Bus

As can be seen from the three graphs above, the disturbance had a drastic and almost immediate effect on the bus voltages which caused the voltages at nearby buses to drop sharply. However, the size of the drop varied between different buses and mainly influenced by the connection strength and distance to the location of fault. Antakya 31 bus, being the closest one to the fault has suffered from the largest voltage drop in the event of a 3-phase short circuit while Tasucu 31 and Iskenderun buses showed similar responses that are smaller than that of Antakya 31.

It can be seen that, at t=1 sec. the voltages at each bus rises noticeably since the circuit breakers at the ends of faulted line are operated, thus, returning the rest of the system to fault-free state. However, the voltage values are not constant at the post-fault state until the new stable system operating state is fully reached. During this state, the oscillations of the voltage values at each bus can be seen. The maximum and minimum values of bus voltages after the fault clearing, as well as their difference in p.u. are provided in Table 4.36.

Table 4.36. Bus Voltages for Case 4.2

	Antakya 31	Tasucu 31	Iskenderun
Vmax	0.9902	0.9876	0.9956
Vmin	0.9392	0.9356	0.9442
Difference	0.051	0.052	0.0514
Vfinal	0.9768	0.9657	0.9861

As Table 4.36 clearly shows, the final values at the end of 5 seconds after the fault are within the normal operational limits. Moreover the voltage oscillatory peak for all buses are well below the specified %10 limit for this case. However, it should be noted that the voltage oscillations in this case are noticeably higher than case 4.1.2 which was the similar case by means of installed capacity and breaker operating time for Bozyaka RES. This implies that the grid strength is relatively lower for case 3 than case 1. This implication will be clarified in the next steps of this case which involve increasing the installed capacity of Şenköy RES according to the aforementioned methodology.

The line loadings before, during and after the fault are also recorded and the related graphs are provided for lines Erzin-Andırın and Yumurtalık-Adana in graphs 4.84 and 4.85, respectively.

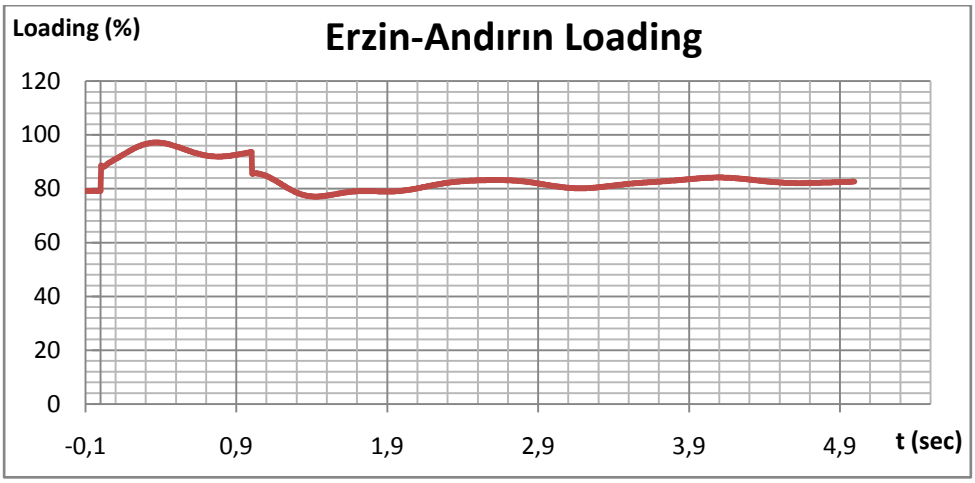

Graph 4.84. Loading of Erzin-Andırın Line

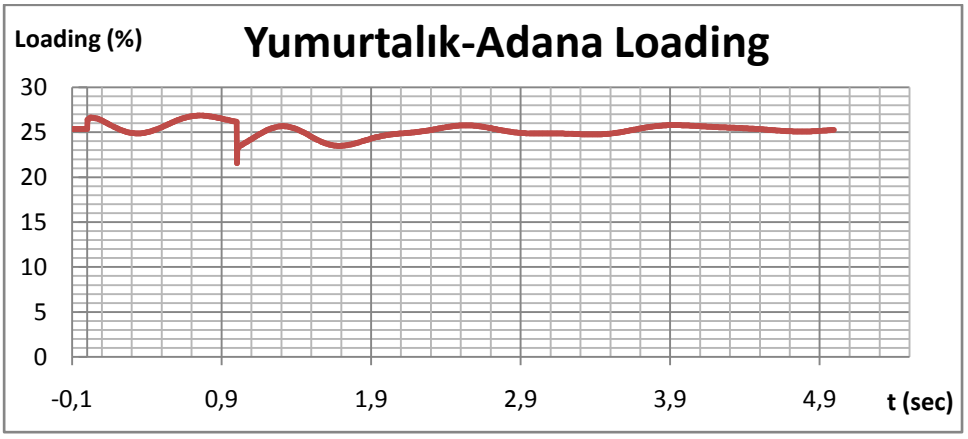

Graph 4.85. Loading Yumurtalık-Adana Line

As can be seen from both graphs, the fault has caused a slight but immediate disturbance on the transmission lines. After the breaker operation, the line loadings have initially decreased immediately but slightly and then, began increasing in an attenuating oscillatory manner to reach the new steady-state values. Since all the transmission lines residing within 250 km radius of the fault point remained under %100 loading at any time before, during or after the fault, it is safe to claim that this case has no threat to the transmission lines by means of overloading. It is

advisable to note that despite the loading of line Erzin-Andırın approaches %100, it never reaches or exceeds full loading at any time.

Table 4.37 provides the initial (t= -0,1 sec.), final (t=5 sec) and maximum rotor angles for Atatürk HPP and İskenderun (Atlas) TPP during this case.

Table 4.37 Rotor Angle Values for Atatürk and Iskenderun Plants.

	Atatürk Rotor Angle (rad)	Iskenderun Rotor Angle (rad)
Initial	0.4948	1.3574
Final	0.4948	1.4072
Maximum	0.4948	1.4607

As can be seen from Table 4.37 the initial and final values of Iskenderun TPP's rotor angle differ only by a small amount (approximately 2,86^{o}) while the Atatürk HPP's rotor angle shows no detectable response to the fault at all. Therefore, the simulation results verify that the generators stay in synchronism with the system without any adverse effect.

Taking the results provided above into consideration, the variations in bus voltages, line loadings after the fault clearance and rotor angles are proven to stay within the limits to ensure a stable operation of the system even with an installed capacity, and hence generation equal to the %7,5 of the short circuit MVA at the bus that the wind farm is connected to. Moreover, the observed parameter variations are far away from approaching the stability limits therefore they imply that the system may be able to handle disturbances for even higher values of installed capacity of the wind farm. This implication will prove true in the next analysis, involving a wind farm installed capacity equal to %10 of the short circuit MVA of the connecting bus.

4.3.3: %10 (120 MW) Installed capacity

Breaker operating time: 1000 ms

For the given fault clearing time, the variations of selected bus voltages are provided in graphs 4.86 to 4.88.

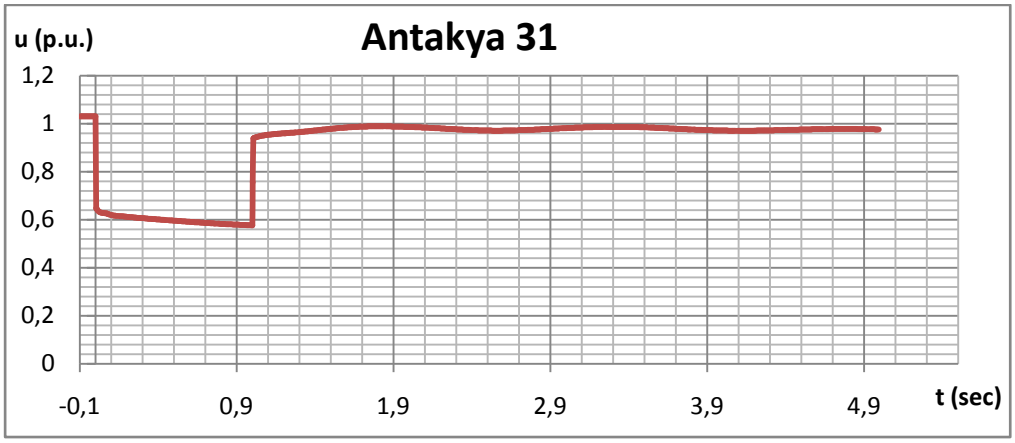

Graph 4.86. Voltage Variation of Antakya 31 Bus

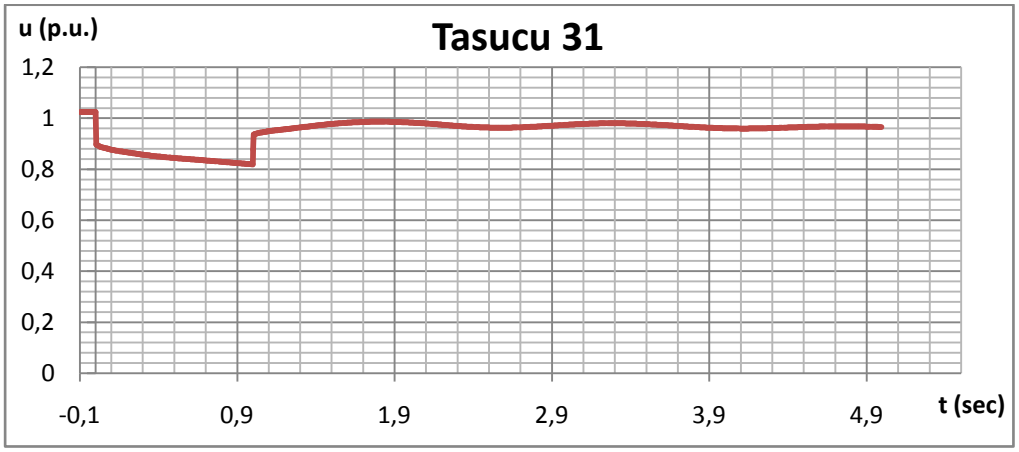

Graph 4.87. Voltage Variation of Tasucu 31 Bus

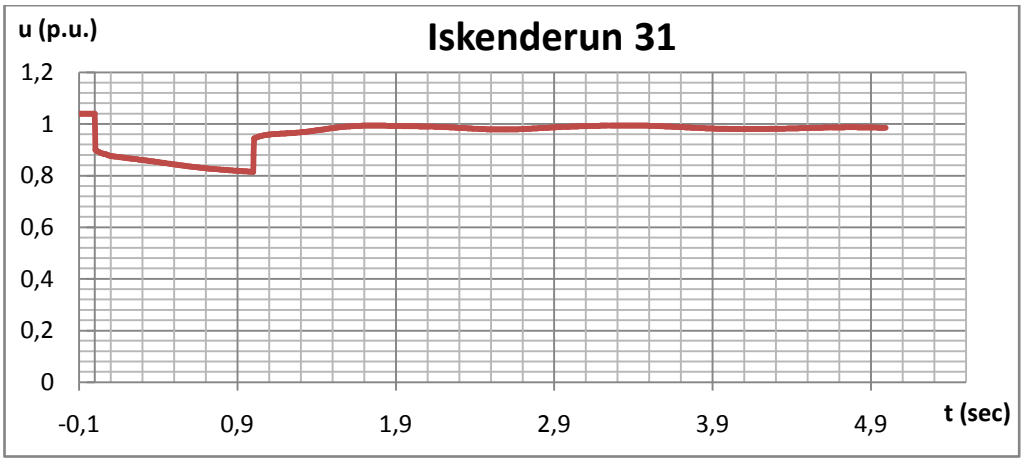

Graph 4.88. Voltage Variation of Iskenderun 31 Bus

As can be seen from the three graphs above, the disturbance had a drastic and almost immediate effect on the bus voltages which caused the voltages at nearby buses to drop sharply. However, the size of the drop varied between different buses and mainly influenced by the connection strength and distance to the location of fault. Antakya 31 bus, being the closest one to the fault has suffered from the largest voltage drop in the event of a 3-phase short circuit while Tasucu 31 and Iskenderun buses showed similar responses that are smaller than that of Antakya 31.

It can be seen that, at t=1 sec. the voltages at each bus rises sharply since the circuit breakers at the ends of faulted line are operated, thus, returning the rest of the system to fault-free state. However, the voltage values are not constant at the post-fault state until the new stable system operating state is fully reached. During this state, the oscillations of the voltage values at each bus can be seen. The maximum and minimum values of bus voltages after the fault clearing, as well as their difference in p.u. are provided in Table 4.38.

Table 4.38. Bus Voltages for Case 3.3

	Antakya 31	Tasucu 31	Iskenderun 31
Vmax	0.9905	0.99	1.0022
Vmin	0.9394	0.936	0.9442
Difference	0.051	0.054	0.058
Vfinal	0.9764	0.9654	0.9855

As Table 4.38 clearly shows, the final values at the end of 5 seconds after the fault are within the normal operational limits. Moreover the voltage oscillatory peak for all buses are well below the specified %10 limit for this case. However, it should be noted that the voltage oscillations in this case are higher than case 4.1.3 which was the similar case by means of installed capacity and breaker operating time for Bozyaka RES. This implies that the grid strength is relatively lower for case 3 than case 1. This implication will be clarified in the next steps of this case according to the aforementioned methodology.

The line loadings before, during and after the fault are also recorded and the related graphs are provided for lines Erzin-Andırın and Yumurtalık-Adana in graphs 4.89 and 4.90, respectively.

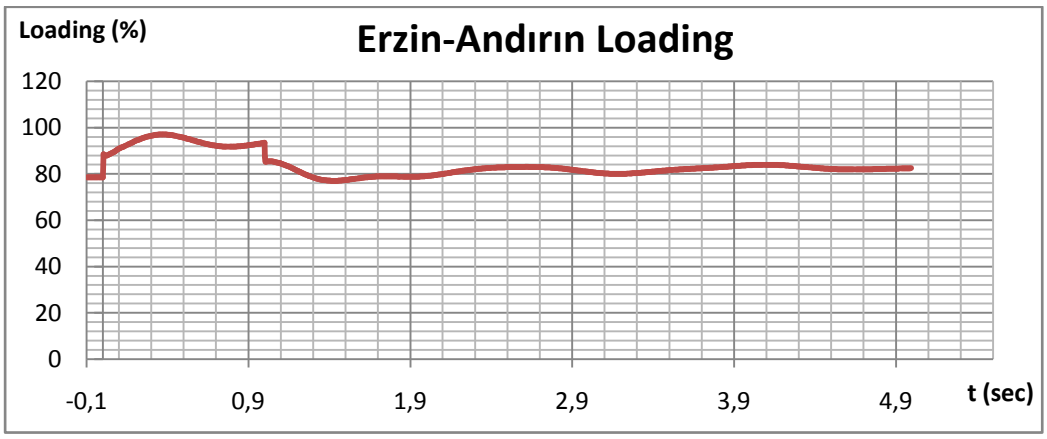

Graph 4.89. Loading of Erzin-Andırın Line

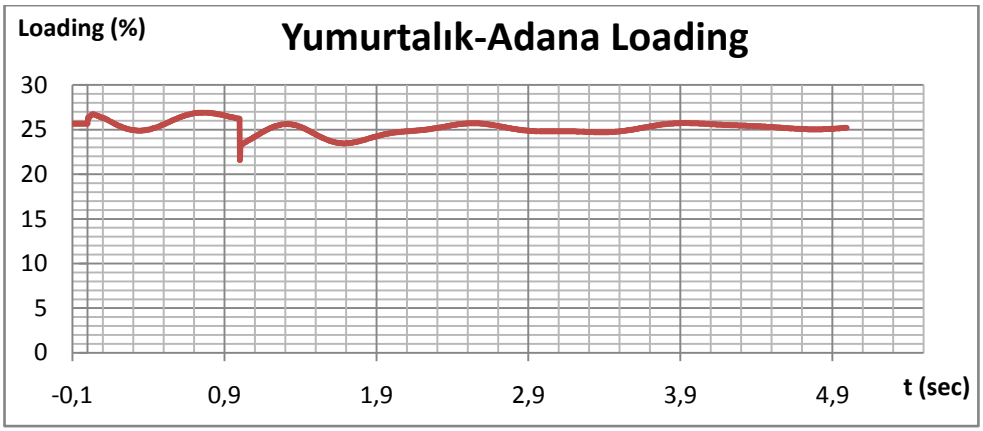

Graph 4.90. Loading of Yumurtalık-Adana Line

As can be seen from both graphs, the fault has caused a slight but immediate disturbance on the transmission lines. After the breaker operation, the line loadings have initially decreased immediately but slightly and then, began increasing in an attenuating oscillatory manner to reach the new steady-state values. Since all the transmission lines residing within 250 km radius of the fault point remained under %100 loading at any time before, during or after the fault, it is safe to claim that this case has no threat to the transmission lines by means of overloading. It is advisable to note that despite the loading of line Erzin-Andırın approaches %100, it never reaches or exceeds full loading at any time.

Table 4.39 provides the initial (t= -0,1 sec.), final (t=5 sec) and maximum rotor angles for Atatürk HPP and İskenderun (Atlas) TPP during this case.

Table 4.39. Rotor Angle Values for Atatürk and Iskenderun Plants

	Atatürk Rotor Angle (rad)	Iskenderun Rotor Angle (rad)
Initial	0.4978	1.3488
Final	0.4948	1.3998
Maximum	0.4948	1.452

As can be seen from Table 4.39 the initial and final values of Iskenderun TPP's rotor angle differ only by a small amount (approximately 2,86^{o}) while the Atatürk HPP's rotor angle shows no detectable response to the fault at all. Therefore, the simulation results verify that the generators stay in synchronism with the system without any adverse effect.

Taking the results provided above into consideration, the variations in bus voltages, line loadings after the fault clearance and rotor angles are proven to stay within the limits to ensure a stable operation of the system even with an installed capacity, and hence generation equal to the %10 of the short circuit MVA at the bus that the wind farm is connected to. Moreover, the observed parameter variations are far away from approaching the stability limits therefore they imply that the system may be able to handle disturbances for even higher values of installed capacity of the wind farm. This implication will be checked to be true in the next analysis, involving a wind farm installed capacity equal to %12,5 of the short circuit MVA of the connecting bus.

4.3.4: %12,5 (150 MW) Installed capacity

Breaker operating time: 1000 ms

For the given fault clearing time, the variations of selected bus voltages are provided in graphs 4.91 to 4.93.

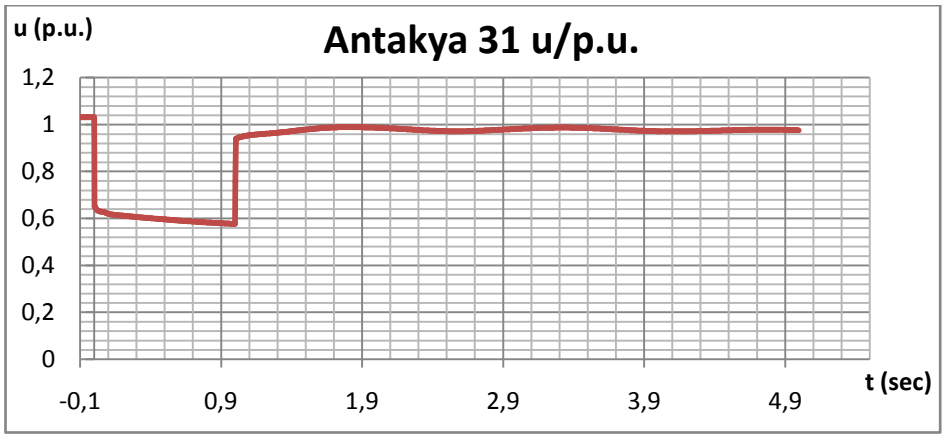

Graph 4.91. Voltage Variation of Antakya 31 Bus

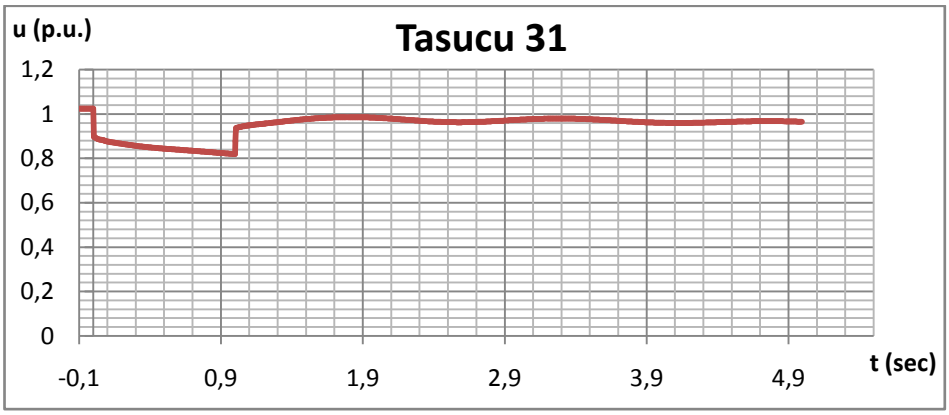

Graph 4.92. Voltage Variation of Tasucu 31 Bus

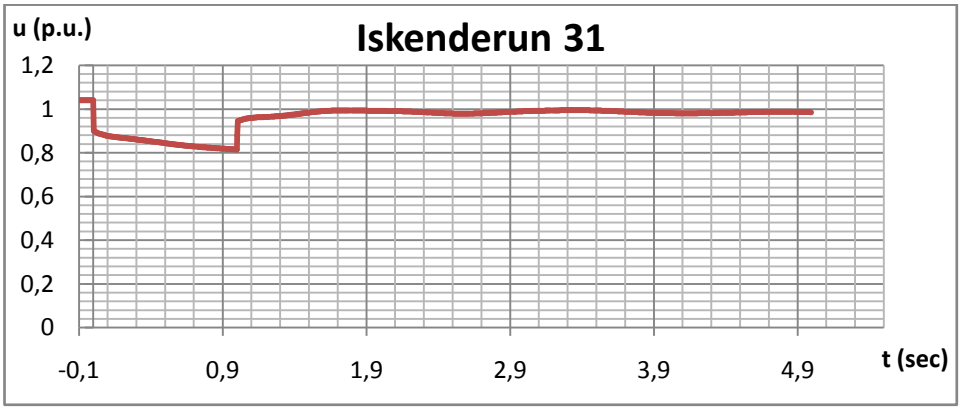

Graph 4.93. Voltage Variation of Iskenderun 31 Bus

As can be seen from the three graphs above, the disturbance had a drastic and almost immediate effect on the bus voltages which caused the voltages at nearby buses to drop sharply. However, the size of the drop varied between different buses and mainly influenced by the connection strength and distance to the location of fault. Antakya 31 bus, being the closest one to the fault has suffered from the largest voltage drop in the event of a 3-phase short circuit while Tasucu 31 and Iskenderun buses showed a similar response that is smaller than that of Antakya 31.

It can be seen that, at t=1 sec. the voltages at each bus rises sharply since the circuit breakers at the ends of faulted line are operated, thus, returning the rest of the system to fault-free state. However, the voltage values are not constant at the post-fault state until the new stable system operating state is fully reached. During this state, the oscillations of the voltage values at each bus can be seen. The maximum and minimum values of bus voltages after the fault clearing, as well as their difference in p.u. are provided in Table 4.40.

Table 4.40 Bus Voltages for Case 3.4

	Antakya 31	Tasucu 31	Iskenderun
Vmax	0.9908	0.9905	1.0027
Vmin	0.9395	0.9363	0.9441
Difference	0.0513	0.0542	0.0586
Vfinal	0.9764	0.9654	0.9855

As Table 4.40 clearly shows, the final values at the end of 5 seconds after the fault are within the normal operational limits. Moreover the voltage oscillatory peak for all buses are still well below the specified %10 limit for this case.

The line loadings before, during and after the fault are also recorded and the related graphs are provided for lines Erzin-Andırın and Yumurtalık-Adana in graphs 4.94 and 4.95, respectively.

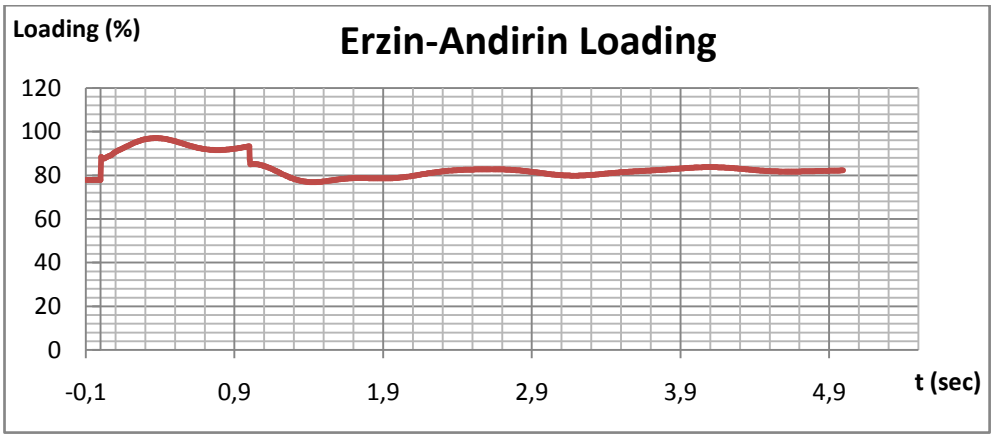

Graph 4.94. Loading of Erzin-Andırın Line

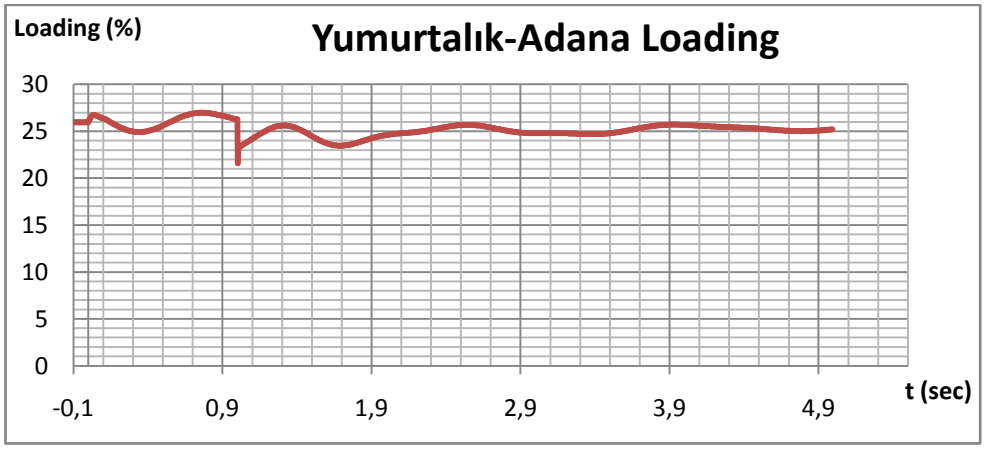

Graph 4.95. Loading of Yumurtalık-Adana Line

As can be seen from both graphs, the fault has caused a slight but immediate disturbance on the transmission lines. After the breaker operation, the line loadings have initially decreased immediately but slightly and then, began increasing in an

attenuating oscillatory manner to reach the new steady-state values. Since all the transmission lines residing within 250 km radius of the fault point remained under %100 loading at any time before, during or after the fault, it is safe to claim that this case has no threat to the transmission lines by means of overloading. It is advisable to note that despite the loading of line Erzin-Andırın approaches %100, it never reaches or exceeds full loading at any time.

Table 4.41 provides the initial (t= -0,1 sec.), final (t=5 sec) and maximum rotor angles for Atatürk HPP and İskenderun (Atlas) TPP during this case.

Table 4.41. Rotor Angle Values for Atatürk and Iskenderun Plants

	Atatürk Rotor Angle (rad)	Iskenderun Rotor Angle (rad)
Initial	0.4948	1.341
Final	0.4948	1.3998
Maximum	0.4948	1.452

As can be seen from Table 4.41 the initial and final values of Iskenderun TPP's rotor angle differ only by a small amount (approximately $3{,}53^{o}$) while the Atatürk HPP's rotor angle shows no detectable response to the fault at all. Therefore, the simulation results verify that the generators stay in synchronism with the system without any adverse effect.

Taking the results provided above into consideration, the variations in bus voltages, line loadings after the fault clearance and rotor angles are proven to stay within the limits to ensure a stable operation of the system even with an installed capacity, and hence generation equal to the %12,5 of the short circuit MVA at the bus that the wind farm is connected to. Moreover, the observed parameter variations are far away from approaching the stability limits therefore they imply that the system may be able to handle disturbances for even higher values of installed capacity of the wind farm. This implication will be checked to be true in the next analysis, involving a

wind farm installed capacity equal to %15 of the short circuit MVA of the connecting bus.

4.3.5: %15 (180 MW) Installed capacity

Breaker operating time: 1000 ms

For the given fault clearing time, the variations of selected bus voltages are provided in graphs 4.96 to 4.98.

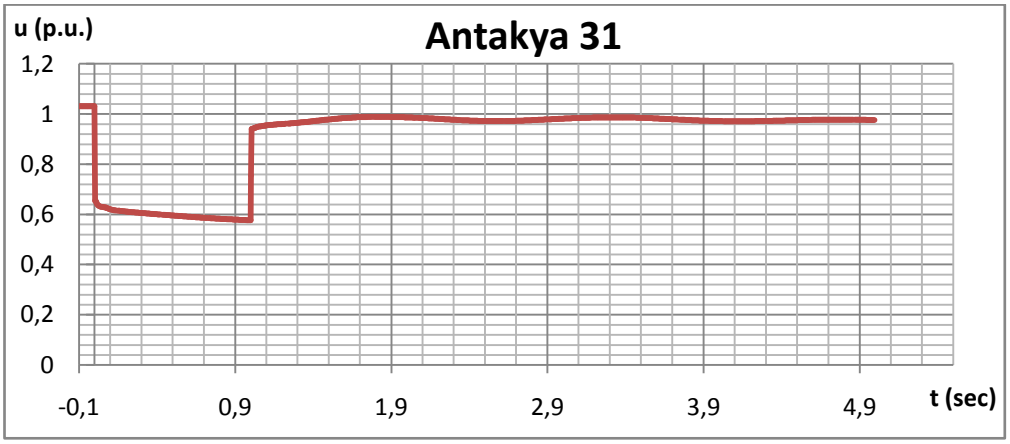

Graph 4.96. Voltage Variation of Antakya 31 Bus

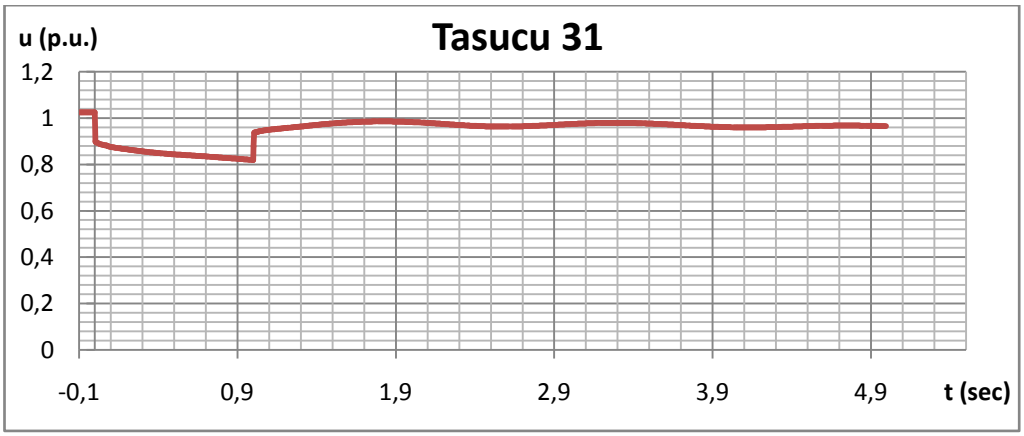

Graph 4.97. Voltage Variation of Tasucu 31 Bus

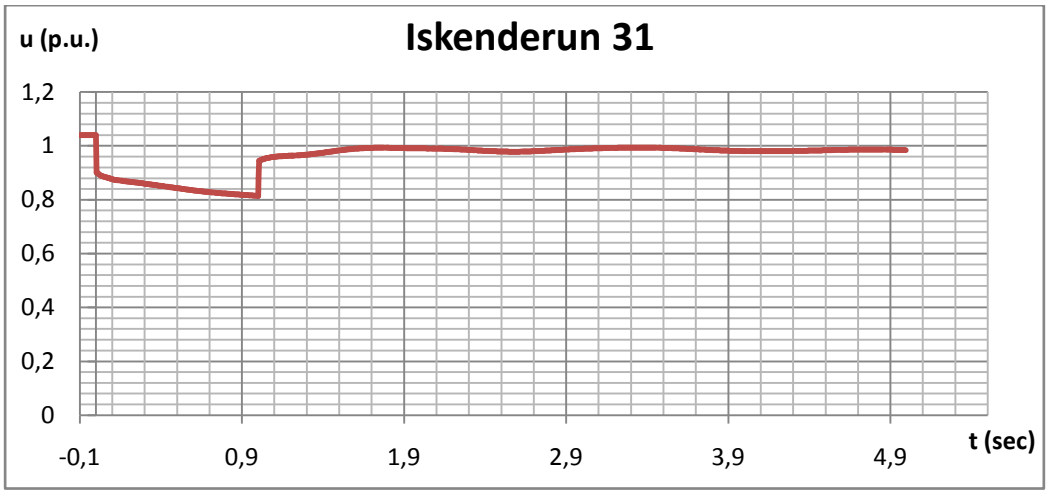

Graph 4.98. Voltage Variation of Iskenderun 31 Bus

As can be seen from the three graphs above, the disturbance had a drastic and almost immediate effect on the bus voltages which caused the voltages at nearby buses to drop sharply. However, the size of the drop varied between different buses and mainly influenced by the connection strength and distance to the location of fault. Antakya 31 bus, being the closest one to the fault has suffered from the largest voltage drop in the event of a 3-phase short circuit while Tasucu 31 and Iskenderun buses showed similar responses that are smaller than that of Antakya 31.

It can be seen that, at t=1 sec. the voltages at each bus rises sharply since the circuit breakers at the ends of faulted line are operated, thus, returning the rest of the system to fault-free state. However, the voltage values are not constant at the post-fault state until the new stable system operating state is fully reached. During this state, the oscillations of the voltage values at each bus can be seen. The maximum and minimum values of bus voltages after the fault clearing, as well as their difference in p.u. are provided in Table 4.42.

Table 4.42. Bus Voltages for Case 3.5

	Antakya 31	Tasucu 31	Iskenderun
Vmax	1.0312	1.0252	1.04
Vmin	0.9398	0.9369	0.9443
Difference	0.0914	0.0883	0.0957
Vfinal	0.9757	0.965	0.9845

As Table 4.42 clearly shows, the final values at the end of 5 seconds after the fault are still within the normal operational limits. However, the oscillation magnitudes are considerably higher than, almost equal to double of the values in case 4.3.4 despite a small increase (30 MW) in the installed capacity of wind farm. The voltage oscillatory peak for all buses are now approaching the specified %10 limit for this case.

The line loadings before, during and after the fault are also recorded and the related graphs are provided for lines Erzin-Andırın and Yumurtalık-Adana in graphs 4.99 and 4.100, respectively.

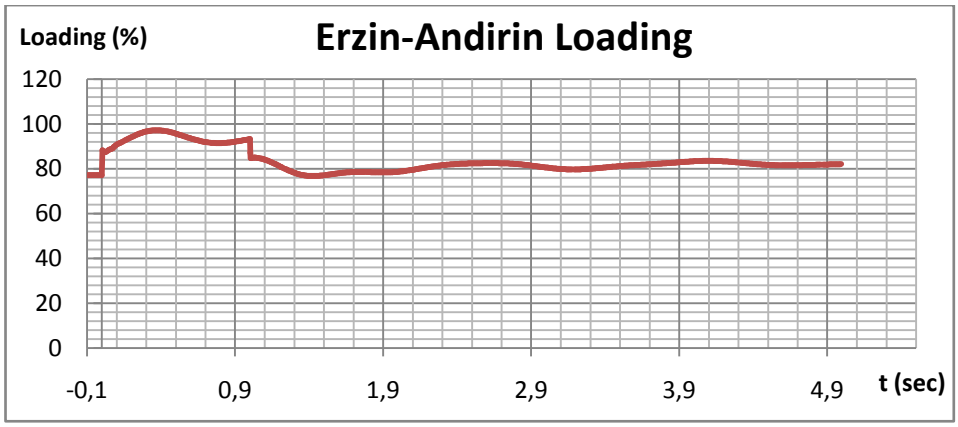

Graph 4.99. Loading of Erzin-Andirin Line

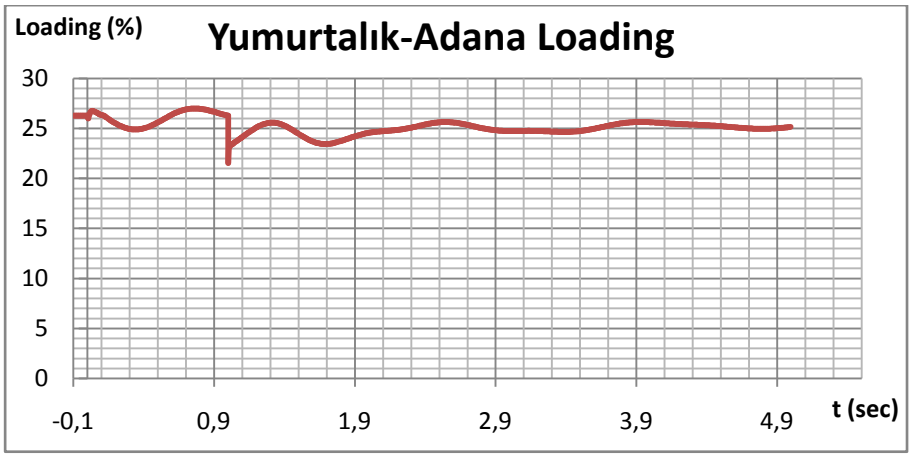

Graph 4.100. Loading of Yumurtalık-Adana Line

As can be seen from both graphs, the fault has caused a slight but immediate disturbance on the transmission lines. After the breaker operation, the line loadings have initially decreased immediately but slightly and then, began increasing in an attenuating oscillatory manner to reach the new steady-state values. Since all the transmission lines residing within 250 km radius of the fault point remained under %100 loading at any time before, during or after the fault, it is safe to claim that this case has no threat to the transmission lines by means of overloading. It is advisable to note that despite the loading of line Erzin-Andırın approaches %100, it never reaches or exceeds full loading at any time.

Table 4.43 provides the initial (t= -0,1 sec.), final (t=5 sec) and maximum rotor angles for Atatürk HPP and İskenderun (Atlas) TPP during this case.

Table 4.43. Rotor Angle Values for Atatürk and Iskenderun Plants

	Atatürk Rotor Angle (rad)	Iskenderun Rotor Angle (rad)
Initial	0.5045	1.3327
Final	0.5045	1.3862
Maximum	0.5045	1.4378

As can be seen from Table 4.43 the initial and final values of Iskenderun TPP's rotor angle differ only by a small amount (approximately 2,86^{o}) while the Atatürk HPP's rotor angle shows no detectable response to the fault at all. Therefore, the simulation results verify that the generators stay in synchronism with the system without any adverse effect.

Taking the results provided above into consideration, the variations in bus voltages, line loadings after the fault clearance and rotor angles are proven to stay within the limits to ensure a stable operation of the system even with an installed capacity, and hence generation equal to the %15 of the short circuit MVA at the bus that the wind farm is connected to. However, unlike previous cases, the observed voltage variations are now approaching the stability limits therefore they imply that the system may not be able to handle disturbances for higher values of installed capacity of the wind farm. This implication will be checked to be true in the next analysis, involving a wind farm installed capacity equal to a considerable %38 of the short circuit MVA of the connecting bus.

4.3.6: %38 (455 MW) Installed capacity

As the final step of this case, the wind farm installed capacity is increased to the maximum possible value that is limited by the system equipment, i.e. the relevant transformers and transmission lines that would be overloaded if further increase took place for Şenköy RES.

Breaker operating time: 1000 ms

For the given fault clearing time, the variations of selected bus voltages are provided in graphs 4.101 to 4.103.

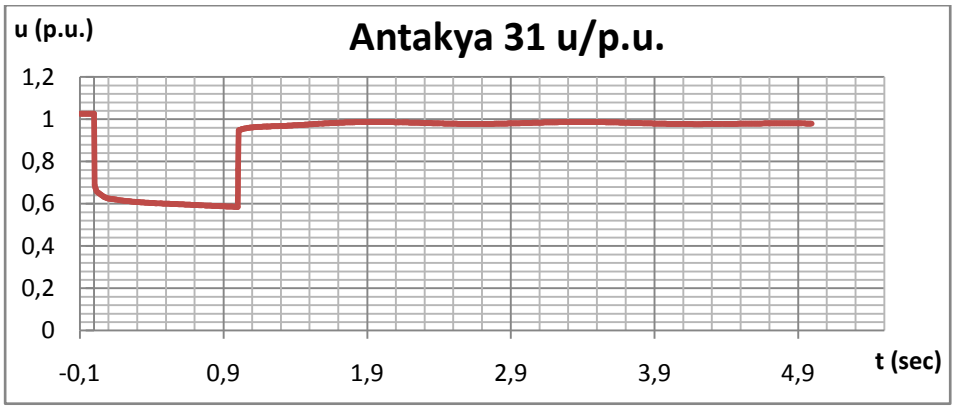

Graph 4.101. Voltage Variation of Antakya 31 Bus

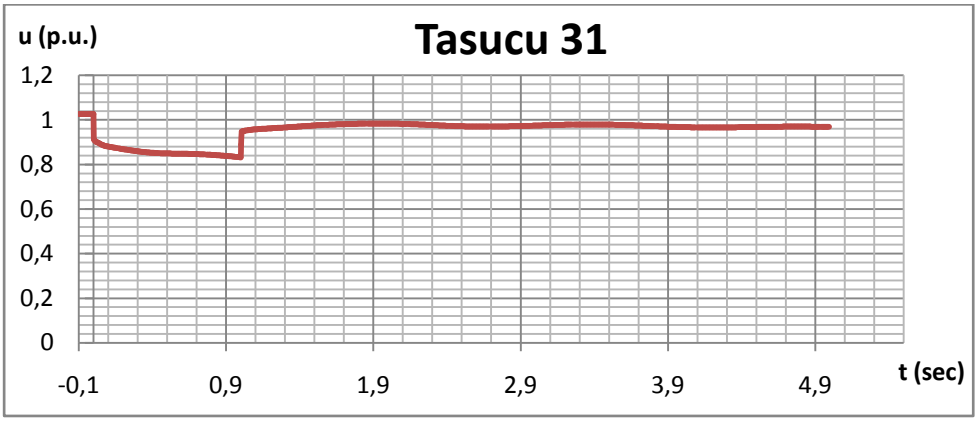

Graph 4.102. Voltage Variation of Tasucu 31 Bus

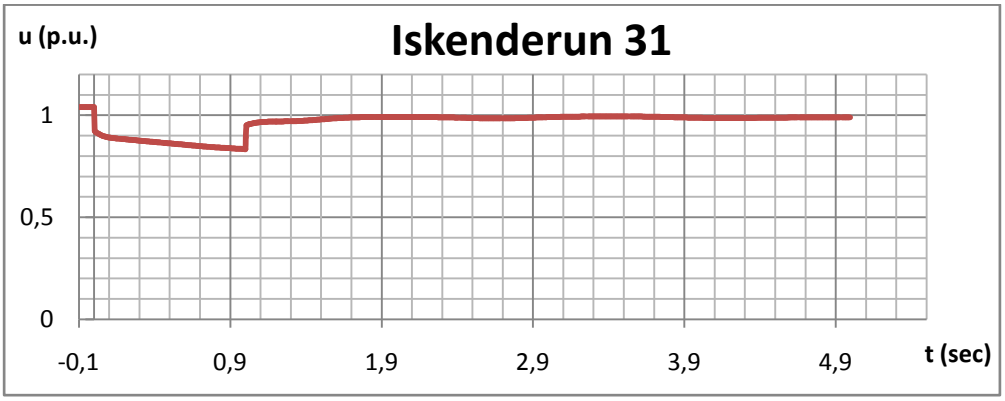

Graph 4.103. Voltage Variation of Iskenderun 31 Bus

As can be seen from the three graphs above, the disturbance had a drastic and almost immediate effect on the bus voltages which caused the voltages at nearby buses to drop sharply. However, the size of the drop varied between different buses and mainly influenced by the connection strength and distance to the location of fault. Antakya 31 bus, being the closest one to the fault has suffered from the largest voltage drop in the event of a 3-phase short circuit while Tasucu 31 and Iskenderun buses showed similar responses that are smaller than that of Antakya 31.

It can be seen that, at t=1 sec. the voltages at each bus rises sharply since the circuit breakers at the ends of faulted line are operated, thus, returning the rest of the system to fault-free state. However, the voltage values are not constant at the post-fault state until the new stable system operating state is fully reached. During this state, the oscillations of the voltage values at each bus can be seen. It is observed that the oscillations in voltages of all three buses have increased considerably when compared to earlier cases involving much smaller installed capacity values. The maximum and minimum values of bus voltages after the fault clearing, as well as their difference in p.u. are provided in Table 4.44.

Table 4.44. Bus Voltages for Case 3.6

	Antakya 31	Tasucu 31	Iskenderun
Vmax	1.041	0.9841	0.994
Vmin	0.9474	0.8894	0.8915
Difference	0.0936	0.0947	0.1025
Vfinal	0.9797	0.969	0.9889

As Table 4.44 clearly shows, the final values at the end of 5 seconds after the fault are still within the normal operational limits. However, the oscillatory peak for Antakya 31 and Tasucu 31 buses are very close to the %10 limit while Iskenderun bus's peak difference has exceeded this value by a small amount.

The line loadings before, during and after the fault are also recorded and the related graphs are provided for lines Erzin-Andırın and Yumurtalık-Adana in graphs 4.104 and 4.105, respectively.

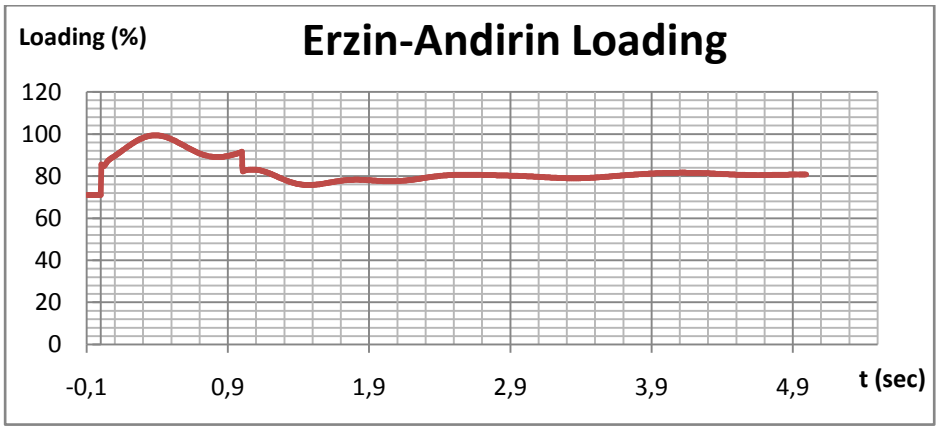

Graph 4.104. Loading of Erzin-Andirin Line

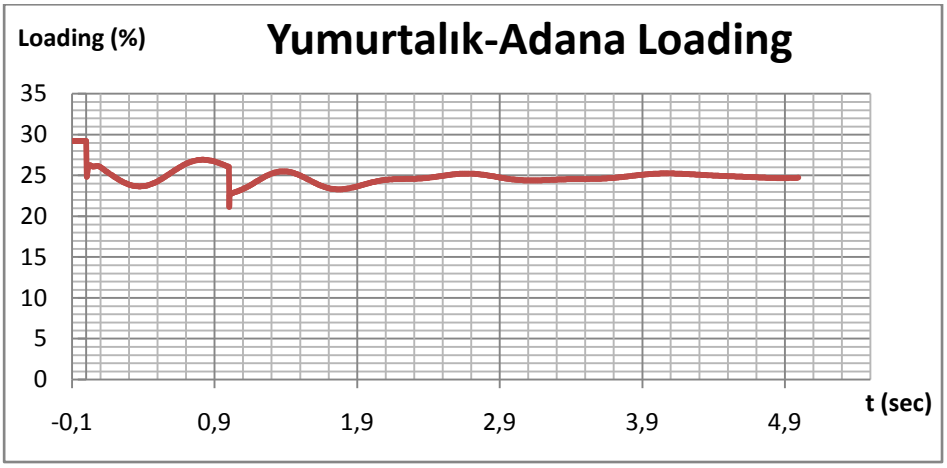

Graph 4.105. Loading of Yumurtalık-Adana Line

As can be seen from both graphs, the fault has caused a slight but immediate disturbance on the transmission lines. After the breaker operation, the line loadings have initially decreased immediately but slightly and then, began increasing in an

attenuating oscillatory manner to reach the new steady-state values. Since all the transmission lines residing within 250 km radius of the fault point remained under %100 loading at any time before, during or after the fault, it is safe to claim that this case has no threat to the transmission lines by means of overloading. It is advisable to note that despite the loading of line Erzin-Andırın approaches %100, it never reaches or exceeds full loading at any time.

Table 4.45 provides the initial (t= -0,1 sec.), final (t=5 sec) and maximum rotor angles for Atatürk HPP and İskenderun (Atlas) TPP during this case.

Table 4.45. Rotor Angle Values for Atatürk and Iskenderun Plants

	Atatürk Rotor Angle (rad)	Iskenderun Rotor Angle (rad)
Initial	0.5422	1.4173
Final	0.5422	1.492
Maximum	0.5422	1.6478

As can be seen from Table 4.45 the initial and final values of Iskenderun TPP's rotor angle varies greatly with time, increasing up to approximately $94{,}4^{o}$. This is an undesired result since the rotor angle, even if for a temporary duration, exceeds the 90^{o} stability limit. Kundur [55] states that under transient conditions, the stability limit may be exceeded for a short time without the loss of stability. Since the final rotor angle of Iskenderun is below 90^{o} (approx. $85{,}2^{o}$) the stability is likely to be preserved under such a disturbance. However, it is a very critical situation that may have catastrophic outcomes in case of an additional disturbance, even a small one, which will certainly cause the already-at-limits Iskenderun TPP to go off synchronism under these circumstances. Atatürk HPP's rotor angle, on the other hand, shows no detectable response to the fault at all.

Therefore, the simulation results show that the probability of stability loss for this case is not negligible as the rotor angle of Iskenderun TPP exceeds 90^o and the aforementioned series of events are assumed to be of considerable probability.

Taking the results provided above into consideration, although the variations in some bus voltages and line loadings after the fault clearance are proven to stay within the limits, the facts that some buses' voltages oscillate unacceptably high and the stability of Iskenderun TPP is arguable as it exceeds the normal stability limit, presence of a wind farm with such a high installed capacity in the given region where the grid relatively weak can be considered as a threat to system stability and operational quality.

4.4 Case 4: Aksu RES

The fourth case, Aksu RES is chosen to be demonstrated fourth since it resides in the central region of Turkey where the grid can be assumed to be strong. Unlike the previous cases, the area where Aksu RES is resided is moderately developed, with more developed centers being in the western part of the area. Aksu wind farm is resided in Yahyalı, a town within the city limits of Kayseri, In the system, the wind farm is connected to the grid at Kayseri 34.5 kV (denoted by Kayseri 34 in the model) bus. Therefore, the connecting line is between the buses Aksu RES 34 and Kayseri 34 The current installed capacity of Aksu RES is 72 MW. The short circuit power at Kayseri 34 bus, on the other hand, is 3800 MVA [54]. Since there were no wind farms with significant capacity near Aksu RES, it is modeled on its own, without any additional capacity coming from nearby wind farms. As can be inferred from its location, the grid where the wind farm is can be considered to be strong since being on the corridor between the eastern parts of Turkey, where the generation levels are high and the western parts, where the consumption is relatively high. Despite being small by means total installed capacity when compared to western part of Turkey, being the only large wind farm in the area makes it possible for the grid to be able to meet the increasing generation levels . Although the position of Aksu RES makes it to be relatively far away from large consumption centers in the grid due to being on

approximately midway between eastern and western ends of Turkey, the fact that it resides on the intersection of many transmission lines providing power flow from east to west implies that the grid around the Aksu RES is relatively strong. This implies that, during simulations, the effects of disturbances will be smaller than what would be expected to be observed at weaker regions of the grid.

As mentioned in the preceding section, the analyses will be carried out for installed capacities of Aksu RES that will be equal to %5, %7.5, %10, %12.5 and %15 of the short circuit MVA at Kayseri 34 bus. The installed capacity values corresponding to these percentages of short circuit power are given in Table 4.46

Table 4.46. Installed Capacity Values for Case 4.

% of Ssc	5	7,5	10	12,5	15
Installed Capacity (MW)	190	285	380	475	570

The buses, transmission lines and generators within 250 km radius of the wind farm are chosen to be observed. However, to avoid overflow of output data, some elements among the initial set are omitted after they are proven not to show any significant variations during the analysis processes. The resulting set of elements to be observed and whose results will be provided in detail are given below.

-Buses (Voltages of) : Kayseri 34, Nevşehir 34, Niğde 154

-Transmission Lines (Loading of): Kayseri-Nevsehir 154, Afsin-Kayseri 154

-Generators (Rotor Angles of): Elbistan A, Elbistan B, Karakaya

Analysis Results

For each given installed capacity value, five individual analyses are carried out regarding circuit breaker operating times. For the sake of keeping the data given here compact, only the cases corresponding to breaker operating time of 1000 ms will be presented unless stated otherwise.

4.4.1: %5 (190 MW) Installed capacity

Breaker operating time: 1000 ms

For the given fault clearing time, the variations of selected bus voltages are provided in graphs 4.106 to 4.108.

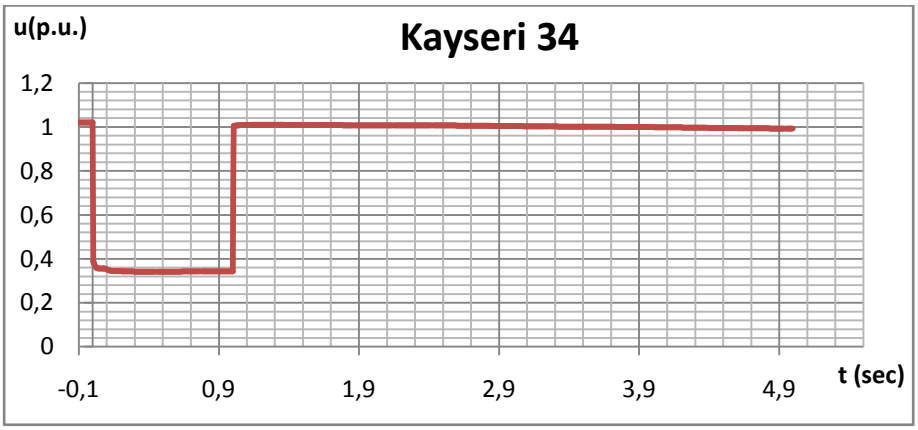

Graph 4.106. Voltage Variation of Kayseri 34 Bus

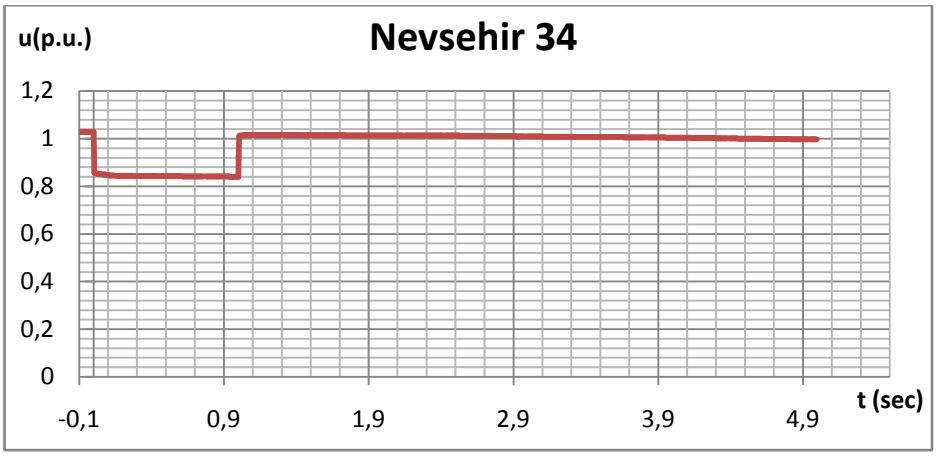

Graph 4.107. Voltage Variation of Nevsehir 34 Bus

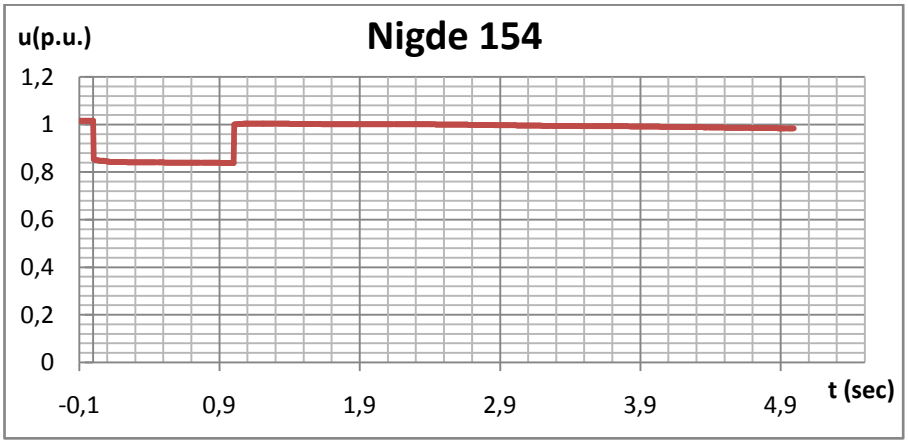

Graph 4.108. Voltage Variation of Nigde 154 Bus

As can be seen from the three graphs above, the disturbance had a drastic and almost immediate effect on the bus voltages which caused the voltages at nearby buses to drop sharply. However, the size of the drop varied between different buses and mainly influenced by the connection strength and distance to the location of fault. Kayseri 34 bus, being the closest one to the fault has suffered from the largest voltage drop in the event of a 3-phase short circuit while Nevsehir 34 and Nigde 154 buses showed similar responses that are smaller than that of Kayseri 34.

It can be seen that, at t=1 sec. the voltages at each bus rises sharply since the circuit breakers at the ends of faulted line are operated, thus, returning the rest of the system to fault-free state. However, the voltage values are not constant at the post-fault state until the new stable system operating state is fully reached. During this state, the oscillations of the voltage values at each bus can be seen. The maximum and minimum values of bus voltages after the fault clearing, as well as their difference in p.u. are provided in Table 4.47.

Table 4.47 Bus Voltages for Case 4.1

	Kayseri 34	Nevsehir 34	Nigde 154
Vmax	1.0205	1.0282	1.0157
Vmin	0.9926	0.9966	0.9835
Difference	0.0279	0.0316	0.0322
Vfinal	0.9926	0.9966	0.9835

As Table 4.47 clearly shows, the final values at the end of 5 seconds after the fault are within the normal operational limits. Moreover the voltage oscillatory peak for all buses are well below the specified %10 limit for this case. Moreover, it should be noted that the voltage oscillations in this case are comparable to case 4.1.1.5 which was the similar case by means of installed capacity and breaker operating time for Bozyaka RES. This implies that the grid strength is similarly strong for case 4 like case 1. This implication will be clarified in the next steps of this case which involve increasing the installed capacity of Aksu RES according to the aforementioned methodology.

The line loadings before, during and after the fault are also recorded and the related graphs are provided for lines Kayseri-Nevsehir 154 and Afsin-Kayseri in graphs 4.109 and 4.110, respectively.

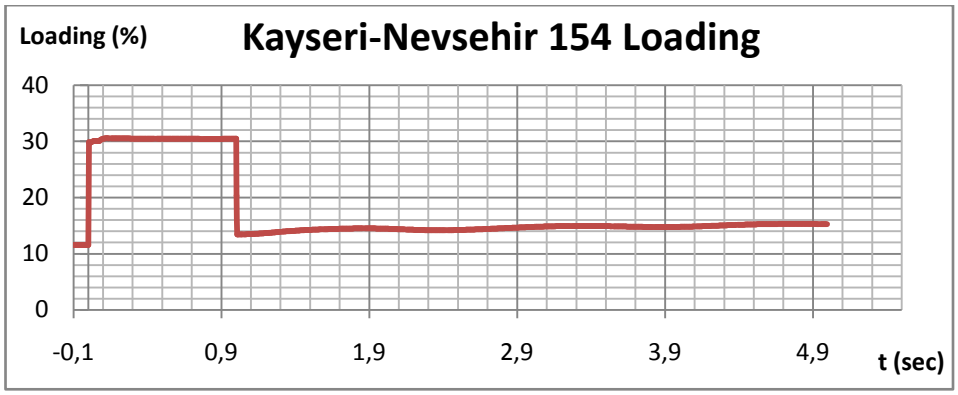

Graph 4.109. Loading of Kayseri-Nevsehir Line

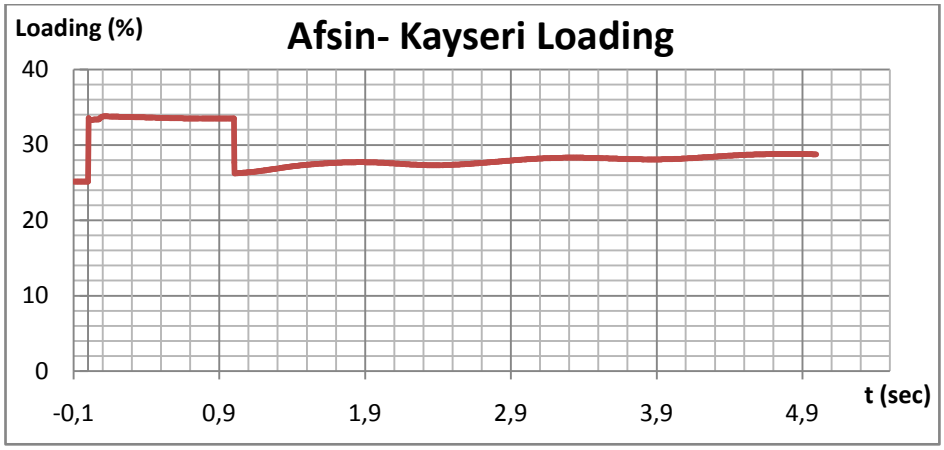

Graph 4.110. Loading of Afsin-Kayseri Line

As can be seen from both graphs, the fault has caused a slight but immediate disturbance on the transmission lines. After the breaker operation, the line loadings have initially decreased immediately and then, began increasing in an attenuating oscillatory manner to reach the new steady-state values. Since all the transmission lines residing within 250 km radius of the fault point remained under %100 loading at any time before, during or after the fault, it is safe to claim that this case has no threat to the transmission lines by means of overloading.

Table 4.48 provides the initial (t= -0,1 sec.), final (t=5 sec) and maximum rotor angles for Afsin-Elbistan A and B TPP and Karakaya HPP during this case.

Table 4.48 Rotor Angle Values for Afsin A & B and Karakaya Plants

	Afsin A Rotor Angle (rad)	Afsin B Rotor Angle (rad)	Karakaya Rotor Angle (rad)
Initial	0.392	0.659	0.5095
Final	0.3931	0.663	0.512
Maximum	0.394	0.663	0.5122

As can be seen from Table 4.48 the initial and final values of all three power plants' rotor angles differ only by a small amount while the Afsin A TPP's rotor angle shows the minimum response to the fault among them. Therefore, the simulation results verify that the generators stay in synchronism with the system without any adverse effect.

Taking the results provided above into consideration, the variations in bus voltages, line loadings after the fault clearance and rotor angles are proven to stay within the limits to ensure a stable operation of the system even with an installed capacity, and hence generation equal to the %5 of the short circuit MVA at the bus that the wind farm is connected to. Moreover, the observed parameter variations are far away from approaching the stability limits therefore they imply that the system may be able to handle disturbances for even higher values of installed capacity of the wind farm. This implication will prove true in the next analysis, involving a wind farm installed capacity equal to %7,5 of the short circuit MVA of the connecting bus.

4.4.2: %7,5 (285 MW) Installed capacity

Breaker operating time: 1000 ms

For the given fault clearing time, the variations of selected bus voltages are provided in graphs 4.111 to 4.113.

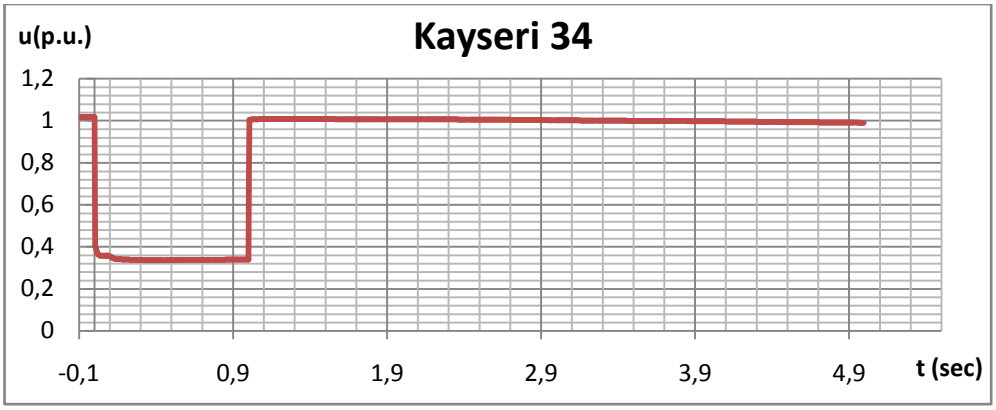

Graph 4.111. Voltage Variation of Kayseri 34 Bus

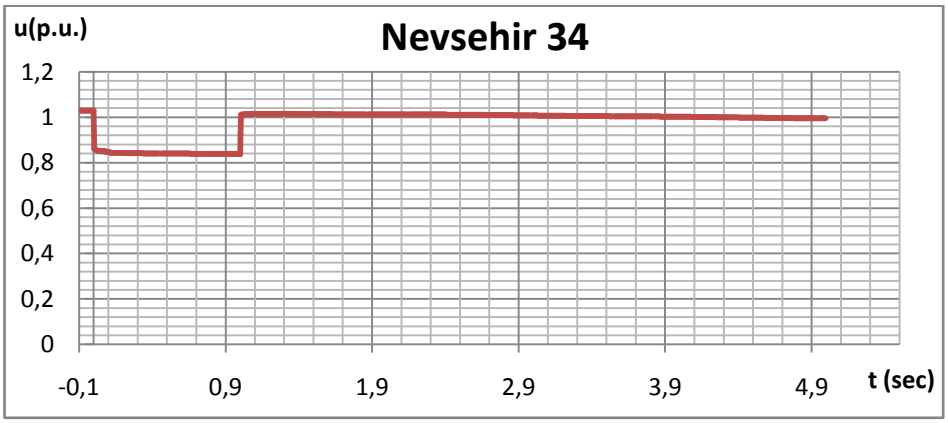

Graph 4.112. Voltage Variation of Nevsehir 34 Bus

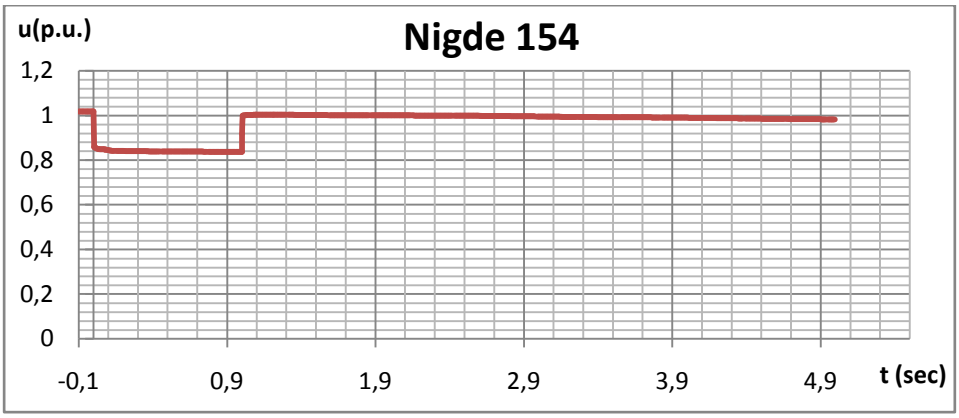

Graph 4.113. Voltage Variation of Nigde 154 Bus

As can be seen from the three graphs above, the disturbance had a drastic and almost immediate effect on the bus voltages which caused the voltages at nearby buses to drop sharply. However, the size of the drop varied between different buses and mainly influenced by the connection strength and distance to the location of fault. Kayseri 34 bus, being the closest one to the fault has suffered from the largest voltage drop in the event of a 3-phase short circuit while Nevsehir 34 and Nigde 154 buses showed similar responses that are smaller than that of Kayseri 34.

It can be seen that, at t=1 sec. the voltages at each bus rises sharply since the circuit breakers at the ends of faulted line are operated, thus, returning the rest of the system to fault-free state. However, the voltage values are not constant at the post-fault state until the new stable system operating state is fully reached. During this state, the oscillations of the voltage values at each bus can be seen. The maximum and minimum values of bus voltages after the fault clearing, as well as their difference in p.u. are provided in Table 4.49.

Table 4.49. Bus Voltages for Case 4.2

	Kayseri 34	Nevsehir 34	Nigde 154
Vmax	1.0205	1.0297	1.0174
Vmin	0.9908	0.995	0.9821
Difference	0.0297	0.0347	0.0353
Vfinal	0.9908	0.995	0.9821

As Table 4.49 clearly shows, the final values at the end of 5 seconds after the fault are within the normal operational limits. Moreover the voltage oscillatory peak for all buses are well below the specified %10 limit for this case. Furthermore, it should be noted that the voltage oscillations in this case are comparable to case 4.1.2. which was the similar case by means of installed capacity and breaker operating time for Bozyaka RES. This implies that the grid strength is similarly strong for case 4 like case 1. This implication will be clarified in the next steps of this case which involve increasing the installed capacity of Aksu RES according to the aforementioned methodology.

The line loadings before, during and after the fault are also recorded and the related graphs are provided for lines Kayseri-Nevsehir 154 and Afsin-Kayseri in graphs 4.114 and 4.115, respectively.

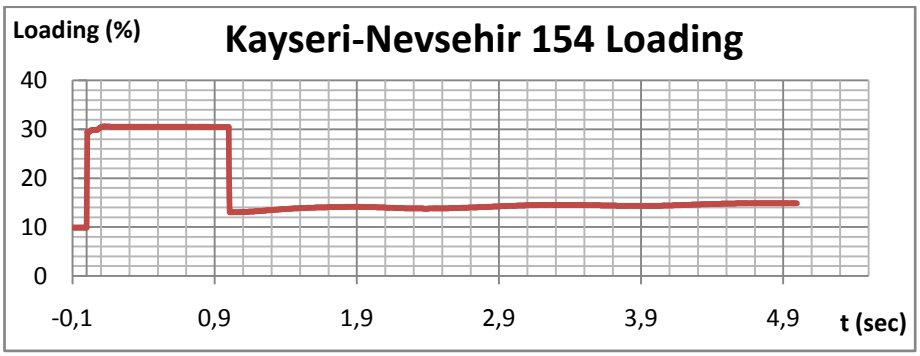

Graph 4.114. Loading of Kayseri-Nevsehir Line

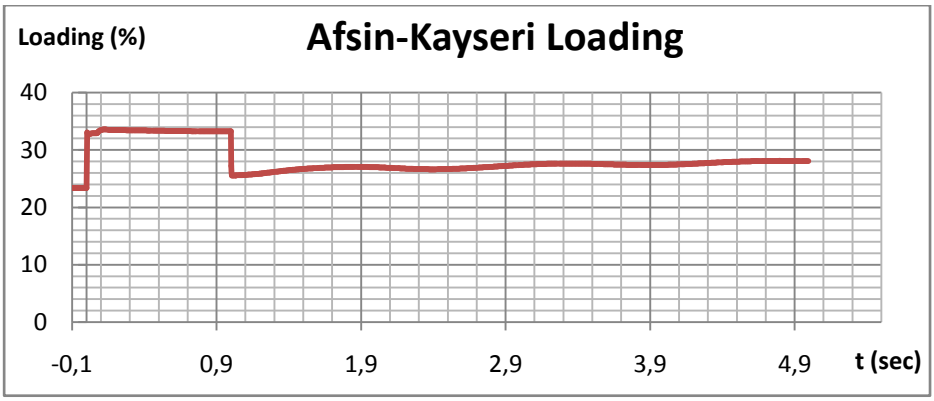

Graph 4.115. Loading of Afsin-Kayseri Line

As can be seen from both graphs, the fault has caused a slight but immediate disturbance on the transmission lines. After the breaker operation, the line loadings have initially decreased immediately yet slightly and then, began increasing in an attenuating oscillatory manner to reach the new steady-state values. Since all the transmission lines residing within 250 km radius of the fault point remained under %100 loading at any time before, during or after the fault, it is safe to claim that this case has no threat to the transmission lines by means of overloading.

Table 4.50 provides the initial (t= -0,1 sec.), final (t=5 sec) and maximum rotor angles for Afsin-Elbistan A and B TPP and Karakaya HPP during this case.

Table 4.50. Rotor Angle Values for Afsin A & B and Karakaya Plants

	Afsin A Rotor Angle (rad)	Afsin B Rotor Angle (rad)	Karakaya Rotor Angle (rad)
Initial	0.3768	0.649	0.4948
Final	0.3763	0.6521	0.496
Maximum	0.3786	0.6522	0.4968

As can be seen from Table 4.50, the initial and final values of all three power plants' rotor angles differ only by a small amount (while the Afsin A TPP's rotor angle shows the minimum response to the fault among them). Therefore, the simulation results verify that the generators stay in synchronism with the system without any adverse effect.

Taking the results provided above into consideration, the variations in bus voltages, line loadings after the fault clearance and rotor angles are proven to stay within the limits to ensure a stable operation of the system even with an installed capacity, and hence generation equal to the %7,5 of the short circuit MVA at the bus that the wind farm is connected to. Moreover, the observed parameter variations are far away from approaching the stability limits therefore they imply that the system may be able to handle disturbances for even higher values of installed capacity of the wind farm. This implication will be checked to be true in the next analysis, involving a wind farm installed capacity equal to %10 of the short circuit MVA of the connecting bus.

4.4.3: %10 (380 MW) Installed capacity

Breaker operating time: 1000 ms

For the given fault clearing time, the variations of selected bus voltages are provided in graphs 4.116 to 4.118.

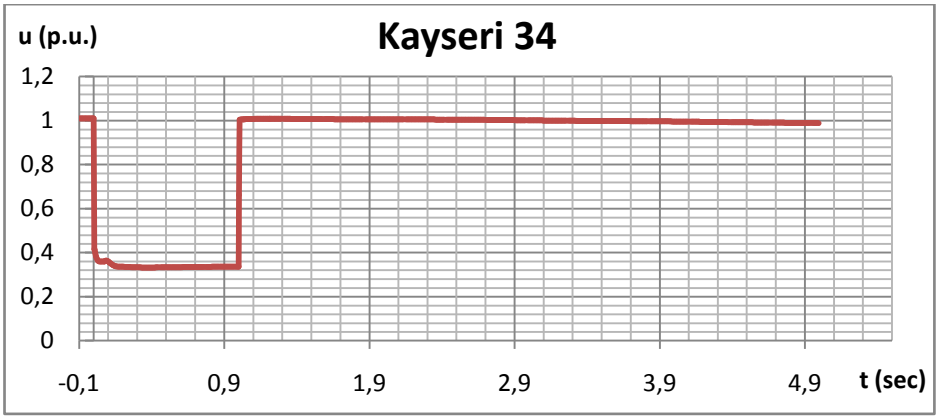

Graph 4.116. Voltage Variation of Kayseri 34 Bus

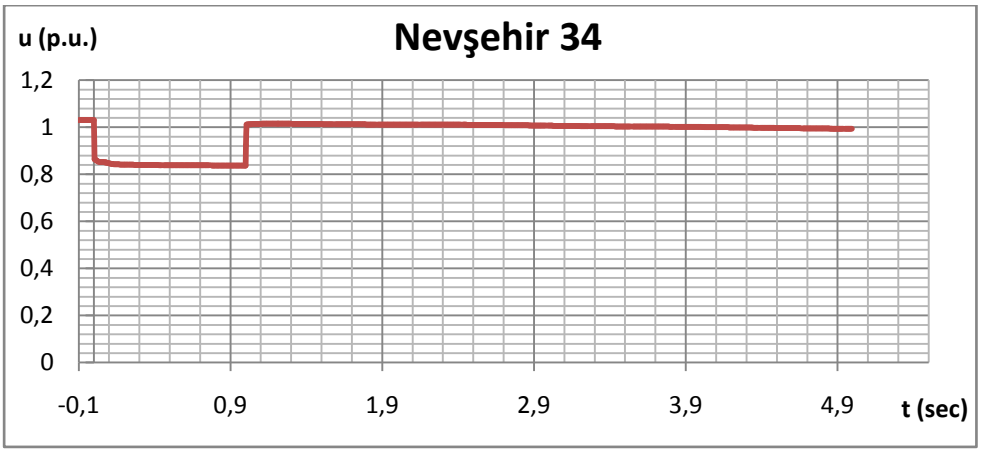

Graph 4.117. Voltage Variation of Nevsehir 34 Bus

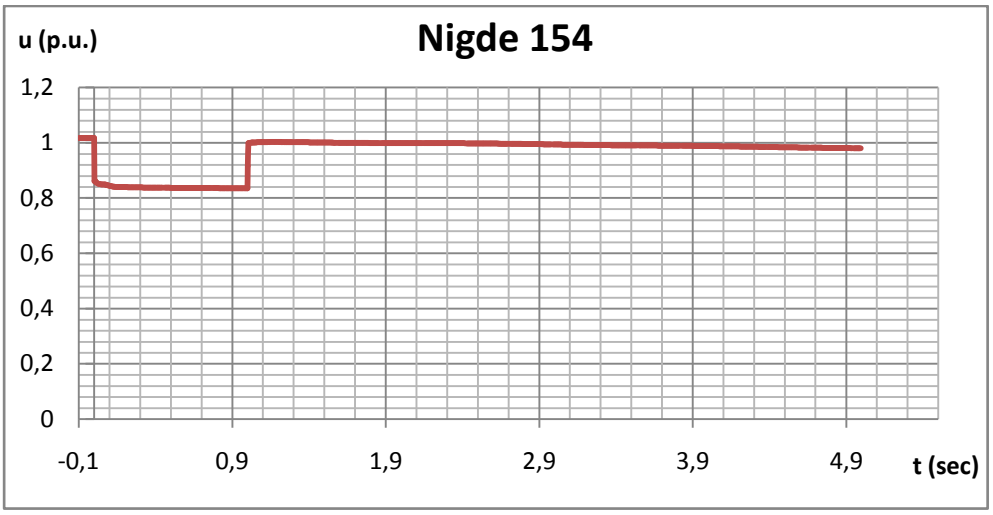

Graph 4.118. Voltage Variation of Nigde 154 Bus

As can be seen from the three graphs above, the disturbance had a drastic and almost immediate effect on the bus voltages which caused the voltages at nearby buses to drop sharply. However, the size of the drop varied between different buses and mainly influenced by the connection strength and distance to the location of fault. Kayseri 34 bus, being the closest one to the fault has suffered from the largest voltage drop in the event of a 3-phase short circuit while Nevsehir 34 and Nigde 154 buses showed similar responses that are smaller than that of Kayseri 34. It can be

seen that, at t=1 sec. the voltages at each bus rises sharply since the circuit breakers at the ends of faulted line are operated, thus, returning the rest of the system to fault-free state. However, the voltage values are not constant at the post-fault state until the new stable system operating state is fully reached. During this state, the oscillations of the voltage values at each bus can be seen. The maximum and minimum values of bus voltages after the fault clearing, as well as their difference in p.u. are provided in Table 4.51

Table 4.51. Bus Voltages for Case 4.3

	Kayseri 34	Nevsehir 34	Nigde 154
Vmax	1.0188	1.0298	1.0178
Vmin	0.9889	0.9933	0.9805
Difference	0.0299	0.0365	0.0373
Vfinal	0.9889	0.9933	0.9805

As Table 4.51 clearly shows, the final values at the end of 5 seconds after the fault are within the normal operational limits. Moreover the voltage oscillatory peak for all buses are well below the specified %10 limit for this case. Moreover, it should be noted that the voltage oscillations in this case are comparable to case 4.1.2 which was the similar case by means of installed capacity and breaker operating time for Bozyaka RES. This implies that the grid strength is similarly strong for case 4 like case 1. This implication will be clarified in the next steps of this case which involve increasing the installed capacity of Aksu RES according to the aforementioned methodology.

The line loadings before, during and after the fault are also recorded and the related graphs are provided for lines Kayseri-Nevsehir 154 and Afsin-Kayseri in 4.119 and 4.120, respectively.

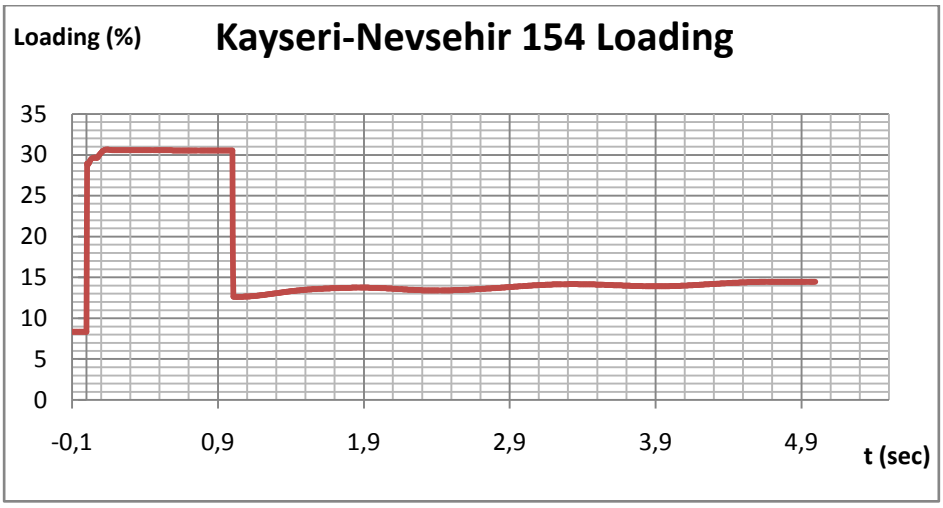

Graph 4.119. Loading of Kayseri-Nevsehir 154 Line

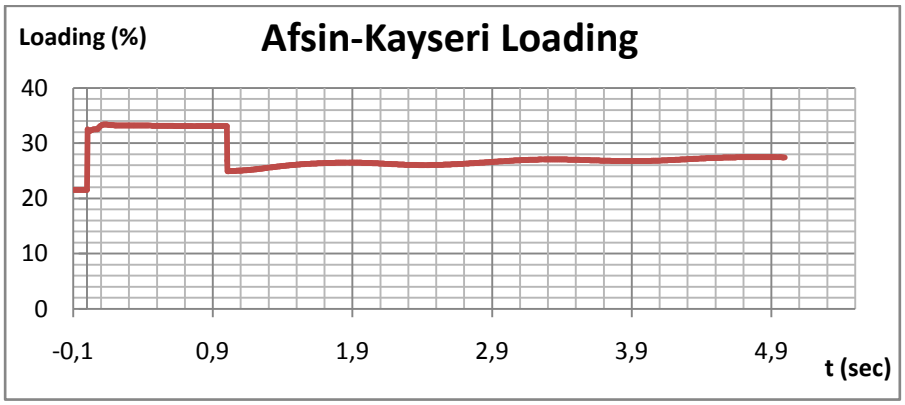

Graph 4.120. Loading of Afsin-Kayseri Line

As can be seen from both graphs, the fault has caused a slight but immediate disturbance on the transmission lines. After the breaker operation, the line loadings have initially decreased immediately yet slightly and then, began increasing in an attenuating oscillatory manner to reach the new steady-state values. Since all the transmission lines residing within 250 km radius of the fault point remained under %100 loading at any time before, during or after the fault, it is safe to claim that this case has no threat to the transmission lines by means of overloading.

Table 4.52 provides the initial (t= -0,1 sec.), final (t=5 sec) and maximum rotor angles for Afsin-Elbistan A and B TPP and Karakaya HPP during this case.

Table 4.52. Rotor Angle Values for Afsin A & B and Karakaya Plants

	Afsin A Rotor Angle (rad)	Afsin B Rotor Angle (rad)	Karakaya Rotor Angle (rad)
Initial	0.3623	0.6392	0.4807
Final	0.3599	0.6412	0.4803
Maximum	0.3641	0.6414	0.4822

As can be seen from Table 4.52, the initial and final values of all three power plants' rotor angles differ only by a small amount (while the Karakaya HPP's rotor angle shows the minimum response to the fault among them. Therefore, the simulation results verify that the generators stay in synchronism with the system without any adverse effect.

Taking the results provided above into consideration, the variations in bus voltages, line loadings after the fault clearance and rotor angles are proven to stay within the limits to ensure a stable operation of the system even with an installed capacity, and hence generation equal to the %10 of the short circuit MVA at the bus that the wind farm is connected to. Moreover, the observed parameter variations are far away from approaching the stability limits therefore they imply that the system may be able to handle disturbances for even higher values of installed capacity of the wind farm. This implication will be checked further in the next analysis, involving a wind farm installed capacity equal to %12.5 of the short circuit MVA of the connecting bus.

4.4.4: %12,5 (475 MW) Installed capacity

Breaker operating time: 1000 ms

For the given fault clearing time, the variations of selected bus voltages are provided in graphs 4.121 to 4.123.

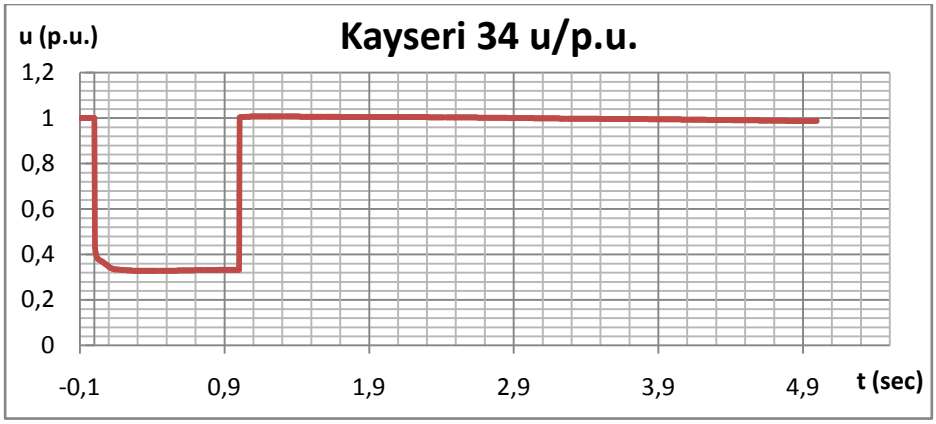

Graph 4.121. Voltage Variation of Kayseri 34 Bus

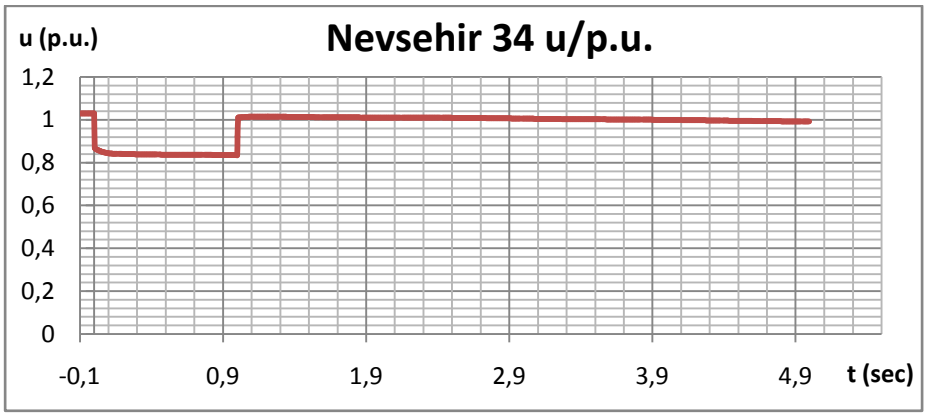

Graph 4.122. Voltage Variation of Nevsehir 34 Bus

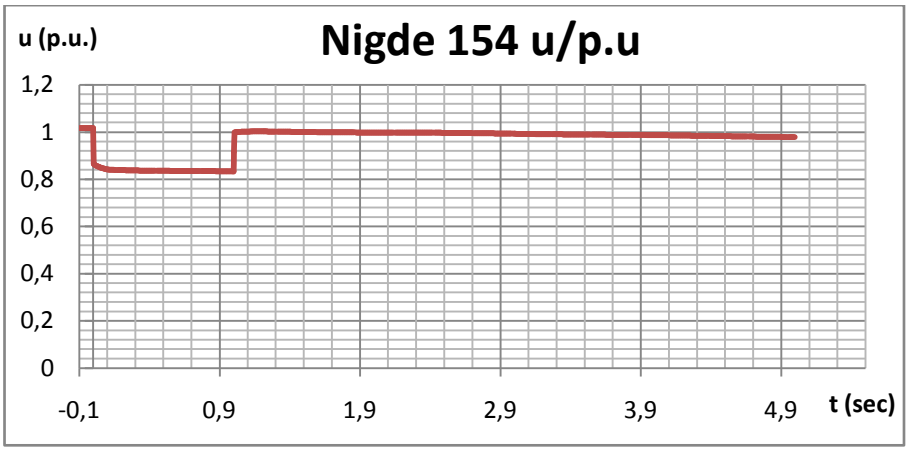

Graph 4.123. Voltage Variation of Nigde 154 Bus

As can be seen from the three graphs above, the disturbance had a drastic and almost immediate effect on the bus voltages which caused the voltages at nearby buses to drop sharply. However, the size of the drop varied between different buses and mainly influenced by the connection strength and distance to the location of fault. Kayseri 34 bus, being the closest one to the fault has suffered from the largest voltage drop in the event of a 3-phase short circuit while Nevsehir 34 and Nigde 154 buses showed a similar response that is smaller than that of Kayseri 34.

It can be seen that, at t=1 sec. the voltages at each bus rises sharply since the circuit breakers at the ends of faulted line are operated, thus, returning the rest of the system to fault-free state. However, the voltage values are not constant at the post-fault state until the new stable system operating state is fully reached. During this state, the oscillations of the voltage values at each bus can be seen. The maximum and minimum values of bus voltages after the fault clearing, as well as their difference in p.u. are provided in Table 4.53.

Table 4.53. Bus Voltages for Case 4.4

	Kayseri 34	Nevsehir 34	Nigde 154
Vmax	1.0176	1.029	1.0173
Vmin	0.987	0.9916	0.9789
Difference	0.0306	0.0374	0.0384
Vfinal	0.987	0.9916	0.9789

As Table 4.53 clearly shows, the final values at the end of 5 seconds after the fault are within the normal operational limits. Moreover the voltage oscillatory peak for all buses are well below the specified %10 limit for this case. Furthermore, it should be noted that the voltage oscillations in this case are comparable to case 4.1.4 which was the similar case by means of installed capacity and breaker operating time for Bozyaka RES. This shows that the grid strength is similarly strong for case 4 similar to case 1.

The line loadings before, during and after the fault are also recorded and the related graphs are provided for lines Kayseri-Nevsehir 154 and Afsin-Kayseri in graphs 4.124 and 4.125, respectively.

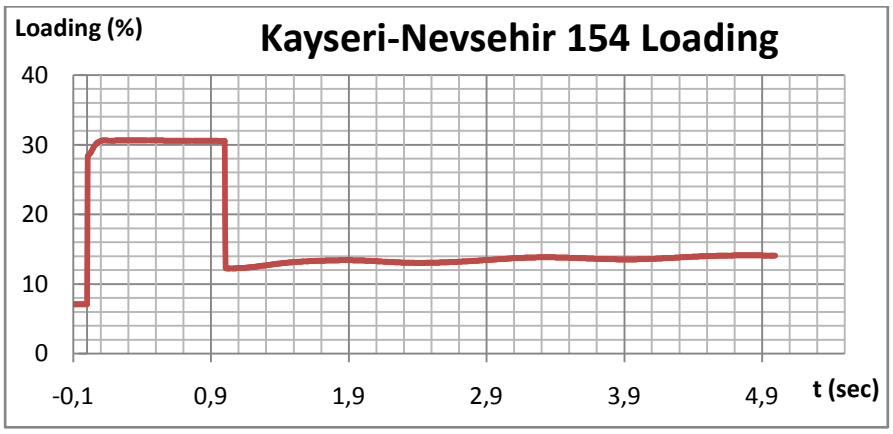

Graph 4.124. Loading of Kayseri-Nevsehir Line

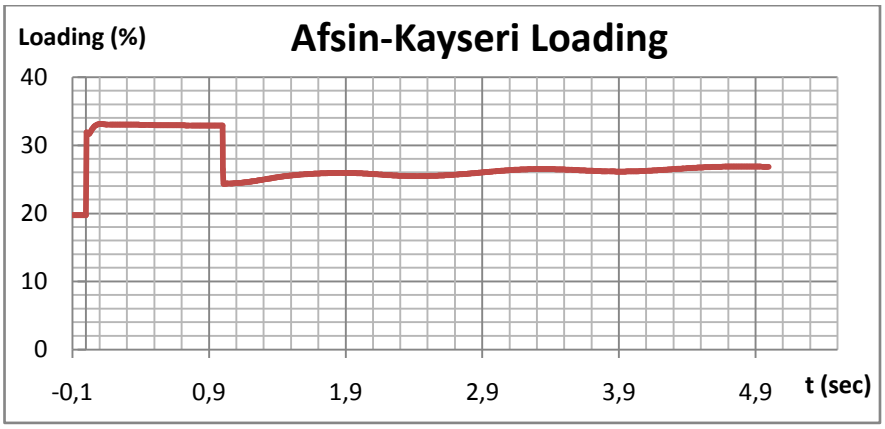

Graph 4.125. Loading of Kayseri-Nevsehir Line

As can be seen from both graphs, the fault has caused a slight but immediate disturbance on the transmission lines. After the breaker operation, the line loadings have initially decreased immediately yet slightly and then, began increasing in an attenuating oscillatory manner to reach the new steady-state values. Since all the transmission lines residing within 250 km radius of the fault point remained under %100 loading at any time before, during or after the fault, it is safe to claim that this case has no threat to the transmission lines by means of overloading.

Table 4.54 provides the initial (t= -0,1 sec.), final (t=5 sec) and maximum rotor angles for Afsin-Elbistan A and B TPP and Karakaya HPP during this case.

Table 4.54. Rotor Angle Values for Afsin A & B and Karakaya Plants

	Afsin A Rotor Angle (rad)	Afsin B Rotor Angle (rad)	Karakaya Rotor Angle (rad)
Initial	0.3484	0.6295	0.4672
Final	0.3438	0.6301	0.4648
Maximum	0.35	0.631	0.4685

As can be seen from Table 4.54 the initial and final values of all three power plants' rotor angles differ only by a small amount (while the Afsin B TPP's rotor angle shows the minimum response to the fault among them). Therefore, the simulation results verify that the generators stay in synchronism with the system without any adverse effect.

Taking the results provided above into consideration, the variations in bus voltages, line loadings after the fault clearance and rotor angles are proven to stay within the limits to ensure a stable operation of the system even with an installed capacity, and hence generation equal to the %12,5 of the short circuit MVA at the bus that the wind farm is connected to. Moreover, the observed parameter variations are far away from approaching the stability limits therefore they imply that the system may be able to handle disturbances for even higher values of installed capacity of the wind farm. This implication will be checked further in the next analysis, involving a wind farm installed capacity equal to %15 of the short circuit MVA of the connecting bus.

4.4.5: %15 (570 MW) Installed capacity

Breaker operating time: 1000 ms

For the given fault clearing time, the variations of selected bus voltages are provided in graphs 4.126 to 4.128.

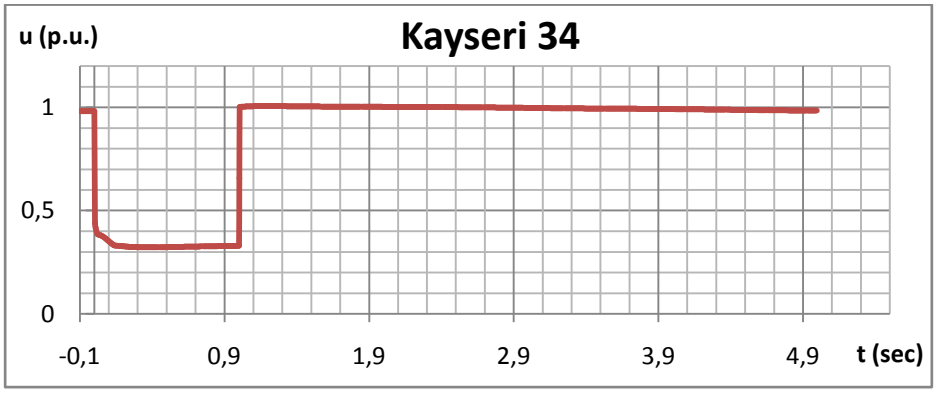

Graph 4.126. Voltage Variation of Kayseri 34 Bus

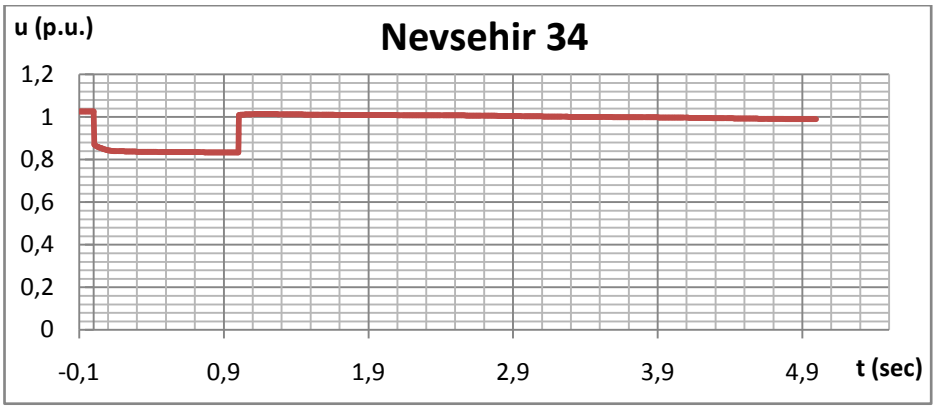

Graph 4.127. Voltage Variation of Nevsehir 34 Bus

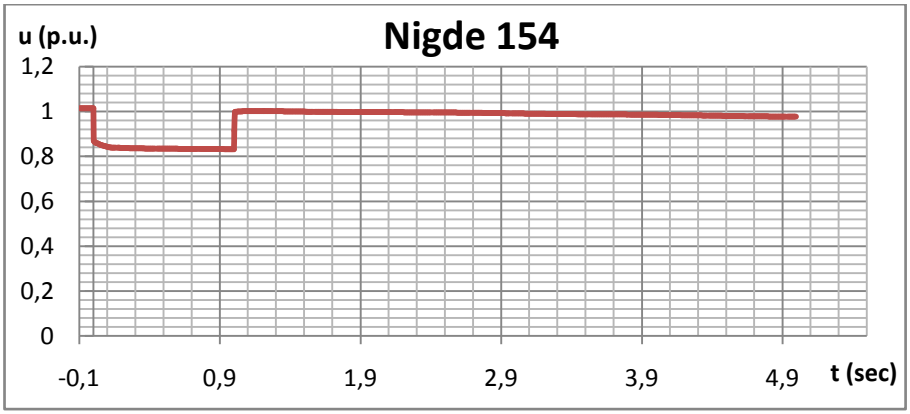

Graph 4.128. Voltage Variation of Nigde 154 Bus

As can be seen from the three graphs above, the disturbance had a drastic and almost immediate effect on the bus voltages which caused the voltages at nearby buses to drop sharply. However, the size of the drop varied between different buses and mainly influenced by the connection strength and distance to the location of fault. Kayseri 34 bus, being the closest one to the fault has suffered from the largest voltage drop in the event of a 3-phase short circuit while Nevsehir 34 and Nigde 154 buses showed similar responses that are smaller than that of Kayseri 34.

It can be seen that, at t=1 sec. the voltages at each bus rises sharply since the circuit breakers at the ends of faulted line are operated, thus, returning the rest of the system

to fault-free state. However, the voltage values are not constant at the post-fault state until the new stable system operating state is fully reached. During this state, the oscillations of the voltage values at each bus can be seen. The maximum and minimum values of bus voltages after the fault clearing, as well as their difference in p.u. are provided in Table 4.55

Table 4.55. Bus Voltages for Case 4.5

	Kayseri 34	Nevsehir 34	Nigde 154
Vmax	1.0152	1.0268	1.015
Vmin	0.9844	0.9892	0.9764
Difference	0.0308	0.0376	0.0386
Vfinal	0.9844	0.9892	0.9764

As Table 4.55 clearly shows, the final values at the end of 5 seconds after the fault are within the normal operational limits. Moreover the voltage oscillatory peak for all buses are well below the specified %10 limit for this case. Moreover, it should be noted that the voltage oscillations in this case are comparable to case 4.1.5 which was the similar case by means of installed capacity and breaker operating time for Bozyaka RES. This is in agreement with the claim that the grid strength is similarly strong for case 4 like case 1.

The line loadings before, during and after the fault are also recorded and the related graphs are provided for lines Kayseri-Nevsehir 154 and Afsin-Kayseri in graphs 4.129 and 4.130, respectively.

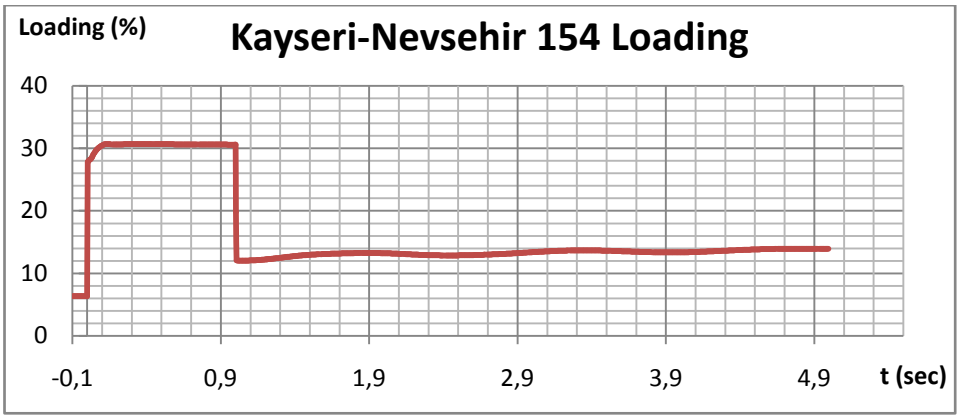

Graph 4.129. Loading of Kayseri-Nevsehir 154 Line

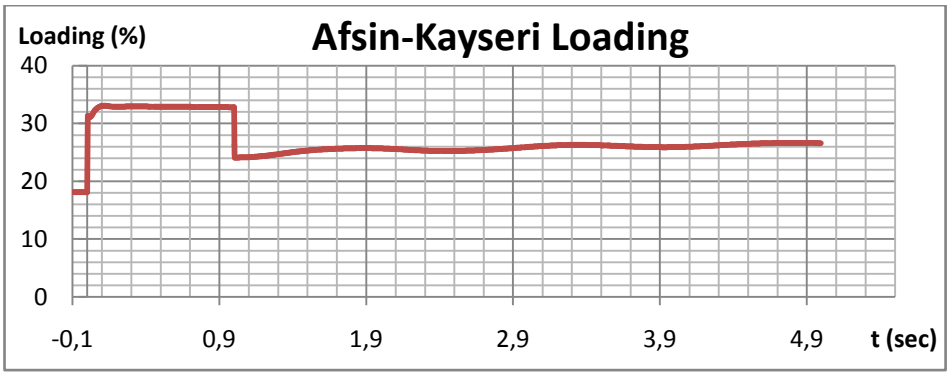

Graph 4.130. Loading of Afsin-Kayseri Line

As can be seen from both graphs, the fault has caused a slight but immediate disturbance on the transmission lines. After the breaker operation, the line loadings have initially decreased immediately yet slightly and then, began increasing in an attenuating oscillatory manner to reach the new steady-state values. Since all the transmission lines residing within 250 km radius of the fault point remained under %100 loading at any time before, during or after the fault, it is safe to claim that this case has no threat to the transmission lines by means of overloading.

Table 4.56 provides the initial (t= -0,1 sec.), final (t=5 sec) and maximum rotor angles for Afsin-Elbistan A and B TPP and Karakaya HPP during this case.

	Afsin A Rotor Angle (rad)	Afsin B Rotor Angle (rad)	Karakaya Rotor Angle (rad)
Initial	0.3418	0.624	0.4634
Final	0.3353	0.6237	0.4595
Maximum	0.3432	0.6254	0.4644

Table 4.56. Rotor Angle Values for Afsin A & B Plants

As can be seen from Table 4.56 the initial and final values of all three power plants' rotor angles differ only by a small amount Therefore, the simulation results verify that the generators stay in synchronism with the system without any adverse effect.

Taking the results provided above into consideration, the variations in bus voltages, line loadings after the fault clearance and rotor angles are proven to stay within the limits to ensure a stable operation of the system even with an installed capacity, and hence generation equal to the %15 of the short circuit MVA at the bus that the wind farm is connected to which is 3 times the given %5 limit claimed for stability. Moreover, the observed parameter variations are still far away from approaching the stability limits therefore they imply that the system may be able to handle disturbances for even higher values of installed capacity of the wind farm. The extent to which this stable operation without deteriorating the power quality will be tried to be determined as the next step for this case which involves increasing the installed capacity to a maximum value that is determined by the limits of power transfer capability of equipment connecting the wind farm to the grid.

4.4.6: %20 (760 MW) Installed capacity

As the final step of this case, the wind farm installed capacity is increased to the maximum possible value that is limited by the system equipment, i.e. the relevant transformers and transmission lines that would be overloaded if further increase took place for Aksu RES and the same fault event is triggered in the identical manner.

Breaker operating time: 1000 ms

For the given fault clearing time, the variations of selected bus voltages are provided in graphs 4.131 to 4.133.

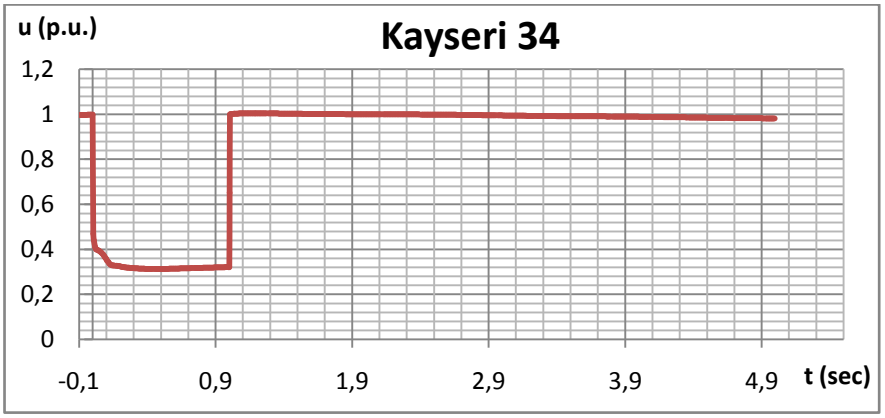

Graph 4.131. Voltage Variation of Kayseri 34 Bus

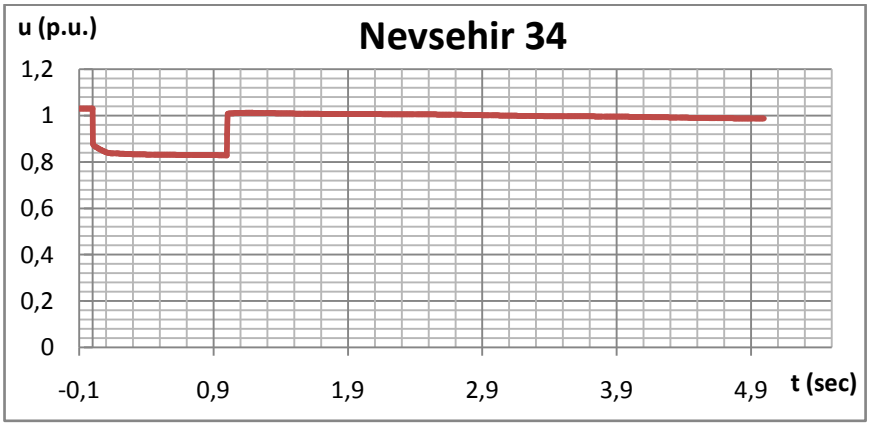

Graph 4.132. Voltage Variation of Nevsehir 34 Bus

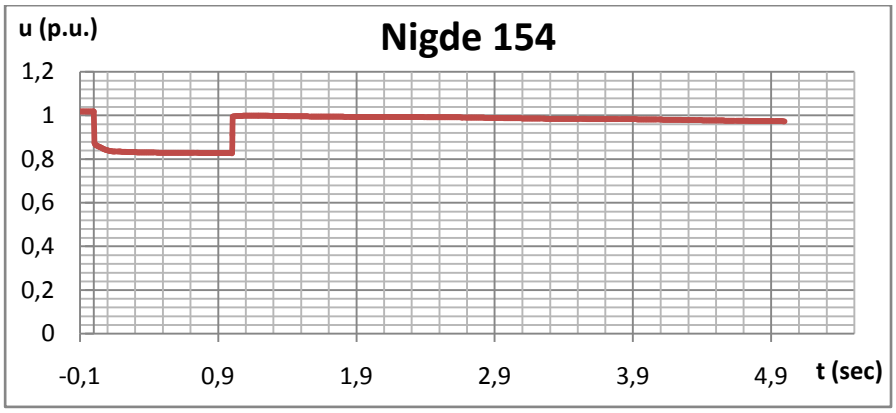

Graph 4.133. Voltage Variation of Nigde 154 Bus

As can be seen from the three graphs above, the disturbance had a drastic and almost immediate effect on the bus voltages which caused the voltages at nearby buses to drop sharply. However, the size of the drop varied between different buses and mainly influenced by the connection strength and distance to the location of fault. Kayseri 34 bus, being the closest one to the fault has suffered from the largest voltage drop in the event of a 3-phase short circuit while Nevsehir 34 and Nigde 154 buses showed similar responses that are smaller than that of Kayseri 34.

It can be seen that, at t=1 sec. the voltages at each bus rises sharply since the circuit breakers at the ends of faulted line are operated, thus, returning the rest of the system to fault-free state. However, the voltage values are not constant at the post-fault state until the new stable system operating state is fully reached. During this state, the oscillations of the voltage values at each bus can be seen. The maximum and minimum values of bus voltages after the fault clearing, as well as their difference in p.u. are provided in Table 4.57

Table 4.57 Bus Voltage Variations for Case 4.6

	Kayseri 34	Nevsehir 34	Nigde 154
Vmax	1.0146	1.0304	1.0185
Vmin	0.9817	0.9867	0.9738
Difference	0.0329	0.0437	0.0447
Vfinal	0.9817	0.9867	0.9738

As Table 4.57 clearly shows, the final values at the end of 5 seconds after the fault are within the normal operational limits. Moreover the voltage oscillatory peak for all buses are well below the specified %10 limit for this case. This suggests that, even if the installed capacity is at its maximum value to ensure proper power transfer to the grid without any overloaded elements, a possible short circuit event will not cause a serious problem regarding the voltage qualities at buses.

The line loadings before, during and after the fault are also recorded and the related graphs are provided for lines Kayseri-Nevsehir 154 and Afsin-Kayseri in graphs 4.134 and 4.135, respectively.

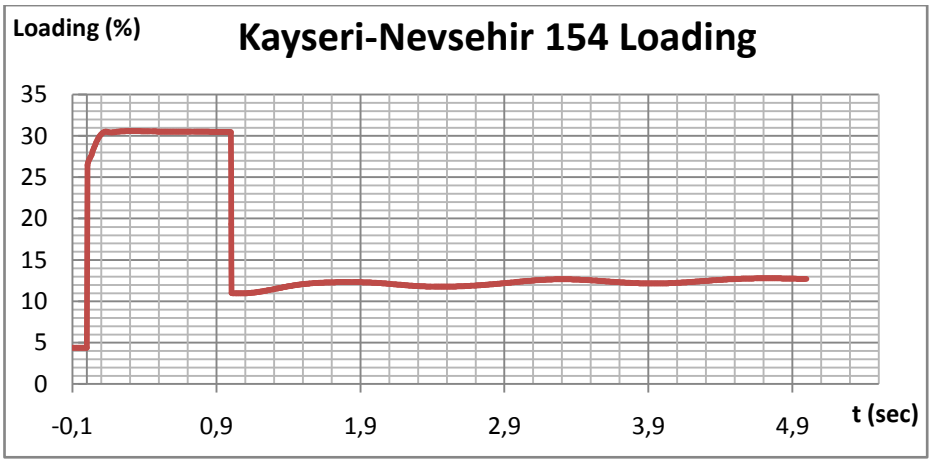

Graph 4.134. Loading of Kayseri-Nevsehir 154 Line

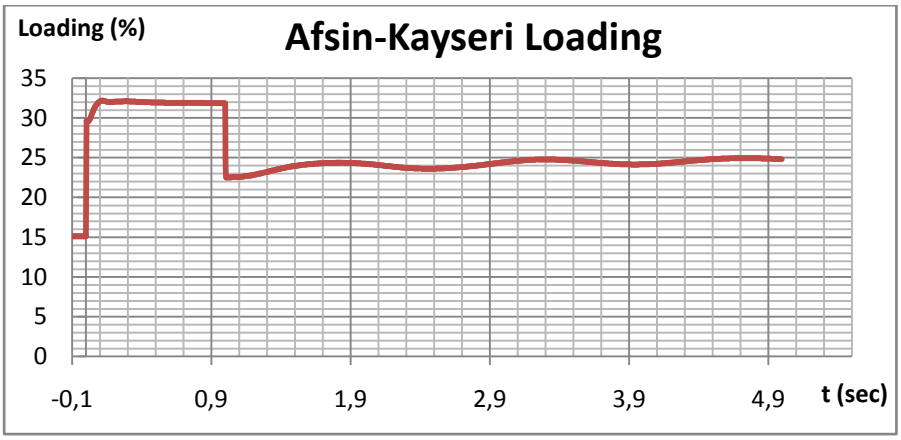

Graph 4.135. Loading of Afsin-Kayseri 154 Line

As can be seen from both graphs, the fault has caused a slight but immediate disturbance on the transmission lines. After the breaker operation, the line loadings have initially decreased immediately yet slightly and then, began increasing in an attenuating oscillatory manner to reach the new steady-state values. Since all the transmission lines residing within 250 km radius of the fault point remained under %100 loading at any time before, during or after the fault, it is safe to claim that this case also has no threat to the transmission lines by means of overloading.

Table 4.58 provides the initial (t= -0,1 sec.), final (t=5 sec) and maximum rotor angles for Afsin-Elbistan A and B TPP and Karakaya HPP during this case.

Table 4.58. Rotor Angle Values for Afsin A & B and Karakaya Plants

	Afsin A Rotor Angle (rad)	Afsin B Rotor Angle (rad)	Karakaya Rotor Angle (rad)
Initial	0.5477	0.5743	0.4849
Final	0.5411	0.5682	0.4768
Maximum	0.5485	0.5748	0.4854

As can be seen from Table 4.58 the initial and final values of all three power plants' rotor angles differ only by a small amount Therefore, the simulation results verify that the generators stay in synchronism with the system without any adverse effect.

Taking the results provided above into consideration, the variations in bus voltages, line loadings after the fault clearance and rotor angles are proven to stay within the limits to ensure a stable operation of the system even with an installed capacity, and hence generation equal to the %20 of the short circuit MVA at the bus that the wind farm is connected to which is 4 times the given %5 limit claimed for stability. Moreover, the observed parameter variations are still far away from approaching the stability limits therefore they imply that the system may be able to handle disturbances for even higher values of installed capacity of the wind farm. However, additional increase in installed capacity is unlikely due to the moderate wind energy potential of the region and, more importantly, the capacity of the equipment (transformers and transmission lines) play a limiting role in the amount of power that can be transferred from Aksu RES to the rest of the grid. All in all, this case analysis shows that it is possible to reach very high generation levels with wind farms without introducing any additional risk to the system security and stability in case of disturbances, especially in the regions where the grid is sufficiently strong.

4.5. Case 5: Çanakkale RES

The fifth and last case to be demonstrated is Çanakkale RES. Çanakkale is stated to be one of the most important cities in Turkey by means of wind energy potential. Therefore it is found to be necessary to include the analysis results as the final case of this section. The geographical properties of Çanakkale also set the wind farms established here in an unique position. Being on two continents with the Bosporus of Çanakkale lying in the north-western direction introduces a wide area that exhibits a high potential by means of wind energy. Çanakkale is a moderately populated city with a modest amount of energy demand. Çanakkale RES is located in Ezine, a town that is resided within the city limits of Çanakkale. However, there are many

individual wind farms in the location that will be included in the given farm in order to be able to simulate their cumulative effect in a clear manner.

In the system, the wind farm is connected to the grid at Çanakkale 34.5 kV (denoted by Çanakkale 34 in the model) bus. Therefore, the connecting line is between the buses Çanakkale RES 34 and Çanakkale 34 The current installed capacity of Çanakkale RES (omitting the nearby wind farms which were actually included in the system model) is 30 MW. The short circuit power at Çanakkale 34 bus, on the other hand, is 1013 MVA, a surprisingly low value considering the population density of the area and larger cities nearby [54]. If the wind farms included in the modeling are also considered, the total installed capacity of the wind farms that are denoted by Çanakkale RES in the model sum up to 68 MW. As can be inferred from the short circuit MVA the grid where the wind farms are connected can be considered to be interestingly weak despite not being noticeably far away to large consumption centers. On the other hand, this situation can be explained considering that the grid's north-western end on the given latitude is Çanakkale, thus forcing the connections to be made mainly from east and partially south. The wind farm concentration in the western part of the country is high, with Çanakkale playing a considerable role by means of installed capacities. These theses bring a controversy regarding the capability of the grid around Çanakkale to cope with increasing wind farm capacities which will be clarified by analyzes to be presented under this case.

As mentioned in the preceding section, the analyses will be carried out for installed capacities of Çanakkale RES that will be equal to %5, %7.5, %10, %12.5 and %15 of the short circuit MVA at Çanakkale 34 bus. The installed capacity values corresponding to these percentages of short circuit power are given in Table 4.59. It is worth to note that, in present case, the %5 limit of short circuit capacity at relevant bus is already exceeded by a slight amount when the nearby wind farms are also considered.

Table 4.59. Installed Capacity Values for Case 5

% of Ssc	5	7,5	10	12,5	15
Installed Capacity (MW)	50	76	101	126	151

The buses, transmission lines and generators within 250 km radius of the wind farm are chosen to be observed. However, to avoid overflow of output data, some elements among the initial set are omitted after they are proven not to show any significant variations during the analysis processes. The resulting set of elements to be observed and whose results will be provided in detail are given below.

-Buses (Voltages of) : Çanakkale 34, Biga 34, Gelibolu 154

-Transmission Lines (Loading of): Balıkesir-Çanakkale 154, Biga-Çanakkale 154

-Generators (Rotor Angles of): Çan TPP, Unimar NGCC Power Plant

Analysis Results

For each given installed capacity value, five individual analyses are carried out regarding circuit breaker operating times. For the sake of keeping the data given here compact, only the cases corresponding to breaker operating time of 1000 ms will be presented.

4.5.1: %5 (50 MW) Installed capacity

Breaker operating time: 1000 ms

For the given fault clearing time, the variations of selected bus voltages are provided in graphs 4.136 to 4.138.

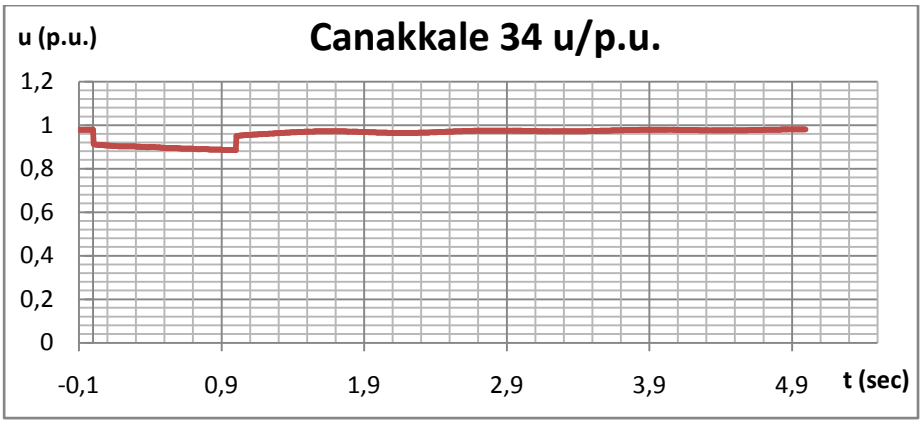

Graph 4.136. Voltage Variation of Canakkale 34 Bus

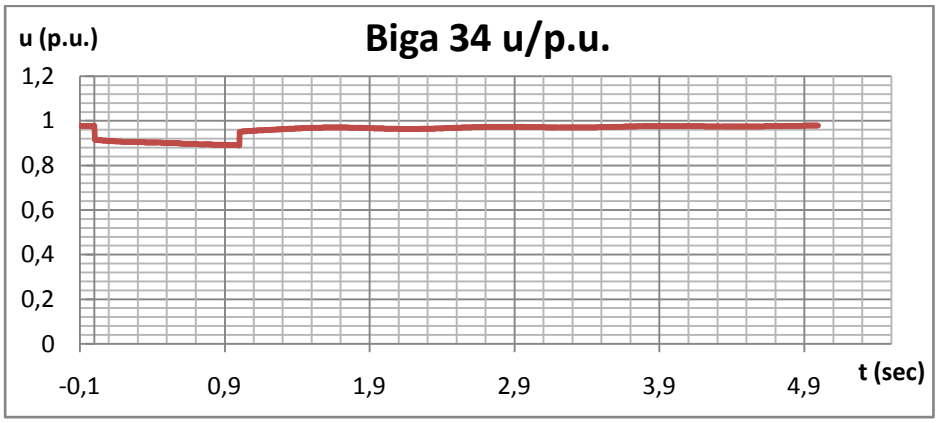

Graph 4.137. Voltage Variation of Biga 34 Bus

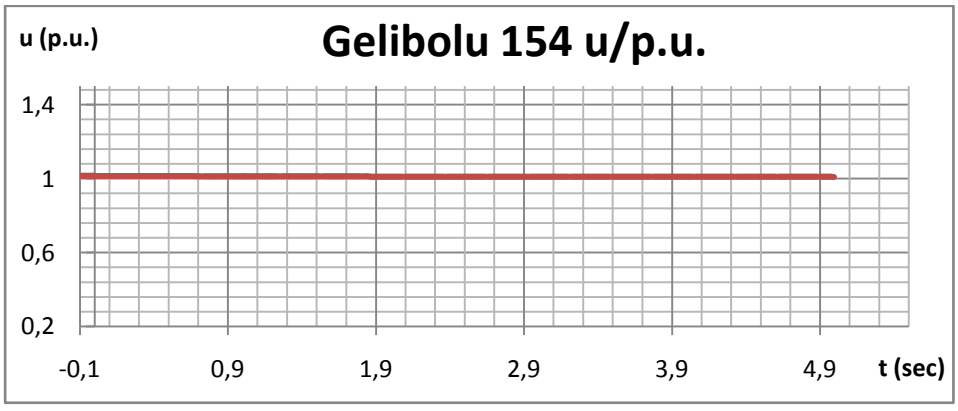

Graph 4.138. Voltage Variation of Gelibolu 154 Bus

As can be seen from the three graphs above, the disturbance had an almost immediate effect on most of the bus voltages which caused the voltages at nearby buses to drop considerably. However, the bus Gelibolu, despite geographically being close to the fault location, is very slightly affected from the fault event. Moreover, size of the drop at many buses are smaller when compared to cases 4.1 to 4.4. It can be seen that, at t=1 sec. the voltages at each bus excluding Gelibolu 154 rise sharply since the circuit breakers at the ends of faulted line are operated, thus, returning the rest of the system to fault-free state. However, the voltage values are not constant at the post-fault state until the new stable system operating state is fully reached. During this state, the oscillations of the voltage values at each bus can be seen. The maximum and minimum values of bus voltages after the fault clearing, as well as their difference in p.u. are provided in Table 4.60.

Table 4.60. Bus Voltages for Case 5.1

	Çanakkale 34	Biga 34	Gelibolu 154
Vmax	0.9808	0.9785	1.013
Vmin	0.9497	0.9501	1.0099
Difference	0.0311	0.0284	0.0031
Vfinal	0.9808	0.9785	1.0099

As Table 4.60 clearly shows, the final values at the end of 5 seconds after the fault are within the normal operational limits. Moreover the voltage oscillatory peak for all buses are well below the specified %10 limit for this case. It should also be noted that the voltage oscillations in this case are comparable to, or even lower than, when Gelibolu 154 bus is considered, case 4.1.1.5 which was the similar case by means of installed capacity and breaker operating time for Bozyaka RES. This implies that the grid strength might be higher than it initially seems. This implication will be clarified in the next steps of this case which involve increasing the installed capacity of Çanakkale RES according to the aforementioned methodology.

The line loadings before, during and after the fault are also recorded and the related graphs are provided for lines Balıkesir-Çanakkale 154 and Biga-Çanakkale in graphs 4.139 and 4.140, respectively.

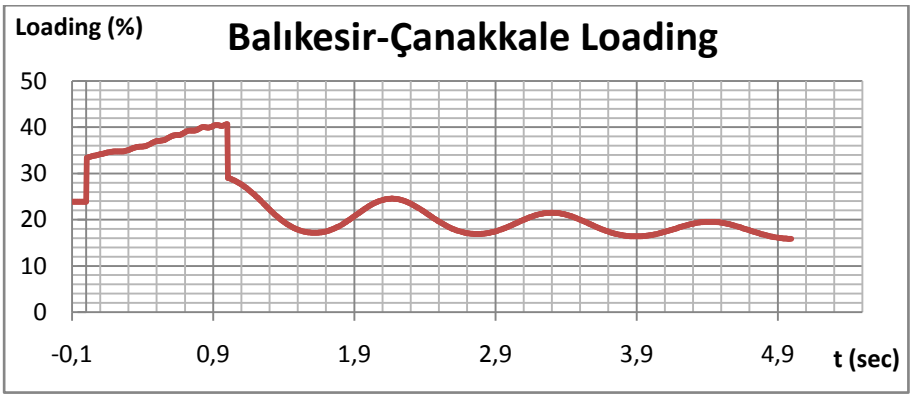

Graph 4.139. Loading of Balıkesir-Çanakkale 154 Line

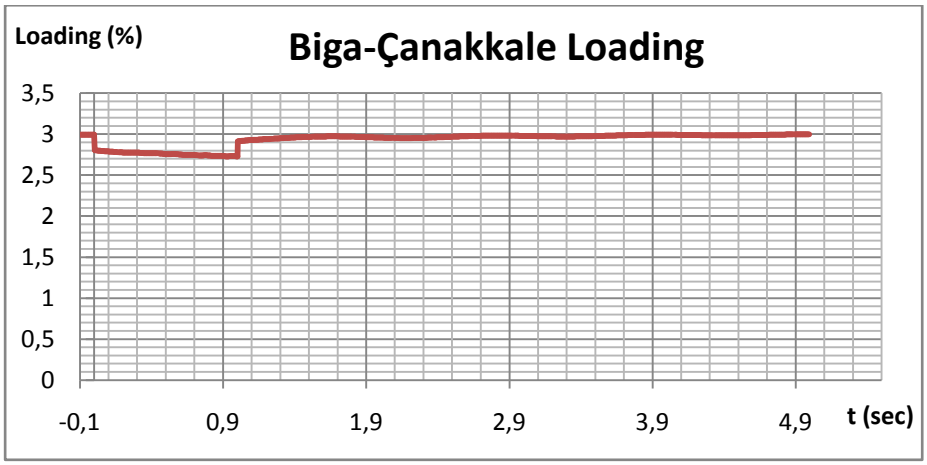

Graph 4.140. Loading of Biga-Çanakkale Line

As can be seen from both graphs, the fault has caused a slight but immediate disturbance on the transmission lines. After the breaker operation, the line loadings have initially changed, leading to an attenuating oscillatory change through time, reaching their steady-state values after the fault. Since all the transmission lines

residing within 250 km radius of the fault point remained under %100 loading at any time before, during or after the fault, it is safe to claim that this case has no threat to the transmission lines by means of overloading.

Table 4.61 provides the initial (t= -0,1 sec.), final (t=5 sec) and maximum rotor angles for Çan TPP and Unimar NGCC Plant during this case.

Table 4.61. Rotor Angle Values for Çan TPP and Unimar NGCC Plants

	Çan Rotor Angle (rad)	Unimar Rotor Angle (rad)
Initial	1.1827	1.4139
Final	1.2366	0.8966
Maximum	1.269	1.4168

As can be seen from Table 4.61 the initial and final values of Çan TPP's rotor angle differ only by a small amount (approximately 2,85^{o}) while the Unimar NGCC's rotor angle shows a higher response to the fault yet ending up with a value that is lower than its initial value. Therefore, the simulation results verify that the generators stay in synchronism with the system without any adverse effect.

Taking the results provided above into consideration, the variations in bus voltages, line loadings after the fault clearance and rotor angles are proven to stay within the limits to ensure a stable operation of the system with an installed capacity, and hence generation equal to the %5 of the short circuit MVA at the bus that the wind farm is connected to. Moreover, the observed parameter variations are far away from approaching the stability limits therefore they imply that the system may be able to handle disturbances for even higher values of installed capacity of the wind farm. This implication will prove true in the next analysis, involving a wind farm installed capacity equal to %7,5 of the short circuit MVA of the connecting bus.

4.5.2: %7,5 (76 MW) Installed capacity

Breaker operating time: 1000 ms

For the given fault clearing time, the variations of selected bus voltages are provided in graphs 4.141 to 4.143.

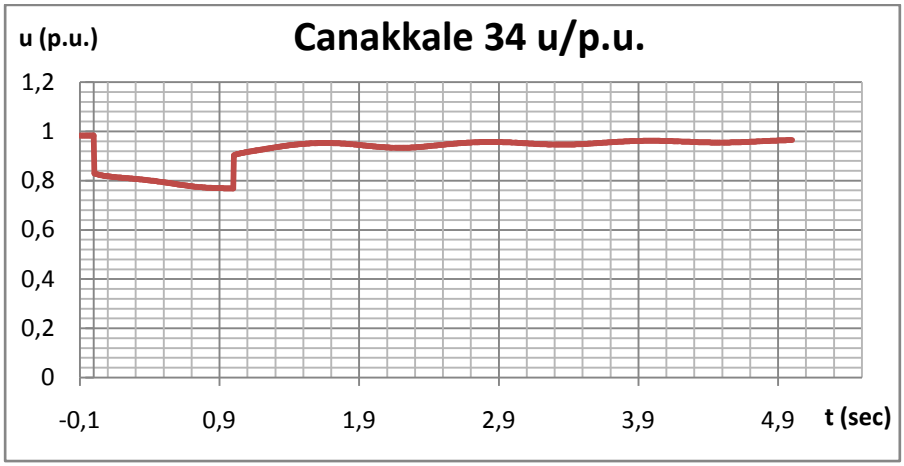

Graph 4.141. Voltage Variation of Canakkale 34 Bus

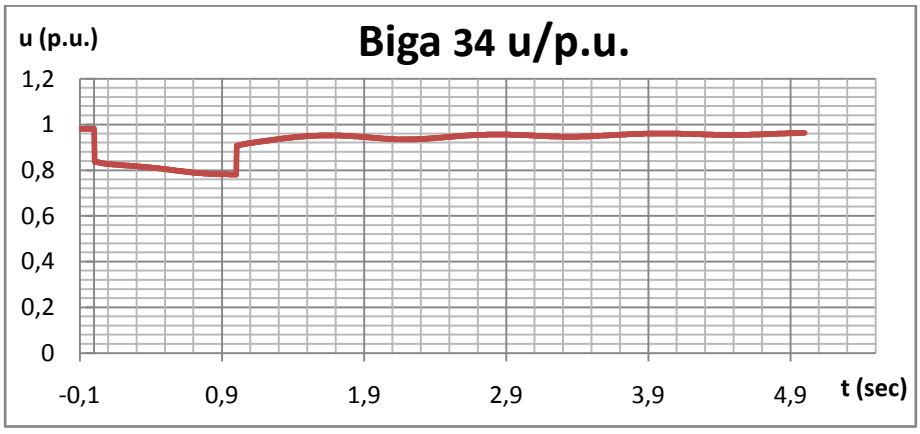

Graph 4.142. Voltage Variation of Biga 34 Bus

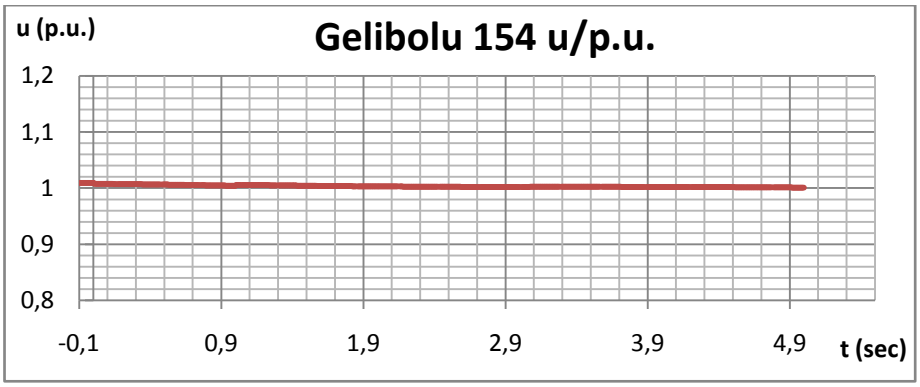

Graph 4.143. Voltage Variation of Gelibolu 154 Bus

As can be seen from the three graphs above, the disturbance had an almost immediate effect on most of the bus voltages which caused the voltages at nearby buses to drop considerably. However, the bus Gelibolu, despite geographically being close to the fault location, is very slightly affected from the fault event. Moreover, size of the drop at many buses are smaller when compared to cases 4.1 to 4.4.

It can be seen that, at t=1 sec. the voltages at each bus excluding Gelibolu 154 rise sharply since the circuit breakers at the ends of faulted line are operated, thus, returning the rest of the system to fault-free state. However, the voltage values are not constant at the post-fault state until the new stable system operating state is fully reached. During this state, the oscillations of the voltage values at each bus can be seen. The maximum and minimum values of bus voltages after the fault clearing, as well as their difference in p.u. are provided in Table 4.62.

Table 4.62. Bus Voltages for Case 5.2

	Çanakkale 34	Biga 34	Gelibolu 154
Vmax	0.9646	0.9632	1.0056
Vmin	0.904	0.9076	1.0011
Difference	0.0606	0.0556	0.0045
Vfinal	0.9646	0.9632	1.0011

As Table 4.62 clearly shows, the final values at the end of 5 seconds after the fault are within the normal operational limits. Moreover the voltage oscillatory peak for all buses are below the specified %10 limit for this case. It should also be noted that the voltage oscillations in this case are still now somewhat higher than case 4.1.2 which was the similar case by means of installed capacity and breaker operating time for Bozyaka RES. This implies that the grid strength might not be as high as it initially seems. It should, be realized that, with a small increase of 26 MW, the differences have risen almost by %100 which can be claimed as a counterargument to the strength of the grid at the present area. This situation will be analyzed in detail in the next steps of this case which involve increasing the installed capacity of Çanakkale RES according to the aforementioned methodology.

The line loadings before, during and after the fault are also recorded and the related graphs are provided for lines Balıkesir-Çanakkale 154 and Biga-Çanakkale in graphs 4.144 and 4.145, respectively.

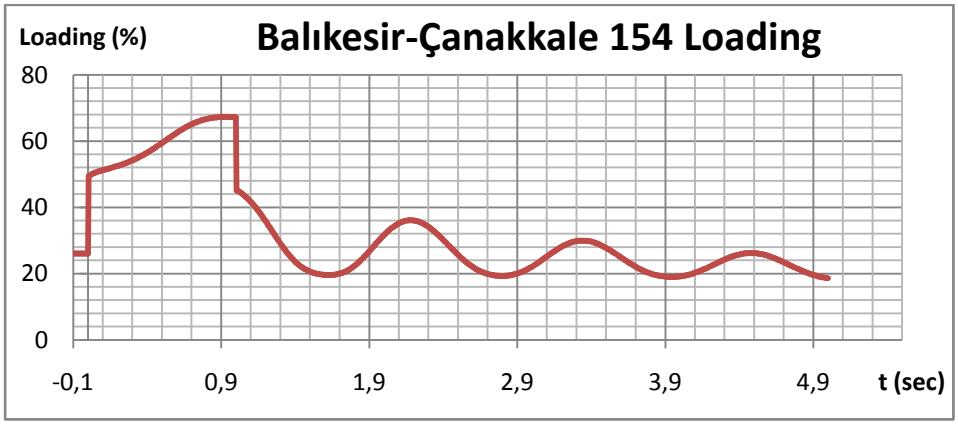

Graph 4.144. Loading of Balıkesir-Çanakkale 154 Line

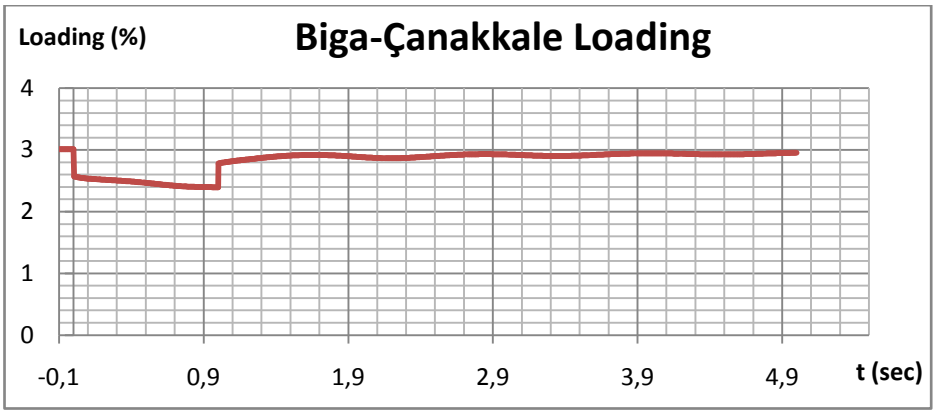

Graph 4.145. Loading of Biga-Çanakkale Line

As can be seen from both graphs, the fault has caused a slight but immediate disturbance on the transmission lines. After the breaker operation, the line loadings have initially changed, leading to an attenuating oscillatory change through time, reaching their steady-state values after the fault. Since all the transmission lines residing within 250 km radius of the fault point remained under %100 loading at any time before, during or after the fault, it is safe to claim that this case has no threat to the transmission lines by means of overloading. It is seen that the peak loading value of Balıkesir-Çanakkale 154 line during the fault has become almost the double of the same line's peak loading in case 4.5.1.

Table 4.63 provides the initial (t= -0,1 sec.), final (t=5 sec) and maximum rotor angles for Çan TPP and Unimar NGCC Plant during this case.

Table 4.63. Rotor Angle Values for Çan TPP and Unimar NGCC Plants

	Çan Rotor Angle (rad)	Unimar Rotor Angle (rad)
Initial	1.1457	1.3896
Final	1.2047	0.9088
Maximum	1.269	1.4168

As can be seen from Table 4.63 the initial and final values of Çan TPP's rotor angle differ only by a small amount (approximately 3,53^{o}) while the Unimar NGCC's rotor angle shows a higher response to the fault. Therefore, the simulation results verify that the generators stay in synchronism with the system without any adverse effect.

Taking the results provided above into consideration, the variations in bus voltages, line loadings after the fault clearance and rotor angles are proven to stay within the limits to ensure a stable operation of the system with an installed capacity, and hence generation equal to the %7,5 of the short circuit MVA at the bus that the wind farm is connected to. Moreover, the observed parameter variations are far away from approaching the stability limits therefore they imply that the system may be able to handle disturbances for even higher values of installed capacity of the wind farm. This implication will be checked to be true in the next analysis, involving a wind farm installed capacity equal to %10 of the short circuit MVA of the connecting bus.

4.5.3: %10 (101 MW) Installed capacity

Breaker operating time: 1000 ms

For the given fault clearing time, the variations of selected bus voltages are provided in graphs 4.146 to 4.148.

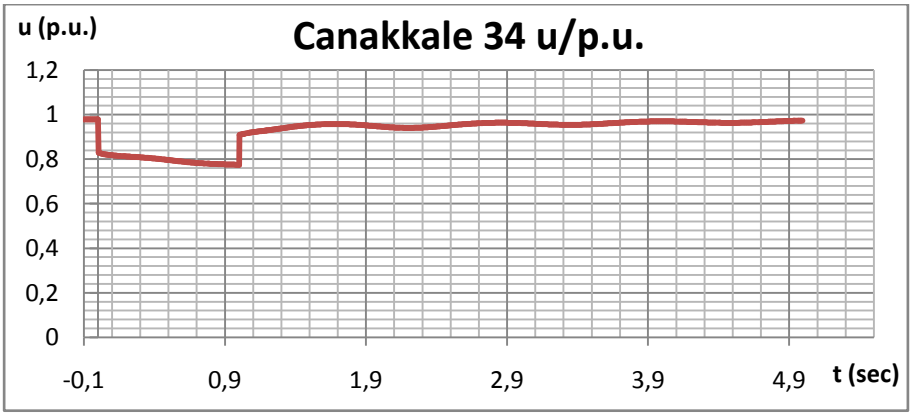

Graph 4.146. Voltage Variation of Canakkale 34 Bus

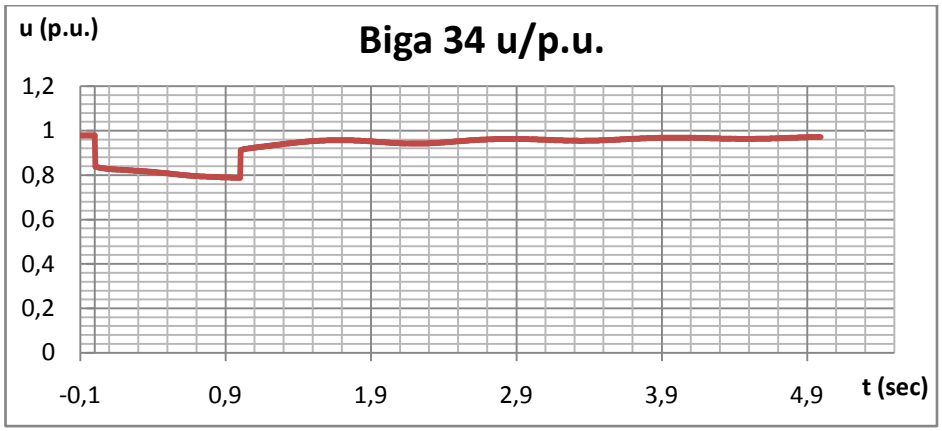

Graph 4.147. Voltage Variation of Biga 34 Bus

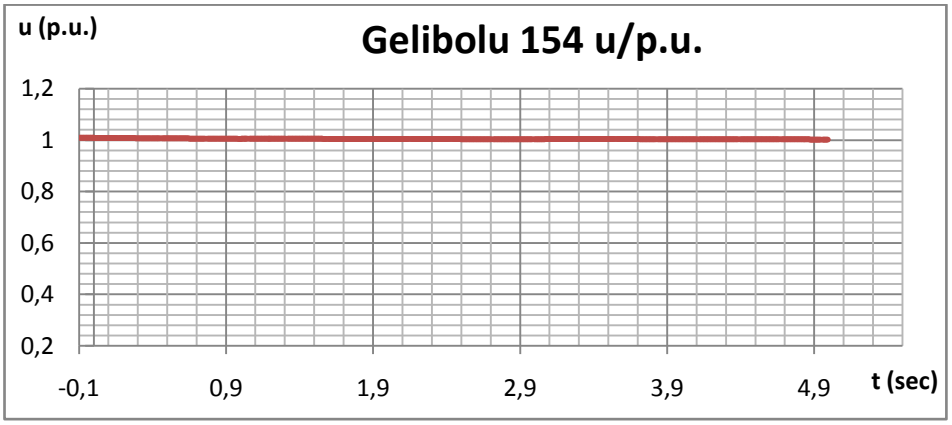

Graph 4.148. Voltage Variation of Gelibolu 154 Bus

As can be seen from the three graphs above, the disturbance had an almost immediate effect on the bus voltages which caused the voltages at nearby buses to drop fairly. However, the bus Gelibolu, despite geographically being close to the fault location, is still very slightly affected from the fault event. However, size of the drop at the other buses have increased slightly.

It can be seen that, at t=1 sec. the voltages at each bus rise sharply with varying magnitudes since the circuit breakers at the ends of faulted line are operated, thus, returning the rest of the system to fault-free state. However, the voltage values are

not constant at the post-fault state until the new stable system operating state is fully reached. During this state, the oscillations of the voltage values at each bus can be seen. The oscillations in buses Çanakkale 34 and Biga 34 are increased slightly when compared to case 4.5.2.The maximum and minimum values of bus voltages after the fault clearing, as well as their difference in p.u. are provided in
Table 4.64.

Table 4.64. Bus Voltages for Case 5.3

	Çanakkale 34	Biga 34	Gelibolu 154
Vmax	0.9736	0.9716	1.0058
Vmin	0.9101	0.9133	1.0019
Difference	0.0635	0.0583	0.0039
Vfinal	0.9736	0.9716	1.0019

As Table 4.64 clearly shows, the final values at the end of 5 seconds after the fault are within the normal operational limits. Moreover the voltage oscillatory peak for all buses are below the specified %10 limit for this case. It should also be noted that the voltage oscillations in this case are higher than case 4.1.3 which was the similar case by means of installed capacity and breaker operating time for Bozyaka RES. This implies that the grid strength around Çanakkale RES is lower than that of Bozyaka RES. However, unlike case 4.5.2, there is not a huge difference between the previous case which involved %25 less installed capacity when compared to case 4.5.3.
The line loadings before, during and after the fault are also recorded and the related graphs are provided for lines Balıkesir-Çanakkale 154 and Biga-Çanakkale in graphs 4.149 and 4.150, respectively.

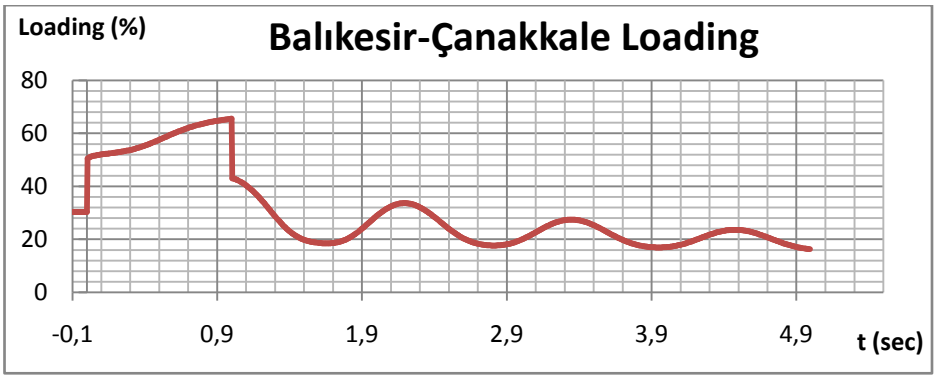

Graph 4.149. Loading of Balıkesir-Çanakkale 154 Line

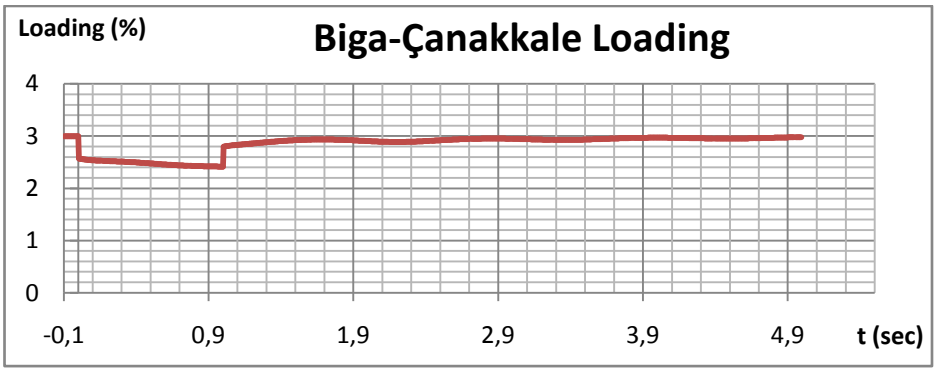

Graph 4.150. Loading of Biga-Çanakkale Line

As can be seen from both graphs, the fault has caused a slight but immediate disturbance on the transmission lines. After the breaker operation, the line loadings have initially changed, leading to an attenuating oscillatory change through time, reaching their steady-state values after the fault. Since all the transmission lines residing within 250 km radius of the fault point remained under %100 loading at any time before, during or after the fault, it is safe to claim that this case has no threat to the transmission lines by means of overloading. It is seen that the peak loading value of Balıkesir-Çanakkale 154 line during the fault has not changed much when compared to case 4.5.2.

Table 4.65 provides the initial (t= -0,1 sec.), final (t=5 sec) and maximum rotor angles for Çan TPP and Unimar NGCC Plant during this case.

Table 4.65. Rotor Angle Values for Çan TPP and Unimar NGCC Plants

	Çan Rotor Angle (rad)	Unimar Rotor Angle (rad)
Initial	1.1293	1.3843
Final	1.2289	0.8618
Maximum	1.2871	1.4079

As can be seen from Table 4.65 the initial and final values of Çan TPP's rotor angle differ by a small amount (approximately $5{,}73^{o}$) while the Unimar NGCC's rotor angle shows a higher response to the fault yet improving to a value that is lower than its initial value. Therefore, the simulation results verify that the generators stay in synchronism with the system without any adverse effect.

Taking the results provided above into consideration, the variations in bus voltages, line loadings after the fault clearance and rotor angles are proven to stay within the limits to ensure a stable operation of the system with an installed capacity, and hence generation equal to the %10 of the short circuit MVA at the bus that the wind farm is connected to. Moreover, the observed parameter variations still far away from approaching the stability limits therefore they imply that the system may be able to handle disturbances for even higher values of installed capacity of the wind farm. This implication will be checked to be true in the next analysis, involving a wind farm installed capacity equal to %12.5 of the short circuit MVA of the connecting bus.

4.5.4: %12,5 (126 MW) Installed capacity

Breaker operating time: 1000 ms

For the given fault clearing time, the variations of selected bus voltages are provided in graphs 4.151 to 4.153.

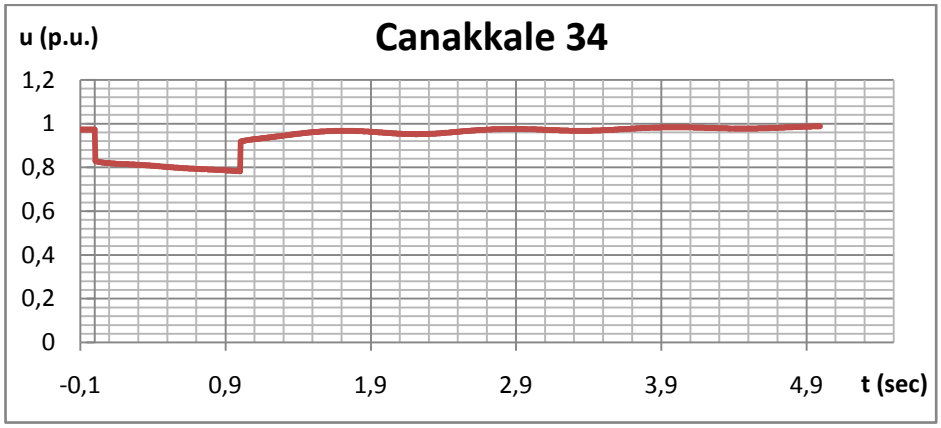

Graph 4.151. Voltage Variation of Canakkale 34 Bus

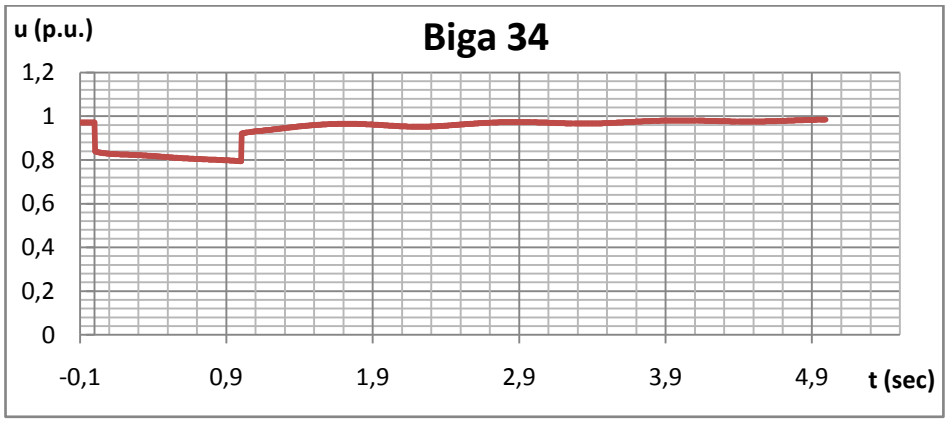

Graph 4.152. Voltage Variation of Biga 34 Bus

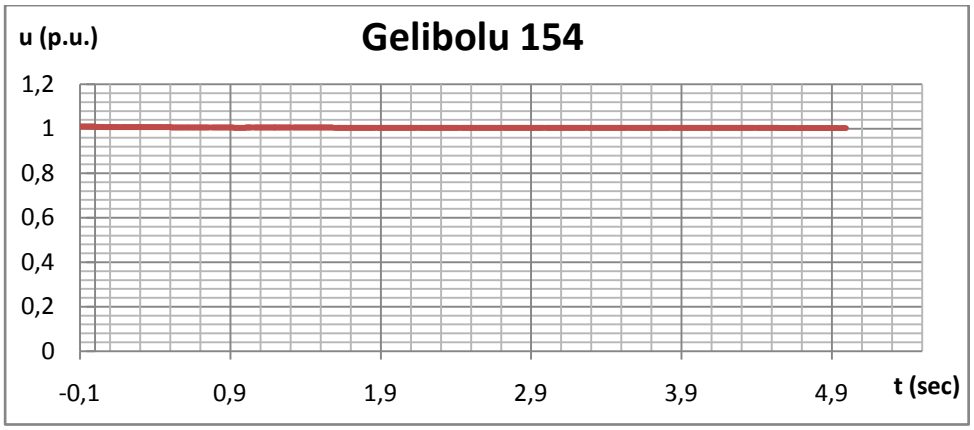

Graph 4.153. Voltage Variation of Gelibolu 154 Bus

As can be seen from the three graphs above, the disturbance had an almost immediate effect on most of the bus voltages which caused the voltages at nearby buses to drop fairly. However, the bus Gelibolu, despite geographically being close to the fault location, is still very slightly affected from the fault event. However, size of the drop at the other buses have increased further.

It can be seen that, at t=1 sec. the voltages at each bus rise sharply with varying magnitudes since the circuit breakers at the ends of faulted line are operated, thus, returning the rest of the system to fault-free state. However, the voltage values are not constant at the post-fault state until the new stable system operating state is fully reached. During this state, the oscillations of the voltage values at each bus can be seen. The oscillations in buses Çanakkale 34 and Biga 34 are increased slightly when compared to case 4.5.3. The maximum and minimum values of bus voltages after the fault clearing, as well as their difference in p.u. are provided in
Table 4.66.

Table 4.66. Bus Voltages for Case 5.4

	Çanakkale 34	Biga 34	Gelibolu 154
Vmax	0.9879	0.9848	1.0096
Vmin	0.9189	0.9215	1.0028
Difference	0.069	0.0633	0.0068
Vfinal	0.9879	0.9848	1.0028

As Table 4.66 clearly shows, the final values at the end of 5 seconds after the fault are within the normal operational limits. Moreover the voltage oscillatory peak for all buses are below the specified %10 limit for this case. It should also be noted that the voltage oscillations in this case are somewhat higher than the similar sub-cases belonging to the ones where the grid strength is shown to be high. This implies that the grid around Çanakkale is not as high as it initially seemed. However, unlike case 4.5.2, there is not a huge difference between the previous case which involved %25 less installed capacity when compared to case 4.5.4.

The line loadings before, during and after the fault are also recorded and the related graphs are provided for lines Balıkesir-Çanakkale 154 and Biga-Çanakkale in graphs 4.154 and 4.155, respectively.

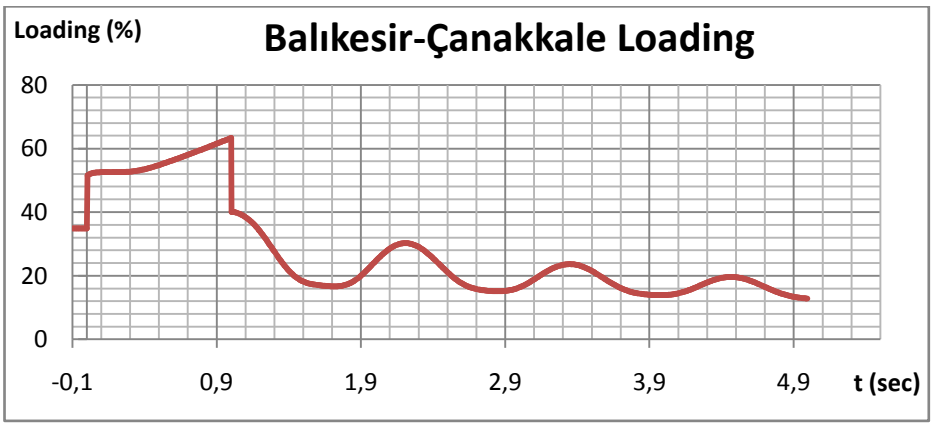

Graph 4.154. Loading of Balıkesir-Çanakkale Line

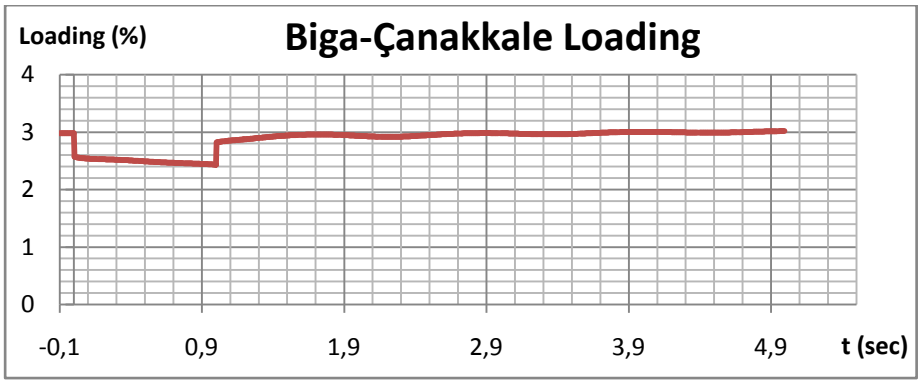

Graph 4.155. Loading of Biga-Çanakkale Line

As can be seen from both graphs, the fault has caused a slight but immediate disturbance on the transmission lines. After the breaker operation, the line loadings have initially changed, leading to an attenuating oscillatory change through time, reaching their steady-state values after the fault. Since all the transmission lines residing within 250 km radius of the fault point remained under %100 loading at any time before, during or after the fault, it is safe to claim that this case has no threat to the transmission lines by means of overloading. It is seen that the peak loading value of Balıkesir-Çanakkale 154 line during the fault has not changed much when compared to case 4.5.3.

Table 4.67 provides the initial (t= -0,1 sec.), final (t=5 sec) and maximum rotor angles for Çan TPP and Unimar NGCC Plant during this case.

Table 4.67. Rotor Angle Values for Çan TPP and Unimar NGCC Plants

	Çan Rotor Angle (rad)	Unimar Rotor Angle (rad)
Initial	1.1205	1.3795
Final	1.2742	0.8055
Maximum	1.3204	1.3869

As can be seen from Table 4.67, the initial and final values of Çan TPP's rotor angle differ by a greater amount (approximately 8,6^{o}) when compared to previous cases, while the Unimar NGCC's rotor angle shows a higher response to the fault. Therefore, the simulation results verify that the generators stay in synchronism with the system without any adverse effect.

Taking the results provided above into consideration, the variations in bus voltages, line loadings after the fault clearance and rotor angles are proven to stay within the limits to ensure a stable operation of the system with an installed capacity, and hence generation equal to the %12,5 of the short circuit MVA at the bus that the wind farm is connected to. Moreover, the observed parameter variations still far away from approaching the stability limits therefore they imply that the system may be able to handle disturbances for even higher values of installed capacity of the wind farm. This implication will be checked in the next analysis, involving a wind farm installed capacity equal to %15 of the short circuit MVA of the connecting bus.

4.5.5: %15 (151 MW) Installed capacity

Breaker operating time: 1000 ms

For the given fault clearing time, the variations of selected bus voltages are provided in graphs 4.156 to 4.158.

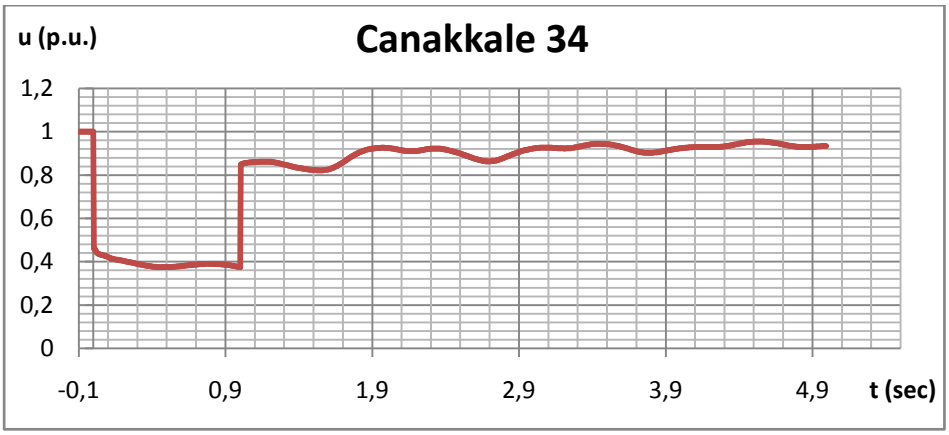

Graph 4.156. Voltage Variation of Çanakkale 34 Bus

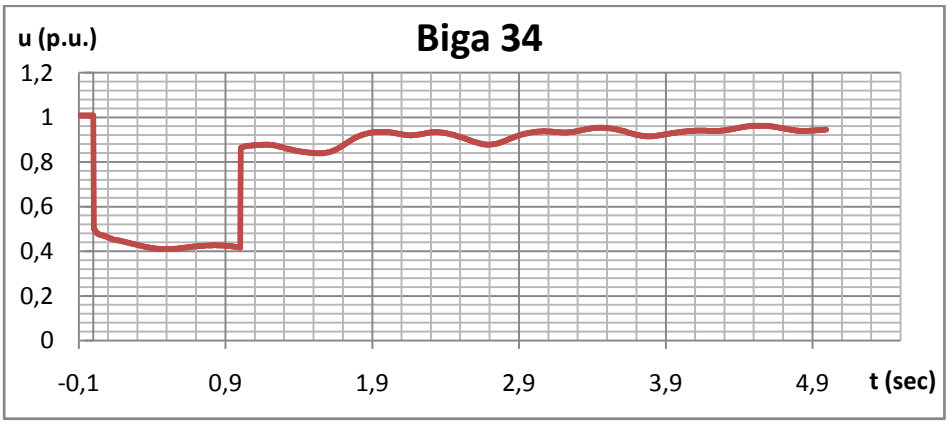

Graph 4.157. Voltage Variation of Biga 34 Bus

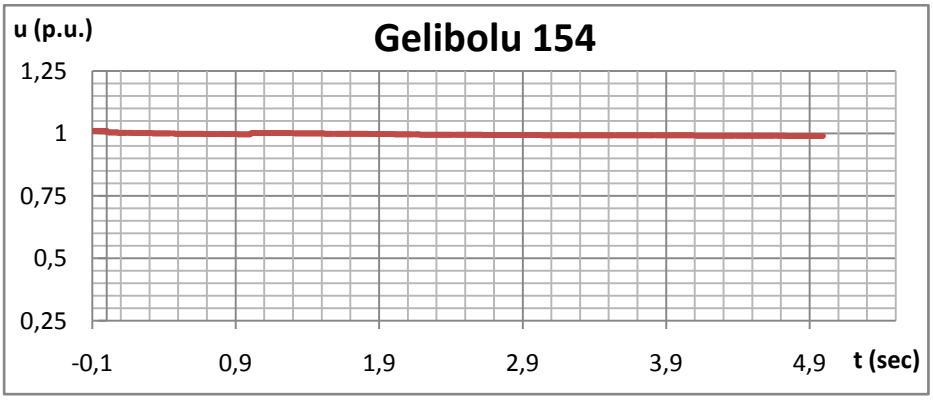

Graph 4.158. Voltage Variation of Gelibolu 154 Bus

As can be seen from the three graphs above, the disturbance had an almost immediate effect on most of the bus voltages which caused the voltages at nearby buses to drop fairly. However, the bus Gelibolu, despite geographically being close to the fault location, is still very slightly affected from the fault event. However, size of the drop at the other buses have increased considerably, and are comparable to similar sub-cases belonging to cases 4.1 to 4.4.

It can be seen that, at t=1 sec. the voltages at each bus rise sharply with varying magnitudes since the circuit breakers at the ends of faulted line are operated, thus, returning the rest of the system to fault-free state. However, the voltage values are not constant at the post-fault state until the new stable system operating state is fully reached. During this state, the oscillations of the voltage values at each bus can be seen. The oscillations in buses Çanakkale 34 and Biga 34 are increased noticeably when compared to case 4.5.4.The maximum and minimum values of bus voltages after the fault clearing, as well as their difference in p.u. are provided in Table 4.68.

Table 4.68. Bus Voltages for Case 5.5

	Çanakkale 34	Biga 34	Gelibolu 154
Vmax	1	1.0079	1.0097
Vmin	0.8219	0.8392	0.99
Difference	0.1781	0.1687	0.0197
Vfinal	0.9346	0.9451	0.9901

As Table 4.68 clearly shows, the final voltages at the end of 5 seconds after the fault for Çanakkale 34 and Biga 34 buses are below 0.95 p.u. which are the lower limit of normal operation. Moreover the voltage oscillatory peak for these buses are considerably over the specified %10 limit for this case. It should also be noted that the voltage oscillations of this size are unacceptably high according to Turkish grid code and need to be prevented by eliminating the cause whenever possible. Here, it brings no question that an increase of 25 MW by means of installed capacity of

Çanakkale RES when compared to case 4.5.4 have played the ultimate role in this increase in oscillations.

The line loadings before, during and after the fault are also recorded and the related graphs are provided for lines Balıkesir-Çanakkale 154 and Biga-Çanakkale in graphs 4.159 and 4.160, respectively.

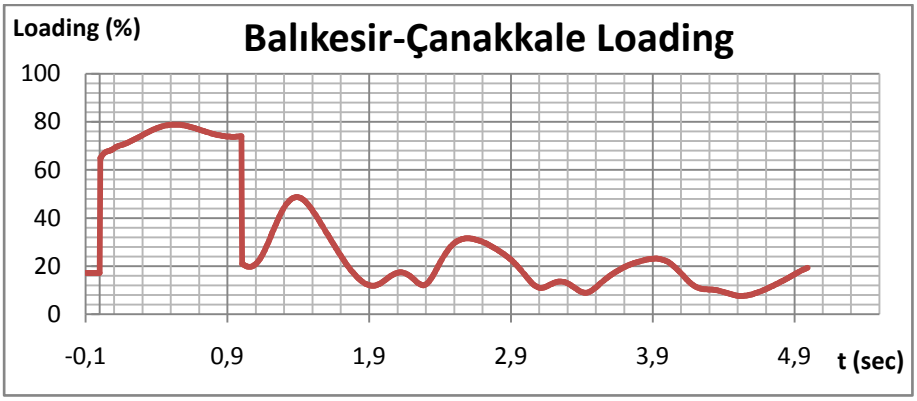

Graph 4.159. Loading of Balıkesir-Çanakkale 154 Line

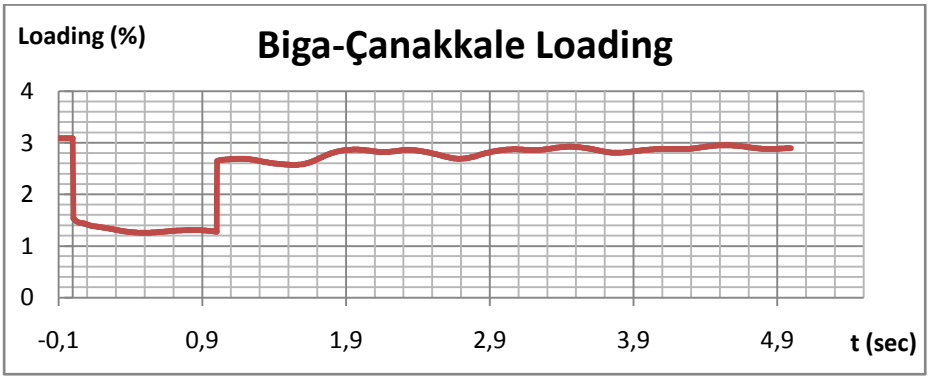

Graph 4.160. Loading of Biga-Çanakkale Line

As can be seen from both graphs, the fault has caused an immediate disturbance on the transmission lines. After the breaker operation, the line loadings have initially

changed, leading to an attenuating oscillatory change through time, reaching their steady-state values after the fault. Since all the transmission lines residing within 250 km radius of the fault point remained under %100 loading at any time before, during or after the fault, it is safe to claim that this case has no threat to the transmission lines by means of overloading. It is seen that the peak loading value of Balıkesir-Çanakkale 154 line during the fault has noticeably increased when compared to case 4.5.4. Moreover, the oscillations in the loading of this line are observed to become larger when compared to previous cases.

Table 4.69 provides the initial (t= -0,1 sec.), final (t=5 sec) and maximum rotor angles for Çan TPP and Unimar NGCC Plant during this case.

Table 4.69. Rotor Angle Values for Çan TPP and Unimar NGCC Plants

	Çan Rotor Angle (rad)	Unimar Rotor Angle (rad)
Initial	1.0377	1.3774
Final	0.9512	1.2377
Maximum	1.2868	1.5348

Although the rotor angle of Çan TPP doesn't exhibit extraordinary behavior, it is not possible to claim the same for Unimar NGCC plant's rotor angle. Despite the initial and final values of rotor angle are far from the stability limit, it is seen that the rotor angle increases up to 1.5348 rad, approximately 87,94^{o} which critically close to the 90^{o} of stability limit. This situation implies that the generator of Unimar NGCC plant has difficulty in staying in synchronism with the system in case of such a disturbance while a high-capacity wind farm is in operation. Therefore, it can be concluded that, the rotor angles of some generators rise up to critical values in the event of a disturbance when Çanakkale RES is expanded to have an installed capacity equal to %15 of the short circuit MVA of the bus via which it's connected to the rest of the system.

Taking the results provided above into consideration, although the variations in some bus voltages and line loadings after the fault clearance are proven to stay within the limits, there have been considerable distortions in the system operational values belonging to certain buss, voltages of which are shown to oscillate at great magnitudes while decreasing below 0.95 p.u. as their steady-state values. Moreover, the rotor angle of Unimar NGCC power plant has increased dangerously, approaching to the stability limit which indicates that the system becomes prone to disturbances when the installed capacity of Çanakkale RES has increased to 151 MW. To sum up, with its present condition, the grid around Çanakkale RES is found not to be strong enough to handle a relatively high amount of wind power generation since the voltage oscillations and final values at given buss failed to meet acceptable criteria, as well as rotor angle of Unimar NGCC power plant has approached to a very critical value. Since the analysis results of case 4.5.5 shown that the installed capacity of wind farm corresponding to %15 of the short circuit MVA of the connecting bus causes problems in the system in case of a short circuit event, no further analyses involving higher installed capacities of Çanakkale RES will be presented here. If desired, the results displaying variations in system parameters due to the same short circuit events for highest installed capacity simulated (corresponding to %20 of short circuit MVA of the related bus) can be accessed from the appendix CD as an Excel file.

4.6 Overview of Simulation Results

In this section, an overview of the simulation results will be made in an commentary and comparative manner. The simulations were carried out in a manner that was described the previous chapter in detail. By means of determining the effect of wind farms on the Turkish transmission system, three main parameters are chosen to be observed. Namely, the bus voltages, transmission line loadings and generator rotor angles. For each wind farm model, these parameters belonging to buses, transmission lines and generators within the circular area centered at fault point and of a radius of 250 km are continuously observed from t= -0.1 sec to t=5 sec.

The effect of a disturbance in a region where wind generation is considerable is shown to be of importance since it plays a large role in determining the acceptability of wind farm investments in the future, as well as questioning the present grid strength by means of being able to handle such disturbances successfully. It is not a straightforward task to evaluate the effect on system security and stability, as well as power quality of existing wind farms in case of a disturbance and the results obtained here can be evaluated by relying on present-case definitions and criteria of system stability, power quality or security. Since determining those criteria is out of scope of this thesis, the comments will be made objectively, stating whether an argument related with aforementioned problems are definite or questionable whenever relevant.

The effects of events will be evaluated according to the bus voltages, line loadings and generator rotor angles according to the criteria provided below. The cases satisfying all the given conditions will be determined as satisfactory, indicating that the system is able to withstand a severe 3-phase to ground fault with the given wind farm and installed capacity level.

Bus Voltages

-Voltages at the end of 5 seconds must be within normal operational limits: 0.95-1.05 pu.

-Voltage oscillations after fault clearing must not exceed %10 of nominal voltage (0.1 p.u.)

Line Loadings

-Loadings at the end of 5 seconds must be within normal operational limits: 0 -100 %.

-Temporary overloadings are acceptable in the transient state, up to %150.

Rotor Angles

-Rotor angle at the end of 5 seconds must be within normal operational limits: 0 - 90^o

-Rotor angles exceeding 90^o slightly (less than %10) and returning to normal limits in the transient state can be acceptable but do not guarantee system stability.

If any of these conditions during the analysis of a case fails to be satisfied, the results will be evaluated to be insufficient, which will imply that presence of a wind farm with given installed capacity in the region can be a threat to the system stability, security or power quality in case of a considerable disturbance.

In the analyzes, all the wind farms simulated are proven to successfully satisfy the given criteria for the installed capacities equal to:

- %5 of short circuit MVA at the connecting bus.

- % 7.5 of short circuit MVA at the connecting bus.

- % 10 of short circuit MVA at the connecting bus.

-% 12.5 of short circuit MVA at the connecting bus.

In the analysis results for 5 cases presented here, it is observed that they include the wind farms resided on both the strong and weak points of the grid. To be more specific, case 1 and case 4 analyzed two wind farms resided on the regions where the grid is stronger while the cases 2,3 and 5 investigated the effects of the wind farms residing on the points where the grid is weaker. Cases 1 and 4 turned out to be more successful at handling the fault for higher wind farm installed capacities while the remaining cases have failed to satisfy the aforementioned criteria at lower values of installed capacities which was an expected result. The Installed capacities, given both

as MW and percentage of short circuit power at relevant bus, at which the system stability and security criteria are failed to be met are given in Table 4.70

Table 4.70. Installed Capacity Limits for Five Cases

Case	Capacity (MW)	% of Ssc at connecting bus
Case 1	600	27.5
Case 2	352	15
Case 3	180	>15*
Case 4	570	>20*
Case 5	151	15

**These cases are proven to critically endure the disturbance at given capacities*

As can be seen from Table 4.70, even the weaker regions in the grid are able to satisfy the given criteria under a disturbance for the installed capacity values up to %12.5 of short circuit MVA at their relevant buses. It's observed that the regions classified as "weak" in the grid are not able to successfully handle the fault event in case that the installed capacity of wind farm is around %15 of the short circuit MVA of the relevant bus. However, the regions classified as "strong" are proven to endure the fault events for even higher installed capacities of the related wind farms. %27.5 was the highest percentage observed to be the first failing point among all wind farms simulated while several wind farms, including that of case 2 and 5 are proven to fail to meet the criteria of system stability, security and power quality for the first time, when the installed capacity of the wind farms were equal to %15 of the short circuit power at connecting buses. In conclusion, for the present case, every region analyzed within the scope of this study is shown to be able to meet the stability, security and power quality criteria for a wind farm having its rating equal to at most %12.5 of the short circuit MVA of the bus that the farm is connected to. The stronger points in the grid, on the other hand, are proven to endure the severe fault

event for wind farm capacities no less than %15, for some cases approaching %30, of the short circuit power at the relevant bus. As the analysis results are investigated further, it is seen that the criteria which tend to be failed to satisfied relatively easily are the ones belonging to bus voltages and rotor angles. The line loadings are proven to rarely be a problem as the system is designed to maintain the unitary structure even during much more severe disturbances. Although occasional overloadings of lines up to %140 at most are observed in transient states of certain cases, these relatively slight overloadings are shown not to cause the loss of the line thanks to the very brief transient period which causes the heating of the lines to stay within acceptable limits. The voltage and rotor angle criteria are in many cases are shown to exceed limits at same or close installed capacity values though the voltage criteria being slightly easier to fail as the installed capacity values approached higher values.

Another discrimination between the stronger and weaker regions in the grid are upon which criteria fails to be satisfied first as the installed capacity of related wind farms are increased to large values. The main problem associated with the stability loss for stronger regions are the rotor angles exceeding 90^o in case of fault events. On the other hand, for other regions, due to the fact that the grid is not as strong as cases 1 and 4, the voltage oscillations have exceeded maximum allowable limits before the rotor angles violated stability conditions. This can be explained with the fact that, presence of a generator implies a certain strength at the bus that the generator is connected to no matter how weak the grid around that bus is. However, the weak regions suffer from lack of ability to effectively attenuate the oscillations in voltages due to the weak connection when compared to stronger regions of the grid. Therefore, some bus voltages in the weaker regions tend to be disturbed easily with a fault involving a considerable wind generation nearby.

Taking everything into account, with the analyzes the results of which are demonstrated in this chapter, it is shown that the Turkish Transmission System is able to handle a severe 3-phase to ground fault at various locations near the wind farms are located with ratings up to at least %12.5 of the short circuit MVA of the bus that the individual wind farms are connected to. Moreover, this limit is shown to

be determined mainly by the bus voltage oscillations which are followed by the rotor angle variations for stronger regions in the system. The bus voltage oscillations are shown to be the main problem introduced with increased wind farm capacity for the weaker regions of the grid while for stronger regions, the rotor angle slip has proved to be the major concern since the grid at those regions are proven to be strong enough to maintain the voltage oscillations at buses within acceptable limits.

This chapter, therefore presented and evaluated the analysis results to investigate the dynamic effects of wind farms in Turkish Transmission System in case of disturbances with relevant numerical values supported by graphs and related observations, statements and comments. As justified by the analysis results, the Turkish grid is shown to be electrically strong and solid enough to handle the wind-farm related disturbances not only for present wind penetration levels, but also for the generation levels that are likely to be realized in the near future.

CHAPTER 5

CONCLUSION AND FUTURE WORK

5.1 Conclusion

The work accomplished in this thesis can be divided into three main parts. Firstly, the Turkish Transmission system structure, as well as generation and consumption centers are modeled in Digsilent Powerfactory with a reduced complexity while trying to match the actual system properties as closely as possible. Then, a large number of transient analyzes are carried out on the system realized with different wind farm installed capacity values, as well as circuit breaker operation times. Finally, the analysis results are examined in detail reaching to a conclusion regarding the dynamic effects of wind farms in Turkish Transmission System.

With the industrial revolution, mankind has discovered the power of steam. Steam was initially used to provide motion for machinery to do heavy physical tasks. Not long after, the discovery of electricity by means of industrial, residential and commercial usage resulted in power plants that use this steam power to generate electricity. In the early days of generation, this was carried out only by combustion process which involved fossil fuels. However, around the middle of 20th century, widespread thermal power plants that are increasing both in numbers and by rating in order to meet the growing energy demand of people have introduced serious air pollution problems. With 21st century drew close, certain alternatives of electrical power generation has been introduced. Among these alternatives, wind power plants took a special place due to its structural simplicity and cheapness despite their considerable efficiency. Starting from the late 1990's, therefore, the wind generation

worldwide has shown a considerable increase by means of the number and size of wind farms, as well as the capacities of individual turbines. This increase in wind generation as a ratio of overall generation, commonly referred as wind penetration, started concerns and arguments regarding the effect of increased levels of wind generation on the electrical systems. Turkey was no different in this manner and in 2004 TEİAŞ has claimed with its report that the presence of wind farms introduces serious problems regarding the system stability and security, especially when the wind farm installed capacity has exceeded %5 of the short circuit power of the bus that the wind farm is connected to. This claim, however, has not been proved to be true neither theoretically nor practically. This thesis aimed to analyze the effects of wind generation on the Turkish Transmission system for the given installed capacities, as well as for increased installed capacities reaching up to around %30 of short circuit MVA at relevant buss and therefore, provide a theoretical conclusion regarding the effects of wind farms in the grid, as well as commenting on the realism of the aforementioned claims. Under this perspective, the steps of the system construction, analysis and result evaluation processes can be briefly summarized with necessary information and comments as follows:

- In Chapter 1, a brief introduction to the thesis topic is made, providing information about the evolution of power generation, early usages of wind power as well as some early wind turbine developments. Moreover, the need for wind power generation is explained alongside a brief overview of growing electricity demand and consequent developments in generation methods starting with industrial revolution. Then, the advantages of wind farms over conventional generation methods are highlighted.

- The growing demand of electricity makes it inevitable to invest for power plants continuously. With natural resources such as fossil fuels getting more and more expensive, the renewable energy plants have become an attractive alternative in the 21st century.

- As the wind farms connected to the grid become more common and larger, arguments regarding their effects on system security, stability and power quality arose. TEİAŞ has provided a report regarding these concerns and claiming that it is necessary to limit the wind farms' allowed installed capacities to low values to prevent such effects.

- In chapter 2, the necessary general background regarding the wind physics and how the wind energy is converted to electrical energy is provided. Important elements in wind power generation such as the Betz limit and wind turbine types are discussed with relevant mathematical proofs.

- Chapter 3 consists of the preparing of the data necessary to build the Turkish electrical system model, as well as explanations regarding the used software: Digsilent Powerfactory. The steps of implementing the system model on the software is also explained in detail.

- In order to be able to simulate the effects of wind farms on the transmission system, firstly the necessary data in order to construct a realistic model of the Turkish Transmission system had to be obtained. For this purpose, the Turkish Generation-Transmission system map prepared by TEİAŞ providing the system data on 2011 is used.

- Due to the tremendous amount of data for the whole system, it was not possible, or within the scope of this study, to exactly model the whole electrical system. Instead, the amount of data is reduced by combining closely oriented equipment as a whole without giving up on realism considerably.

- A realizable yet realistic model of the system is constructed using Digsilent Powerfactory software using the edited data. The system is subjected to several tests involving different load conditions representing the minimum, maximum or average demand levels throughout the year.

- With the tests verifying healthy operation of the system, the transient analyzes are carried out for the wind farms modeled in the system. The analysis processes are performed individually for each wind farm, with different installed capacity values and different circuit breaker operation times. The installed capacity values to be implemented in analyzes are chosen to be equal to %5, %7.5, %10, %12.5 and %15 of short circuit MVA at the bus that the wind farm is connected to. The circuit breaker operation times are determined regarding real cases, as well as theoretical minimum values. Namely; 60, 120, 200, 500 and 1000 milliseconds of breaker operation times are chosen for analyzes.

- Chapter 4 provides and discusses the analysis results regarding the dynamical effects of wind farms in the Turkish Transmission System model. The results are provided and discussed both quantitatively and qualitatively.

- During each of the analyzes bus voltages, line loadings and rotor angles within 250 km radius of fault point are continuously observed and necessary data is recorded. These data made up the basis of evaluations regarding the system stability and security.

- For each wind farm, a certain set of the observed parameters are chosen to be demonstrated in order to avoid excessive data presented here. Graphs showing time variation of bus voltages and line loadings are also provided to aid visualizing the effects of disturbances to the system.

- After providing the results for each analysis, these results are commented on regarding the severity of the consequences of fault. For this purpose, widely accepted definitions for system stability, security and power quality are used and taken as the necessary criteria to be satisfied.

- When all the analyses at different installed capacities of a wind farm are carried out, the overall results are overviewed and the extent of wind farm's installed capacity up to which the disturbance's effects are held within acceptable limits are determined.

- In the last part of Chapter 4, the results of all analyses are overviewed. The facts and observations regarding the system strength at different points of the grid where the wind farms are connected to are stated. Moreover, the causes of system security, stability and power quality violations under disturbance with increasing wind farm capacities are determined and commented on.

The results of analyses are important since they lead the key role in determining the size of effects of wind farms on the transmission system under dynamic events i.e. disturbances. The outcomes of these results can be summarized as follows:

- The grid strength is not uniform as expected. However, the regions close to large generation or consumption centers are turned out to be stronger when compared to regions far away from large generation or consumption centers.

- Majority of wind farms analyzed belong to the regions where the grid is stronger. This is, again, an expected situation considering the fact that wind farms are highly concentrated on western coastline of Turkey where the grid is strong by structure due to large number of populated areas with high power demands.

- The severity of consequences of a disturbance is determined by the voltage oscillations and final values of bus voltages, line loadings and the generators' rotor angle variations.

- The severity of consequences of the fault event is inversely proportional with the grid strength around the location of fault. That is, same 3 phase to ground fault event has caused smaller disturbances in the system parameters for the regions where the grid is stronger.

- The disturbances caused by the fault became more severe as the installed capacity of the nearby wind farms increased. This provides a proof to the fact that wind generation does affect the system stability under fault conditions.

- The most commonly observed effects of disturbances in cases involving high levels of wind generation are the voltage oscillations and rotor angle variations exceeding the limits for system security, stability and quality of electricity. The events of rotor angles exceeding 90^{o} took place earlier than excessive oscillations in the bus voltages for the stronger regions in the grid while the oscillations of bus voltages became the dominant problem for the regions where the grid is relatively weaker. Line loadings are shown to be far away from being a problem even at very high levels of wind penetration.

- On the other hand, these dynamical effects of wind generation on the electrical system is proven to be stay within safe limits unless the generation levels increase to large values. The analysis results showed that the system is able to withstand a severe disturbance around any wind farm provided that the installed capacity of that wind farm does not exceed %12.5 of short circuit MVA belonging to the bus that the wind farm is connected to. For stronger regions in the grid, this value increased up to, and sometimes above %20.

- The installed capacity of the wind farms as the percentage of short circuit MVA at related bus is shown to be the main factor affecting the severity of the consequence of the fault event in the system, rather than the sole MW rating. This is justified further by the fact that different regions having similar properties related to strength of the grid have performed similarly well by means of satisfying the required criteria for stability, system security and power quality at similar wind farm installed capacity in terms of percentage of the short circuit MVA at related buses despite the actual capacities (in terms of MW) of the wind farms varied greatly.

To sum up, with the given analyses, the dynamical effects of wind farms to Turkish Transmission System are theoretically observed through several simulations involving different cases. As opposed to some claims, the severity of these effects are proven to be small and of little importance unless extremely high wind generation levels are reached. Therefore, with present case of Turkish grid, it is safe to state that the present, and planned wind farms are far away from being a threat to the system stability, security or power quality.

5.2 Suggestions for Future Work

Wind power generation is a very important and dynamical field that is under constant development with new discoveries and contributions from all over the world. It is, therefore, not possible to limit the issues related to wind generation to a single study. Instead, every study made in this field ought to have something to contribute to the

field by means of new discoveries and developments. The work carried out in this thesis can be improved or developed further in the possible future works as follows:

- Due to tremendous amount of data belonging to the electrical system, it was not possible to develop an exact model of the generation-transmission system. Although the realism of given model is sufficient for the analyzes given here, in order to determine exact effects and limits for stability, security and power quality, an exact model of the Turkish grid can be used.

- In the system model, the existing wind farms are modeled and connected to the relevant buses. The future investments are assumed to be made on the locations where wind generation already existed in order to be able to increase the installed capacities of wind farms properly. However, the investments to be made in locations where no wind farm existing nearby are not included within this study. Therefore, these planned investments can be also included in the system model to simulate future effects of the given wind farms.

- Although small in numbers and ratings, remaining renewable energy plants including geothermal and solar power plants, as well as bio-fuel burning plants are not included in the system model. Including these in the model can increase the accuracy of the simulation results.

- Lastly but most importantly, although being considerably broad, the analyzes carried out in this thesis should not be regarded as ultimate results since it is not possible to consider every possible disturbance or event combination regarding the wind power plants within the whole country. Therefore, the dynamical effects of wind farms in Turkish transmission system can be investigated in more detail considering different aspects such as flicker or harmonics with different scenarios involving various disturbances.

REFERENCES

[1] R.Miller et. al., 21st Century Technologies Promises and Perils of a Dynamic Future, OECD, 1998

[2] J.R. Luoma, "The Challenge for Green Energy: How to Store Excess Electricity", in *Yale Environment*, Yale University, 2009

[3] Union of Concerned Scientists, "Benefits of Renewable Energy Use", [Online]. Available: http://www.ucsusa.org/clean_energy/our-energy-choices/renewable-energy/public-benefits-of renewable.html#.VbyT0vnASX8. [Accessed 13.05.2015]

[4] T.Petru, "Modeling of Wind Turbines for Power System Studies", Dept. of Electric Power Engineering, Chalmers University of Technology, Göteborg, Sweeden, 2003

[5] I. Spreeuwenberg, "National Grid Input into UK Offshore Energy SEA Impact on Onshore Electricity Transmission System", in *Offshore Energy Strategic Environmental Assessment programme*, UK Department of Energy and Climate Change, London, 2008

[6] World Nuclear Association, "Renewable Energy and Electricity", [Online]. Available: http://www.world-nuclear.org/info/Energy-and-Environment/Renewable-Energy-and-Electricity/. [Accessed 14.06.2015]

[7] European Wind Energy Association, "Powering Europe: Wind Energy and the Electricity Grid", EWEA, 2010

[8] TEİAŞ, "Bölgesel Bazda Sisteme Bağlanabilecek Rüzgar Enerjisine Dayalı Üretim Tesisi Kapasiteleri", TEİAŞ, Ankara, 2013

[9] L.Wang et. al., Wind Power Systems Applications of Computational Intelligence, Berlin: Springer, 2010

[10] T.Ackermann, Wind Power in Power Systems, Stockholm: John Wiley & Sons Ltd., 2012

[11] P.Jain, Wind Energy Engineering, Mc Graw Hill, 2011

[12] Conservation of Energy, [Online]. Available: http://hyperphysics.phy-astr.gsu.edu/hbase/conser.html. [Accessed 01.02.2015]

[13] M. Ragheb and A. M. Ragheb, "Wind Turbines Theory - The Betz Equation and Optimal Rotor Tip Speed Ratio" , Fundamental and Advanced Topics in Wind Power, InTech, 2011

[14] D. Milkborrow, "Annual Power Costs Comparison: What a Difference a Year Can Make.", WindPower Monthly, January 2010

[15] Greenhouse Gas Emissions, [Online]. Available: http://www.theguardian.com -/environment/2015/may/06/carbon-dioxide-record-levels-noaa. [Accessed 14.04.2015]

[16] United States Environmental Protection Agency, [Online]. Available: http://www.epa.gov/climatechange/ghgemissions/gases/co2.html. [Accessed 07.04.2015]

[17] Inventory of U.S. Greenhouse Gas Emissions and Sinks: 1990-2012, National Service Center for Environmental Publications, 2014

[18] United States Environmental Protection Agency, Clean Energy, [Online]. Available:http://www.epa.gov/cleanenergy/energy-and-you/affect/air-emissions.html. [Accessed 03.03.2015]

[19] %20 Wind Energy By 2030 Technical Report, U.S. Department of Energy, 2008

[20] Global Trends in Renewable Energy Investment, Frankfurt School FS-Unep Collaborating Centre, Bloomberg L.P., 2014

[21] Global Wind Energy Council, "Global statistics", [Online]. Available: http://www.gwec.net/global-figures/graphs/. [Accessed 15.02.2015]

[22] Technology Roadmap: Wind energy, International Energy Agency, 2013

[23] Union of Concerned Scientists, "How Geothermal Energy Works", [Online]. Available:http://www.ucsusa.org/clean_energy/our-energy-choices/renewable-energy/how-geothermal-energy-works.html#.VbuMM_nASX8. [Accessed 18.07.2015]

[24] Energy Informative, "Wind Energy Pros and Cons", [Online]. Available :http://energyinformative.org/wind-energy-pros-and-cons/. [Accessed 18.07.2015]

[25] U.S. Department of Energy, "Installed Wind Capacity", [Online]. Available: http://apps2.eere.energy.gov/wind/windexchange/wind_installed_capacity.asp [Accessed 12.07.2015]

[26] Government of U.K., "Land eligibility under the Basic Payment Scheme", Department for Environment, Food & Rural Affairs, 2013

[27] University of Delaware, "What is Wind Energy?", [Online]. Available: http://www.ceoe.udel.edu/lewesturbine/faq.shtml. [Accessed 18.02.2015]

[28] Energy Center of Wisconsin, "Parts of a Wind Turbine" [Online]. Available: http://www.ecw.org/windpower/web/cat2a.html. [Accessed 10.03.2015]

[29] A.Rivkin, M. Randall et. al., Wind Power Generation and Distribution, Burlington: Jones & Bartlett Learning, 2014

[30] M. Ragheb, "Vertical Axis Wind Turbines", University of Illinois, " *Popular Science*, Vol. 274, No. 4, pp. 18-39, 2008

[31] M. Pöller and S. Achilles, "Aggregated Wind Park Models for Analyzing Power System Dynamics", *4th International Workshop on Large Scale Integration of Wind Power and Transmission Networks for Offshore Wind-Farms*, 2003

[32] M. B. Turi and C. S. Marks, "Beaiıng Selectıon Techniques As Applied to Mainshaft Direct and Hybrid Drives for Wind Turbines", *Timken Technical Paper*, No:1, pp. 1-16, 2009

[33] Treehugger, "Is Direct Drive the Future? Wind Turbines Without Gears are Lighter, Cheaper, More Reliable" [Online]. Available: http://www.treehugger.com/renewable-energy/is-direct-drive-the-future wind-turbines-without-gears-are-lighter-cheaper-more-reliable.html. [Accessed 19.03.2015]

[34] A.Benlevi, "Engineering Model for Automatic Design of Rotor Nacelle Assemblies", Delft University of Technology, Faculty of Aerospace Engineering, 2014

[35] National Renewable Energy Laboratory, "Wind Resource Assessment", [Online]. Available: http://www.nrel.gov/wind/resource_assessment.html [Accessed 20.07.2015]

[36] Türeb, "Türkiye Rüzgar Enerjisi İstatistik Raporu", Türeb, Ankara, 2015.

[37] M. Çalışkan, "Türkiye Rüzgar Enerjisi Potansiyeli ve Mevcut Yatırımlar", in *Rüzgar Enerjisi ve Santralleri Semineri*, Tucsa, İstanbul, 2011

[38] H.Alış, "Türkiye'de Rüzgar Enerjisi", EÜAŞ, Ankara, 2012

[39] M.H.J. Bollen, F.Hassan, Integration of Distributed Generation in the Power System, New Jersey: John Wiley & Sons Inc., 2011

[40] Z.T.Altuntaşoğlu, "Türkiye'de Rüzgâr Enerjisi, Mevcut Durum, Sorunlar", in *Mühendis ve Makine*, 2011, Issue: 617

[41] L.Yılmaz, "Yenilenebilir Enerji Kaynakları Açısından Rüzgar Enerjisinin Türkiye'deki Kapasitesi", İstanbul Teknik Üniversitesi İnşaat Fakültesi Hidrolik ve Su Yapıları Kürsüsü, İstanbul, 2002

[42] Elektrik Üreticileri Derneği, "EnerjiSA Türkiye'nin En Büyük RES'ini Açtı", [Online].Available: http://www.eud.org.tr/TR/Genel/Belge Goster.aspx?F6E10F8892433CFF-2395174CFB32E16D0BC216A9778CD0. [Accessed 24.07.2015]

[43] MHI Vestas Offshore Wind, "V164-8.0 MW breaks world record for wind energy production", [Online]. Available: http://www.mhivestasoffshore.com/v164-8-0-mw-breaks-world-record-for-wind-energy-production/. [Accessed 20.04.2015]

[44] Ö.Güler, "Dünya'da ve Türkiye'de Rüzgar Enerjisi", İstanbul Teknik Üniversitesi Enerji Enstitüsü, İstanbul, 2005

[45] T.C. Enerji ve Tabii Kaynaklar Bakanlığı, "T.C. Enerji ve Tabii Kaynaklar Bakanlığı Stratejik Planı 2010-2014", T.C. Enerji ve Tabii Kaynaklar Bakanlığı, Ankara, 2009

[46] Integreen, "Türkiye'de Rüzgar Enerjisi", [Online]. Available: http://www.integreen.com.tr/Neden-Ruzgar-Enerjisi.html. [Accessed 22.04.2015]

[47] Tures, "Rüzgar ve Güneş Enerjisi Ölçüm Tebliği", in *Türkiye Rüzgar Enerjisi Sektör Buluşması*, Ankara, 2011

[48] Z.Eriş, "Rüzgar Lisans Başvuruları Açılsın",in *Enerjigazetesi*, [Online]. Available: http://www.enerjigazetesi.com/eris-ruzgar-lisans-basvurulari-acilsin/. [Accessed 18.04.2015]

[49] D.Taylor, Renewable Energy: Power for a Sustainable Future, Oxford, UK : Oxford University Press in association with the Open University, 2012.

[50] S.Soter and R.Wegener, "Development of Induction Machines in Wind Power Technology", Institute of Electrical Drives and Mechatronics University of Dortmund, Germany, 2007

[51] E.H. Camm et. al., "Characteristics of Wind Turbine Generators for Wind Power Plants", IEEE PES Wind Plant Collector System Design Working Group, 2009

[52] Z. Chen, "Issues of Connecting Wind Farms into Power Systems", in *IEEE/PES Transmission and Distribution Conference & Exhibition: Asia and Pacific Dalian,*China, 2005

[53] EPDK, "Elektrik Şebeke Yönetmeliği", in *T.C. Resmi Gazete*, no: 29013, 2014

[54] K.Aktaş, G.Gündoğmuş, 2009 Puant (yaz) Yük Şartlarında Yük Akışı, Üç Faz ve Faz Toprak Kısa Devre Etüdü, TEİAŞ, Ankara, 2009

[55] P.Kundur, Power System Stability and Control, Mc Graw Hill, 1994

APPENDIX A

DETAILED RESULTS OF TRANSIENT SIMULATIONS INCLUDING ALL CIRCUIT BREAKER OPERATION TIMES

The variations of bus voltages, generator rotor angles and line loadings belonging to elements observed for each wind farm presented in the thesis can be accessed from the MS Excel tables in the CD provided inside the back cover of this thesis.